

---

# The Momentum Amplituhedron

## Scattering Amplitudes from Geometry

David Damgaard

---



München 2022



---

# **The Momentum Amplituhedron**

## **Scattering Amplitudes from Geometry**

**David Damgaard**

---

Dissertation  
der Fakultät für Physik  
der Ludwig-Maximilians-Universität  
München

vorgelegt von  
David Damgaard  
aus Kopenhagen, Dänemark

München, den 27. Oktober 2021

Erstgutachter: Dr. Livia Ferro

Zweitgutachter: PD Dr. Michael Haack

Tag der Einreichung: 27. Oktober 2021

Tag der mündlichen Prüfung: 16. Dezember 2021

# Contents

<b>1</b>	<b>Introduction</b>	<b>1</b>
<b>2</b>	<b>Scattering Amplitudes</b>	<b>9</b>
2.1	Scattering Amplitudes . . . . .	9
2.2	Poincaré Group and Little Group Scaling . . . . .	12
2.3	On-Shell Methods . . . . .	16
2.4	Non-Abelian Gauge Theory . . . . .	20
2.4.1	BCFW recursion relations . . . . .	23
2.4.2	Singularities of Non-Abelian Gauge Theories: Collinear and Soft Limits . . . . .	26
2.5	Bi-Adjoint $\phi^3$ Theory . . . . .	28
2.6	On-shell Supersymmetry . . . . .	31
2.6.1	$\mathcal{N} = 4$ Supersymmetry . . . . .	32
2.7	Super-BCFW Recursion for $\mathcal{N} = 4$ sYM . . . . .	35
2.8	Symmetries of $\mathcal{N} = 4$ sYM . . . . .	40
2.8.1	Superconformal symmetry . . . . .	40
2.8.2	Dual Superconformal symmetry . . . . .	41
2.9	Loops . . . . .	46
2.9.1	The Scalar Box Integral . . . . .	47
2.9.2	Generalized Unitarity . . . . .	49
<b>3</b>	<b>The Grassmannian</b>	<b>53</b>
3.1	Projective Space . . . . .	54
3.2	The Grassmannian . . . . .	55
3.2.1	Grassmannians as permutations . . . . .	57
3.2.2	Grassmannians as plabic graphs . . . . .	58
3.3	The Positive Grassmannian . . . . .	63
3.3.1	Boundary Stratification . . . . .	67
3.4	Scattering Amplitudes from the Grassmannian . . . . .	68
3.4.1	BCFW Bridge Construction . . . . .	70
3.5	Scattering Amplitudes from Grassmannian Integrals . . . . .	75

<b>4</b>	<b>Positive Geometries</b>	<b>79</b>
4.1	Positive Geometries and Canonical Forms . . . . .	79
4.2	Morphisms of Positive Geometries . . . . .	83
4.3	Adding Positive Geometries . . . . .	85
4.4	The Amplituhedron . . . . .	89
4.4.1	Tree Amplituhedron . . . . .	90
4.4.2	Extracting scattering amplitudes . . . . .	93
4.4.3	The Loop Amplituhedron . . . . .	95
4.4.4	Emergent Unitarity and Locality . . . . .	96
<b>5</b>	<b>Kinematic Associahedron</b>	<b>99</b>
5.1	Kinematic Space . . . . .	99
5.2	The Planar Scattering Form . . . . .	100
5.3	The Kinematic Associahedron . . . . .	102
5.4	Examples . . . . .	103
5.5	Kinematic Associahedron for Arbitrary Color Orderings . . . . .	107
5.6	Factorization and Boundaries of the Kinematic Associahedron . . . . .	110
<b>6</b>	<b>The Momentum Amplituhedron</b>	<b>111</b>
6.1	Scattering Amplitudes as Differential Forms . . . . .	112
6.2	The Momentum Amplituhedron . . . . .	116
6.3	The Momentum Amplituhedron Boundaries and Volume Form . . . . .	120
6.3.1	Boundaries of the Momentum Amplituhedron . . . . .	121
6.3.2	The Momentum Amplituhedron Canonical Form . . . . .	121
6.3.3	Scattering Amplitudes from the Volume Function . . . . .	123
6.4	Factorization Properties . . . . .	123
6.5	Extra positivity conditions . . . . .	125
6.6	Examples . . . . .	126
<b>7</b>	<b>Momentum Amplituhedron &amp; Kinematic Associahedron Map</b>	<b>131</b>
7.1	Momentum Amplituhedron in Kinematic Space . . . . .	131
7.2	Kinematic Spaces and their Maps . . . . .	132
7.2.1	Kinematic spaces . . . . .	132
7.2.2	Maps between kinematic spaces . . . . .	134
7.2.3	Comparing canonical forms . . . . .	135
7.3	Examples . . . . .	138
7.3.1	Four-point amplitudes . . . . .	138
7.3.2	Five-point amplitudes . . . . .	139
7.3.3	Six-point amplitudes . . . . .	141
7.3.4	Beyond $n = 6$ . . . . .	145
7.4	The Inverse-Soft Construction for $\omega_{n,k}$ . . . . .	145

---

<b>8</b>	<b>Momentum Amplituhedron &amp; Kleiss-Kuijf Relations</b>	<b>149</b>
8.1	Non-Standard Orderings of the Momentum Amplituhedron . . . . .	149
8.2	Simplicial realization of KK relations for MHV Amplitudes . . . . .	150
8.3	Ray-based Homological Algorithm . . . . .	157
8.4	Kleiss-Kuijf Relations for the Kinematic Associahedron . . . . .	164
8.5	Poset-based Homological Algorithm . . . . .	170
8.5.1	Revisiting MHV amplitudes . . . . .	171
8.5.2	All Helicity Sectors . . . . .	179
<b>9</b>	<b>Conclusion and Outlook</b>	<b>183</b>
<b>A</b>	<b>Orthogonal complement</b>	<b>187</b>
<b>B</b>	<b>Extended Fock-Goncharov Parametrization for <math>n = 5</math></b>	<b>189</b>
<b>C</b>	<b>Formulae for Six-point Amplitudes</b>	<b>191</b>
<b>D</b>	<b>Geometry of the Differential Form <math>\nu_{6,2}</math></b>	<b>193</b>
<b>E</b>	<b>Positivity conditions on <math>\mathcal{V}_{5,2}</math> from <math>\mathcal{W}_{5,2}^{(\sigma)}</math></b>	<b>195</b>
<b>F</b>	<b>Poset Intervals for MHV Four-point Amplitudes</b>	<b>197</b>



# Zusammenfassung

Diese Dissertation befasst sich mit einigen der jüngeren theoretischen Entwicklungen auf dem Gebiet der Streuamplituden. In den letzten Jahren wurde immer mehr der traditionelle Ansatz der Extraktion von Streuamplituden aus Feynman-Diagrammen zugunsten von Techniken, die als On-Shell-Methoden bekannt sind, aufgegeben. Diese Methoden offenbaren eine interessante Beziehung zwischen Streuamplituden und einer Geometrie, die als positive Grassmannsche Geometrie bekannt ist und zu einer radikalen Neuformulierung von Streuamplituden durch so genannte positiven Geometrien geführt hat. Positive Geometrien sind Geometrien mit Rändern aller Kodimensionen und gewissen zugehörigen *kanonischen Formen*, aus denen Streuamplitude extrahiert werden können. Der zentrale Akteur dieser Dissertation ist das *Impulsamplituhedron*, welches durch die Positive Geometrie gegeben ist und die on-shell Amplituden auf Baumniveau in der maximal supersymmetrischen Yang-Mills-Theorie kodiert, die im Raum der Spinor-Helizitätsvariablen definiert ist. Die *canonical* Form das Impulsamplituhedron verfügt über eine besondere Singularitätsstruktur, die die physikalischen Singularitäten der Streuamplituden in allen Helizitätssektoren auf Baumniveau kodiert, aus denen die Streuamplituden extrahiert werden können. Dies ermöglicht es, Streuamplituden in maximal supersymmetrischen Yang-Mills Theorie zu bestimmen ohne Bezug auf Felder, Lagrangedichten, Raumzeit oder Feynman-Diagramme zu nehmen. In neueren Arbeiten über das Impulsamplituhedron konnten wir sehen, das seine kanonische Form mit der kanonischen Form – die mit einer Geometrie assoziiert ist, welche die Streuamplituden für bi-adjungierte Skalare – dem kinematischen Associahedron kodiert, in Verbindung gebracht werden kann.

Die Definition des Impusamplituhedron auf dem Raum der Spinor-Helizitäts-Variablen ermöglicht einen direkten Vergleich von Geometrien, mit unterschiedlich Farb-geordneten Streuamplituden im selben Raum verbunden sind. Die wird genutzt, um die Kleiss-Kuijf-Relationen – eine Reihe von Beziehungen zwischen Streuamplituden verschiedener Farbordnungen, wiederherzustellen, die sich aus der Farbzerlegung von Streuamplituden ergeben. Die Kleiss-Kuijf-Relationen manifestieren sich als orientierte Summen von Impulsamplituhedronen verschiedener Farbordnungen ohne Vertices in ihren Rändern. Wir leiten einen homologischen Algorithmus ab, der auf diesem Prinzip basiert, um Kleiss-Kuijf-Beziehungen für Impulsamplituhedronen zu finden.



# Abstract

This dissertation focus on some of the modern theoretical developments in the field of scattering amplitudes. Recent years have seen a departure from the traditional approach of extracting scattering amplitudes in terms of Feynman diagrams in favor of techniques known as on-shell methods. These methods reveal a striking relationship between scattering amplitudes and a geometry known as the positive Grassmannian, leading to a radical reformulation of scattering amplitudes in terms of so-called positive geometries. Positive geometries are geometries with boundaries of all codimensions and have a certain associated *canonical form*. In some special cases, physical observables can be extracted from the canonical forms of positive geometries.

The central player in this dissertation is the *momentum amplituhedron* which is the positive geometry encoding on-shell tree-level amplitudes in maximally supersymmetric Yang-Mills theory defined on the space of spinor helicity variables. The momentum amplituhedron is equipped with a canonical form with a particular singularity structure, encoding the physical singularities of scattering amplitudes in all helicity sectors at tree-level, from which scattering amplitudes can be extracted. This allows us to determine scattering amplitudes in maximally supersymmetric Yang-Mills without reference to fields, Lagrangians, space-time, or Feynman diagrams. We will in this dissertation report on the most recent results for the momentum amplituhedron obtained in collaboration with other authors. In particular, we will see that its canonical form can be related to the canonical form associated with a geometry encoding scattering amplitudes for bi-adjoint scalars – the kinematic associahedron. Furthermore, since we can define the momentum amplituhedron on the space of spinor helicity variables, it allows for a direct comparison of geometries associated with differently color-ordered scattering amplitudes in the same space. This ability to compare momentum amplituhedra of different color orderings will be employed to rederive the Kleiss-Kuijf relations, a set of relations between scattering amplitudes of different color orderings stemming from the color decomposition of scattering amplitudes. The Kleiss-Kuijf relations will appear as oriented sums of momentum amplituhedra of different color orderings with no vertices in their boundary stratifications. We will use this fact to derive a homological algorithm based on this principle to find Kleiss-Kuijf relations for

momentum amplituhedra.

# Acknowledgements

First of all, I wish to express my deep gratitude to my doctoral advisor, Professor Livia Ferro who, with seemingly infinite patience, has not only introduced me to this fascinating field of study but also provided invaluable guidance in every aspect of academic life. Second, I would like to extend my thanks to P.D. Dr. Michael Haack for agreeing to be my second “Gutachter”. I would also like to thank Professor Tomasz Lukowski, whose technical overview and deep knowledge have been a continuous boon to me. Furthermore, I wish to thank Robert Moerman for innumerable discussions and whose close collaboration has helped me improve my own understanding immensely. I would also like to thank Robert for his assistance in running the successful journal club “Geometry and Scattering Amplitudes”, aimed at the scientific community of young researchers interested in the field of scattering amplitudes and geometry during the Corona pandemic of 2020/21. Furthermore, I would like to extend my thanks to Matteo Parisi for great cooperation on the original Momentum Amplituhedron paper. I also wish to extend my thanks to Gabriele Dian for many stimulating discussions both in-person and later online when the pandemic made physical interaction impossible. I wish you all the best in all personal and academic endeavors in the future. Moreover, I would like to also extend my deep gratitude to Professor Jacob Bourjaily for many interesting discussions in Copenhagen and for the development of the Mathematica<sup>TM</sup> package `positroids`, which has been an invaluable tool in the calculations presented in the dissertation.

I believe this work would not have been possible without the great support from my friends and family in Denmark and abroad. I would in particular like to extend my gratitude to everyone who has listened, provided feedback, or otherwise put up with me as I immersed myself in my studies. There are too many to mention individually, but I would like to especially thank Abdurrahman Barzinji, Bjarke Reimann, and Professor N. Emil Bjerrum-Bohr who all those years ago encouraged me to pursue theoretical physics. Further, I wish to extend my deep gratitude to everyone who has made my time in Munich special: here I wish to especially thank Fabrizio Cordonier-Tello, Pantelis Fragkos, Nicolas Gonzáles, Alexander Tabler, and Marc Syvari for our wonderful, if tumultuous, time together at the Arnold-Sommerfeld-Center. Lastly, I would like to thank everyone who has provided helpful suggestions to clear up the language in this dissertation including Abdurrahman Barzinji, Fabrizio Cordonier-Tello, Sionainn Ditto, Nicolas Gonzáles, Christian Schneider, and Marc Syvari. All

mistakes in language or otherwise are of course my own.

# Chapter 1

## Introduction

One of the most outstanding questions in theoretical physics concerns the discrepancy between quantum mechanics and gravity. This discrepancy can be illustrated in the following thought experiment by Arkani-Hamed in his 2013 paper cited in [1]

“Quantum mechanics forces us to divide the world in two pieces—an infinite measuring apparatus and a finite system being observed. However, for any observations made in a finite region of space-time, gravity makes it impossible to make the apparatus [arbitrarily] large, since it also becomes heavier, and collapses the observation region into a black hole” [1].

The problem is usually circumvented by considering the measuring apparatus on some boundary of space-time, as is done when considering boundary correlators in AdS space [2] and the  $S$ -matrix of flat space [3]. In these examples, bulk space-time and quantum mechanics seem to *emerge* from some deeper *new physics*, which is still unknown. In order to shed light on this potential *new physics*, we take a clue from the transition from classical to quantum physics in early the 20th century, the quantum revolution, where the well-understood predictions of classical physics appear as emergent from the deeper principles of quantum mechanics.

Before the quantum revolution, the principle of determinism was crucial for the predictive success of physics. The principle of determinism states that given sufficient information about every particle configuration in the universe, including position and momentum, one would in principle be able to predict how this configuration would evolve in time, given infinite calculation power [4]. Any future configuration is therefore completely determined by its past. This is beautifully illustrated by P.S. Laplace in his 1814 treatise “A Philosophical Essay on Probabilities”:

“We ought then to regard the present state of the universe as the effect of its anterior state and as the cause of the one which is to follow. Given for one instant an intelligence which could comprehend all the forces by which nature is animated and the respective situation of the beings who compose it – an intelligence sufficiently vast to submit these data to analysis [...] for it, nothing would be uncertain and the future, as the past, would be present to its eyes.” [5]

This aforementioned “intelligence” has later been dubbed Laplace’s Demon and the forces referred to are that of (classical) mechanics which Laplace played an integral part in developing (see e.g. *Traité de Mécanique Céleste*, his work from 1829-1839 [6]). Of course, Laplace stresses later in the book, that indeed no human will ever have access to this intelligence and we have to content ourselves with statistics, thus the title of the book from which the former quote is taken “A Philosophical Essay on Probabilities” [5].

The concept of time plays a crucial role in the above quote. Here, we have an understanding of the universe in one configuration at an initial time  $t_i$ , and then at a final time  $t_f$ , in another configuration which is strictly dependent on the first and is encapsulated by the dynamics of the laws of Nature acting in the time interval from  $t_i$  to  $t_f$ . Time and space are completely separated aspects following the traditions of classical mechanics. The notion of time and space as separated concepts has long been discarded, along with the belief in a perfectly deterministic, “clock-work” universe, as time and space have become linked in Einstein’s seminal work from the first decade of the 20th century [7, 8]. This work paved the departure from the classical understanding of gravity and muddled the concept of simultaneity [9]. Around the same time, in the early decades of the 20th century, the groundwork which would develop into quantum mechanics (QM) was being laid by Einstein [10], Planck [11] and Bohr [12], among others: the physics of the very small was concluded to be probabilistic in nature [13]! The worldview of relativity, which pertains to<sup>1</sup> very fast-moving objects [7] (Special Relativity, SR) and massive objects [8, 9] (General Relativity, GR), and the worldview of QM [13], necessary for a proper description of very small objects, are in tension<sup>2</sup>. There exists a reconciliation between QM and SR, known as Quantum Field Theory (QFT) which as the name suggests has quantized fields as its degrees of freedom [3, 14, 15]. Still, today, a completely established theory of Nature unifying GR and QM is not available.

The concept of determinism has been discarded both due to the problem with

<sup>1</sup>In the sense that it is meaningfully distinct from the Newtonian or classical worldview.

<sup>2</sup>For instance, the passage of time is unambiguously uniform in QM, while in GR it is associated with an index of a four-vector which is dependent on the curvature of space-time and thus on the presence of massive objects.

irreversibility of the arrow of time<sup>3</sup> from the second law of thermodynamics and the inherently probabilistic QM. However, despite its apparent failures in extreme (very heavy, small, or fast moving) physical settings, the classical picture of the universe, involving point particles, bulk continuous matter, and forces acting thereupon is still highly relevant in many fields of study [18]: in many regimes, physical observables are well described by classical predictions. In certain well behaved sectors, e.g. objects with mass of order  $\mathcal{O}(\text{kg})$  and sizes  $\mathcal{O}(\text{m})$  moving at relative speeds  $\mathcal{O}(\frac{\text{m}}{\text{s}})$ , classical physics *emerges* in the limit of relativity and/or QM.

The development of QFT has been derived from three important underpinnings [3, 14, 15]:

I **Causality:** The principle of causality states that an event in space-time has an associated *light-cone*, and only events inside this light-cone can be influenced by the original event and therefore implies that cause and effect are time-like separated.

II **Locality:** The principle of locality states that an action on a point in space-time can only influence another point if there is a particle or wave traveling the distance between the points, mediating the action.

III **Unitarity:** The principle of unitarity states that the space of wave-functions constitutes a complete set, or rather, the sum of all possible probabilities of occurrences in any quantum mechanical event is equal to 1.

These notions should be interpreted as fundamental features of space-time, the synthesis of spatial and temporal dimensions into one fabric which is dynamic and plastic. While determinism is no longer a fundamental aspect of microscopic physics, we accept that the world very much behaves as though it is deterministic on macroscopic scales. *We understand deterministic systems to be emergent from the deeper laws of non-deterministic quantum mechanics.* Inspired by this, an immediate, albeit ambitious question would be if any notions exist giving rise to causality, locality, and unitarity. To find potential notions or principles from scratch is a daunting task, but we can guide ourselves with the following question in mind: to what mathematical problems are the results of QFT the answer? Or equivalently, can we reformulate the predictions of QFT as answers to mathematical questions without any reference to space-time at all? This question is motivated by history: different formulations of classical physics are not created equal from the point of view

---

<sup>3</sup>The irreversibility of the arrow of time is the statement that entropy in a closed system must increase, breaking the symmetry between past and present. This implies that there is not enough information in the past to uniquely determine the future even in classical settings. Here one may raise the counterargument that entropy is itself a statistical notion stemming from the lack of information about a given system [16, 17].

of QM: when approaching a classical limit of QM, the resulting formulation is much closer to the principle of least action [18] than Newtonian Laws [19], since in the former determinism is a derived notion while in the latter determinism is manifest in the formulation [1]. As we shall see throughout this dissertation, one reformulation of fundamental physics is geometric in nature and the underlying notion is that of *positivity*, giving rise to QFT observables without any reference to space-time at all.

The observables we are interested in are derived from the so-called *scattering amplitudes*, a group of functions encoding the quantum mechanical overlap of an initial and final multi-particle state. The initial and final states are completely separated from each other, with the initial particle state being prepared at the far past, and the final state in the far future, equivalent to being prepared on the “boundary” of flat space. We can think of scattering amplitudes as encoding the (square root of the) probability of interaction between the states, usually organized into the so-called *S*-matrix first introduced by Wheeler in [35]. The *S*-matrix is assumed to be unitary and we assume it can be expressed as a power series in a small parameter associated with the couplings in a given theory.

The standard method of extracting scattering amplitudes in terms of Feynman diagrams [20] holds the three concepts of causality, locality, and unitarity manifest: at every step in a given QFT calculation these principles hold. The Standard Model (SM) of particle physics is an example of a QFT and has proven extremely successful in describing and interpreting the results of some of the most advanced physics experiments such as the Large Hadron Collider (LHC) and is considered one of the most successful theories in physics [21]. While SM has had immense predictive power, the actual calculations involving Feynman diagrams are often quite cumbersome to the degree that some calculations are intractable, even on powerful computers. This is due to the inherent gauge redundancies introduced in the theory and are ubiquitous in the intermediate steps of a given calculation, but absent in the final results comparable to experimental data from, for instance, the LHC. These complications with performing computations lead us back to the challenge of finding mathematical problems to which the predictions of SM are answers. The hope here is that these problems are *easier* than their QFT counterparts and thus could provide the practical benefit of pushing the theoretical limit on the precision of the QFT results, which can be compared to data in addition to hinting at a deeper framework, akin to what QM is to classical mechanics. It should be noted, that there has been incredible progress in our ability to extract scattering amplitudes, including the work of Parke and Taylor [22], Berends and Giele [23], Bern, Dixon and Kosover [24–27] among many others [28–34]. Some of these techniques shall be reviewed in this dissertation.

The standard approach of obtaining scattering amplitudes is ultimately derived from the path integral over quantized fields: the dynamics of a given theory is encoded in the *Lagrangian density* from which the path integral is defined. The

---

variational principle is employed to obtain time-ordered correlation functions for different numbers of external fields and subsequently related to scattering amplitudes through the Lehmann-Symanzik-Zimmerman reduction formula [36]. For details, we refer to the standard textbooks of Weinberg [3], Peskin and Schröder [14] and Srednicki [15]. In lieu of keeping track of the variational techniques and the several integrations over internal degrees of freedom, one usually recasts the problem in terms of Feynman diagrams. In this framework, scattering amplitudes are expressed as a sum over graphs. The perturbative nature of scattering amplitudes is made clear through the identification of loops, closed circuits in each graph. These loops are associated with unfixed internal momenta, which require integration over their full phase-space and in many cases yield infinities in the low-energy (IR) and/or high-energy (UV) sectors. In the following, we will not make direct contact with this framework and rather introduce the notion of scattering amplitudes through the approach laid out in [34]. This framework employs powerful techniques based on recursion, analyticity, and the highly restrictive Lorentz group to fix scattering amplitudes.

In this dissertation, we will focus on scattering amplitudes in *maximal supersymmetric* Yang-Mills theory (msYM). We will not speculate on whether supersymmetry is a *real actual* symmetry of space-time, rather we will treat the theory as a toy model in the tradition of the hydrogen atom and the harmonic oscillator. The msYM is highly symmetric making it a useful laboratory to study the universal dynamics of the scattering of particles. Due to its highly restrictive symmetries of superconformal and dual superconformal symmetry in the planar sector, (planar) msYM has been described as the simplest example of a QFT [37]. This theory acts as a simplified setting in which we can explore general important features of scattering amplitudes. Following the question regarding reformulations of QFT raised earlier in this introduction, in this dissertation, we shall see how theoretical results from msYM can emerge from geometric considerations. In particular, when imposing a notion of *positivity* on certain geometric spaces, the consequences of unitarity and locality appear hand-in-hand, without having introduced a notion of space-time! This idea was first put forth by Arkani-Hamed and Trnka in their seminal paper from 2013 on the *amplituhedron* [1], a geometry associated with planar scattering amplitudes in msYM defined in the kinematic space of momentum twistor variables. Here, the physical manifestations of locality and unitarity, the singularity structure of the scattering amplitudes, arise as boundaries of the amplituhedron once the notion of positivity is invoked.

An important step in making contact between scattering amplitudes and geometry is to rewrite scattering amplitudes as differential forms on the space of kinematic variables used to express the amplitudes themselves. The differential forms associated with scattering amplitudes are conjectured to be *canonical* forms of certain *positive geometries* [38], a class of real, oriented geometries with boundaries

of all co-dimensions which are themselves positive geometries. Positive geometries admit a unique differential form on the spaces in which they are defined. The differential form is dubbed the canonical form and has logarithmic singularities on-and-only-on the co-dimension-1 boundaries of the positive geometry. The residues on the logarithmic singularities are simply the canonical forms associated with boundary components of the positive geometry [38].

The *momentum amplituhedron* is a positive geometry first described in [39], encoding scattering amplitudes in msYM in terms of spinor helicity variables and is the central player in this dissertation. We define the momentum amplituhedron on bosonized spinor helicity variables subject to certain positivity conditions ensuring its boundaries correspond to the physical singularities of the msYM. We will discuss how scattering amplitudes can be extracted from the volume form of the momentum amplituhedron. In this dissertation, we shall also discuss recent results related to the momentum amplituhedron, including a map between the canonical forms of the momentum amplituhedron and the kinematic associahedron, another positive geometry associated with the scattering of bi-colored scalars with  $\phi^3$  interactions. The canonical forms of the momentum amplituhedron and the kinematic associahedron is found to be equal when stripping off a universal differential form, associated with the little group invariance of the Lorentz group [40], from the canonical form of the momentum amplituhedron. We will also discuss how certain amplitude relations appear as geometric statements when cast in the framework of the momentum amplituhedron. This was explored in the paper [41], where we found the relations between color-ordered amplitudes due to Kleiss-Kuijf [42], emerging as beautiful geometric statements about unions of different momentum amplituhedra. This is a surprising result, given the Kleiss-Kuijf relations stem from group-theoretic considerations not encoded in the definition of the momentum amplituhedron. The existence of the momentum amplituhedron provides an important clue towards a geometric description of more physically realistic theories, such as SM, without reference to space-time.

## Plan of the Dissertation

The dissertation is structured as follows:

- In Chapter 2 we provide an introduction to the field of scattering amplitudes, focusing on concepts and techniques that will be used later. We will introduce the spinor helicity formalism and the modern approach of extracting scattering amplitudes based on recursion techniques. Here we will encounter the main theories which will be considered throughout this dissertation: the Yang-Mills (YM) theory, the bi-adjoint  $\phi^3$  theory, and msYM. We will also provide a discussion of the highly restrictive symmetries of the latter. All three theories admit a color decomposition, disentangling the color degrees of freedom from

---

the kinematic degrees of freedom, leading to interesting relations between partial amplitudes carrying the kinematic degrees of freedom, which will also be discussed in this chapter. While the original work presented in this dissertation is primarily concerned with tree-level scattering amplitudes, we will end the chapter by making contact with loop level scattering amplitudes, albeit briefly.

- In Chapter 3 we introduce the Grassmannian: a generalization of the projective space naturally suited for studying scattering amplitudes in msYM. We will begin the chapter with a discussion of projective spaces and subsequently generalize to the Grassmannian, the space of  $k$ -vectors in  $n$ -dimensions. We will discuss various methods of representing an element in the Grassmannian by way of decorated permutations and plabic graphs. Then, we proceed to discuss the positive part of the Grassmannian, which is interpreted as the generalization of the projective polytope. Here, lower-dimensional configurations of the positive Grassmannian represent boundaries of the top-dimensional element. The chapter ends with a discussion of how scattering amplitudes in their BCFW representation can be extracted from the positive Grassmannian.
- In Chapter 4 we discuss a class of geometries, known as *positive geometries*, which will play a crucial role in the definition of the momentum amplituhedron, introduced later in the dissertation. Here we discuss standard features of positive geometries and provide primitive examples of them. Techniques such as triangulations, pull-backs, and push-forwards will be discussed and illustrated. We will also review how the *oriented sum* of positive geometries can give rise to geometries, which are no longer positive geometries. In this chapter, we shall also introduce the prime example of positive geometries, the amplituhedron and its generalization to the loop amplituhedron, and discuss how the notions of locality and unitarity appear as consequences of positivity conditions imposed on the amplituhedron geometry.
- In Chapter 5 we introduce the kinematic associahedron. The kinematic associahedron is the positive geometry associated with scattering amplitudes in bi-adjoint  $\phi^3$  theory and its canonical form is the so-called *planar scattering form*. Here we introduce the planar scattering form related to scattering amplitudes in bi-adjoint  $\phi^3$  theory and provide a definition of the kinematic associahedron due to Arkani-Hamed, Bai, He, and Yan [43]. We provide a few examples of kinematic associahedra and end the chapter by discussing their factorization and boundary properties.

- In Chapter 6 we introduce the *momentum amplituhedron* first defined in [39]. Here we review the main new object of research found during this Ph.D. program. We discuss how to define scattering amplitudes as differential forms on spinor helicity space and how to organize the external data into bosonized spinor helicity variables. Then, after having discussed certain positivity constraints on external data, we provide the original definition of the momentum amplituhedron. We analyze the boundary structure of the momentum amplituhedron and its factorization properties as well as discuss how to obtain its canonical form. We then proceed to describe how to extract scattering amplitudes from the canonical form of the momentum amplituhedron and we close the chapter by providing examples of the momentum amplituhedron in different helicity sectors.
- In Chapter 7 we elucidate on an interesting relationship between the canonical forms of the momentum amplituhedron and the kinematic associahedron found in [40]. Here we provide a detailed discussion of the kinematic spaces on which the geometries are defined and the maps between them. Performing morphisms using these maps, we relate the canonical forms of the kinematic associahedron and the momentum amplituhedron. This feature is encapsulating the fact that certain elements of the boundary structure of the two geometries are similar, as both the momentum amplituhedron and the kinematic associahedron have boundaries where planar Mandelstam variables vanish.
- In Chapter 8 we return to the amplitude relations discussed back in Chapter 2: the Kleiss-Kuijf relations. We see how they can be naturally cast in the framework of momentum amplituhedron geometry as oriented sums of momentum amplituhedra of different color ordering, combining together to no longer have any 0-dimensional boundaries in their boundary stratification. We review the result of our paper [41] and show two different approaches to find amplitude relations: one that is applicable for the MHV sector of momentum amplituhedra and the kinematic associahedron and one that is suitable for the momentum amplituhedron beyond the MHV sector.
- The dissertation concludes with Chapter 9, which provides a summary and outlook for future research inspired by or continuing along the lines of the work presented here.

# Chapter 2

## Scattering Amplitudes

Scattering amplitudes are usually derived from quantum field theory as path integrals over field configurations controlled by a certain action [3, 14]. We will instead consider scattering amplitudes as naturally emergent objects stemming from the Wignerian definition of particles with natural transformation properties [34, 44]. In this chapter, we start by reviewing scattering amplitudes from an on-shell perspective and introduce relevant kinematic spaces on which they are defined. We then discuss modern methods of calculation, including the color-kinematic decomposition [45–47]. We then provide a discussion of the three specific theories of interest in this dissertation: Yang-Mills theory, bi-adjoint scalar theory with cubic interactions [31, 33] and  $\mathcal{N} = 4$  super Yang-Mills theory. The chapter concludes with a brief discussion on loop amplitudes.

### 2.1 Scattering Amplitudes

Scattering amplitudes are, as laid out in the introduction, the mathematical structures which encode the quantum mechanical information about a scattering process of interacting particles [45]. We can understand the scattering amplitude  $\mathcal{A}_n$  of  $n$  interacting particles labeled by  $i = \{1, 2, \dots, n\}$ , as a complex scalar function of *external data*, which takes the form of a list  $\{E_i, p_i; \mathbf{a}_i\}$  encoding energy,  $E_i$ , relativistic momentum,  $p_i$ , and  $\mathbf{a}_i$  denotes the type of each particle participating in the scattering process

$$\mathcal{A}_n : \quad \{E_i, p_i, \mathbf{a}_i\} \rightarrow \mathcal{A}_n(\{E_i, p_i, \mathbf{a}_i\}) \in \mathbb{C}^1. \quad (2.1)$$

Generically, the external data here are subject to constraints. First momentum conservation, related to overall translation invariance of flat space-time<sup>1</sup>, imposes the

---

<sup>1</sup>We take scattering amplitudes as living in the four dimensional Minkowski space in the mostly negative signature, unless otherwise stated.

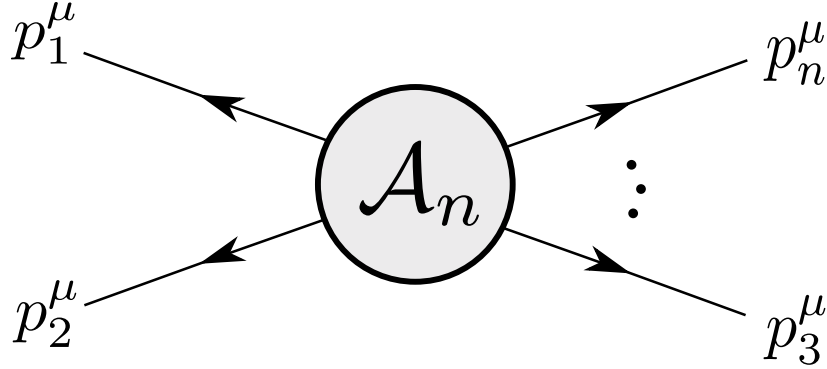


Figure 2.1: A graphic representation of an arbitrary scattering amplitude with  $n$  outgoing momenta labeled  $p_1^\mu, p_2^\mu, \dots, p_n^\mu$ .

following linear condition on the relativistic four-momenta

$$\sum_i p_i^\mu = 0, \quad (2.2)$$

where  $\mu = 0, \dots, D-1$ . A further constraint is the so-called on shell condition, which can be understood as the generalization of Einstein's famous dispersion relation

$$(p_i^2 - m_i^2) = 0, \quad (2.3)$$

where  $p_i^2 = p_{i\mu} p_i^\mu = \eta_{\mu\nu} p_i^\mu p_i^\nu$  with  $\eta_{\mu\nu}$  being the Minkowski metric in the mostly minus convention and  $m_i$  is the mass of particle  $i$ . Of course, any actual physical observable will be a real number, however since scattering amplitudes as defined in (2.1) are complex, any physical observable are proportional to the absolute square of the scattering amplitude, e.g. the differential of the total cross section of a process,  $\sigma$ , with respect to a solid angle element  $d\Omega$  is

$$\frac{d\sigma}{d\Omega} \propto |\langle \mathcal{A}_n \rangle|^2, \quad (2.4)$$

proportional to the absolute value squared of the scattering amplitudes averaged over indistinguishable states. In this dissertation, the scattering amplitudes themselves are the primary focus.

Throughout this dissertation we will assume that the scattering amplitudes admit a perturbation expansion, i.e. that there exists a small parameter  $g$ , such that the amplitudes can be expressed as a power expansion

$$\mathcal{A}_n = \sum_{i=0}^{\infty} g^{2(i+1)} \mathcal{A}_n^{(i)} = g^2 \mathcal{A}_n^{(0)} + g^4 \mathcal{A}_n^{(1)} + \mathcal{O}(g^6), \quad (2.5)$$

---

<sup>2</sup>Greek labels are in general over the  $D$ -dimensional spacetime indices.

where the first term in (2.5),  $\mathcal{A}_n^{(0)}$ , is labeled *tree* since using the Feynman diagram expansion, the diagrams contain no loops and have simple structure resembling tree graphs. The higher order terms in this expansion are called loop amplitudes and involve integrals over internal degrees of freedom [15]. In this dissertation, the primary focus will be on the leading order contribution, however we briefly touch upon loop corrections in the end of this chapter in section 2.9.

## The $S$ -Matrix

The scattering process can be interpreted from the point of view of quantum states, where we consider the evolution in the bulk of space-time from some multiparticle states defined on the boundary:  $|i\rangle$  and  $|f\rangle$ , which are interpreted as the *initial* and *final* states, respectively. The scattering probability is governed by the  $S$ -matrix, mapping initial to final states

$$\sigma \sim |\langle f|S|i\rangle|^2. \quad (2.6)$$

We expect such a matrix to be constructed from two parts: one governing the case where no transition between states occurs and one governing transitions between initial and final states.

$$S = 1 + iT. \quad (2.7)$$

In this framework, the scattering amplitudes are simply identified as

$$i\delta(p_1 + p_2 + \dots + p_n)\mathcal{A}_{i\rightarrow f} = \langle f|T|i\rangle, \quad (2.8)$$

with the statement of momentum conservation explicitly factorized as a  $\delta$ -function. There are important lessons about the scattering amplitude to be learned from the  $S$ -matrix. In particular, unitarity is simply encoded in this formulation, as it is just the statement that

$$S^\dagger S = 1. \quad (2.9)$$

Expanding the  $S$ -matrix in terms of the transition matrix (2.7), we obtain

$$-i(T - T^\dagger) = T^\dagger T, \quad (2.10)$$

This statement is known as the optical theorem [3]. We can find an equivalent statement on the level of scattering amplitudes by sandwiching (2.10) between the two state brackets as follows

$$i\langle f|(T - T^\dagger)|i\rangle = i(\mathcal{A}_{i\rightarrow f} - \mathcal{A}_{f\rightarrow i}^*) = 2\Im\mathcal{A}_{i\rightarrow f} = \langle f|T^\dagger T|i\rangle, \quad (2.11)$$

where  $\Im\mathcal{A}_{i\rightarrow f}$  is the imaginary part of the scattering amplitude. Inserting a complete set of states  $\sum_k |k\rangle\langle k| = 1$  on the right hand side, we get

$$\langle f|T^\dagger T|i\rangle = \sum_k \langle f|T^\dagger|k\rangle\langle k|T|i\rangle = \sum_{h_k, \mathbf{a}_k} \int \Pi_k \mathcal{A}_{i\rightarrow k} \mathcal{A}_{k\rightarrow f}^*, \quad (2.12)$$

where the sum is over all discrete quantum number of the intermediate state,  $\int d\Pi_k$  amounts to integrating over the continuous quantum numbers, e.g. momentum, of the intermediate state. Collecting both sides, we obtain the optical theorem for scattering amplitudes

$$2\Im\mathcal{A}_{i\rightarrow f} = \sum_{h_k, \mathbf{a}_k} \int \Pi_k \mathcal{A}_{i\rightarrow k} \mathcal{A}_{k\rightarrow f}^*. \quad (2.13)$$

Treating  $\mathcal{A}^*$  as a scattering amplitude in its own right, we can expand the scattering amplitude loop-by-loop order as in (2.5) and matching powers of the coupling constant

$$\Im\mathcal{A}_n^{(1)} = \sum_{h_k, \mathbf{a}_k} \int d\Pi_k \mathcal{A}_n^{(0)}(k) \times \mathcal{A}_n^{(0)}(k), \quad (2.14)$$

where the integration is over all internal on-shell momentum of the internal state  $k$ , and we sum the possible helicity states,  $h_k$  and particle types  $\mathbf{a}_k$ . This is a very important result as it relates the complex structure of the scattering amplitude at loop-level with a sum over factorized tree-level amplitudes [14]. We shall return to this point at the end of this chapter in section 2.9.

## 2.2 Poincaré Group and Little Group Scaling

Before embarking on a further discussion of scattering amplitudes in specific theories, we review how to construct particles, the objects participating in the scattering process. Conventionally, particle information is encoded in quantum fields, which allow for the treatment of quantum mechanical objects using techniques from classical field theory ensuring that the given theory respects special relativity. The conventional way of extracting scattering amplitudes using Feynman diagrams has the consequence of keeping the notions of causality, locality, and unitarity strictly manifest at the cost of introducing gauge redundancies complicating intermediate steps, but never manifesting in the final result. In this work, we shall treat particles as irreducible representations of the Poincaré group, governing four-dimensional translations and Lorentz transformations [34].

In (2.1), we label the external data using four-momentum labels  $p_i^\mu$ . This is done explicitly by starting from some reference momentum,  $k_i^\mu$ , and relate it to the specific

momenta we are interested in by way of a Lorentz transformation  $p^\mu = L_\nu^\mu(p_i; k)k^\nu$ . We note, that  $L_\nu^\mu(p_i; k)$  is not unique and there are particular Lorentz transformations that leave  $p_i^\mu$  invariant, for instance rotations around the axis in the direction of  $p_i^\mu$ . This is the *little group* of Lorentz transformations and shall play an important role throughout this dissertation, especially in chapter 7. Assuming there exists a unitary representation of the Lorentz group,  $U(\Lambda)$ :  $U(\Lambda_1\Lambda_2) = U(\Lambda_1)U(\Lambda_2)$ , and choosing a specific Lorentz transformation,  $L$ , allows us to define the one-particle states  $|p, \mathbf{a}\rangle$  as

$$|p, \mathbf{a}\rangle = U(L(p; k)) |k, \mathbf{a}\rangle. \quad (2.15)$$

Applying an arbitrary Lorentz transformation to  $|p, \mathbf{a}\rangle$  we obtain

$$\begin{aligned} U(\Lambda) |p, \mathbf{a}\rangle &= U(\Lambda)U(L(p; k)) |k, \mathbf{a}\rangle = U(\Lambda L(p; k)) |k, \mathbf{a}\rangle, \\ &= U(L(\Lambda p; k)L^{-1}(\Lambda p; k))U(\Lambda L(p; k)) |k, \mathbf{a}\rangle, \\ &= U(L(\Lambda p; k))U(L^{-1}(\Lambda p; k)\Lambda L(p; k)) |k, \mathbf{a}\rangle, \\ &= U(L(\Lambda p; k))U(W(\Lambda, p; k)) |k, \mathbf{a}\rangle, \end{aligned} \quad (2.16)$$

where  $W(\lambda, p; k)$  is a subgroup of the Lorentz group leaving the momentum vector invariant, thus the little group. A particle can then be labeled by its momentum and transforms under a certain representation of the little group

$$U(W(\Lambda, p, k)) |k, \mathbf{a}\rangle = D_{\mathbf{a}, \mathbf{b}}(W(\Lambda, p; k)) |k, \mathbf{b}\rangle. \quad (2.17)$$

Scattering amplitudes, as they are assumed to obey Poincaré invariance, are then assumed to be Lorentz scalars and obey conservation of external momenta, meaning that they must transform nicely according to

$$\mathcal{A}_n^\Lambda(\{p_i, \mathbf{a}_i\}) = \prod_{i=1}^n (D_{\mathbf{a}_i, \mathbf{b}_i}(W)) \mathcal{A}_n(\{\Lambda p_i, \mathbf{b}_i\}), \quad (2.18)$$

acting on each participating particle individually [34].

We can now discuss the label  $\mathbf{a}$ , which we use to distinguish between different particles states with the same momenta and energy. In four dimensions, we can label massless particles by their helicity,  $h = \pm s$ , where  $s$  is the spin of the particle. In this dissertation, we will make contact with scalars of spin-0, fermions of spin-1/2 and vector bosons (gluons) of spin-1. We label scattering amplitudes by their momentum and helicity as follows

$$\mathcal{A}_n(\{p_1^{h_1}, \mathbf{A}_1\}, \dots, \{p_n^{h_n}, \mathbf{A}_n\}), \quad (2.19)$$

where  $\mathbf{A}_i$  encodes the remaining distinguishing labels of particle states such as color-charge.

The four-momentum vectors  $p_i^\mu$ , might not be the best choice of variables however, and in general we wish to linearize the on-shell conditions:  $p_i^2 = m^2$ . We do this by contracting the four-momentum vectors with the  $SU(2)$  Pauli matrices  $\sigma_\mu^{a\dot{a}} = \{\mathbb{1}, \sigma_i\}$  with  $i = 1, 2, 3$ , such that we obtain the matrix

$$p_i^{a\dot{a}} = \sigma_\mu^{a\dot{a}} p_i^\mu = \begin{pmatrix} p^0 - p^3 & p^1 - ip^2 \\ p^1 + ip^2 & p^0 + p^3 \end{pmatrix}, \quad (2.20)$$

associated with each particle. This matrix is not full rank and its determinant for generic momenta just imposes the on-shell condition

$$\det p_i^{a\dot{a}} = p_i^2 = -m^2. \quad (2.21)$$

This allows for the definition of two spinor helicity variables given by

$$p_i^{a\dot{a}} = \begin{cases} \lambda_i^a \tilde{\lambda}_i^{\dot{a}} & m^2 = 0 \\ \lambda_{iI}^a \tilde{\lambda}^{\dot{a}I} & \text{else.} \end{cases} \quad (2.22)$$

In the massless case, the matrix  $p_i^{a\dot{a}}$  is of rank 1 and we can decompose it to a product of two 2-vectors denoted  $\lambda$  and  $\tilde{\lambda}$ . They can be generically thought of as complex. For real momenta,  $p_i^{a\dot{a}}$  is a Hermitian matrix and  $\lambda$  and  $\tilde{\lambda}$  are related by complex conjugation. In the following, we shall keep them independent, which can either be done by taking complex momenta, or keeping momenta real but working in the so-called split-signature,  $\eta_{\mu\nu} = \text{diag}(-1, +1, -1, +1)$ . The spinor helicity variables for the massless case is usually collected into two  $2 \times n$  matrices as follows

$$\lambda_i^a = \begin{pmatrix} \lambda_1^1 & \lambda_2^1 & \dots & \lambda_n^1 \\ \lambda_1^2 & \lambda_2^2 & \dots & \lambda_n^2 \end{pmatrix}, \quad \tilde{\lambda}_i^{\dot{a}} = \begin{pmatrix} \tilde{\lambda}_1^{\dot{1}} & \tilde{\lambda}_2^{\dot{1}} & \dots & \tilde{\lambda}_n^{\dot{1}} \\ \tilde{\lambda}_1^{\dot{2}} & \tilde{\lambda}_2^{\dot{2}} & \dots & \tilde{\lambda}_n^{\dot{2}} \end{pmatrix}. \quad (2.23)$$

Since scattering amplitudes are Lorentz scalars, no free Lorentz indices are floating in (2.1), we are interested in  $SL(2) \times SL(2)$  invariants of these matrices

$$\det \lambda_i \lambda_j = \epsilon_{ab} \lambda_i^a \lambda_j^b := \langle ij \rangle, \quad (2.24)$$

$$\det \tilde{\lambda}_i \tilde{\lambda}_j = \epsilon_{\dot{a}\dot{b}} \tilde{\lambda}_i^{\dot{a}} \tilde{\lambda}_j^{\dot{b}} := [ij]. \quad (2.25)$$

Importantly, the Mandelstam variables can be expressed using massless spinor helicity variables

$$s_{ij} = (p_i + p_j)^2 = 2p_i \cdot p_j = \langle ij \rangle [ij], \quad (2.26)$$

which can be shown using  $\eta^{\mu\nu} = -\frac{1}{2} \text{tr} \sigma^\mu \bar{\sigma}^\nu$ , with  $\bar{\sigma}^\nu = (\mathbb{1}, -\sigma^i)$ . Momentum conservation has to be imposed by hand and is found to be the constraint

$$\begin{aligned} 0 &= p_1 + p_2 + \dots + p_n = 2p_1 \cdot (p_1 + p_2 + \dots + p_n) = \\ &= 2p_1^2 + 2p_1 \cdot p_2 + 2p_1 \cdot p_3 + \dots + p_1 \cdot p_n = \\ &= s_{12} + s_{13} + \dots + s_{1n} \Rightarrow \sum_{i=1}^n \langle qi \rangle [ir] = 0, \end{aligned} \quad (2.27)$$

where in the last line we have contracted the spinor helicity variables by two reference variables  $\lambda_q^a$  and  $\tilde{\lambda}_r^{\dot{a}}$ . Another constraint the variables have to fulfill is Cramer's rule, also known as the Plücker identity, which is a standard statement about vectors in  $\mathbb{R}^d$ , stating that we can expand any  $d$ -vector as a linear combination of  $d$  basis vectors. Choosing  $\lambda_i$  and  $\lambda_j$  as the basis vectors, we can write  $\lambda_k$  as an expansion

$$\lambda_k = \alpha\lambda_i + \beta\lambda_j, \quad (2.28)$$

by contracting with  $\lambda_i$  and  $\lambda_j$  we can find  $\alpha$  and  $\beta$  as follows

$$\langle kj \rangle = \alpha \langle ij \rangle, \quad (2.29)$$

$$\langle ki \rangle = \beta \langle ji \rangle, \quad (2.30)$$

such that we get

$$\langle ij \rangle \lambda_k = \langle kj \rangle \lambda_i - \langle ki \rangle \lambda_j, \quad (2.31)$$

These rules are usually cast as identities on spinor brackets, by contracting with an arbitrary reference spinor,  $\lambda_r$ , as follows

$$\langle kr \rangle \langle ij \rangle - \langle kj \rangle \langle ir \rangle + \langle ki \rangle \langle jr \rangle = 0. \quad (2.32)$$

Of course the construction follows identically for the square brackets, and we have

$$[kr][ij] - [kj][ir] + [ki][jr] = 0. \quad (2.33)$$

We can easily encode the ten generators of the Poincaré group in the language of spinor helicity as follows [45]:

$$p^{a\dot{a}} = - \sum_i \lambda_i^a \tilde{\lambda}_i^{\dot{a}}, \quad m_{ab} = \sum_i \lambda_{i(a} \frac{\partial}{\partial \lambda_i^{b)}, \quad \tilde{m}_{\dot{a}\dot{b}} = \sum_i \tilde{\lambda}_{i(\dot{a}} \frac{\partial}{\partial \tilde{\lambda}_i^{\dot{b})}, \quad (2.34)$$

taking (...) as meaning symmetrization of enclosed indices. Here  $p^{a\dot{a}}$  is the generator of translations and  $m_{ab}$  and  $\tilde{m}_{\dot{a}\dot{b}}$  are the generators for the Lorentz group.

The spinor helicity variables provide an excellent parameterization of scattering amplitudes, in particular in gauge theories. In the following sections, we will explore the Parke-Taylor amplitude [22] of  $n$  color-ordered gluons with all but two helicities positive. For now, we will just quote it to visualize the compactness of the parameterization

$$A_n(1^+, 2^+, \dots, i^-, \dots, j^-, \dots, n^+) = \frac{\langle ij \rangle^4}{\langle 12 \rangle \langle 23 \rangle \dots \langle n-1n \rangle \langle n1 \rangle}, \quad (2.35)$$

which of course, has the correct scaling under little group transformations. We will review the explicit construction of  $A_n$  in section 2.4. In the following, we shall derive this very simple formula by way of recursion of simple three-particle scattering amplitudes.

## 2.3 On-Shell Methods

### Three Particle Kinematics

The choice of working in spinor helicity variables makes on-shell conditions (2.21) manifest and in the massless case any three-point scattering amplitude, denoted three-point functions in the following, can only be a function of either  $\lambda$  or  $\tilde{\lambda}$  [48]. This can be seen by expressing the Mandelstam variables using momentum conservation

$$\langle 12 \rangle [12] = 2p_1 \cdot p_2 = (p_1 + p_2)^2 = (-p_3)^2 = 0 \quad (2.36)$$

This requires either  $\langle 12 \rangle$  or  $[12]$  (or both) must vanish. In the case where  $\langle 12 \rangle$  is finite,

$$\langle 12 \rangle [23] = \langle 1|(p_2)|3\rangle = -\langle 1|(p_1 + p_3)|3\rangle = 0, \quad (2.37)$$

tells us that  $[23] = 0$ . By similar arguments, we can claim  $[13] = 0$  and therefore

$$\tilde{\lambda}_1 \propto \tilde{\lambda}_2 \propto \tilde{\lambda}_3. \quad (2.38)$$

Another valid choice in (2.36) would be to take  $[12]$  finite. In that case, in complete analogy we obtain

$$\lambda_1 \propto \lambda_2 \propto \lambda_3, \quad (2.39)$$

and thus all angle brackets vanish, telling us either that the three-point function is either a function of angle **or** square brackets. Furthermore, if using real momenta in mostly-minus signature, we have  $\lambda_1^* = \tilde{\lambda}_1$  and all real three massless particle scattering amplitudes vanish! We keep momenta complex or work in the split signature [49], and construct an ansatz for the structure of three-point function

$$\mathcal{A}_3(p_1, p_2, p_3) = \begin{cases} \langle 12 \rangle^{a_{12}} \langle 23 \rangle^{a_{23}} \langle 13 \rangle^{a_{13}} & \text{or} \\ [12]^{\tilde{a}_{12}} [23]^{\tilde{a}_{23}} [13]^{\tilde{a}_{13}}, \end{cases} \quad (2.40)$$

up to a coupling constant.

The little group of Lorentz transformations, discussed above in section 2.2, acts as a complex  $U(1)$  transformation on the spinor helicity variables.

$$\lambda_i \sim t_i \lambda_i, \quad \tilde{\lambda}_i \sim t_i^{-1} \tilde{\lambda}_i. \quad (2.41)$$

A massless scattering amplitude is fixed by Lorentz invariance to transform under the little group transformation as [34],

$$\mathcal{A}_n(t_i \lambda_i, t_i^{-1} \tilde{\lambda}_i) = t_i^{-2h_i} \mathcal{A}_n(\lambda_i, \tilde{\lambda}_i), \quad (2.42)$$

where  $h_i$  is the helicity of the particle labeled,  $i$ . This restriction completely fixes the coefficients of (2.40). By scaling (2.40) with respect to each particle

$$t_1^{a_{12}+a_{13}} t_2^{a_{12}+a_{23}} t_3^{a_{23}+a_{13}} \langle 12 \rangle^{a_{12}} \langle 23 \rangle^{a_{23}} \langle 13 \rangle^{a_{13}} = t_1^{-2h_1} t_2^{-2h_2} t_3^{-2h_3} \langle 12 \rangle^{a_{12}} \langle 23 \rangle^{a_{23}} \langle 13 \rangle^{a_{13}}. \quad (2.43)$$

We need to solve the equations

$$a_{12} + a_{13} = -2h_1 \quad (2.44)$$

$$a_{12} + a_{23} = -2h_2 \quad (2.45)$$

$$a_{23} + a_{13} = -2h_3 \quad (2.46)$$

which fixes the powers to be

$$\mathcal{A}_n = \langle 12 \rangle^{h_3-h_1-h_2} \langle 23 \rangle^{h_1-h_2-h_3} \langle 13 \rangle^{h_2-h_1-h_3}, \quad (2.47)$$

independent of which particles exists in the theory of interest. If we have a theory of only gluons, the helicities can be  $\pm 1$  and the only scaleless three-point function is the one where two legs have positive helicity and one leg has negative, e.g.

$$\mathcal{A}_3^{\text{MHV}} \sim 1^- \rightarrow \text{circle with } \mathcal{A}_3^{\text{MHV}} \text{ inside, legs } 2^- \text{ and } 3^+ \left. \right\} \propto \frac{\langle 12 \rangle^3}{\langle 13 \rangle \langle 23 \rangle}, \quad (2.48)$$

where we have taken  $(h_1, h_2, h_3) = (-1, -1, 1)$ . We can also follow the same line of argument in the second case, where  $\lambda_1 \propto \lambda_2 \propto \lambda_3$ . The solution in that case is

$$\mathcal{A}_3^{\overline{\text{MHV}}} \sim 1^+ \rightarrow \text{circle with } \mathcal{A}_3^{\overline{\text{MHV}}} \text{ inside, legs } 2^+ \text{ and } 3^- \left. \right\} \propto \frac{[12]^3}{[23][13]}, \quad (2.49)$$

where the helicity state is  $(h_1, h_2, h_3) = (1, 1, -1)$ . We call these two solutions the maximally helicity violating (MHV) and anti-maximally helicity violating ( $\overline{\text{MHV}}$ ) amplitudes<sup>3</sup>. The three-point functions act as building blocks for higher  $n$ -point scattering amplitudes, as we will show in the following.

## Analytical Structure and Recursion

Scattering amplitudes are functions obeying unitarity, locality, and causality, and this is reflected in their analytic structure. In the following, we take four-momentum

<sup>3</sup>The notation was historically introduced from the point of view of  $2 \rightarrow (n-2)$  scattering, where notion of ‘‘helicity violation’’ refers to the difference between the in and out state and the ‘‘maximal’’ refers to the fact that when all helicities are the same, the amplitude is identically 0:

$$\mathcal{A}(1^\pm, 2^+, \dots, n^+) = \mathcal{A}_n(1^\pm, 2^-, \dots, n^-) = 0. \quad (2.50)$$

complex and we have that scattering amplitudes are complex rational functions of Lorentz invariants. In this section, we have seen that scattering amplitudes are restricted to have the correct little group scaling and this restriction determines the three-point functions in (2.48) and (2.49). Locality and unitarity specifically fix  $n$ -point scattering amplitudes to either be governed by local  $n$ -point interactions or built up from local  $m$ -point interactions with momentum transferred between them by an internal off-shell particle. In theories where amplitudes can be built up solely by three-point functions, (2.48) and (2.49), we call the theory *constructable*. Locality implies that scattering amplitudes have simple poles exactly when the particle goes on-shell and the residue around these poles are factorizations over scattering amplitudes constructed by lower point functions. Schematically,

$$\partial \quad \begin{array}{c} \diagup \quad \diagdown \\ \circlearrowleft \mathcal{A}_n \\ \diagdown \quad \diagup \\ \vdots \end{array} = \sum_{L,R} \begin{array}{c} \diagup \quad \diagdown \\ \circlearrowleft \mathcal{A}_L \\ \diagdown \quad \diagup \\ \vdots \end{array} \text{---} \begin{array}{c} \diagup \quad \diagdown \\ \circlearrowleft \mathcal{A}_R \\ \diagdown \quad \diagup \\ \vdots \end{array} \quad (2.51)$$

where  $\partial$  is associated with the residue on the singularity of the amplitude related to the internal particle going on-shell, and  $\mathcal{A}_L$  and  $\mathcal{A}_R$  are scattering amplitudes of lower-point amplitudes, such that  $n = L + R - 2$ , as each part shares the on-shell propagator as an external leg. Locality tells us, that the two subamplitudes  $\mathcal{A}_L$  and  $\mathcal{A}_R$  in principle can be separated by an arbitrary distance. This implies that they are independent functions and must therefore be multiplied together [72]. Unitarity, on the other hand, tells us we have to integrate over the internal momentum transfer and summing over quantum numbers such as helicity of the propagator, corresponding to inserting a complete set of internal states. This is equivalent to summing over each combination of  $\mathcal{A}_L$  and  $\mathcal{A}_R$ , since the on-shell condition and momentum conservation completely fixes the transferred momenta. Thus the tree-level scattering amplitude can only have singularities on special isolated points in momentum space, associated with certain internal degrees of freedom going on-shell. To find the exact locations, we specialize to the case when  $\mathcal{A}_L = \mathcal{A}_L(p_1, p_2, \dots, p_k, P_I)$  is a  $k + 1$  point amplitude and  $P_I$  is the momentum of the internal particle. In that case, the pole occurs exactly when the internal state goes on-shell, that is  $p_I^2 = (p_1 + p_2 + \dots + p_k)^2 = s_{12\dots k} = 0$  for all massless particles.

A general scattering amplitude can be evaluated in terms of lower point scattering amplitudes using the following recursion technique [29]. Consider the  $n$ -point scattering amplitude in some theory. We perform a complex deformation:  $\mathcal{A}_n \rightarrow \mathcal{A}_n(z)$ , by way of  $n$  complex 4-vectors,  $r_i^\mu$ , constrained by the properties

$$\sum_{i=1}^n r_i^\mu = 0, \quad (2.52)$$

$$r_i \cdot r_j = 0, \quad (2.53)$$

$$r_i \cdot p_i = 0. \quad (2.54)$$

such that the external particle momenta deformed by

$$\hat{p}_i^\mu \equiv p_i^\mu + z r_i^\mu. \quad (2.55)$$

Due to the defining properties of  $r_i^\mu$ , all shifted momenta are on-shell  $\hat{p}_i^2 = 0$ , obey momentum conservation  $\sum_{i=1}^n \hat{p}_i^\mu$ , and each multiparticle Mandelstam variable in shifted momenta

$$\hat{s}_{ij\dots k} = (\hat{p}_i + \hat{p}_j + \hat{p}_k)^2 = s_{ij\dots k} + 2z \left( \sum_{a=i}^k p_a \right) \cdot \left( \sum_{b=i}^k r_b \right), \quad (2.56)$$

is at most linear in  $z$ . We can thus express  $\hat{s}_{ij\dots k}$  as a zero on  $z$

$$\hat{s}_{ij\dots k} = -\frac{s_{ij\dots k}}{z^*} (z - z^*), \quad (2.57)$$

with  $z^*$  being the solution

$$z^* = -\frac{s_{ij\dots k}}{2P \cdot R}, \quad (2.58)$$

where we have defined  $P = \sum_{a=i}^k p_a$  and  $R = \sum_{b=i}^k r_b$ . Taking  $z \rightarrow 0$  in  $\mathcal{A}(z)$  just returns the unshifted scattering amplitude. This means the residue of the pole  $\frac{\mathcal{A}_n(z)}{z}$  at  $z = 0$ , is equal to the unshifted scattering amplitude, therefore Cauchy's theorem states

$$0 = \oint_{\mathcal{C}} \frac{\mathcal{A}_n(z)}{z} = \mathcal{A}_n(z=0) + \sum_{z=z^*} \text{Res}_{z=z^*} \frac{\mathcal{A}_n(z)}{z} + \mathcal{B}_n, \quad (2.59)$$

where  $\mathcal{C}$  is a contour surrounding all poles in the complex plane. We explicitly include the *boundary term*,  $\mathcal{B}_n$ , a rational function encoding the residue of a potential pole at  $z \rightarrow \infty$ . In most cases<sup>4</sup>, we can choose the shift vectors in such a way that the boundary term vanishes. The residues away from  $z = 0$  are just where internal propagators go on-shell and in the neighborhood of  $z^*$  we simply obtain that  $\mathcal{A}_n(z)$  factorizes in the following manner

$$\mathcal{A}_n(z) \rightarrow \mathcal{A}_L(z^*) \frac{1}{\hat{s}_{ij\dots k}} \mathcal{A}_R(z^*) = -\frac{z^*}{z - z^*} \mathcal{A}_L(z^*) \frac{1}{s_{ij\dots k}} \mathcal{A}_R(z^*), \quad (2.60)$$

Meaning that the residue of  $\frac{\mathcal{A}_n(z)}{z}$  on the pole  $z = z^*$  is simply

$$-\text{Res}_{z=z^*} \frac{\mathcal{A}_n(z)}{z} = \mathcal{A}_L(z^*) \frac{1}{s_{ij\dots k}} \mathcal{A}_R(z^*). \quad (2.61)$$

---

<sup>4</sup>For more details about the shifts from the point of view of field theory we refer to [50]. We will in the following assume that a choice of deformation vectors, leading to vanishing of the boundary term, exists.

Summing over all possible internal particles and integrating over their momentum  $P_I$ , and taking all residues into account, we obtain

$$\mathcal{A}_n = \sum_{I=2}^{n-2} \sum_{h=\pm} \frac{1}{s_{1\dots I}} \mathcal{A}_{I+1}(1, 2, \dots, I^h) \mathcal{A}_{n-I+1}(-I^{-h}, I+1, \dots, n), \quad (2.62)$$

which is only true when  $\mathcal{B}_n = 0$ . This can be justified if, under a particular shift, we have

$$\mathcal{A}_n(z) \rightarrow 0, \quad z \rightarrow \infty. \quad (2.63)$$

In the next section, we shall review how using a particular choice of shift vectors, we can prove the Parke-Taylor formula (2.35) in just a few lines of algebra.

## 2.4 Non-Abelian Gauge Theory

Scattering amplitudes in non-abelian gauge theories, called Yang-Mills theories, are of primary interest in this dissertation. Here, particles carry color charge, transforming under an  $SU(N)$  gauge group, where  $N$  denotes the number of independent colors existing in the theory. The spectrum is  $N^2 - 1$  adjoint particles with spin 1 called gluons, though one can add additional spin- $\frac{1}{2}$  particles to the spectrum to obtain a theory similar to the quantum chromodynamics sector of the Standard Model. Each external particle in the adjoint representation is equipped with a color matrix  $T^a$  with the following commutator relations

$$[T^a, T^b] = if^{abc}T^c, \quad (2.64)$$

with  $f^{abc}$  being the structure constants of the given theory. The color information carried by the generator of the gauge group  $T^a$  can be disentangled from the kinematic information of a scattering amplitude by color-kinematic decomposition [42,45,51]. For instance, consider the scattering of  $n$  colored gluons at leading order in perturbation theory:

$$\mathcal{A}_{n,k}^{\text{tree}}(\{p_i, h_i, a_i\}) = g^{n-2} \sum_{\sigma \in \mathcal{O}_n} \text{Tr}(T^{a_1} T^{a_{\sigma(2)}} \dots T^{a_{\sigma(n)}}) A_{n,k}^{\text{tree}}[1^{h_1}, \sigma(2^{h_2}), \dots, \sigma(n^{h_n})], \quad (2.65)$$

where  $\mathcal{O}_n \simeq S_n/Z_n$  are  $(n-1)!$  non-cyclic permutations of the tuple  $\{1, 2, \dots, n\}$ ,  $T^a$  are the color generators of the given theory, and  $A_n[1, \dots, n]$  are *color-ordered* or *partial* amplitudes<sup>5</sup>. The argument refers to a specific labeling of external particles according to their position in a planar embedding. We distinguish between helicity amplitudes

<sup>5</sup>We will sometimes suppress the labels of the partial ordering when referring to the *standard ordering*, i.e.  $A_{n,k} := A_{n,k}[1, 2, \dots, n]$ .

by the label  $k$ , denoting the number of negative helicity gluons in the scattering, such that  $k = 2$  refers to amplitudes in the MHV configuration, or sector, and  $k = 3$  refers to the NMHV, et cetera. We write  $A_{n,k}$  referring to the  $n$ -point scattering amplitudes in the  $N^{k-2}$ MHV sector and we have that “worse-than-MHV” scattering amplitudes vanish as follows

$$A_{n,0} = A_{n,1} = 0, \quad (2.66)$$

along with

$$A_{n,n} = A_{n,n-1} = 0. \quad (2.67)$$

We therefore have non-zero amplitudes for  $2 \leq k \leq n - 2$  and the  $k = n - 2$  is referred to as anti-MHV or  $\overline{\text{MHV}}$  amplitude.

The partial amplitudes fulfill the following conditions:

I Cyclic identity

$$A_{n,k}[1, 2, \dots, n] = A_{n,k}[2, 3, \dots, n, 1]. \quad (2.68)$$

II Reflection identity

$$A_{n,k}[1, 2, \dots, n] = (-1^n)A_{n,k}[n, \dots, 2, 1]. \quad (2.69)$$

III Photon- or U(1) decoupling identity

$$A_{n,k}[1, 2, \dots, n] + A_{n,k}[2, 1, 3, \dots, n] + \dots + A_{n,k}[2, 3, \dots, 1, n] = 0. \quad (2.70)$$

These equations can be seen as consequences of color group structures. The first identity comes from the standard cyclic property of traces and allows us to fix the first leg in (2.65) and thus the basis of scattering amplitudes consists only of  $(n - 1)!$  distinct elements associated with all the ways we can permute the remaining  $(2, \dots, n)$  elements. The photon decoupling relation can be found from the decomposition of the color group  $U(N) \simeq U(1) \times SU(N)$  [45] and taking one of the color matrices,  $T^{a_i} = \mathbb{1}$ , to be the identity matrix, thus making it commute with all other color matrices. Since gluon amplitudes in  $U(N)$  theories must vanish [45], the photon decoupling identity drops out as an immediate consequence.

There exists another color decomposition of scattering amplitudes, the Del Duca, Dixon, Maltoni (DDM) decomposition [51] where the scattering amplitude can be decomposed in terms of the structure constants, as follows

$$\mathcal{A}_{n,k}^{\text{tree}}(\{p_i, h_i, a_i\}) = g^{n-2} \sum_{\sigma \in S_n} f^{a_1 \sigma_1 b_1} f^{b_1 a_{\sigma_2} b_2} \dots f^{b_{n-3} a_{\sigma_{n-2}} a_n} A_{n,k}^{\text{tree}}[1, \sigma(2 \dots n - 1), n], \quad (2.71)$$

where we have expanded in a basis of  $(n-2)!$  partial amplitudes. Using the identity  $[T^a, T^b] = -if^{abc}T^c$ , we can relate the two decompositions through a set of relations

$$A_{n,k}^{\text{tree}}[1, \{\alpha\}, n, \{\beta\}] = (-1)^{n_\beta} \sum_{\omega \in \{\alpha\} \sqcup \{\beta^T\}} A_{n,k}^{\text{tree}}[1, \{\omega\}, n], \quad (2.72)$$

where  $\sqcup$  is the *shuffle product* instructing us to shuffle the set  $\{\beta^T\}$ , the reverse of the set  $\{\beta\}$ , into the set  $\{\alpha\}$ , respecting their internal orderings. These are the Kleiss-Kuijf (KK) relations [42] and reduce our basis of partial amplitudes down to  $(n-2)!$ . It is clear, that both the reflection and photon decoupling identity can be cast on a form of (2.72), by taking  $\beta = 0$  and  $\beta = 1$ , thus they are included in the Kleiss-Kuijf relations.

It turns out we can reduce the basis even further [52, 53]: if we take as an ansatz that the full scattering amplitude can be written as a sum over factorization channels

$$\mathcal{A}_{n,k} = \sum_i \frac{c_i n_i}{\prod_{a \in i} s_a} \quad (2.73)$$

where we have factored the numerator as  $c_i$ , consisting of the color factors, times  $n_i$  consisting of Lorentz contractions of momentum and spinors. We can relate certain factorization channels by the Jacobi identity on the color numerators  $c_i$

$$c_i + c_j + c_k = 0, \quad (2.74)$$

which usually is visualized as a relation between Feynman diagrams, where the indices refers to a labeling of the specific channels, e.g. for  $n = 4$  particle scattering  $i = s_{12}$ ,  $j = s_{23}$ , and  $k = s_{13}$ , with  $c_{s_{12}}$  being the color factor associated with the factorization channel where  $s_{12} \rightarrow 0$  etc. as visualized in the following:

$$\begin{array}{c} \begin{array}{ccc} 2 & 3 & \\ | & | & \\ 1 \text{---} & & \text{---} 4 \end{array} + \begin{array}{ccc} 4 & 3 & \\ | & | & \\ 1 \text{---} & & \text{---} 2 \end{array} - \begin{array}{ccc} 3 & 2 & \\ | & | & \\ 1 \text{---} & & \text{---} 4 \end{array} = \\ f^{a_1 a_2 b} f^{b a_3 a_4} + f^{a_1 a_4 b} f^{b a_2 a_3} - f^{a_1 a_3 b} f^{b a_2 a_4} = 0. \end{array} \quad (2.75)$$

Since the choice of expansion is not unique, e.g. we can always transform  $n_i \rightarrow n_i + s_{12}\Delta$ , where  $\Delta$  is an arbitrary function, we assume that there exists a choice of numerator coefficients,  $n_i$ , such that they too fulfill the Jacobi identities of (2.75) [52]

$$n_i + n_j + n_k = 0. \quad (2.76)$$

In that case, we have that the scattering amplitudes fulfill another set of relations, namely the Bern-Carrasco-Johansson (BCJ) relations [52], which can be cast in the following form [45] (known as the fundamental BCJ relations)

$$\sum_{i=3}^n \left( \sum_{j=3}^i s_{2j} \right) A_{n,k}^{\text{tree}}[1, 3, \dots, i, 2, i+1, \dots, n] = 0. \quad (2.77)$$

These relations further reduce the basis down to  $(n-3)!$  and can be obtained from e.g. string theory, where they appear as the infinite tension limit of the imaginary part of the Kawai-Lewellen-Tye (KLT) relations found as certain monodromy relations between sectors of open string integrals [54].

### 2.4.1 BCFW recursion relations

Armed with these relations, we now wish to evaluate the partial amplitudes described above in (2.65) and (2.71). To that end, we exploit the recursion relations (2.62) as presented in the previous section 2.3, making a choice of  $r_i^\mu$ , such that we do not obtain any boundary term in (2.59). A standard choice due to Britto, Cachazo, Feng, and Witten (BCFW) [28, 29] is shifting the spinor helicity variables of two external legs

$$\lambda_i \rightarrow \hat{\lambda}_i = \lambda_i + z\lambda_j, \quad (2.78)$$

$$\tilde{\lambda}_j \rightarrow \hat{\tilde{\lambda}}_j = \tilde{\lambda}_j - z\tilde{\lambda}_i. \quad (2.79)$$

This is denoted as a  $[j, i]$ -shift and is of course equivalent to an explicit shift on momenta, as can be seen by projecting in

$$\sigma_\mu^{a\dot{a}} \hat{p}_i^\mu = \hat{\lambda}_i^a \hat{\tilde{\lambda}}_i^{\dot{a}} = \lambda_i^a \tilde{\lambda}_i^{\dot{a}} + z\lambda_j^a \tilde{\lambda}_i^{\dot{a}} \Rightarrow \sigma_\mu^{a\dot{a}} r_i^\mu = \lambda_j^a \tilde{\lambda}_i^{\dot{a}}, \quad (2.80)$$

$$\sigma_\mu^{a\dot{a}} \hat{p}_j^\mu = \hat{\lambda}_j^a \hat{\tilde{\lambda}}_j^{\dot{a}} = \lambda_j^a \tilde{\lambda}_j^{\dot{a}} - z\lambda_j^a \tilde{\lambda}_i^{\dot{a}} \Rightarrow \sigma_\mu^{a\dot{a}} r_j^\mu = -\lambda_j^a \tilde{\lambda}_i^{\dot{a}}. \quad (2.81)$$

The shift vectors  $r_i$  and  $r_j$  fulfills the defining identities for shifted momenta as laid out in the previous section

$$\sum_l r_l = \lambda_j^a \tilde{\lambda}_i^{\dot{a}} - \lambda_j^a \tilde{\lambda}_i^{\dot{a}} = 0 \quad (2.82)$$

$$r_i \cdot r_j = \langle jj \rangle [ii] = 0, \quad (2.83)$$

$$p_i \cdot r_i = \langle ij \rangle [ii] = 0, \quad (2.84)$$

$$p_j \cdot r_j = \langle jj \rangle [ji] = 0, \quad (2.85)$$

and therefore are valid shift vectors for setting up the recursion of section 2.3. To get the most out of a  $[j, i]$ -shift, we need to ensure that there is no pole of the shifted amplitude at infinity. For the time being, we are going to assume the Parke-Taylor amplitude (2.35) and study how it scales under shifts.

$$A_{n,2}[1^-, 2^-, 3^+, \dots, n^+] = \frac{\langle 12 \rangle^4}{\langle 12 \rangle \langle 23 \rangle \dots \langle n-1n \rangle \langle n1 \rangle}. \quad (2.86)$$

If we shift  $[j, i] = [1, 2]$ , we note that the numerator does not contribute with any factors of  $z$  as the shifted term is proportional to  $\langle 11 \rangle = 0$ . Therefore the only contribution is from the denominator, where we have  $\langle \hat{2}3 \rangle = \langle 23 \rangle + z\langle 13 \rangle$ . Thus the

Parke Taylor factor (2.86) scales as  $\frac{1}{z}$  under  $z \rightarrow \infty$ . Considering instead the  $[1, 3]$ -shift, the only factors of  $z$  arise from the denominators  $\langle 2\hat{3} \rangle$  and  $\langle \hat{3}4 \rangle$  each scaling with a factor of  $\frac{1}{z}$ . Therefore the Parke-Taylor amplitude (2.35) scales as  $\frac{1}{z^2}$  as  $z \rightarrow \infty$  under the  $[1, 3]$ -shift. Following a similar line of argument, we can obtain the scaling properties for (2.86) under shifts of different adjacent helicity legs.

$[+, +\rangle$	$[+, -\rangle$	$[-, +\rangle$	$[-, -\rangle$
$\frac{1}{z}$	$z^3$	$\frac{1}{z}$	$\frac{1}{z}$

If  $i$  and  $j$  are non-adjacent as in the  $[1, 3]$ -shift, each shift scales further by an extra factor of  $\frac{1}{z}$ . The scalings can be argued in generality from field theory [55]. Since  $[1, 2]$  is a valid shift, we will proceed with this shift. The recursion relations tells us

$$\begin{aligned}
A_{n,2}[1^-, 2^-, 3^+, \dots, n^+] = & \\
& \sum_{h=\pm} \sum_{m=4}^n \frac{1}{s_{23\dots m-1}} \hat{A}_{n-m+3, k_L}[\hat{1}^-, \hat{P}_{23\dots m-1}^h, m^+, \dots, n^+] \times \\
& \hat{A}_{m-1, k_R}[-\hat{P}_{23\dots m-1}^{-h}, \hat{2}^-, 3^+, \dots, (m-1)^+], \quad (2.87)
\end{aligned}$$

where we sum over all amplitudes with the shifted legs belonging to different local contributions connected by the propagator  $s_I$  with  $I = (2, 3, \dots, (k-1))$ , and  $k_L$  and  $k_R$  are defined such that  $k_L + k_R = k + 1 = 3$ . Only a few terms in this sum survive in (2.87) due to the vanishing of “worse-than-MHV” amplitudes (2.66): in the first term,  $h$  must be equal to  $-1$  in order for the left amplitude not to vanish, unless  $k = n - 2$  in which case the left amplitude is the  $\overline{\text{MHV}}$  three-point function discussed in section 2.3. A similar analysis can be performed for the right amplitude leading to only two surviving terms in the sum (2.87).

$$\begin{aligned}
A_{n,k}[1^-, 2^-, 3^+, \dots, n^+] = & \frac{1}{s_{23}} \hat{A}_{n-1,2}[\hat{1}^-( -\hat{P}_{23}^-), 4^+, \dots, n^+] \hat{A}_{3,1}[(-\hat{P}_{23}^+), \hat{2}^-, 3^+] \\
& + \frac{1}{s_{1n}} \hat{A}_{3,1}[\hat{1}^-, (-P_{1n})^+, n^+] \hat{A}_{n-1,2}[\hat{P}_{1n}^-, \hat{2}^-, 3^+, \dots, (n-1)^+]. \quad (2.88)
\end{aligned}$$

Under the induction hypothesis that the  $(n-1)$ -point MHV amplitudes are described by (2.35) and using the three-point functions derived earlier (2.48) and (2.49), we have all the tools to derive the  $n$ -point case. Inserting spinor helicity expressions and analytically continuing the momenta<sup>6</sup>  $\lambda_{-p} = -\lambda_p$  and  $\tilde{\lambda}_{-p} = \tilde{\lambda}_p$ , we get

$$A_{n,2}[1^-, 2^-, \dots, n^+] = \frac{1}{s_{23}} \frac{\langle \hat{1}\hat{P}_{23} \rangle^3}{\langle \hat{P}_{23}4 \rangle \langle 45 \rangle \dots \langle n\hat{1} \rangle} \frac{[\hat{P}_{23}3]^3}{[\hat{2}3][\hat{2}\hat{P}_{23}]}. \quad (2.89)$$

<sup>6</sup>the opposite choice is also completely valid.

The second term of (2.88) vanishes on support of  $\hat{P}_{1n}^2 = 0$ , while the first term is non-vanishing for generic momenta since  $[\hat{2}^*] = [2^*]$ . We can write the numerator as

$$\langle \hat{1} \hat{P}_{23} \rangle^3 [\hat{P}_{23} 3]^3 = \langle 1(\hat{P}_{23}) 3 \rangle^3 = (\langle 1(\hat{2} + 3) 3 \rangle)^3 = \langle 12 \rangle^3 [23]^3, \quad (2.90)$$

and the shifted term in the denominator is  $[2\hat{P}_{23}] \langle \hat{P}_{23} 4 \rangle = \langle 34 \rangle [23]$ . Reinserting into (2.89), yields

$$A_{n,2}[1^-, 2^-, \dots, n^+] = \frac{1}{s_{23}} \frac{\langle 12 \rangle^3 [23]^3}{[23] \langle 34 \rangle [23] \langle 45 \rangle \dots \langle n1 \rangle} = \frac{\langle 12 \rangle^3}{\langle 23 \rangle \langle 34 \rangle \langle 45 \rangle \dots \langle n1 \rangle}. \quad (2.91)$$

which is exactly the Parke-Taylor scattering amplitude (2.35) for  $n$  gluons in the MHV sector.

The recursion relations are powerful tools for evaluating scattering amplitudes, however, they are not always applicable. Indeed here  $n$ -point amplitudes are assumed to be constructible from three-point functions (2.48) and (2.49), and thus no information about higher point local interactions are taken into account. In the case of Yang-Mills theories, all information of the  $S$ -matrix (at tree-level) can be constructed from recursion over three-point functions, as argued in [45]!

### Non-Adjacent Shifts and Bonus Relations

As mentioned earlier, there is an extra factor of  $\frac{1}{z}$  in the  $z$ -scaling of amplitudes under non-adjacent BCFW shifts. This ensures an extra set of relations between scattering amplitudes referred to “bonus relations”. In particular, they can be cast on the form [45]

$$\oint_C \hat{A}_n(z) = 0, \quad (2.92)$$

where the integration contour is the same as for (2.59). This statement has played an important role as consistency conditions of graviton scattering amplitudes [56]<sup>7</sup>. For gluon scattering, the bonus relations have a curious implication, as they encode the BCJ relations (2.77) [57]. Here we outline the general idea for 4-point scattering of gluons. For simplicity we consider the  $[1^-, 2^-]$ -shift. We then consider the integral

$$\oint_C \frac{dz}{z} \hat{s}_{23}(z) \left( \hat{A}_{4,2}[\hat{1}, \hat{2}, 3, 4] + \hat{A}_{4,2}[\hat{1}, 4, \hat{2}, 3] + \hat{A}_{4,2}[\hat{1}, 3, 4, \hat{2}] \right), \quad (2.93)$$

where for notational purposes, we have neglected to write the helicities of the external particles  $[1, 2, 3, 4] := [1^-, 2^-, 3^+, 4^+]$ . The integrand consists of a kinematic

<sup>7</sup>Here the double  $\frac{1}{z^2}$  scaling of graviton amplitudes can be verified by the double-copy construction of graviton amplitudes from gluon amplitudes.

function  $\hat{s}_{23}(z)$  multiplied by the shifted  $U(1)$  decoupling identity and can be set to 0. Breaking the integral up term-by-term, we realize that the middle term  $\hat{A}(\hat{1}, 3, \hat{2}, 4) \sim \frac{1}{z^2}$ , meaning that even when taking into account the extra scaling of  $z$  from the coefficient  $\hat{s}_{23}$ , the integral vanish

$$\oint_{\mathcal{C}} \frac{dz}{z} \hat{s}_{23}(z) \hat{A}_{4,2}[\hat{1}, 3, \hat{2}, 4] = 0, \quad (2.94)$$

where again  $\mathcal{C}$  covers every pole of  $A_{4,2}(1, 3, 2, 4)$ . For the first and third term, we have to evaluate the residues on the poles in  $z$ . In the first term, the only residue appears at  $z = 0$  and therefore the integral just evaluates to

$$\oint_{\mathcal{C}} \frac{dz}{z} \hat{s}_{23}(z) \hat{A}_{4,2}[\hat{1}, \hat{2}, 3, 4] = s_{23} A_{4,2}[1, 2, 3, 4], \quad (2.95)$$

while in the third term we have a pole in  $z = 0$  and a pole at  $z = z_{13} = \frac{[13]}{[23]}$ , therefore we obtain by Cauchy's theorem

$$\oint_{\mathcal{C}} \frac{dz}{z} \hat{s}_{23}(z) A_{4,2}[\hat{1}, 3, 4, \hat{2}] = (s_{23} - s_{23}(z_{13})) A_{4,2}[1, 3, 4, 2] = -s_{13} A_{4,2}[1, 3, 4, 2]. \quad (2.96)$$

Putting it all together we get

$$0 = s_{23} A_{4,2}[1, 2, 3, 4] - s_{13} A_{4,2}[1, 3, 4, 2], \quad (2.97)$$

which is one representation of the BCJ relations (2.77). We could in general have started from another  $U(1)$  relation and multiplied by a different propagator to obtain different representations of the BCJ relations. We refer to the work cited in [57], where the authors inductively prove the BCJ relations can be obtained from the bonus scaling of non-adjacent legs for all  $n$ .

## 2.4.2 Singularities of Non-Abelian Gauge Theories: Collinear and Soft Limits

The partial amplitudes have certain universal behavior associated with specific momentum configurations. The two types of configurations are the collinear limits, where two external particles become collinear and their momenta become proportional, and soft limits, where a certain external momentum vanishes. We can employ the BCFW recursion relations to study these limits [46].

### Collinear Limit

The collinear behavior of a scattering amplitude can be explored by taking two consecutive particles (in the color orderings)  $p_i \sim p_{i+1}$ , which can be parameterized as  $p_i = zP$  and  $p_{i+1} = (1 - z)P$ , with the total collinear momentum  $P = p_i + p_{i+1}$ .

Since this momentum is null, we can write spinor helicity variables for the total collinear momentum  $P = \lambda_P \tilde{\lambda}_P$ , and therefore

$$\lambda_i = \sqrt{z} \lambda_P, \quad \tilde{\lambda}_i = \sqrt{z} \tilde{\lambda}_P, \quad (2.98)$$

$$\lambda_{i+1} = \sqrt{1-z} \lambda_P, \quad \tilde{\lambda}_{i+1} = \sqrt{1-z} \tilde{\lambda}_P. \quad (2.99)$$

Considering the  $n$ -point MHV amplitudes  $A_{n,2}[1^-, 2^-, 3^+, 4^+, 5^+, \dots, n^+]$  with  $p_4$  and  $p_5$  collinear, we can extract the universal behavior

$$\begin{aligned} A_{n,2}[1^-, 2^-, 3^+, 4^+, 5^+, \dots, n^+] &= \frac{\langle 12 \rangle^3}{\langle 23 \rangle \langle 34 \rangle \langle 45 \rangle \langle 56 \rangle \dots \langle n1 \rangle} \xrightarrow{p_4 \parallel p_5} \\ &= \frac{1}{\sqrt{z(1-z)} \langle 45 \rangle} \times \frac{\langle 12 \rangle^3}{\langle 23 \rangle \langle 3P \rangle \langle P6 \rangle \dots \langle n1 \rangle} \\ &= \text{Split}_-(z, 4^+, 5^+) A_{n-1,2}[1^-, 2^-, 3^+, P^+, 6^+, \dots, n^+]. \end{aligned} \quad (2.100)$$

The remaining splitting functions can be found by taking other legs collinear, we get [58]

$$\text{Split}_-(z; i^+, (i+1)^-) = -\frac{z^2}{\sqrt{z(1-z)} [ii+1]}, \quad (2.101)$$

$$\text{Split}_-(z; i^-, (i+1)^+) = -\frac{(1-z)^2}{\sqrt{z(1-z)} [ii+1]}, \quad (2.102)$$

$$\text{Split}_-(z; i^-, (i+1)^-) = 0, \quad (2.103)$$

where  $\text{Split}_+(z; i^{h_i}, (i+1)^{h_{i+1}})$  is the parity conjugate of  $\text{Split}_-(z; i^{h_i}, (i+1)^{h_{i+1}})$ .

### Soft Limits

Another interesting class of limits of scattering amplitudes is the *soft limits*: here we obtain the following factorization for the MHV amplitude with a positive helicity gluon going soft

$$\begin{aligned} A_{n,2}[1^-, 2^-, 3^+, \dots, n^+] &= \frac{\langle 12 \rangle^3}{\langle 23 \rangle \langle 34 \rangle \langle 45 \rangle \langle 56 \rangle \dots \langle n1 \rangle} \\ &\xrightarrow{p_4^+ \rightarrow 0} \frac{\langle 35 \rangle}{\langle 34 \rangle \langle 45 \rangle} \times \frac{\langle 12 \rangle^3}{\langle 23 \rangle \langle 35 \rangle \langle 56 \rangle \dots \langle n1 \rangle}. \end{aligned} \quad (2.104)$$

Had we taken a negative gluon, say particle 2, as the soft particle, the amplitude would simply vanish. This is because taking a negative helicity gluon soft reduces  $k$  by one and we are left with a  $k=1$  scattering amplitude which vanishes as per (2.66). Had we instead used an NMHV or  $\overline{\text{MHV}}$  scattering amplitude, we would simply have obtained that the soft factors can be written as

$$\text{Soft}(i^-) = \frac{\langle i-1i+1 \rangle}{\langle i-1i \rangle \langle ii+1 \rangle}, \quad (2.105)$$

and

$$\text{Soft}(i^+) = \frac{[i-1i+1]}{[i-1i][ii+1]}. \quad (2.106)$$

## 2.5 Bi-Adjoint $\phi^3$ Theory

Arguably one of the simplest theories from the point of view of scattering amplitudes is the bi-adjoint  $\phi^3$  theory. It is a theory of scalars that transform under a product of gauge groups, are exclusively in the adjoint representation, and are thus charged under two color groups,  $SU(N) \times SU(\tilde{N})$ . Tree-level scattering amplitudes in this theory admit a double color decomposition:

$$\mathcal{M}_n = \sum_{\alpha \in S_n/Z_n} \text{Tr}(T^{\alpha_{(1)}} T^{\alpha_{(2)}} \dots T^{\alpha_{(n)}}) M_n(\alpha), \quad (2.107)$$

$$M_n(\alpha) = \sum_{\beta \in S_n/Z_n} \text{Tr}(T^{\alpha_{\beta(1)}} T^{\alpha_{\beta(2)}} \dots T^{\alpha_{\beta(n)}}) m_n(\alpha|\beta), \quad (2.108)$$

where the *double partial amplitudes*,  $m_n(\alpha|\beta)$  are understood to be planar with respect to both orderings  $(\alpha, \beta)$  and are naturally expressed on the kinematic space of Mandelstam variables, which is the  $\frac{n(n-3)}{2}$  dimensional space under momentum conservation

$$X_{ij} := s_{ii+1\dots j-1}, \quad X_{ii+1} = X_{1n} = 0. \quad (2.109)$$

Partial amplitudes can be found by

$$m_n(\alpha|\beta) = (-1)^{n-3+n_{\text{flip}}(\alpha|\beta)} \sum_{\text{planar}\{\alpha|\beta\}} \prod_{a=1}^{n-3} \frac{1}{X_{i_a, j_a}}, \quad (2.110)$$

where  $\{\alpha|\beta\}$  refers to the *mutually compatible* planar graphs with respect to the orderings  $\alpha$  and  $\beta$ . Mutually compatible planar graphs are the Feynman diagrams which are planar with respect to both orderings  $\alpha$  and  $\beta$ . We will postpone the definition of  $n_{\text{flip}}$  to later in this section. There exists a beautiful formalism due to Cachazo, He, and Yuan (CHY) [30–33] for obtaining the partial amplitudes. The CHY formalism realizes  $n$ -point scattering amplitudes in different theories as integrals over an  $n$  punctured Riemann sphere, localized on the solutions to the so-called scattering equations. Denoting the position of  $n$  punctures in  $\mathbb{C}$  as  $\sigma_a$  for  $a = 1, \dots, n$ , the set of  $n$  equations is then

$$0 = S_a = \sum_{b \neq a} \frac{S_{ab}}{\sigma_{ab}}, \quad (2.111)$$

is invariant under  $SL(2, \mathbb{C})$  transformations, acting as

$$\sigma_a \rightarrow \sigma'_a = \frac{A\sigma_a + B}{C\sigma_a + D}, \quad AD - BC = 1, \quad (2.112)$$

fulfilling the following non-trivial equations

$$\sum_a S_a = \sum_a \sigma_a S_a = \sum_a \sigma_a^2 S_a = 0, \quad (2.113)$$

meaning that the space of non-trivial solutions to (2.111) is  $(n - 3)!$  dimensional. The origin of these equations is the twistor string theory of Witten [59] and is beyond the scope of this dissertation. The scattering equations have an interesting manifestation in the Gross-Mende limit of open string theory amplitudes [60], where they appear using the method of steepest descent as explored in section 6 of [30]<sup>8</sup>. The partial amplitudes in bi-adjoint  $\phi^3$  theory are found by integration over punctures on a Riemann sphere

$$m_n(\alpha|\beta) = \int \prod_{i=1}^n \frac{d\sigma_i}{\text{vol}(SL(2, \mathbb{C}))} \prod_{a=1}^n \delta'(S_a) \frac{1}{\sigma_{\alpha_1\alpha_2}\sigma_{\alpha_2\alpha_3}\dots\sigma_{\alpha_n\alpha_1}} \frac{1}{\sigma_{\beta_1\beta_2}\sigma_{\beta_2\beta_3}\dots\sigma_{\beta_n\beta_1}}. \quad (2.114)$$

Here the  $\text{vol}(SL(2, \mathbb{C}))$  and  $\delta'$  instruct us to fix the  $SL(2; \mathbb{C})$  invariance by anchoring 3 of the  $n$  coordinates, conventionally  $\sigma_1 = 0$ ,  $\sigma_{n-1} = 1$ , and  $\sigma_n = \infty$ . The integrands  $(\sigma_{\alpha_1\alpha_2}\sigma_{\alpha_2\alpha_3}\dots\sigma_{\alpha_n\alpha_1})^{-1}$  are referred to as the Parke-Taylor factors, as their cyclic structure is reminiscent of the denominator of (2.35)<sup>9</sup>.

The integral (2.114) can be evaluated using the following algorithm proposed in [33] and described as follows. Since the partial amplitudes are both  $\alpha$  and  $\beta$  color-ordered, only the relative ordering of the two sets is relevant. Therefore, without loss of generality, we take  $\alpha = \{1, 2, \dots, n\}$  in the following.

1. Draw a circle with  $n$  nodes on its boundary and label the nodes by the standard ordering – we call this the external ordering – and link the nodes by a path inside the circle according to the other ordering  $\beta$  – the internal ordering.
2. Locate a set  $\{i, i + 1, \dots, i + r\}$  of at least two external labels,  $r > 1$ , that are consecutive with respect to both the external and internal ordering in the circle.
3. Assuming this set is maximal, that it cannot be extended by further consecutive labels and it is non-empty, we redraw the circle by moving all points along the boundary until they are close together.

<sup>8</sup>It is curious that the scattering equations, relevant for scattering of particles, appear in the high-energy limit of string theories, as usually the particle or “field-theory” limit is associated with the low-energy of string theory.

<sup>9</sup>It is possible to find Yang-Mills and even gravity scattering amplitudes among many others by similar integrals, where the Parke-Taylor factors are replaced by other integrands. We will not review this construction here.

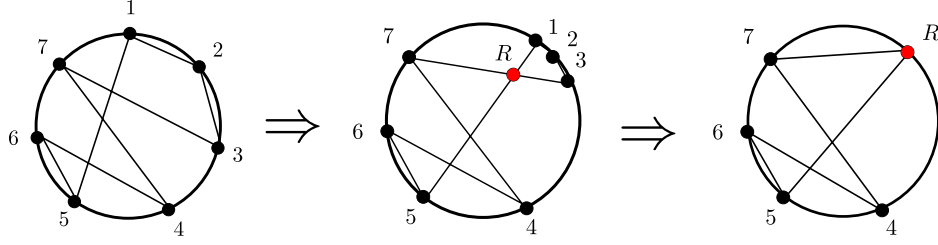


Figure 2.2: The algorithm for evaluating the CHY integral (2.114), by finding the polygon decomposition. We draw the ordering  $\alpha = \{1, 2, 3, 4, 5, 6, 7\}$  on the boundary of the disc and the ordering  $\beta = \{1, 2, 3, 7, 4, 6, 5\}$  in the interior. We then identify the mutually consecutive labels  $\{1, 2, 3\}$  and redraw the circle with the vertices drawn close together, with the intersection of the line starting at 1 and the line starting at 3 as the red vertex  $R$ . Lastly, we remove the polygon and move the point  $R$  to the boundary of the disc. The procedure repeats until both orderings  $\alpha$  and  $\beta$  agree.

4. Assuming the lines starting at  $i$  and  $i + r$  intersect at the point  $R$ , we note that  $\{i, i + 1, \dots, i + r, R\}$  forms a convex polygon, which we can remove from the graph, bringing  $R$  to the boundary of the disc, and repeat the procedure from step 2 until both orderings agree completely.

The method is sketched in Figure 2.2 for a particular example.

Collecting all the polygons, we can calculate the sub-amplitudes according to equally ordered amplitudes  $m(\alpha|\alpha)$ , which can be found by the following: draw a convex  $n$ -gon with vertices labeled by  $\alpha$ . Then triangulate the  $n$ -gon using diagonals and label each diagonal  $X_{a,b}$  as the diagonal connecting vertex  $a$  and  $b$ , such that  $b > a + 1$ . Then the partial amplitude is just

$$m_n(\alpha|\alpha) = \sum_{\mathcal{T} \in \Delta} \frac{1}{\prod_{e \in \mathcal{T}} X_e}, \quad (2.115)$$

where we sum over all possible triangulations of the  $n$ -gon,  $\Delta$ , and take the product of the internal diagonals  $X_e$  in a given triangulation,  $\mathcal{T}$ .

The problem of finding the overall sign for distinct double partial ordered amplitudes is reduced to finding  $n_{\text{flip}}(\alpha|\beta)$ . The procedure to find  $n_{\text{flip}}(\alpha|\beta)$  is described in [33] and discussed presently: starting from from the polygon decomposition described above under equation (2.114)

- Determine the overall orientation of the exterior disc according to the set  $\alpha$ .
- Determine the orientation of each loop segment by the ordering  $\beta$ , inducing an orientation of each convex polygon in the polygon decomposition.
- For each polygon with an **odd** number of vertices we associate a plus sign. If the orientation for the polygon is the same as the orientation of the external disc and a minus sign if it is oriented oppositely.

- For each polygon with an **even** number of vertices we contribute a minus sign
- For each *intersection point* we contribute a minus sign.

The product of the signs obtained from this procedure generates the overall sign of the double-partial amplitude.

The bi-adjoint  $\phi^3$  amplitudes have an interesting manifestation in the so-called KLT-kernal, giving the kinematic factors in the BCJ relation (2.77), or similarly for kinematic factors in the double copy construction relating gravity and gluon amplitudes. It was proposed in [61] that the BCJ relations can be found by expanding a collection of  $|\sigma|$  color-ordered Yang-Mills amplitude in a basis of  $(n-3)!$  color ordered amplitudes labeled  $\gamma$ .

$$A_{n,k}(\sigma) = m_n(\sigma|\beta)m_n^{-1}(\beta|\gamma)A_{n,k}(\gamma), \quad (2.116)$$

where the  $m_n(\sigma|\beta)$  is a matrix of dimension  $|\sigma| \times (n-3)!$  and the matrix  $m_n^{-1}(\beta|\gamma)$  is the matrix-inverse of the  $(n-3)! \times (n-3)!$  matrix with entries taken from  $m_n(\gamma_i|\beta_j)$ . For instance, for the  $n=4$  case, we take the orderings  $\sigma = (1243)$ ,  $\beta = (1324)$  and  $\gamma = (1234)$ , then we obtain from (2.116)

$$\begin{aligned} A_{4,2}(1, 2, 4, 3) &= m_4(1243|1324)m_4^{-1}(1324|1234)A_{4,2}(1, 2, 3, 4) = -\frac{s_{23}}{s_{12} + s_{23}}A_{4,2}(1, 2, 3, 4) \\ &\Rightarrow s_{13}A_{4,2}(1, 2, 4, 3) = s_{23}A_{4,2}(1, 2, 3, 4). \end{aligned} \quad (2.117)$$

which is a standard BCJ relation.

## 2.6 On-shell Supersymmetry

In this section, we introduce the notion of maximal supersymmetry. It is a symmetry of a physical setup under exchange of bosonic degrees of freedom with fermionic degrees of freedom and vice versa [45]. While supersymmetry is lacking in direct observational evidence [62] at least in its unbroken form<sup>10</sup>, supersymmetry highly simplifies calculations of scattering amplitudes. Indeed scattering amplitudes in maximally supersymmetric Yang-Mills theory (msYM) provide a laboratory where we can study the mathematical structure of scattering amplitudes in general and the planar sector of msYM has been dubbed “the simplest quantum field theory” [37]. In the following, we shall review supersymmetry from the perspective of the on-shell formulation of scattering amplitudes, introduced in the earlier parts of this chapter.

<sup>10</sup>It is clear that if we assume unbroken supersymmetry, each fermion in the standard model would have a bosonic counterpart with exactly the same mass, color charge, etc., and vice versa. Such degrees of freedom would have left clear experimental evidence in physics experiments throughout the last century.

Particle name	label	number of states
positive helicity gluon	$g^+$	1
positive helicity gluinos	$\Gamma^A$	4
real scalars	$S^{AB}$	6
negative helicity gluinos	$\Gamma^{ABC} \sim \bar{\Gamma}_D$	4
negative helicity gluon	$g^-$	1

Table 2.1: The states in  $\mathcal{N} = 4$  super Yang-Mills. We note the presence of the 6 real scalars, which are not present in non-supersymmetric Yang-Mills theory. The six real scalars can in general acquire a vacuum expectation value and thus break the supersymmetry.

### 2.6.1 $\mathcal{N} = 4$ Supersymmetry

We take as the starting point of our discussion of supersymmetry the supercharges  $(q, \bar{q})$ , which act in the following manner on maximal spin- $s$  one-particle states with momentum  $p$ ,

$$q_{aI} |p, s, a\rangle = 0, \quad (2.118)$$

$$\bar{q}^{\dot{a}I} |p, -s, a\rangle = 0, \quad (2.119)$$

$$q_{aI} |p, -s, a\rangle = \lambda_a |p, -s + \frac{1}{2}, a\rangle_I, \quad (2.120)$$

$$\bar{q}^{\dot{a}I} |p, s, a\rangle = \tilde{\lambda}_p^{\dot{a}} |p, s - \frac{1}{2}, a\rangle^I, \quad (2.121)$$

where  $a$  counts the remaining particle labels aside from spin and the index  $I$  labels the so-called  $R$  symmetry which rotates the generators  $q^I$  and  $\bar{q}_I$  into each other. This tells us something interesting: if we have enough supercharges we can organize all external on-shell states into a coherent multiplet. Letting  $\mathcal{N}$  denote number of supercharges, it is natural to introduce  $\mathcal{N} = 4$  supercharges for Yang-Mills theory by counting helicity from  $-1 \rightarrow 1$  in steps of  $\frac{1}{2}$ . A careful analysis yields the spectrum as in [45] is summarized in Table 2.1

The presence of the scalars in the spectrum of  $\mathcal{N} = 4$  implies the existence of a moduli space of different supersymmetric vacua. In particular, at the origin of this space, where the vacuum expectation value vanishes, the theory is conformal and contains no dimensionful parameters. When the scalars obtain a vacuum expectation value (vev) such that the supersymmetry is unbroken, we say the theory is on the *Coulomb branch* and in the following, we consider scattering amplitudes in the zero-vev limit of the Coulomb branch [45].

#### On-shell superspace

Remarkably, it is possible to organize the entire 16 state particle spectrum of  $\mathcal{N} = 4$  sYM into an on-shell chiral supermultiplet by introducing four Grassmann-odd

variables,  $\eta_A$  transforming in the fundamental representation of the  $SU(4)$   $R$ -symmetry index  $A = 1\dots 4$ ,

$$\Phi = g^+ + \eta_A \Gamma^{+,A} + \frac{1}{2!} \eta_A \eta_B S^{AB} + \frac{1}{3!} \eta_A \eta_B \eta_C \epsilon^{ABCD} \bar{\Gamma}_D + \eta_1 \eta_2 \eta_3 \eta_4 g^-. \quad (2.122)$$

We could just as well have started from the parity conjugate state  $g^-$  and establishing the supermultiplet by the  $\bar{\eta}$  Grassmann variables transforming in the antifundamental representation of  $SU(4)$   $R$ -symmetry as follows

$$\bar{\Phi} = g^- + \bar{\eta}_A \bar{\Gamma}^{-,A} + \frac{1}{2!} \bar{\eta}_A \bar{\eta}_B S^{AB} + \frac{1}{3!} \bar{\eta}^A \bar{\eta}^B \bar{\eta}^C \Gamma^{+,D} + \bar{\eta}_1 \bar{\eta}_2 \bar{\eta}_3 \bar{\eta}_4 g^+. \quad (2.123)$$

We will employ the former supermultiplet (2.122), however, we note that we can relate the two supermultiplets by a Fourier transformation [63] as follows

$$\bar{\Phi}(\bar{\eta}) = \int d^4 \eta e^{\eta \cdot \bar{\eta}} \Phi(\eta). \quad (2.124)$$

The Grassmann variables are anti-commuting variables,  $\eta_A \eta_B = -\eta_B \eta_A$  and therefore they have some interesting properties: first, the square of a Grassmann variable vanish  $\eta_A^2 = 0$ , meaning that any series expansion of a function of a Grassmann variable terminates after two terms  $f(\eta) = a + \eta b$ . The integration over Grassmann variables simply follows two rules

$$\int d\eta \eta = 1, \quad (2.125)$$

$$\int d\eta = 0, \quad (2.126)$$

which tells us integration of any function with respect to Grassmann variables, by a series expansion

$$\int d\eta f(\eta) = \int d\eta (a + \eta b) = b, \quad (2.127)$$

which is the same result as performing differentiation on the same function

$$\frac{\partial}{\partial \eta} f(\eta) = \frac{\partial}{\partial \eta} (a + \eta b) = b. \quad (2.128)$$

We can extract the specific external particle states from the supermultiplet by applying sequences of either derivatives or integrations with respect to the Grassmann-odd parameters  $\eta_A$  on  $\Phi$ . Supercharges can be expressed in terms of the Grassmann-odd parameters<sup>11</sup>  $\eta_A$  as

$$q^{A\dot{a}} \equiv \tilde{\lambda}^{\dot{a}} \frac{\partial}{\partial \eta_A}, \quad \tilde{q}^{Aa} \equiv \lambda^a \eta_A, \quad (2.129)$$

<sup>11</sup>Here we follow the convention of Elvang and Huang [45].

whose anti-commutator is simply the translation operator  $\{\tilde{q}^{aA}, q_B^{\dot{a}}\} = \delta_B^A p^{a\dot{a}}$  [58]. We define the *superamplitude* as the scattering of  $n$  states each organized into a supermultiplet  $\mathcal{A}(1, 2, \dots, n) := \mathcal{A}(\Phi_1, \Phi_2, \dots, \Phi_n)$  which will be a function of the spinor helicity variables  $(\lambda_i, \tilde{\lambda}_i)$  and four Grassmann variables  $\eta_{iA}$  for each supermultiplet. In general, a superamplitude can be expressed as a polynomial in  $\eta$ s as follows

$$\mathcal{A}_n = \mathcal{A}_n^{\text{MHV}} + \mathcal{A}_n^{\text{NMHV}} + \mathcal{A}_n^{\text{N}^2\text{MHV}} + \dots + \overline{\mathcal{A}_n^{\text{MHV}}}, \quad (2.130)$$

where each  $\text{N}^{k'}$ MHV scattering amplitude is of Grassmann degree  $4(k' + 2)$ <sup>12</sup>. The actual scattering of particles states can be projected out so-called *component amplitudes* from the superamplitude by applying sequences of derivatives or integrations of the Grassmann-odd variables as follows. For instance for an MHV gluon scattering amplitude is extracted from the superamplitude as follows

$$\mathcal{A}_n(1^+ \dots i^- \dots j^- \dots n^+) = \left( \prod_{A=1}^4 \partial_{iA} \right) \left( \prod_{B=1}^4 \partial_{jB} \right) \mathcal{A}_n(\Phi_1, \dots, \Phi_n) |_{\eta_{kC}}, \quad (2.131)$$

where  $\partial_{iA} \equiv \frac{\partial}{\partial \eta_{iA}}$ . Since the supermultiplet  $\Phi$  transforms in the adjoint of  $SU(N)$  [45], we can repeat the analysis of section 2.4 to decompose the color degrees of freedom from the kinematic using the standard color decomposition at tree-level

$$\mathcal{A}_n^{\text{N}^{k-2}\text{MHV}}(\{p_i, h_i, a_i\}) = g^{n-2} \sum_{\sigma \in \mathcal{O}_n} \text{Tr}(T^{a_1} T^{a_{\sigma(2)}} \dots T^{a_{\sigma(n)}}) A_{n,k}(1^{h_1}, \sigma(2^{h_2}), \dots, \sigma(n^{h_n})), \quad (2.132)$$

and thus the amplitude relations (2.72) discussed in section 2.4 also holds for msYM. Supersymmetry demands that the superamplitude must be annihilated by the generators of supersymmetry

$$q^A \mathcal{A}_n = \tilde{q}_A \mathcal{A}_n = 0. \quad (2.133)$$

Which we can naturally satisfy if the superamplitude appear on the form taking  $k' = k - 2$  as follows

$$\mathcal{A}_n^{\text{N}^{k'}\text{MHV}} = \delta^{2 \times 4}(\tilde{q}) \mathcal{P}_n^{(4k')}, \quad (2.134)$$

where  $\mathcal{P}_n^{4k}$  is a degree- $4k$  polynomial of the Grassmann variables,  $\eta$ . We have defined the fermionic  $\delta$ -functions as follows

$$\delta^{2 \times 4}(\tilde{q}) = \frac{1}{2^4} \prod_{A=1}^4 \tilde{q}_{Aa} \tilde{q}_A^a = \frac{1}{2^4} \prod_{A=1}^4 \sum_{i < j=2}^n \langle ij \rangle \eta_{iA} \eta_{jA}. \quad (2.135)$$

<sup>12</sup>In this dissertation we shall encounter two helicity label conventions  $k$  and  $k'$ , where  $k = k' + 2$ , as  $k$  measures the actual helicity state of a scattering amplitude, while  $k'$  measure how far it is from the MHV state as in  $\text{N}^{k'}\text{MHV}$

Since  $\delta^{2 \times 4}(\tilde{q})$  is a degree-8 polynomial, all  $\eta$  dependence for the MHV amplitude is fixed and  $P^{(0)}$  is just a function of the external momenta. Since the component amplitude associated with 4-gluon scattering should match the Yang-Mills partial amplitudes, we can match the MHV partial superamplitude to be

$$A_{n,2}[1, \dots, n] = \frac{\delta^{(2 \times 4)}(\tilde{q})}{\langle 12 \rangle \langle 23 \rangle \dots \langle n1 \rangle}, \quad (2.136)$$

In particular, the MHV three-point function can be expressed as

$$A_{3,2}[1, 2, 3] = \frac{\delta^{(2 \times 4)}(\lambda_1 \eta_1 + \lambda_2 \eta_2 + \lambda_3 \eta_3)}{\langle 12 \rangle \langle 23 \rangle \langle 31 \rangle}. \quad (2.137)$$

We can find the  $\overline{\text{MHV}}$  three-point function by conjugation, exchanging  $\lambda$  with  $\tilde{\lambda}$  and  $\eta$  to  $\bar{\eta}$  in the MHV function to reach the  $\overline{\text{MHV}}$  amplitude in the anti-fundamental on-shell superspace (2.123) and then performing a Fourier transform on the anti-fundamental Grassmann variables  $\bar{\eta}$  to obtain the superamplitude in the standard on-shell superspace as follows

$$\begin{aligned} A_{3,1}[1, 2, 3] &= \int \prod_{i=1}^3 d^4 \bar{\eta} e^{i \sum_{i=1}^3 \eta_i^A \bar{\eta}_{iA}} \frac{\delta^{(2 \times 4)}(\tilde{\lambda}_1 \bar{\eta}_1 + \tilde{\lambda}_2 \bar{\eta}_2 + \tilde{\lambda}_3 \bar{\eta}_3)}{[12][23][31]} \\ &= \frac{\delta^{(1 \times 4)}([12]\eta_3 + [23]\eta_1 + [31]\eta_2)}{[12][23][31]}. \end{aligned} \quad (2.138)$$

Before moving on, we will briefly introduce the notion of non-chiral on-shell variables, which will be employed when introducing the momentum amplituhedron later. The idea of non-chiral on-shell supersymmetry is to bring the Grassmann-odd parameters,  $\eta_{iA}$ , with  $A = 1, \dots, 4$ , on the same footing as the spinor helicity variables  $(\lambda_i^a, \tilde{\lambda}_i^{\dot{a}})$  where  $(a, \dot{a}) = 1, 2$ . This is done by a half-Fourier transform on half of the  $\eta$ s e.g. the variables  $\eta_{i3}$  and  $\eta_{i4}$  [64]. This leads to the following set of Grassmann variables  $\eta^{r=1,2}$  and  $\tilde{\eta}^{\dot{r}=1,2}$ .

## 2.7 Super-BCFW Recursion for $\mathcal{N} = 4$ sYM

The maximally supersymmetric Yang-Mills theory is highly constrained by its inherent symmetries. Indeed, we shall provide a discussion on these exact symmetries in the next section 2.8, however for now, we wish to arm ourselves with some scattering amplitudes to make this discussion more concrete. In particular, we review how the BCFW recursion discussed in section 2.4 is naturally adapted to msYM. The extra condition of supermomentum conservation,  $\sum_i \lambda_i \eta_i = 0$ , implores us to modify the complex deformation in the BCFW shift (2.78), to account for the enhanced symmetry.

This is achieved by an accompanying shift of the Grassmann variables [37]. Taking for instance the  $[1, 2]$ -shift, we have

$$\hat{\tilde{\lambda}}_1 = \tilde{\lambda}_1 + z\tilde{\lambda}_2, \quad \hat{\lambda}_2 = \lambda_2 - z\lambda_1, \quad \hat{\eta}_{1A} = \eta_{1A} + z\eta_{2A}. \quad (2.139)$$

Using the same arguments as in section 2.3, we can express the recursion schematically as

$$A_{n,k} = \int d^4\eta_{\hat{P}} \hat{A}_{n_L, k_L} \frac{1}{P^2} \hat{A}_{n_R, k_R}, \quad (2.140)$$

where the integral over the shifted Grassmann variables automatically encodes the sum over all possible particles in our spectrum. These recursion relations can be solved analytically as was done in [65]. We will review the construction for MHV and NMHV amplitudes in the following.

### Super-BCFW Recursion for the MHV Sector

For the MHV sector we perform the  $[1, 2]$ -shift according to (2.139). In the case of proper  $z$  scaling, Cauchy's theorem (2.59) implores us to write

$$\begin{aligned} A_{n,2}[1, 2, \dots, n] &= \begin{array}{c} \hat{1} \\ \diagup \\ n \\ \vdots \\ \vdots \\ \vdots \\ \vdots \\ 4 \\ \diagdown \end{array} \hat{A}_{n-1}^{\text{MHV}} \xrightarrow{\hat{P}_{2,3}} \hat{A}_3^{\text{MHV}} \begin{array}{c} \hat{2} \\ \diagdown \\ 3 \end{array} \\ &= \int d^4\eta_{\hat{P}} \frac{1}{P^2} \hat{A}_{n-1,2}[\hat{1}, \hat{P}, 4, \dots, n] \hat{A}_{3,1}[-\hat{P}, \hat{2}, 3] \\ &= \int d\eta_{\hat{P}} \frac{1}{s_{23}} \frac{\delta^{(2 \times 4)}(\sum_{i \in L} \hat{\lambda}_i \hat{\eta}_i)}{\langle 1\hat{P} \rangle \langle \hat{P}4 \rangle \dots \langle n1 \rangle} \frac{\delta^{(1 \times 4)}([\hat{P}2]\eta_3 + [23]\eta_{\hat{P}} + [3\hat{P}]\eta_2)}{[\hat{P}2][23][3\hat{P}]}, \quad (2.141) \end{aligned}$$

where we have analytically continued  $\tilde{\lambda}_{-\hat{P}} = \tilde{\lambda}_{\hat{P}}$ . We have inductively inserted the MHV super-amplitude  $A_{n-1,2}$ . We can evaluate the integral by localizing the last  $\delta$ -function, we have

$$\delta^{(1 \times 4)}([\hat{P}2]\eta_3 + [23]\eta_{\hat{P}} + [3\hat{P}]\eta_2) = [23]^4 \delta^{(1 \times 4)} \left( \eta_{\hat{P}} + \frac{[\hat{P}2]\eta_3 + [3\hat{P}]\eta_2}{[23]} \right). \quad (2.142)$$

Inserting this solution into the remaining  $\delta$ -function, we obtain

$$\begin{aligned}
 \delta^{(2 \times 4)}\left(\sum_{i \in L} \hat{\lambda}_i \hat{\eta}_i\right) &= \delta^{(2 \times 4)}\left(\lambda_1 \tilde{\eta}_1 + \lambda_{\hat{P}} \eta_{\hat{P}} + \sum_{i=4}^n \lambda_i \eta_i\right) \\
 &= \delta^{(2 \times 4)}\left(\lambda_1 \tilde{\eta}_1 - \left(\frac{[\hat{P}2] \eta_3 + [3\hat{P}] \eta_2}{[23]}\right) \lambda_{\hat{P}} + \sum_{i=4}^n \lambda_i \eta_i\right) \\
 &= \delta^{(2 \times 4)}\left(\lambda_1 \tilde{\eta}_1 + \lambda_3 \eta_3 + \lambda_2 \eta_2 + \sum_{i=4}^n \lambda_i \eta_i\right) \\
 &= \delta^{(2 \times 4)}\left(\lambda_1 \eta_1 + \lambda_3 \eta_3 + \lambda_2 \eta_2 + \sum_{i=4}^n \lambda_i \eta_i\right), \quad (2.143)
 \end{aligned}$$

which is exactly the statement of supermomentum conservation for  $n$  supermomenta. The full integration just yields

$$\begin{aligned}
 A_{n,2}[1, 2, \dots, n] &= \int d^4 \eta_{\hat{P}} \hat{A}_{n-1,2}[\hat{1}, \hat{P}, 4, \dots, n] \frac{1}{s_{23}} \hat{A}_{3,1}[-\hat{P}, 2, 3] \\
 &= [23]^2 \frac{\delta^{(1 \times 4)}\left(\sum_{i=1}^n \lambda_i \eta_i\right)}{\langle 23 \rangle \langle 45 \rangle \dots \langle n1 \rangle} \frac{1}{\langle 1(\hat{2}+3)2 \rangle [3(\hat{2}+3)4]} \\
 &= \frac{\delta^{(1 \times 4)}\left(\sum_{i=1}^n \lambda_i \eta_i\right)}{\langle 23 \rangle \langle 45 \rangle \dots \langle n1 \rangle} \frac{1}{\langle 13 \rangle (\langle 24 \rangle - z \langle 14 \rangle)}. \quad (2.144)
 \end{aligned}$$

After evaluating  $z = \frac{\langle 23 \rangle}{\langle 13 \rangle}$  and applying the Schouten identity (2.32), we obtain the super Parke-Taylor formula

$$A_{n,2}[1, 2, \dots, n] = \frac{\delta^{(2 \times 4)}(\tilde{q})}{\langle 12 \rangle \langle 23 \rangle \dots \langle n1 \rangle}. \quad (2.145)$$

### Super-BCFW Recursion for the NMHV Sector

When moving beyond the MHV sector, more diagrams appear in the recursion. We can collect the diagrams into two types as follows

$$A_{n,3}[1, 2, \dots, n] = \sum_{m=5}^n \underbrace{\begin{array}{c} \hat{1} \\ \vdots \\ \overset{n}{\circlearrowleft} \hat{A}_{n-m-1,2} \text{---} \hat{P}_I \text{---} \hat{A}_{m-1,2} \overset{3}{\circlearrowright} \\ \underset{m}{\circlearrowright} \text{---} \text{---} \underset{m-1}{\circlearrowleft} \end{array}}_{\text{type A}} + \underbrace{\begin{array}{c} \hat{1} \\ \vdots \\ \overset{n}{\circlearrowleft} \hat{A}_{n-1,3} \text{---} \hat{P}_{2,3} \text{---} \hat{A}_{3,1} \overset{2}{\circlearrowright} \\ \underset{4}{\circlearrowright} \text{---} \text{---} \underset{3}{\circlearrowleft} \end{array}}_{\text{type B}}. \quad (2.146)$$

The first diagrams we assign to be of type A and involves two MHV functions, while the second type of diagrams, of type B, is only appearing for  $n \geq 6$  since the left

subamplitudes is NMHV and therefore requires at least 5 external legs. The first type of diagrams can be expressed as

$$\text{type A} = \int d^4\eta_{\hat{P}} \frac{\delta^{(2 \times 4)}(L)}{\langle \hat{1}\hat{P} \rangle \langle \hat{P}m \rangle \langle mm+1 \rangle \dots \langle n\hat{1} \rangle} \frac{1}{P^2} \frac{\delta^{(2 \times 4)}(R)}{\langle \hat{P}\hat{2} \rangle \langle \hat{2}3 \rangle \dots \langle m-1\hat{P} \rangle}, \quad (2.147)$$

where we write  $P = p_2 + p_3 + \dots + p_{m-1}$ . The  $\delta$ -functions are simply the statement of supermomentum conservation for each subdiagram, as follows

$$\delta^{(2 \times 4)}(L) = \delta^{(2 \times 4)}(-\lambda_{\hat{P}}\eta_{\hat{P}} + \lambda_{\hat{1}}\eta_{\hat{1}} + \sum_{r=m}^n \lambda_r\eta_r), \quad (2.148)$$

and

$$\delta^{(2 \times 4)}(R) = \delta^{(2 \times 4)}(\lambda_{\hat{P}}\eta_{\hat{P}} + \lambda_{\hat{2}}\eta_{\hat{2}} + \sum_{r=3}^{k-1} \lambda_r\eta_r). \quad (2.149)$$

We localize the integral by first combining these two  $\delta$ -functions to obtain

$$\delta^{(2 \times 4)}(L)\delta^{(2 \times 4)}(R) = \delta^{(2 \times 4)}(L+R)\delta^{(2 \times 4)}(R) = \delta^{(2 \times 4)}\left(\sum_{i=1}^n \lambda_i\eta_i\right)\delta^{(2 \times 4)}(R), \quad (2.150)$$

which is exactly the statement of supermomentum conservation times a remaining  $\delta$ -function, which we can write as

$$\delta^{(2 \times 4)}(R) = \frac{1}{\langle 1\hat{P} \rangle^4} \delta^{(1 \times 4)}(\langle 1\hat{P} \rangle\eta_{\hat{P}} + \langle 1\hat{2} \rangle\eta_{\hat{2}} + \sum_{r=3}^{m-1} \langle 1r \rangle\eta_r) \delta^{(1 \times 4)}(\langle \hat{P}\hat{2} \rangle\eta_{\hat{2}} + \sum_{r=3}^{m-1} \langle \hat{P}r \rangle\eta_r). \quad (2.151)$$

The only remaining dependence on  $\eta_P$  is thus in the first of these two  $\delta$ -functions, the integration over which simply yields a factor of  $\langle 1\hat{P} \rangle^4$ , canceling the Jacobian in (2.151). Since (2.147) only contains  $\eta_P$  dependence in the numerator, the denominator factorizes, and performing the integral therefore simply yields the following for the  $\delta$ -functions

$$\int d^4\eta_{\hat{P}} \delta^{(2 \times 4)}(L) \delta^{(2 \times 4)}(R) = \delta^{(2 \times 4)}(\tilde{q}) \delta^{(1 \times 4)}(\langle \hat{P}\hat{2} \rangle\eta_{\hat{2}} + \sum_{r=3}^{m-1} \langle \hat{P}r \rangle\eta_r). \quad (2.152)$$

We can use the  $\delta^{(2 \times 4)}(\tilde{q})$  to pull out a factor of  $A_{n,2}$  (2.145) to obtain

$$\text{Diagram A} = A_{n,2} \frac{\langle 12 \rangle \langle 23 \rangle \langle m-1m \rangle \delta^{(1 \times 4)}(\langle \hat{P}\hat{2} \rangle\eta_{\hat{2}} + \sum_{r=1}^{m-1} \langle \hat{P}r \rangle\eta_r)}{\langle m\hat{P} \rangle \langle m-1\hat{P} \rangle \langle \hat{2}\hat{P} \rangle \langle \hat{2}3 \rangle \langle 1\hat{P} \rangle P^2}. \quad (2.153)$$

We write this using the *dual* momenta variables, which we will return to in section 2.8, but for now only consider shorthand

$$x_{ij}^{a\dot{a}} = \sum_{r=i}^{j-1} \lambda_r^a \tilde{\lambda}_r^{\dot{a}}, \quad (2.154)$$

and

$$\theta_{ij,A}^a = \sum_{r=i}^{j-1} \lambda_r^a \eta_{rA}. \quad (2.155)$$

Then after several algebraic manipulations, we find the following expression for type A diagrams (2.153) after integration

$$\text{Diagram A} = A_{n,2} \frac{\langle 23 \rangle \langle m-1 \cdot m \rangle \delta^{(1 \times 4)} (\langle 1 | x_{1m} \cdot x_{m3} | \theta_{31} \rangle + \langle 1 | x_{13} \cdot x_{3m} | \theta_{m1} \rangle)}{x_{3m}^2 \langle 1 | x_{13} \cdot x_{3m} | m \rangle \langle 1 | x_{13} \cdot x_{3m} | m-1 \rangle \langle 1 | x_{1m} \cdot x_{m3} | 3 \rangle \langle 1 | x_{1m} \cdot x_{m3} | 2 \rangle}. \quad (2.156)$$

The factor multiplied by the MHV amplitude is called the  $R$ -invariant and is labeled by three indices,  $R_{13m}$ , and is defined as follows

$$R_{ijk} = \frac{\langle j-1j \rangle \langle k-1k \rangle \delta^{(1 \times 4)} (\Xi_{ijk})}{x_{jk}^2 \langle i | x_{ij} \cdot x_{jk} | k \rangle \langle i | x_{ij} \cdot x_{jk} | k-1 \rangle \langle i | x_{ik} \cdot x_{kj} | j \rangle \langle i | x_{ik} \cdot x_{kj} | j-1 \rangle}, \quad (2.157)$$

using the shorthand

$$\Xi_{ijk,A} = \langle i | x_{ik} \cdot x_{kj} | \theta_{ji,A} \rangle + \langle i | x_{ik} x_{kj} | \theta_{ki,A} \rangle, \quad (2.158)$$

where we have suppressed the  $A$  index in the  $\delta$ -function of (2.157). The choice of BCFW shift fixes the indices labeling the relevant  $R$ -invariants. For  $n = 5$ , only type-A diagrams with  $R_{135}$  contribute to the NMHV amplitude and we can write

$$A_{5,3} = A_{5,2} R_{135}, \quad (2.159)$$

while for  $n > 5$ , the type  $B$  diagrams simply recurses this formula and the result is remarkably simple [65]

$$A_{n,3} = A_{n,2} \times P_n^{(4)} = A_{n,2} \sum_{j=3}^{n-2} \sum_{k=j+2}^n R_{1jk}, \quad (2.160)$$

where  $P_n^{(4)}$  is the color-stripped Grassmannian polynomial of degree 4 defined in (2.134). We notice, that each  $R$ -invariant share the first index 1. This is a consequence of the choice of BCFW-shift, and we refer to this choice to have *anchored* leg 1. We could in general have anchored any external leg,  $m$ , by choosing the  $[m, m+1]$ -supershift.

## 2.8 Symmetries of $\mathcal{N} = 4$ sYM

The  $\mathcal{N} = 4$  sYM is a remarkably simple theory [37]. With that, we mean that the theory is highly constrained by a list of symmetries beyond Poincaré symmetry, introduced in the beginning of this chapter in section 2.2. These symmetries are listed below and are the *superconformal symmetry*, which together with the *dual superconformal symmetry* generates the infinite-dimensional symmetry algebra *Yangian* [66].

### 2.8.1 Superconformal symmetry

We split the symmetries of msYM into the bosonic and the supersymmetric sectors, starting with the bosonic. First, we have the generators of translations

$$p^{a\dot{a}} = \sum_{i=1}^n \lambda_i^a \tilde{\lambda}_i^{\dot{a}}, \quad (2.161)$$

which, together with Lorentz transformations constitutes the Poincaré group. The six generators of the Lorentz group read

$$m_{ab} = \sum_i \lambda_{i(a} \frac{\partial}{\partial \lambda_i^{b)}, \quad \tilde{m}_{\dot{a}\dot{b}} = \sum_i \tilde{\lambda}_{i(\dot{a}} \frac{\partial}{\partial \tilde{\lambda}_i^{\dot{b})} \quad (2.162)$$

as briefly discussed in (2.34). Furthermore in  $\mathcal{N} = 4$  sYM, we have supersymmetry generators for  $q^A$  and  $\tilde{q}_A$  explored in (2.133), enlarging the Poincaré group to the super-Poincaré group. The theory also respects a conformal symmetry, consisting of conformal boosts, dilatation, the  $SU(4)$   $R$ -symmetries, and the fermionic conformal supersymmetry generators [45]. Using the collective index  $\alpha = (a, \dot{a}, A)$ , we denote the generators of the group as  $G_\beta^\alpha$ , which is in the graded Lie algebra  $\mathfrak{su}(2, 2|4)$  [2]. The remaining generators can be written as

$$d = \sum_i \left( \frac{1}{2} \lambda_i^a \partial_{\lambda_i^a} + \frac{1}{2} \tilde{\lambda}_i^{\dot{a}} \partial_{\tilde{\lambda}_i^{\dot{a}}} + 1 \right), \quad (2.163)$$

$$r_A^B = \sum_i \left( \eta_{iA} \partial_{\eta_{iB}} - \frac{1}{4} \delta_A^B \eta_{iC} \partial_{\eta_{iC}} \right), \quad (2.164)$$

$$s_a^A = \sum_i \partial_{\lambda_i^a} \partial_{\eta_{iA}}, \quad \bar{s}_{\dot{a}A} = \sum_i \partial_{\tilde{\lambda}_i^{\dot{a}}} \partial_{\eta_{iA}}, \quad k_{a\dot{a}} = -\partial_{\lambda_i^a} \partial_{\tilde{\lambda}_i^{\dot{a}}}. \quad (2.165)$$

### Supertwistors

Clearly, the generators above appear with a certain number of derivatives from 0 in the case of the generator of translations,  $p^{a\dot{a}}$ , to 2 in the case of conformal boost  $k_{a\dot{a}}$ . This hints that another choice of variables might be available to make all the

generators act linearly. Indeed the *twistor* variables, first proposed by Penrose in [67], and the *supertwistor* variables later studied by Hodges [68] and Mason and Skinner [69], are precisely such a set of variables, linearising the generators of the conformal and superconformal group. The twistors can easily be constructed from the conventional spinor helicity variables, by way of a Fourier transform, as follows

$$\lambda_i^a \rightarrow i\partial_{\tilde{\mu}_{ia}}, \quad \partial_{\lambda_i^a} \rightarrow -i\tilde{\mu}_{ia}, \quad (2.166)$$

assuming split-Minkowski signature  $(+, +, -, -)$ . We notice, that the little group action on these new variables is simply  $\mu_i \rightarrow t_i^{-1}\mu_i$  and therefore we simply collect the supertwistor  $\mathcal{W}$ , such that

$$\mathcal{W}_i^\alpha = (\tilde{\mu}^a, \tilde{\lambda}^{\dot{a}}, \eta^A) \sim t_i^{-1}(\tilde{\mu}^a, \tilde{\lambda}^{\dot{a}}, \eta^A), \quad (2.167)$$

with the collective index  $\alpha = (a, \dot{a}, A)$ . The external data is now completely described by a projective vector, the *supertwistor* in  $\mathbb{CP}^{3|4}$  and in this formulation the generators of the superconformal groups simply become

$$G_\beta^\alpha = \sum_i (G_i)_\beta^\alpha = \sum_i \left( \mathcal{W}_i^\alpha \partial_{\mathcal{W}_i^\beta} - \frac{1}{4} \delta_\beta^\alpha \mathcal{W}_i^\gamma \partial_{\mathcal{W}_i^\gamma} \right). \quad (2.168)$$

Here the term  $\frac{1}{4} \delta_\beta^\alpha \mathcal{W}_i^\gamma \partial_{\mathcal{W}_i^\gamma}$  ensures that the bosonic subgroups  $SU(2)$  and  $SU(4)$  are traceless [45], and counts the degree of  $\mathcal{W}_i^A$  of whatever expression the generator is applied to. While we can write scattering amplitudes in twistor space, we are mainly interested in twistors as an illustration of how we can linearize the generators of superconformal symmetry. In the following, we will introduce the emergent *dual* superconformal symmetry and their associated dual-twistor formulation, the momentum twistors, which are particularly suited to discuss planar scattering amplitudes.

### 2.8.2 Dual Superconformal symmetry

As we saw in section 2.2, the choice of spinor helicity variables is very useful in the calculation of scattering amplitudes as they make the on-shell condition manifest. Momentum conservation has to be plugged in by hand, however, leading to a proliferation of  $\delta$ -functions in our calculations. In the end of the previous section, we encountered the supertwistors, linearising the superconformal symmetry group, and therefore placing all symmetries on the same footing. In this section, we shall see the emergence of the *dual* conformal invariance and proceed to generate a set of dual supertwistor variables.

In section 2.7, we introduced new shorthand variables  $x_{ij}^{a\dot{a}}$  and  $\theta_{ij,A}^a$  in (2.154) and in (2.155), we will now provide a few more details on their construction. The statement of momentum conservation  $p_1 + p_2 + \dots + p_n = 0$ , for an  $n$ -point scattering amplitude can be understood geometrically as a set of four-vectors forming a loop as sketched

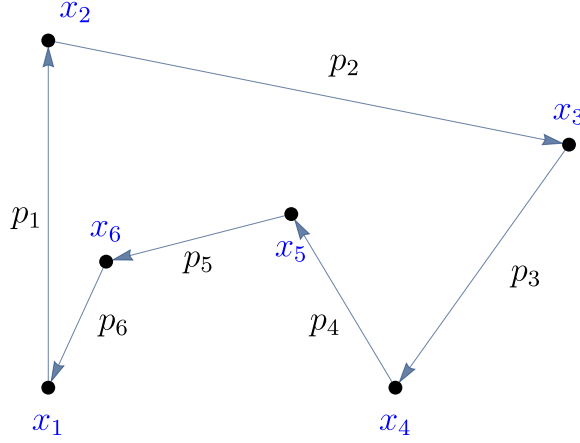


Figure 2.3: A two dimensional projection of the four momentum vectors in a scattering process. Momentum conservation restricts the shape to be a closed loop. We can either describe the loop using the variables associated with its edges (momenta) or the vertices (dual space coordinates)

on Figure 2.3. We can choose to describe this loop in terms of its edges (momenta) or its nodes. Choosing the latter define for us the *dual* momentum variables, subject to the following condition

$$x_i^{\dot{a}a} - x_{i+1}^{\dot{a}a} = p_i^{\dot{a}a} = \tilde{\lambda}_i^{\dot{a}} \lambda_i^a, \quad (2.169)$$

and similarly for the case of supermomentum conservation, we get

$$\theta_{i,A}^a - \theta_{i+1,A}^a = \lambda_i^a \eta_{i,A}, \quad (2.170)$$

making momentum conservation and supermomentum conservation manifest by simply identifying  $x_{n+1} = x_1$  and  $\theta_{n+1} = \theta_1$ . Of course, this is only valid for a scattering amplitude with a distinct ordering of external momentum. This means that we are restricting our discussion to a single partial superamplitude, or we can consider only the *planar* sector of msYM, where we can unambiguously define an ordering of consecutive external momenta.

We can easily express the tree-level MHV superamplitudes for msYM in dual coordinates as

$$A_{n,2} = \frac{\delta^4(x_1 - x_{n+1}) \delta^8(\theta_1 - \theta_{n+1})}{\langle 12 \rangle \langle 23 \rangle \cdots \langle n1 \rangle}, \quad (2.171)$$

and the NMHV superamplitude as

$$A_{n,3} = A_{n,2} \times P_n^{(4)} = A_{n,2} \sum_{j=2}^{n-3} \sum_{k=i+2}^{n-1} R_{njk}, \quad (2.172)$$

where the  $R$ -invariants are exactly the same as defined in (2.157)

$$R_{njk} = \frac{\langle j-1j \rangle \langle k-1k \rangle \delta^{(1 \times 4)}(\Xi_{njk})}{y_{jk}^2 \langle n|x_{nj} \cdot x_{jk}|k \rangle \langle n|x_{nj} \cdot x_{jk}|k-1 \rangle \langle n|x_{nk} \cdot x_{kj}|j \rangle \langle n|x_{nk} \cdot x_{kj}|j-1 \rangle}, \quad (2.173)$$

$$\Xi_{njk,A} = \langle n|x_{nk} \cdot x_{kj}|\theta_{jn,A} \rangle + \langle n|x_{nk} \cdot x_{jk}|\theta_{kn,A} \rangle, \quad (2.174)$$

where we have anchored the  $R$ -invariant with respect to leg  $n$  instead of 1 as in (2.157). The appearance of the superamplitudes in dual space as similar to their momentum-space counterparts, hints at a hidden symmetry – a superconformal symmetry for the dual coordinates, *the dual superconformal symmetry* [66]. We will discuss the bosonic sector of this symmetry presently. First and foremost, the  $x$  variables are naturally translation invariant, as can be seen from their definition in (2.169). Therefore, the scattering amplitude must be invariant under translations in the dual space [45]. Denoting the dual translation operator as  $P^\mu$ , we can express the generator of dual conformal boosts in terms of the dual translations and dual inversions [45]

$$K^\mu = I P^\mu I. \quad (2.175)$$

Therefore we should study of the scattering amplitudes act under dual inversion,  $I$ , in order to describe the dual conformal generators. The dual inversion acts as follows

$$I x_i^\mu = \frac{x_i^\mu}{x_i^2}, \quad I (\theta_i)_a^A = \frac{x_i^{Ab}}{x_i^2} (\theta_i)_b^A, \quad I (\tilde{\lambda}_i)_b = (\tilde{\lambda}_i)_a \frac{x_i^{ab}}{x_i^2}, \quad I (\lambda_i)_a = \frac{x_{i+1}^{ba}}{x_{i+1}^2} (\lambda_i)_a. \quad (2.176)$$

Applying the dual inversion operator to the MHV superamplitude for msYM, we obtain the following uniform scaling

$$I A_{n,2} = \left( \prod_{i=1}^n x_i^2 \right) A_{n,2} \quad (2.177)$$

Applying dual inversion to the  $R$ -invariants, however, we obtain that they are completely invariant under such transformations

$$I R_{njk} = R_{njk}, \quad (2.178)$$

and therefore the only contribution to the scaling of NMHV superamplitude under dual inversion is from the MHV superamplitude [45], as follows

$$I A_{n,3} = \left( \prod_{i=1}^n x_i^2 \right) A_{n,3}. \quad (2.179)$$

Since the superamplitude is not invariant under dual inversions, the dual conformal boost generator generates an ‘‘anomaly’’ term, as follows

$$K^\mu = I P^\mu I A_{n,k} = \left( - \sum_{i=1}^n x_i^\mu \right) A_{n,k}. \quad (2.180)$$

We can define the “shifted” dual conformal boost generator, which precisely annihilates the superamplitude as follows

$$\hat{K}^\mu A_{n,k} = \left( K^\mu + \sum_i x_i^\mu \right) A_{n,k} = 0. \quad (2.181)$$

Following a similar line of argument as above, we can list the generators of dual superconformal symmetry in its entirety [66]

$$\begin{aligned} P_\mu &= \sum_i \partial_{x_i^\mu}, & Q_{Aa} &= \sum_i \partial_{\theta_i^{Aa}}, & \bar{Q}_{\dot{a}}^A &= \sum_i \theta_i^a \partial_{\theta_i^{\dot{a}a}}, \\ K^{\dot{a}a} &= \sum_i \left( x_i^{\dot{a}b} x_i^{ba} \partial_{x_i^{bb}} + x_i^{\dot{a}b} \theta_i^{aB} \partial_{\theta_i^{\beta B}} + x_i^{\dot{a}b} \lambda_i^a \partial_{\lambda_i^b} \right), \\ D &= \sum_i \left( x_i^{\dot{a}a} \partial_{x_i^{\dot{a}a}} + \frac{1}{2} \left[ \theta_i^{aA} \partial_{\theta_i^{aA}} + \lambda_i^a \partial_{\lambda_i^a} \right] \right), & R_B^A &= \sum_i \left( \theta_i^{aA} \partial_{\theta_i^{aB}} - \frac{1}{4} \delta_B^A \theta_i^{aC} \partial_{\theta_i^{aC}} \right), \\ M_{ab} &= \sum_i \left( x_{i(a}^{\dot{a}} \partial_{x_i^{b)\dot{a}}} + \theta_{i(a}^A \partial_{\theta_i^{b)A}} + \lambda_{i(a} \partial_{\lambda_i^{b)}} \right), & \bar{M}_{\dot{a}b} &= \sum_i x_{i(\dot{a}}^a \partial_{x_i^{b)a}}, \\ S^{aA} &= \sum_i \left( \theta_i^{aB} \theta_i^{bA} \partial_{\theta_i^{\beta B}} + x_i^{ba} \theta_i^{bA} \partial_{x_i^{bb}} + \lambda_i^a \theta_i^{bA} \partial_{\lambda_i^b} \right), & \bar{S}_{\dot{a}}^A &= \sum_i x_i^{\dot{a}a} \partial_{\theta_i^{aA}}. \end{aligned} \quad (2.182)$$

Organizing these generators into  $j_a = \{P_{aa}, Q_{Aa}, \hat{Q}_{\dot{a}}^A, K^{\dot{a}a}, D, R_B^A, M_{ab}, \bar{M}_{\dot{a}b}, S^{aA}, \bar{S}_{\dot{a}}^A\}$ , then we have

$$j_a R_{nj k} = 0. \quad (2.183)$$

The dual superconformal generators are similar to the superconformal generators discussed in the beginning of this section 2.8, and thus constitutes another  $SU(2, 2|4)$  group. Together with the ordinary  $SU(2, 2|4)$  superconformal symmetry group, the two sets of generators spans an infinite dimensional algebra known as the *Yangian*. The generators of the Yangian are organized into levels. Taking  $\mathbf{A} = (\dot{a}, a, A)$ , the level-0 generators are as follows

$$\text{level } 0 : \quad \sum_{i=1}^n G_{i\mathbf{B}}^{\mathbf{A}}, \quad (2.184)$$

where  $G_{i\mathbf{B}}^{\mathbf{A}}$  is the set of superconformal generators defined in (2.168). We can construct the higher level generators

$$\text{level } 1 : \quad \sum_{i < j}^n (-1)^{|\mathbf{C}|} [G_{i\mathbf{C}}^{\mathbf{A}} G_{j\mathbf{B}}^{\mathbf{C}} - (i \leftrightarrow j)], \quad (2.185)$$

where  $|\mathbf{C}|$  is 0 when  $\mathbf{C} \in \dot{a}, a$  and 1 when  $\mathbf{C} \in A$ . A non-trivial observation [45] is that the *shifted* dual conformal boost generator belong to level 1. We can generate the higher level generators by repeated commutations and anti-commutations of level-0 and level-1 generators. For more details on the Yangian, we refer to the paper by Drummond, Henn, and Plefka [66].

### Supermomentum Twistors

We define a new set of variables using the so-called *incidence relations*

$$\mu_i^{\dot{a}} \equiv x_i^{\dot{a}a} \lambda_{ia} = x_i^{\dot{a}a} \lambda_{i+1a}, \quad (2.186)$$

and

$$\chi_i^A = \theta_i^{aA} \lambda_{ia} = \theta_{i+1}^{aA} \lambda_{ia}, \quad (2.187)$$

and collect them into the *supermomentum twistors* as follows

$$\mathcal{Z}_i^\alpha = (\lambda_i^a, \mu_i^{\dot{a}}, \chi_i^A), \quad (2.188)$$

with  $\alpha = (a, \dot{a}, A) = (1, \dots, 8)$ , scaling uniformly under little group transformations  $\mathcal{Z}_i^\alpha \sim t \mathcal{Z}_i^\alpha$ . This means that the momentum twistors are purely projective vectors in  $\mathbb{P}^{3|4}$  [1]. The momentum twistors are completely unconstrained and any choice of data is physically viable, which is a benefit when comparing numeric results. We can relate the momentum twistors to the spinor helicity variables through the incidence relations:

$$\tilde{\lambda}_i^{\dot{a}} = \frac{\langle i+1i \rangle \mu_{i-1}^{\dot{a}} + \langle ii-1 \rangle \mu_{i+1}^{\dot{a}} + \langle i-1i+1 \rangle \mu_i^{\dot{a}}}{\langle i-1i \rangle \langle ii+1 \rangle}, \quad (2.189)$$

and

$$\eta_i^A = \frac{\langle i+1i \rangle \chi_{i-1}^A + \langle ii-1 \rangle \chi_{i+1}^A + \langle i-1i+1 \rangle \chi_i^A}{\langle i-1i \rangle \langle ii+1 \rangle}. \quad (2.190)$$

Since the  $\lambda_i$  variables can just be read off from the first two entries of the supermomentum twistor,  $\mathcal{Z}_i^a = \lambda_i^a$ , for  $a = 1, 2$ , we can always translate back to the chiral on-shell spinor helicity variables. The bosonic part of the super-momentum twistors  $z^a$  carrying a dual conformal  $SU(2, 2)$  index  $\mathbf{a}$ . We can construct 4-brackets of  $z^a$

$$\begin{aligned} \langle ijkl \rangle = \epsilon_{abcd} z_i^a z_j^b z_k^c z_l^d = & \langle ij \rangle [\widehat{kl}] + \langle ik \rangle [\widehat{lj}] + \langle il \rangle [\widehat{jk}] + \\ & + \langle kl \rangle [\widehat{ij}] + \langle lj \rangle [\widehat{ik}] + \langle jk \rangle [\widehat{il}], \end{aligned} \quad (2.191)$$

where we have expanded the momentum twistors in terms of  $\langle ij \rangle = \epsilon_{ab} \lambda_i^a \lambda_j^b$  and  $[\widehat{ij}] = \epsilon_{ab} \mu_i^a \mu_j^b$ . We can express the planar Mandelstam variables

$$\begin{aligned} \langle j-1jk-1k \rangle = \langle j-1j \rangle \langle k-1|x_{k-1j}x_{jk}|k \rangle = \langle j-1j \rangle \langle k-1k \rangle x_{jk}^2 \\ \Rightarrow x_{jk}^2 = \frac{\langle j-1jk-1k \rangle}{\langle j-1j \rangle \langle k-1k \rangle}, \end{aligned} \quad (2.192)$$

where  $x_{jk} = x_j - x_k$ . In particular, we can express the  $R$ -invariants (2.157) of the previous section 2.6 in terms of supermomentum twistors as follows

$$R_{njk} = \frac{\langle j-1j \rangle^4 \langle k-1k \rangle^4 \delta^{(4)}(\Xi_{njk})}{\langle nj-1jk-1 \rangle \langle j-1jk-1k \rangle \langle jk-1kn \rangle \langle k-1knj \rangle \langle knj-1j \rangle} \quad (2.193)$$

while the argument of the delta function is

$$\Xi_{njk,A} = -\frac{[\langle j-1kk-1k \rangle \chi_{n,A}] + \text{cyclic}}{\langle j-1j \rangle \langle k-1k \rangle}, \quad (2.194)$$

again suppressing the index  $A$  in the  $\delta$ -function. Plugging this into the former expression we encode the  $R$ -invariants as so-called *five-bracket*

$$\begin{aligned} [nj-1jk-1k] := R_{njk} = \\ \frac{\delta^{1 \times 4}(\langle j-1jk-1k \rangle \chi_n + \text{cyclic})}{\langle nj-1jk-1 \rangle \langle j-1jk-1k \rangle \langle jk-1kn \rangle \langle k-1knj-1 \rangle \langle knj-1j \rangle}. \end{aligned} \quad (2.195)$$

We can then write the NMHV amplitude as

$$A_{n,3} = A_{n,2} \sum_{k=2}^{n-3} \sum_{k=j+2}^{n-1} [n, j-1, j, k-1, k]. \quad (2.196)$$

In general, it can be shown that  $N^{k-2}$ MHV superamplitude can be cast as a polynomial of five brackets times the MHV superamplitude [45].

## 2.9 Loops

In this section, we briefly touch upon loop corrections to scattering amplitudes. Here the notion of unitarity, in particular generalized unitarity, allows us to evaluate certain cuts on the amplitudes, basically probing the complex structure of the function. From standard quantum field theory [14], we have that each term in (2.5) can be put on the form

$$\mathcal{A}_n^{(L)} = \sum_j \prod_{l=1}^L \int \frac{d^D \ell_l}{(2\pi)^D} \frac{n_j}{\prod_{i \in n_{\text{int}}(j)} (D_i)^2}, \quad (2.197)$$

where  $j$  counts the number of Feynman diagrams,  $n_j$  is the numerator for the Feynman diagrams  $n_{\text{int}}(j)$  are the number of internal lines and  $D_i$  is the propagator associated with each internal line. Before discussing how to actually evaluate loop contributions to scattering amplitudes, let us remind ourselves of the color-decomposition of the one-loop scattering amplitudes: we discussed the color decompositions of tree-level scattering amplitudes in (2.65), where the scattering amplitude was decomposed a sum

over *partial* amplitudes multiplied by a trace over color matrices. Here, the partial amplitudes are planar with respect to the external ordering of particles. For one-loop contributions we have a similar decomposition, however we now obtain sub-leading terms with non-planar contributions [70]

$$\begin{aligned} \mathcal{A}_{n,k}^{(1)} &= g^n N \sum_{\sigma \in S_n / \mathbb{Z}_n} \text{Tr}(T^{a_1} T^{a_{\sigma(2)}} \dots T^{a_{\sigma(n)}}) A_{n,k}^{(1)}[\sigma(1^{h_1}, 2^{h_2}, \dots, n^{h_n})] \\ &\quad + g^n \sum_{c=3}^{\lfloor \frac{n}{2} \rfloor + 1} \sum_{\sigma \in S_n / S_{n,c}} \text{Tr}(T^{a_{\sigma(1)}} \dots T^{a_{\sigma(c)}}) \text{Tr}(T^{a_{\sigma(c+1)}} \dots T^{a_{\sigma(n)}}) (A_{n,k}^{(1)})_c, \end{aligned} \quad (2.198)$$

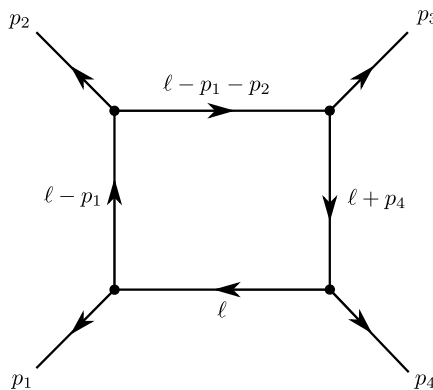
where  $S_{n,c}$  is some set of permutations leaving the product

$$\text{Tr}(T^{a_{\sigma(1)}} T^{a_{\sigma(2)}} \dots T^{a_{\sigma(c)}}) \text{Tr}(T^{a_{\sigma(c+1)}} T^{a_{\sigma(2)}} \dots T^{a_{\sigma(n)}}), \quad (2.199)$$

invariant. The non-planar contributions are sub-leading in the number of colors  $N$ , therefore it is common to take the *planar limit* of scattering amplitudes by considering  $\frac{1}{N} \rightarrow 0$ , keeping  $\lambda = g^2 N$  constant. This is known as the 't Hooft limit [71] and in this limit only planar diagrams contribute. This construction is generalized for all  $\ell$ , and planar  $\mathcal{N} = 4$  sYM refers to this specific limit of  $\mathcal{N} = 4$  sYM theory.

### 2.9.1 The Scalar Box Integral

In order to discuss the standard techniques for evaluating loop scattering amplitudes, we take as an example the scalar box integral relevant for the 1-loop corrections the scattering amplitudes in bi-adjoint  $\phi^3$  theory, discussed at tree level in section 2.5. The integral also has a non-obvious relevance to one-loop corrections to  $\mathcal{N} = 4$  sYM. We will return to this point in the end of this section. For now, we define the integral as



$$= \int \frac{d^D \ell}{(2\pi)^D} \frac{1}{\ell^2 (\ell - p_1)^2 (\ell - p_1 - p_2)^2 (\ell + p_4)^2}. \quad (2.200)$$

This can be expressed in the *Feynman representation* where we rewrite denominators appearing inside the integral as another integral

$$\begin{aligned} & \frac{1}{\ell^2(\ell - p_1)^2(\ell - p_1 - p_2)^2(\ell + p_4)^2} \\ &= \int dF_4 \frac{1}{(x_1\ell^2 + x_2(\ell^2 - p_1)^2 + x_3(\ell - p_1 - p_2)^2 + x_4(\ell + p_4)^2)^4} \\ &= \int dF_4 \frac{1}{(\ell^2 - 2\ell \cdot (p_1(x_2 + x_3) + x_3p_2 - x_4p_4) + x_3s_{12})^4}, \end{aligned} \quad (2.201)$$

where  $\int dF_4 = (n-1)! \int_0^1 dx_1 \int_0^{1-x_1} dx_2 \dots \int_0^{1-x_1-x_2-x_3} dx_4 \delta(1-x_1-x_2-x_3-x_4)$ . We can complete the square appearing in the denominator such that the integral becomes

$$\int dF_4 \frac{1}{(q^2 + \Delta)^4} \quad (2.202)$$

where we have changed variables from  $\ell$  to  $q$ , by way of

$$q = \ell - p_1(x_2 + x_3) - p_2x_3 + p_4x_4, \quad (2.203)$$

$$\Delta = (s_{23}x_2x_4 - s_{12}x_1x_3), \quad (2.204)$$

found from completing the square in (2.201) and using  $s_{12} + s_{23} + s_{13} = 0$ . We can now perform the space-time integration

$$\text{Box}_4 = \int \frac{d^D q}{(2\pi)^D} \int dF_4 \frac{1}{(q^2 + (tx_2x_4 - sx_1x_3))^4}. \quad (2.205)$$

The space-time integral over  $d^4 q$  can be performed using a *Wick rotation*, such that we go from a Minkowskian integral to an Euclidian integral. The Wick rotation rotates the contour integration of the  $q^0$  complex plane, which is justified if the new contour does not contain additional singularities [15]. Writing the propagators in (2.197) as  $D_i \rightarrow D_i + i\epsilon$  and keeping track of the  $i\epsilon$  factors in the integration, we note there are two poles in the complex  $q_0$  plane, but none in the  $(+, +)$  quadrant or the  $(-, -)$  quadrant, allowing us to rotate the contour counterclockwise by  $90^\circ$ , equivalent to substituting

$$q^0 = iq_E^0, \quad q^{i=1\dots 3} = \vec{q}_E, \quad (2.206)$$

into the expression

$$\text{Box}_4 = \int \frac{d^D q_E}{(2\pi)^D} dF_4 \frac{1}{(q_E^2 + \Delta)^4}. \quad (2.207)$$

The Euclidian integral over  $q_E$  is only dependent on the magnitude of  $q_E$ ; we can therefore perform the integration over the  $D$ -sphere first

$$\text{Box}_4 = \int \frac{d\Omega_D}{(2\pi)^D} \int_0^\infty dq_E \int dF_4 \frac{q_E^{D-1}}{(q_E^2 + \Delta)^4}. \quad (2.208)$$

The volume integral of the  $D$  dimensional sphere is simply

$$\int d\Omega_D = \frac{2\pi^{D/2}}{\Gamma(D/2)}, \quad (2.209)$$

which we substitute into the expression (2.208) to find

$$\text{Box}_4 = \frac{1}{2} \frac{2\pi^{D/2}}{\Gamma(D/2)} \int dF_4 \int_0^\infty d(q_E^2) \frac{(q_E^2)^{D/2-1}}{(q_E^2 + \Delta)^4}. \quad (2.210)$$

Performing the remaining integration, we obtain

$$\text{Box}_4 = \int dF_4 \frac{\Gamma(5 - D/2)\Gamma(D - 1)}{(4\pi)^{D/2}\Gamma(4)\Gamma(D/2)} \Delta^{-(5-D/2)}. \quad (2.211)$$

Now, we just need to evaluate the remaining integral over  $\int dF_4$ . The integral is divergent in  $D = 4$  dimensions, so we are required to regularize it. We make the standard choice of dimensional regularization [15] by choosing to evaluate the integral in  $D = 4 + 2\epsilon$  dimensions. Expanding in  $\epsilon$ , we obtain the following result for the scalar box integral

$$\begin{aligned} \text{Box}_4 &= \int dF_4 \frac{\Gamma(1 - \epsilon)\Gamma(3 - 2\epsilon)}{(4\pi)^{2+\epsilon}\Gamma(4)\Gamma(2 + \epsilon)} (-s_{23}x_2x_4 - s_{12}x_1x_3)^{-1+\epsilon} \\ &= \left( \frac{2}{\epsilon^2} [(-s_{12})^{-\epsilon} + (-s_{23})^{-\epsilon}] - \log \frac{s_{12}}{s_{23}} - \pi^2 \right) + O(\epsilon). \end{aligned} \quad (2.212)$$

## 2.9.2 Generalized Unitarity

The scalar box integral is just one Feynman diagram out of many required to determine the full one loop scattering amplitude for the bi-adjoint  $\phi^3$  theory described earlier in this chapter. So even after the efforts of the previous section, we still have a long ways ahead before we have the full contribution to the scattering amplitude, let alone the scattering amplitude in  $\mathcal{N} = 4$  sYM. We therefore discuss the method of *generalized unitarity*, where the integral we just performed plays a large part. The method was first developed by Bern et al [27] in the 1990's. The general idea is to harness the power of unitarity to recycle information about tree-level scattering amplitudes into loop level calculations as in (2.14). The way we are going to apply this principle is by considering the  $\mathbb{R}^{3,1}$  loop integrals on subspaces defined by certain propagators going on-shell, e.g. we could study the integral (2.200) on the subspace defined by

$$\ell^2 = (\ell - p_1 - p_2)^2 = 0. \quad (2.213)$$

We refer to taking  $m$  loop momenta on-shell as an *m-cut*, for instance the above cut is a 2-cut. On this subspace, the box-integrand becomes singular and the sum of residues

from all integrands is equal to the products of two on-shell amplitudes with some of the legs being the external legs of the one-loop amplitudes while others are *internal* and therefore integrated over and all possible helicity configurations are summed. This has two powerful uses: first, if one hands us a function and claims it is a one-loop integrand, we can verify it by taking residues on the loop variables and observing the factorization into products of tree-level amplitudes, second, if we already know a complete basis of integrals that can appear in the one-loop scattering amplitudes, we can use this fact to *bootstrap* the full amplitude. For instance, we expand a one-loop amplitude in a basis of *scalar integrals* like the one evaluated earlier, as follows

$$A_n^{(1)} = \sum_i C_D^{(i)} I_D^{(i)} + \sum_j C_{D-1}^{(j)} I_{D-1}^{(j)} + \dots + \sum_k C_2^{(k)} I_2^{(k)}. \quad (2.214)$$

Here we have expanded the amplitude in terms of  $m$ -gon integrals, where  $2 \leq m \leq D$ , with  $D$  denoting the space-time dimension, as there are only  $D$  independent vectors in  $D$  dimensions. The universal scalar integrands are much easier to evaluate than Feynman integrals in specific theories and the problem of evaluating the one-loop amplitude becomes a matter of determining the coefficients  $C_m$  of the  $m$ -gon integrals. Let us consider a simple example, making use of the box-integral evaluated in the previous section 2.9.

Consider the 4-point 1-loop superamplitude in  $D = 4$  [45]. We consider the two-cut, associated with putting two internal propagators on-shell as illustrated in the following

$$\text{cut}_s \left( A_{4,2}^{(1)} \right) = \begin{array}{c} \text{Diagram: Two vertices } A_4^{(0)} \text{ connected by two internal lines } \ell_1 \text{ and } \ell_2. \text{ External legs } 1, 2, 3, 4 \text{ are attached to the vertices.} \end{array} = \int d\mu_4 A_{4,2}[-\ell_1, 1, 2, \ell_2] \times A_{4,2}[-\ell_2, 3, 4, \ell_1], \quad (2.215)$$

with  $d\mu_4 := d^4\ell_1 d^4\eta_{\ell_1} d^4\ell_2 d^4\eta_{\ell_2} \delta^+(\ell_1^2) \delta^+(\ell_2^2) \delta^4(\ell_1 + \ell_2 + p_1 + p_2)$ . We can simply evaluate these expressions using (2.145) to

$$A_4[-\ell_1, 1, 2, \ell_2] = \frac{\delta^{(2 \times 4)}(q_L)}{\langle \ell_1 1 \rangle \langle 1 2 \rangle \langle 2 \ell_2 \rangle \langle \ell_2 \ell_1 \rangle}, \quad (2.216)$$

$$A_4[-\ell_2, 3, 4, \ell_1] = \frac{\delta^{(2 \times 4)}(q_R)}{\langle \ell_2 3 \rangle \langle 3 4 \rangle \langle 4 \ell_1 \rangle \langle \ell_1 \ell_2 \rangle}, \quad (2.217)$$

with  $q_L = -\lambda_{\ell_1} \eta_{\ell_1} + \lambda_1 \eta_1 + \lambda_2 \eta_2 + \lambda_{\ell_2} \eta_{\ell_2}$  and  $q_R = -\lambda_{\ell_2} \eta_{\ell_2} + \lambda_3 \eta_3 + \lambda_4 \eta_4 + \lambda_{\ell_1} \eta_{\ell_1}$ . The remaining integration in (2.215) is over Grassmann variables and is evaluated to

$$\begin{aligned} \text{cut}_s \left( A_{4,2}^{(1)} \right) &= \frac{1}{\langle 1 2 \rangle \langle 3 4 \rangle} \int d^4\eta_{\ell_1} d^4\eta_{\ell_2} \frac{\delta^{(2 \times 4)}(q_L) \delta^{(2 \times 4)}(q_R)}{\langle \ell_1 1 \rangle \langle 2 \ell_2 \rangle \langle \ell_2 3 \rangle \langle 4 \ell_1 \rangle \langle \ell_1 \ell_2 \rangle} \\ &= -\frac{\delta^{(2 \times 4)}(q)}{\langle 1 2 \rangle \langle 3 4 \rangle} \frac{\langle \ell_1 \ell_2 \rangle^2}{\langle \ell_1 1 \rangle \langle 2 \ell_2 \rangle \langle \ell_2 3 \rangle \langle 4 \ell_1 \rangle}, \end{aligned} \quad (2.218)$$

where we have used

$$\delta^{(2 \times 4)}(q_L) \delta^{(2 \times 4)}(q_R) = \delta^{(2 \times 4)}(q_L + q_R) \delta^{(2 \times 4)}(q_R) = \delta^{(2 \times 4)}(q) \delta^{(2 \times 4)}(q_R), \quad (2.219)$$

where  $q^{aA} = \sum_i \lambda_i^a \eta_i^A$  is the standard statement of supermomentum conservation, and the Grassmann integral is just localized by the remaining  $\delta$ -function. We can factor out a copy of the tree level amplitude  $A_4(1, 2, 3, 4)$

$$\text{cut}_s \left( A_{4,2}^{(1)} \right) = A_{4,2}[1, 2, 3, 4] \frac{\langle 23 \rangle \langle 14 \rangle \langle \ell_1 \ell_2 \rangle^2}{\langle \ell_1 1 \rangle \langle 2 \ell_2 \rangle \langle \ell_2 3 \rangle \langle 4 \ell_1 \rangle}. \quad (2.220)$$

We can compare this to the cut on the double box discussed in the last section (2.200), as evaluated in the example in the last section

$$\text{cut}_s(\text{Box}_4) = \int d\mu_4 \frac{1}{(\ell_1 + p_4)^2 (\ell_2 + p_2)^2} = \int d\mu \frac{1}{\langle \ell_1 4 \rangle [\ell_1 4]} \frac{1}{\langle \ell_2 2 \rangle [\ell_2 2]}. \quad (2.221)$$

Comparing to (2.220), we can see that

$$\begin{aligned} \frac{\langle 23 \rangle \langle 14 \rangle \langle \ell_1 \ell_2 \rangle^2}{\langle \ell_1 1 \rangle \langle 2 \ell_2 \rangle \langle \ell_2 3 \rangle \langle 4 \ell_1 \rangle} &= \frac{1}{(\ell_1 + p_4)^2 (\ell_2 + p_2)^2} \frac{\langle \ell_1 \ell_2 \rangle^2 \langle 23 \rangle \langle 14 \rangle [\ell_1 4] [\ell_2 2]}{\langle \ell_1 4 \rangle \langle \ell_2 2 \rangle} \\ &= \frac{s_{23} s_{34}}{(\ell_1 + p_4)^2 (\ell_2 + p_2)^2}, \end{aligned} \quad (2.222)$$

after making repeated use of the Schouten identity (2.32). This means the  $s$ -channel singularity structure of the one-loop scattering amplitude is totally encapsulated in the box integral and we have evaluated

$$\text{cut}_s \left( A_{4,2}^{(1)} \right) = s_{23} s_{34} A_{4,2} \text{cut}_s(\text{Box}_4). \quad (2.223)$$

An important result, that we will not review here (see [58] or [45]), is that this is the *only* contribution to the one-loop amplitude, and the full one-loop amplitude in  $\mathcal{N} = 4$  sYM for  $n = 4$ ,  $k = 2$  is simply

$$\begin{aligned} A_{4,2}^{(1)} &= s_{23} s_{34} A_{4,2}[1, 2, 3, 4] \text{Box}_4(p_1, p_2, p_3, p_4) \\ &= \frac{\delta^{(2 \times 4)}(q)}{\langle 12 \rangle \langle 23 \rangle \langle 34 \rangle \langle 14 \rangle} \times \left( \frac{2}{\epsilon^2} [(-s)^{-\epsilon} + (-t)^{-\epsilon}] - \log \frac{s}{t} - \pi^2 \right) + O(\epsilon). \end{aligned} \quad (2.224)$$

Interestingly, this also contributes to the  $n = 4$  point scattering amplitude at one-loop in standard Yang-Mills theory; however, in this case we also get contributions from triangles, bubbles and rational parts, as per (2.214).



# Chapter 3

## The Grassmannian

In this chapter, we will review the *Grassmannian* and in particular the *positive* Grassmannian. Both spaces have deep connections to scattering amplitudes and the geometric constructions to be introduced in the following chapters. We will start from a treatment of projective spaces, in order to build up a basic intuition about these kinds of spaces. We will then proceed to discuss the Grassmannian, including its different representations as on-shell diagrams and permutations. We then introduce the *positive* Grassmannian. As we shall see, by invoking the seemingly innocuous criteria of positivity of the Plücker variables of the Grassmannian, we obtain a rich geometric structure, interpreted as a generalization of the projective simplex. Afterwards, we will discuss the boundary structure of the positive Grassmannian in terms of *positroid cells*, and review the invariant differential form associated with the top-dimensional element of the positive Grassmannian. We then return to scattering amplitudes in msYM, introduced in the previous chapter, and review their connection to the positive Grassmannian. In particular, we review their representation as on-shell diagrams, as well as how we can construct the on-shell diagrams for all scattering amplitudes by the BCFW construction. We will also discuss how to represent tree-level scattering amplitudes and all  $\ell$ -loop integrands as Grassmannian integrals. For further reading on the Grassmannian, and in particular, its relation to scattering amplitudes, we refer to the book “Grassmannian Geometry of Scattering Amplitudes” by Arkani-Hamed, Bourjaily, Cachazo, Goncharov, Postnikov, and Trnka [72].

The *Grassmannian*, denoted  $G(k, n)$ , is defined as the space of  $k$  planes in  $n$  dimensions. This can be seen as a generalization of the *projective space*, the space of lines in  $n$  dimensions. We have already encountered an example of projectivity in section 2.8, where supertwistors and the supermomentum twistors are defined up to linear rescaling, and thus can be seen as points in projective space. Let us initiate our discussion by reviewing projective spaces, in general.

### 3.1 Projective Space

The complex projective  $n$ -dimensional space,  $\mathbb{CP}^n$ , is defined as the space of lines in  $n$  complex dimensions through the origin. This can be phrased as the space of non-zero  $n$ -dimensional complex vectors defined up to an equivalence relation, as follows

$$u \sim v \quad \text{iff} \quad v = \lambda u, \quad (3.1)$$

where  $u, v \in \mathbb{C}_{\neq 0}^n$  are non-zero complex  $(n+1)$ -vectors, and  $\lambda \in \mathbb{C}_{\neq 0}$  is some non-zero complex number. We refer to all vectors up to this equivalence class as *points*. The coordinates of  $u$  are referred to as homogeneous coordinates. We can relate a point in  $\mathbb{CP}^n$  to a point in  $\mathbb{C}^n$ , the standard non-projective *affine* space, as follows. For a given vector  $u^A \equiv (u_0, u_1, \dots, u_n)^T \in \mathbb{CP}^n$ , we have

$$\begin{pmatrix} u_0 \\ u_1 \\ \vdots \\ u_n \end{pmatrix} \sim u_0^{-1} \begin{pmatrix} u_0 \\ u_1 \\ \vdots \\ u_n \end{pmatrix} \equiv \begin{pmatrix} 1 \\ z_1 \\ z_2 \\ \vdots \\ z_n \end{pmatrix}. \quad (3.2)$$

Here we have defined

$$z_i \equiv \frac{u_i}{u_0}. \quad (3.3)$$

This new vector  $z^a \equiv (z_1, \dots, z_{n-1}) \in \mathbb{C}^n$  is just a point in the affine complex space. Going from a point in  $\mathbb{CP}^n$  to a point in  $\mathbb{C}^n$  amounts to choosing a coordinate patch in  $\mathbb{CP}^n$ , equivalent to intersecting the space of lines with a  $(n-1)$ -dimensional hyperplane localizing the coordinates. We note that a given patch will not cover all points of  $\mathbb{CP}^n$ , specifically the points with  $u_0 = 0$  do not have a representation in the affine space and are referred to as “points at infinity” in  $\mathbb{CP}^n$ .

The most general coordinate transformations in this space are  $SL(n)$ -transformations, generic transformations by an  $n \times n$  matrix with unit determinant, since a generic transformation

$$u' = L \cdot u, \quad (3.4)$$

scales the homogeneous coordinates of the point  $u'$  by  $\det L$ , which is the same point according to (3.1). This ensures that  $\mathbb{CP}^1$  is diffeomorphic to a Riemann sphere, as can be seen by applying arbitrary  $SL(2)$  transformations on a point in  $\mathbb{CP}^1$  as follows. Take  $u^I = (u^0 \ u^1)^T$  and take

$$u'^J = M_I^J u^I = \begin{pmatrix} a & b \\ c & d \end{pmatrix} \begin{pmatrix} u^0 \\ u^1 \end{pmatrix} = \begin{pmatrix} au^0 + bu^1 \\ cu^0 + du^1 \end{pmatrix}, \quad (3.5)$$

then choosing the coordinate patch where  $u^0 = 1$ , we obtain

$$\begin{pmatrix} 1 \\ z \end{pmatrix} \rightarrow \begin{pmatrix} a + bz \\ c + dz \end{pmatrix} \sim (a + bz) \begin{pmatrix} 1 \\ \frac{c+dz}{a+bz} \end{pmatrix}. \quad (3.6)$$

If  $\det M = 1$ , this amounts to a Möbius transformation characteristic of the Riemann sphere briefly discussed in section 2.5. Since we can always rescale each point by a complex constant, we cannot meaningfully define distance on  $\mathbb{CP}^n$ . Therefore the only meaningful  $SL(n+1)$  tensor we can define, is the Levi-Civita tensor,  $\epsilon_{I_0 I_1 \dots I_n}$ . Full contraction of  $n+1$  points using the Levi-Civita tensor is interpreted as a statement of collinearity, that is, for  $n$  points  $X_0^I, \dots, X_n^I$ , we interpret the quantity

$$\epsilon_{I_0 I_1 \dots I_n} X_0^{I_0} X_1^{I_1} \dots X_n^{I_n} = 0, \quad (3.7)$$

to mean that the points  $X_0, \dots, X_n$  inhabit the same hyperplane. As a consequence of this, in projective spaces *all lines intersect!*, with lines that we would label as parallel in the euclidean space intersecting at the point at infinity.

## 3.2 The Grassmannian

The Grassmannian,  $G(k, n)$ , is the space of  $k$ -hyperplanes in  $n$  complex dimensions through the origin [72]. We represent a point in the Grassmannian  $C \in G(k, n)$  as a  $(k \times n)$ -matrix

$$G(k, n) \ni C \in M(k, n) / \sim, \quad (3.8)$$

where the equivalence class is

$$C \sim C' \quad \text{iff} \quad C' = \Lambda \cdot C, \quad (3.9)$$

where  $\Lambda \in M(k, k)$ , is a  $(k \times k)$ -matrix, representing a complex general linear transformation,  $GL(k)$ . The Grassmannian can be seen as a generalization of the (complex) projective space by the following identification  $G(1, n) = \mathbb{CP}^{n-1}$ . A generic point in the Grassmannian can be seen to have dimensionality

$$\dim G(k, n) = n \times k - k^2 = (n - k)k, \quad (3.10)$$

as the dimensionality of a  $n \times k$  matrix minus the redundancy of  $GL(k)$ , the set of generic  $k \times k$  matrices. We can fix the  $GL(k)$  redundancy by fixing a  $k \times k$  submatrix of  $C$  to the identity matrix. A standard choice is

$$C = \begin{pmatrix} 1 & 0 & \dots & 0 & c_{1k+1} & c_{1k+2} & \dots & c_{1n} \\ 0 & 1 & \dots & 0 & c_{2k+1} & c_{2k+2} & \dots & c_{2n} \\ \vdots & \vdots & \ddots & \vdots & \vdots & \vdots & & \vdots \\ 0 & 0 & \dots & 1 & c_{kk+1} & c_{kk+2} & \dots & c_{kn} \end{pmatrix}, \quad (3.11)$$

where we have fixed the first  $k \times k$ -submatrix to the identity matrix. We realize, that we cannot cover the complete Grassmannian manifold in this coordinate chart, however the collection of  $\binom{n}{k}$  coordinates charts, represented by fixing different  $k \times k$  submatrices to the identity, suffices to cover the entire Grassmannian [72]. The invariant information of  $G(k, n)$  is stored in the *Plücker* coordinates. Denoting the columns of  $c_a \in C$ , we identify a  $k$ -element subset  $I \in [n] = \{1, 2, \dots, n\}$  and we define the Plücker coordinates as

$$(I) \equiv \det C_I = \det c_{I_1} c_{I_2} \cdots c_{I_k}. \quad (3.12)$$

Applying an arbitrary  $GL(k)$  transformation to  $C$ , represented by multiplying with a  $k \times k$  matrix  $\Lambda$ , rescales each Plücker coordinate with the homogeneous weight as

$$C \rightarrow \Lambda \cdot C \quad \Rightarrow \quad (I) \rightarrow \det(\Lambda)(I) \quad \forall \quad I \in [n]. \quad (3.13)$$

Therefore the  $GL(k)$  invariant data appear as *ratios* of Plücker coordinates and a set of relations between Plücker coordinates must exist [72], giving rise to this redundancy. The set of relations is called *Cramer's rule* and is simply the statement that any  $k$ -vector can be expanded in a basis of  $k$  independent  $k$ -vectors, as follows

$$c_{a_1}(a_2 \cdots a_{k+1}) - c_{a_2}(a_1 a_3 \cdots a_{k+1}) + \dots + (-1)^k c_{a_{k+1}}(a_1 \cdots a_k). \quad (3.14)$$

We have already seen (3.14) in section 2.3 in equation (2.32) for  $k = 2$  where we referred to it as the *Schouten Identity*, where we implicitly took  $\lambda \in G(2, n)$ . We will return to this choice in section 3.4.

Throughout this dissertation, we will make use of the *orthogonal complement* of the matrix  $C \in G(k, n)$ , the existence of which exploits the natural isomorphism between  $G(k, n)$  and  $G(n - k, n)$ , reflected in their dimensionality (3.10). We define the orthogonal complement as the matrix  $C^\perp$ , such that

$$C^\perp \cdot C = 0, \quad (3.15)$$

up to a  $GL(n - k)$  transformation. For further details on the orthogonal complement, we refer to the Appendix A, where we specify how to extract Plücker coordinates of  $C^\perp$  from the Plücker coordinates on  $C$ .

A generic point in the Grassmannian,  $C \in G(k, n)$ , is represented by a matrix  $C$  with none of its Plücker coordinates vanishing, having precisely  $k(n - k)$  degrees of freedom, as discussed above. If a single Plücker coordinate vanishes, we have certain linear relations between the columns,  $c_a \in C$ , due to Cramer's rule (3.14). We consider a stratification of  $G(k, n)$  in terms of consecutive Plücker coordinates, called the *positroid stratification* of the Grassmannian,  $G(k, n)$ . We refer to the stratifying subvarieties of  $G(k, n)$  as *cells* represented by matrices of ranks  $k$  to  $k(n - k)$ , the generic element of the Grassmannian. We organize the positroid cells by rank into a

partial ordered set – a poset.

In this dissertation, we are going to be interested in defining differential forms on Grassmannian spaces. A generic top-form on  $G(k, n)$  can be written as follows

$$\Omega = \frac{d^{k \times n} C}{\text{vol}(GL(k))} \frac{1}{f(C)}. \quad (3.16)$$

Since we require the differential top-form to scale homogeneously under  $GL(k)$  transformations, we have that  $f(C)$  must be a function scaling as

$$f(\Lambda \cdot C) = \Lambda^{k \times n} f(C). \quad (3.17)$$

We can write (3.16) on a  $GL(k)$  invariant form by the *rows* of  $C$ ,  $C_\alpha$

$$\Omega = \langle C_1 \cdots C_k d^{(n-k)} C_1 \rangle \cdots \langle C_1 \cdots C_k d^{(n-k)} C_k \rangle \frac{1}{f(C)}, \quad (3.18)$$

where we define

$$\langle C_1 \cdots C_k d^{(n-k)} C_\alpha \rangle = \epsilon^{a_1 a_2 \cdots a_n} c_{1 a_1} \cdots c_{k a_k} d c_{1 a_{k+1}} \wedge \cdots \wedge c_{1 a_n}, \quad (3.19)$$

with  $\alpha = 1, \dots, k$ .

### 3.2.1 Grassmannians as permutations

We can associate a *permutation* to each element of  $G(k, n)$  defined as follows [72]: for each  $a \in [n]$ , the permutation  $\sigma(a) \geq a$  labels the first column  $c_{\sigma(a)} \in C$ , for which

$$c_a \in \text{span} \{c_{a+1}, \dots, c_{\sigma(a)}\}. \quad (3.20)$$

In particular we notice that if the column is empty,  $c_a = \vec{0}$ , then the permutation  $\sigma(a) = 0$ , since the vector  $\vec{0}$  is spanned by the empty consecutive chains of columns “ $\{c_{a+1}, \dots, c_a\}$ ”. We will in the following make use of *decorated* permutations where we add  $n$  to each  $\sigma$  if  $\sigma(i) < i$ . For instance, we can label a generic point  $C \in G(2, 4)$  with no vanishing Plücker coordinates as the permutation  $\sigma = \{3, 4, 5, 6\}$ , meaning that the columns  $c_1 \in \text{span}\{c_2, c_3\}$ ,  $c_2 \in \text{span}\{c_3, c_4\}$ ,  $c_3 \in \text{span}\{c_4, c_1\}$ , and  $c_4 \in \text{span}\{c_1, c_2\}$ . It is natural that this decorated permutation is associated with the generic element in  $G(2, 4)$ , since Cramer’s rule dictates that any two-vector can be expressed linearly in terms of any two independent two-vectors. Taking the Plücker coordinate  $(12) = 0$  in  $G(2, 4)$ , we have by Cramer’s rule

$$(13)(24) = (23)(14) + (34)(12) \xrightarrow{(12)=0} (13)(24) = (23)(14). \quad (3.21)$$

Therefore we must have the decorated permutation  $\sigma' = \{2, 4, 5, 7\}$  when  $(12) = 0$ , since the column  $c_1$  is now collinear with  $c_2$ , while the column  $c_4 \in \text{span}\{c_1, c_2, c_3\}$ . The

number of degrees of freedom of the configuration associated with this permutation is simply given by  $k(n - k) - 1 = 3$ . For a generic permutation, one can read off the dimension of the given positroid cell by

$$\dim C_\sigma = \left( \sum_{a=1}^n r[a; \sigma(a)] \right) - k^2, \quad (3.22)$$

where we denote by  $r[a; b] \equiv \text{rank}\{c_a, c_{a+1}, \dots, c_b\}$ , and we subtract  $k^2$  representing the  $GL(k)$  redundancy. There exists a method of extracting  $r[a; b]$  from so-called “hook diagrams”. We will not review this construction here, but refer to [72] for more details. We can easily read off  $k$  from a given permutation as the number of elements,  $a$ , in the permutation  $\sigma$  for which  $\sigma(a) > a$ . We classify the points of  $G(k, n)$  according to decorated permutation  $\sigma$  as the disjoint union

$$G(k, n) = \bigsqcup_{\sigma} \mathring{\Pi}_\sigma, \quad (3.23)$$

where  $\mathring{\Pi}_\sigma$  is the set of matrices  $C$  whose columns fulfill (3.20) for all  $a$ , which are just the positroid cells discussed earlier and naturally represented by decorated permutations. Taking  $G(1, n) = \mathbb{CP}^{n-1}$ , the positroid stratification just amounts to decomposing the projective space into coordinate patches as was done in section 3.1.

### 3.2.2 Grassmannians as plabic graphs

An element of the Grassmannian can also be represented by a *plabic*-(planar, bi-colored) graph with  $n$  external legs and some number of internal legs connected by vertices, each with one of two colors, empty or shaded. We draw the plabic graphs in the interior of a disc with  $n$  marked points on its boundary. We assume that the graph is simple, meaning it does not contain multiple edges or self-loops. A generic plabic graph associated with a cell in  $G(3, 7)$  is sketched in Figure 3.1. We can identify a decorated permutation associated with each plabic graph. In order to do so, we define the Left-Right (LR)-path between all external edges  $a \rightarrow \sigma(a)$ , where we turn left at each empty vertex and turn right at each shaded vertex. This gives us the decorated permutation,  $i \rightarrow \sigma(i)$  defined above, if we appropriately add  $n$  such that  $\sigma(a) \geq a$ . For instance, following the LR-path on the plabic graph Figure 3.1, as seen in Figure 3.2, we obtain the permutation  $\sigma = \{5, 6, 4, 7, 9, 10, 8\}$ .

Not only can we obtain the decorated permutation of a point in the Grassmannian from the plabic graph, but we can also obtain a direct representation of the point  $C \in G(3, 7)$  by the so-called “boundary measurements”. We first label each face of the plabic graph with a variable  $f_i$ , e.g. for the Figure 3.1, we label its 9 faces according to Figure 3.3 and choose a common orientation for the faces. Second, we assign a *perfect orientation* to the graph, meaning that we assign arrows to edges, such that for each empty vertex there are exactly two outgoing and one incoming arrow,

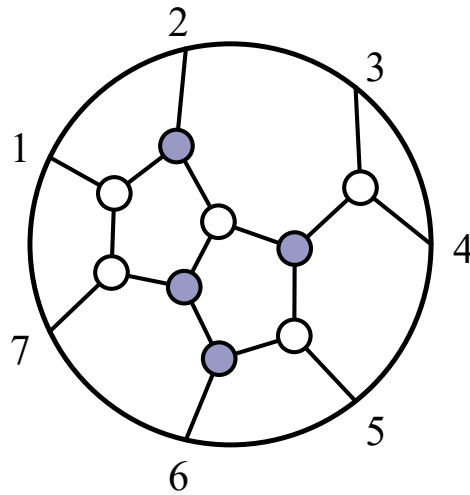


Figure 3.1: A generic plabic graph associated with a configuration of planes  $C \in G(3, 7)$ , with  $\dim C = 8$ . The figure is generated using the `positroid` Mathematica<sup>TM</sup> package [73].

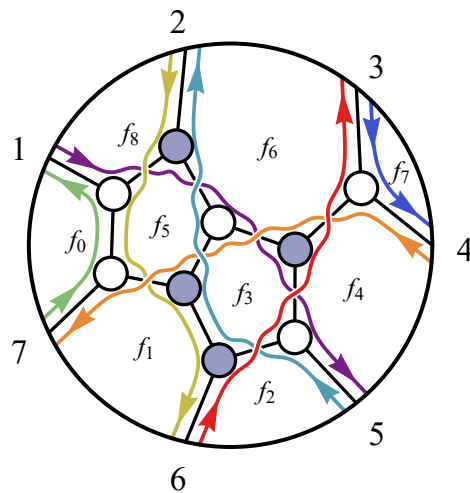


Figure 3.2: The  $LR$ -path defined for the plabic graph in 3.1 for an element in  $G(3, 7)$ . Starting from each external leg,  $a$ , we take a left at a empty vertex and a right at a shaded vertex until encountering another external leg, which is just the permutation of the first  $\sigma(i)$ , up to addition of  $n$ . The decorated permutation of this particular plabic graph is given by  $\sigma = \{5, 6, 4, 7, 9, 10, 8\}$ . The figure is generated using the `positroid` Mathematica<sup>TM</sup> package [73].

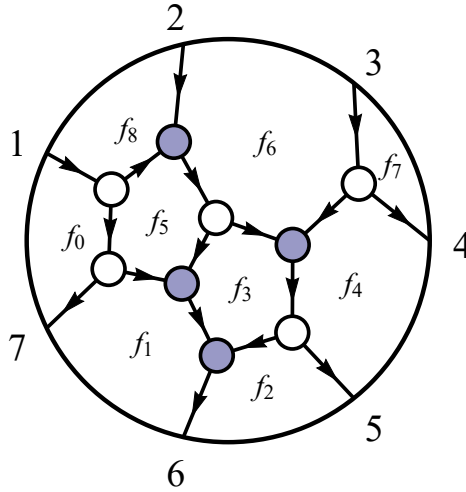


Figure 3.3: The assignment of face labels and perfect orientation on the plabic graph of Figure 3.1. The perfect orientation is given by any assignment of arrows, such that there is one incoming and two outgoing edges to each empty vertex, and two incoming and one outgoing for each shaded vertex. The figure is generated using the `positroid` Mathematica<sup>TM</sup> package [73].

while for each shaded vertex there are exactly two incoming and one outgoing arrow. Summing over all paths  $A \rightsquigarrow a$ , we assign minus the product of all faces  $f_i$  to the *left* of the paths to  $c_a^A \in C$ , as follows

$$c_a^A = - \sum_{\Gamma \in \{A \rightsquigarrow a\}} \prod_{f \in \hat{\Gamma}} (-f), \quad (3.24)$$

where  $\hat{\Gamma}$  is the clockwise closures of  $\Gamma$ . If any path contains a closed, directed loop we take a geometric series of faces in the loop [72]. A few examples of boundary measurements are sketched on Figure 3.4. Note that the face labels overcount the degrees of freedom in  $C \in G(k, n)$  by 1, reflected in the condition  $\prod_i (-f_i) = 1$ .

### Moves on Plabic Graphs

The invariant information of the Grassmannian is stored in the decorated permutation, as discussed earlier. We identify certain *moves* on a plabic graph that leave a given permutation unchanged. There are two types of these moves: flip moves and square moves.

- I The *flip move* allows us to collapse any two adjacent vertices of the same color and expand it in any way we want as depicted on Figure 3.5

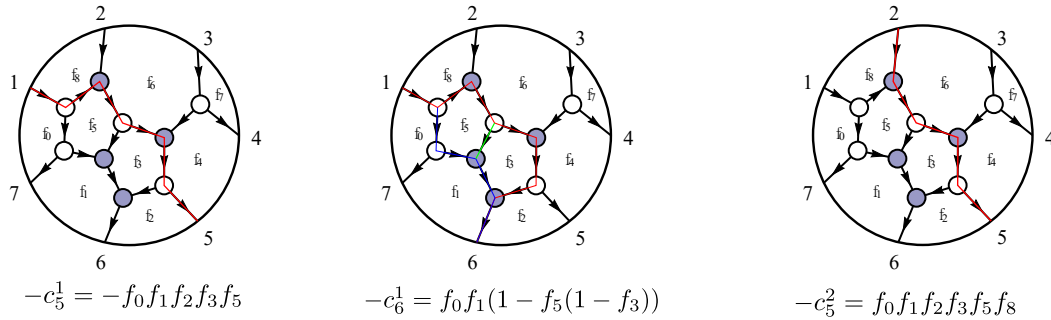


Figure 3.4: A few boundary measurements for the configuration of  $G(3, 7)$  labeled by the affine permutation  $\{5, 6, 4, 7, 9, 10, 8\}$ , based on the face labeling. Note that the degrees of freedom in the configuration labeled by  $\{5, 6, 4, 7, 9, 10, 8\}$  is 8 by (3.22), while there are 9 face labels. This can be remedied by setting  $f_0f_1\dots f_8 = -1$ .

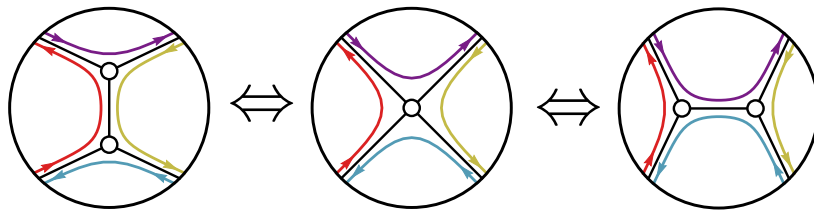


Figure 3.5: The flip move amounts to collapse any two adjacent vertices of the same color to a single vertex, which is no longer trivalent, and vice versa. These graphs are understood to be subgraphs of any larger plabic graph. The figure is generated using the `positroid` Mathematica™ package [73]

II The *square move* amounts to identifying a square subgraph with vertices of alternating colors. Then exchanging the empty and shaded vertices leaves the decorated permutation invariant, as shown in Figure 3.6. .

Performing these moves on a given subgraph leaves the LR's unchanged and thus the two plabic graphs, before and after the move, refer to the same permutation and therefore the same element in  $G(n, k)$ .

### Amalgamation of Plabic Graphs

In three dimensions, we can have one-planes and two-planes. We represent the generic (top dimensional) one-plane in  $G(1, 3)$  and the two-plane in  $G(2, 3)$ , as the following

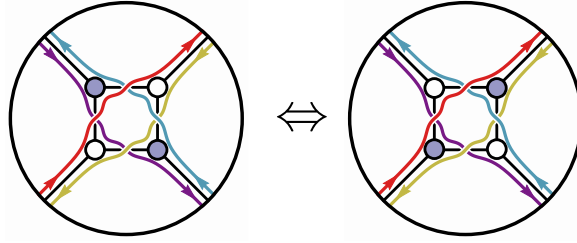


Figure 3.6: The square move consists of exchanges the colors of the vertices in any square subgraph of a larger plabic graph. Following the LR paths on both graphs reveals that the square move leaves the overall permutation invariant and therefore they reflect the same configuration in  $G(k, n)$ . The figure is generated using the `positroid` Mathematica<sup>TM</sup> package [73]

graphs

$$\begin{array}{c}
 \begin{array}{c} 1 \\ \diagdown \\ \bigcirc \\ \diagup \\ 3 \end{array} \begin{array}{c} 2 \\ \text{---} \\ \bigcirc \end{array} \\
 \end{array} \Leftrightarrow C \equiv \begin{pmatrix} 1 & \alpha_1 & \alpha_2 \end{pmatrix} \in G(1, 3), \quad (3.25)$$

$$\begin{array}{c}
 \begin{array}{c} 1 \\ \diagdown \\ \bigcirc \\ \diagup \\ 3 \end{array} \begin{array}{c} 2 \\ \text{---} \\ \bullet \end{array} \\
 \end{array} \Leftrightarrow C \equiv \begin{pmatrix} 1 & 0 & \alpha_1 \\ 0 & 1 & \alpha_2 \end{pmatrix} \in G(2, 3), \quad (3.26)$$

where both matrices are defined up to a  $GL(1)$  and  $GL(2)$  equivalence, respectively. These plabic graphs are also called on-shell diagrams due to their relationship with physics, as we will discuss in section 3.4. We can construct elements of the generic Grassmannian,  $G(k, n)$  by repeated *amalgamation* of (3.25) and (3.26). The amalgamation procedure is defined in the following two steps:

**I Direct product.** We take the direct products of two Grassmannians. Consider two planes  $C_L \in G(k_L, n_R)$  and  $C_R \in G(k_R, n_R)$ . We construct an element  $C \in G(k_L + k_R, n_L + n_R)$ , by the operation on Figure 3.7 with representation in terms plabic graphs on Figure 3.8.

The non-zero Plücker coordinates on  $C$  can be obtained from  $C_L$  and  $C_R$  by the following

$$(a_1 \cdots a_{k_L} b_1 \cdots b_{k_R})_C = (a_1 \cdots a_{k_L})_{C_L} \times (b_1 \cdots b_{k_R})_{C_R}. \quad (3.27)$$

$$\left( \begin{array}{|c|} \hline C_L \\ \hline \end{array} \right) \otimes \left( \begin{array}{|c|} \hline C_R \\ \hline \end{array} \right) \Rightarrow \left( \begin{array}{|cc|} \hline C_L & 0 \\ \hline 0 & C_R \\ \hline \end{array} \right)$$

Figure 3.7: The direct product at the level of Grassmannians. Here we take  $C_L \in G(k_L, n_L)$  and  $C_R \in G(k_R, n_R)$  giving rise to the matrix on the right.

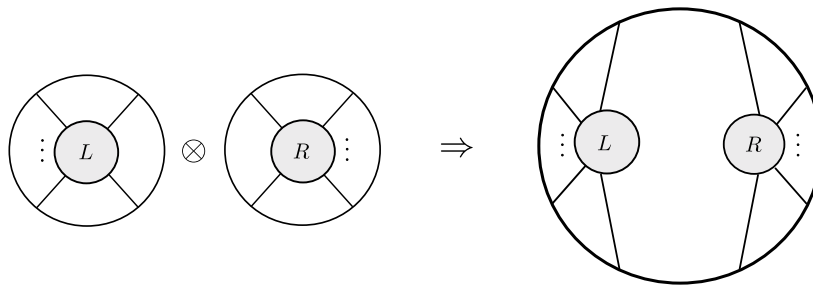


Figure 3.8: The direct product of two plabic graphs  $L$  and  $R$  giving rise to the on-shell diagram on the right.

**II Projection.** The projection operation amounts to reducing a point in the Grassmannian  $C \in G(k + 1, n + 2)$  to a point of the Grassmannian  $\hat{C} \in G(k, n)$ , by identifying two columns,  $c_A$  and  $c_B$  and projecting the remaining columns of  $C$  onto the quotient space of  $C$  modulo the difference  $(c_A - c_B)$ . This can be readily understood as connecting two external edges of a plabic graph into an internal edge, reducing the number of external edges by two and increasing the number of internal edges by one as seen on Figure 3.9. Taking the columns of the original matrix ordered according to  $(A, B, 1, \dots, n)$ , we identify the columns  $A$  and  $B$ , the Plücker coordinates of the resulting point  $\hat{C} \in G(k, n)$  in terms of the Plücker coordinates of the original  $C \in G(k + 1, n + 2)$  are given by

$$(a_1 \cdots a_k)_{\hat{C}} = (Aa_1 \cdots a_k)_C + (Ba_1 \cdots a_k)_C. \tag{3.28}$$

### 3.3 The Positive Grassmannian

The totally non-negative Grassmannian,  $G_+(n, k) \subset G(n, k)$  is a subspace of the Grassmannian,  $G(n, k)$ , with the constraint that the  $k \times n$  matrix representing  $k$ -planes in  $G(k, n)$ , up to  $GL(k)$  transformations, has *consecutive* Plücker coordinates

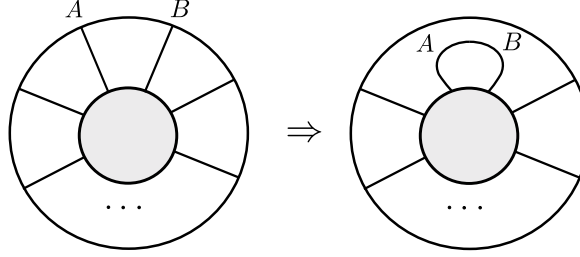


Figure 3.9: The projection operation on an on-shell diagram. We identify two legs, reducing the number of external legs of the on-shell diagram.

greater than or equal to 0. Due to convention, we will refer to the totally non-negative Grassmannian as the *positive* Grassmannian by slight abuse of notation [72]<sup>1</sup>. The positive Grassmannian is intrinsically linked to the plabic graphs described earlier in this chapter and has a natural geometric interpretation as a generalization of the projective simplex. An element of the positive Grassmannian is defined as a matrix with entries restricted such that the Plücker coordinates are non-negative, as follows

$$C \in G_+(k, n) \Rightarrow \det(c_{i_1} c_{i_2} \dots c_{i_k}) \geq 0 \quad \text{for } (i_1 < i_2 < \dots < i_k), \quad (3.29)$$

where  $C$  is defined up to  $GL(k)$  transformations, which just scale each Plücker coordinate by a constant.

Let us consider a simple example: the simplest real Grassmannian is  $G_{\mathbb{R}}(1, n) \simeq \mathbb{R}\mathbb{P}^{n-1}$ , which is the real slice of  $\mathbb{C}\mathbb{P}^n$ . Consider a generic, top dimensional point  $C \in G_{\mathbb{R}}(1, 3)$ , represented by the  $(1 \times 3)$  matrix  $C = (c_1, c_2, c_3)$ , where  $c_i$  are real numbers up to rescaling, the positive Grassmannian  $G_+(1, 3)$  is just the part of the coordinate space of  $G(1, 3)$ , where all the homogeneous coordinates are positive or zero. Positivity carves up the 1-plane into a closed region, bounded by inequalities. Choosing the coordinate patch  $c_1 = 1$ , the boundaries are at  $c_2 = 0$ ,  $c_3 = 0$ , and at the point at infinity. This is the projective simplex, or equivalently a cone in  $\mathbb{R}^2$ . Since we can rescale each coordinate with an arbitrary sign  $c_a \sim t_a c_a$ , we can select different equivalent closed regions as sketched in Figure 3.10 .

For  $k > 1$ , positivity of the Plücker coordinates implies a fixed ordering of the columns of  $C$ , since the minors are antisymmetric with respect to their internal ordering, e.g. if  $(c_i c_j c_k) > 0$ , then  $C$  can be said to be an element of the positive Grassmannian with the ordering  $i < j < k$  [72]. One would assume, that we need to describe distinct positivity conditions for each  $n!$  ordering of columns. This is however not required, as we have twisted cyclic symmetry, that is, under shifting of

<sup>1</sup>The *positive* Grassmannian would be the Grassmannian where all consecutive Plücker coordinates are strictly positive. We will not make use of this space in this dissertation and no ambiguities should occur.

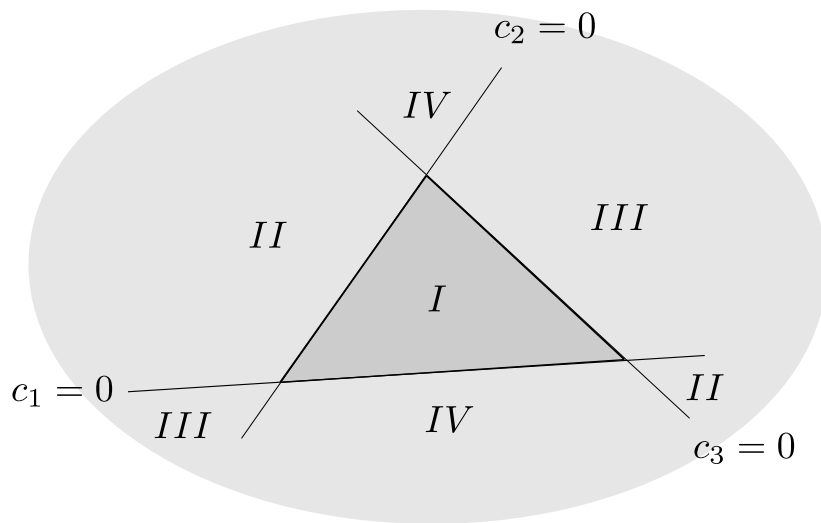


Figure 3.10: The real Grassmannian  $G(1,3) \simeq \mathbb{RP}^2$ . The 1-plane is represented by a matrix  $C = (c_1, c_2, c_3)$ . The positive space *I*, is simply the space where all the homogeneous coordinates are positive. Rescaling each homogeneous coordinate  $c_i \rightarrow t_i c_i$  will select a different “positive part” e.g. region *II*, *III*, or *IV*, where we have identified sign configurations that are the same up to the overall sign to the same region, e.g. region *II* can be denoted by  $\{c_1 > 0, c_2 < 0, c_3 > 0\}$  or by  $\{c_1 < 0, c_2 > 0, c_3 < 0\}$ .

the columns in  $G_+(k, n)$  according to

$$c_1 \rightarrow c_2, c_2 \rightarrow c_3, \dots, c_n \rightarrow (-1)^{k+1} c_1, \quad (3.30)$$

ensuring positivity is retained in the shifted ordering [72].

There exists a particularly natural set of coordinates to describe an element of the positive Grassmannian, the *canonical coordinates*. They can be constructed for any given permutation, starting from the trivial  $k \times n$  matrix and subsequently shifting columns multiplying positive parameters. We will review the construction for the top dimensional element of  $G_+(3, 6)$ , by first finding a plabic graph representation<sup>2</sup> and subsequently construct the matrix representation of  $C \subset G_+(3, 6)$ , starting from a trivial element denoted by the permutation  $\sigma_0 = \{7, 8, 9, 4, 5, 6\}$ . The permutation for the top-dimensional element of  $G_+(3, 6)$  is just the permutation  $\sigma = \{4, 5, 6, 7, 8, 9\}$ , which is exactly the case the Plücker coordinates are only restricted by Cramer's rule. We can exchange elements in the permutation by  $(ij)$  as follows

$$(ij) \circ \{\sigma(1), \sigma(2), \dots, \sigma(i), \dots, \sigma(j), \dots, \sigma(n)\} = \{\sigma(1), \sigma(2), \dots, \sigma(j), \dots, \sigma(i), \dots, \sigma(n)\}. \quad (3.31)$$

We then exchange consecutive elements  $(a, b)$  in the permutation, such that  $a$  and  $b$  are consecutive or only separated by elements which are in the correct position  $\{a, \sigma(z), b\}$ , if  $\sigma(z) = z \pmod n$ . This operation is repeated until we reach the trivial element with all  $\sigma(a) = a \pmod n$ , keeping track of which elements in the decorated permutation we have permuted. For instance, we take the *lexicographic decomposition scheme*, where we perform the exchanges in the lexicographic order [73]

$$\begin{aligned} (12) \circ \{4, 5, 6, 7, 8, 9\} &= \{5, 4, 6, 7, 8, 9\} \\ (23) \circ \{5, 4, 6, 7, 8, 9\} &= \{5, 6, 4, 7, 8, 9\} \\ (12) \circ \{5, 6, 4, 7, 8, 9\} &= \{6, 5, 4, 7, 8, 9\} \\ (34) \circ \{6, 5, 4, 7, 8, 9\} &= \{6, 5, 7, \mathbf{4}, 8, 9\} \\ (23) \circ \{6, 5, 7, \mathbf{4}, 8, 9\} &= \{6, 7, 5, \mathbf{4}, 8, 9\} \\ (12) \circ \{6, 7, 5, \mathbf{4}, 8, 9\} &= \{\mathbf{7}, 6, 5, \mathbf{4}, 8, 9\} \\ (35) \circ \{\mathbf{7}, 6, 5, \mathbf{4}, 8, 9\} &= \{\mathbf{7}, 6, 8, \mathbf{4}, \mathbf{5}, 9\} \\ (23) \circ \{\mathbf{7}, 6, 8, \mathbf{4}, \mathbf{5}, 9\} &= \{\mathbf{7}, \mathbf{8}, 6, \mathbf{4}, \mathbf{5}, 9\} \\ (36) \circ \{\mathbf{7}, \mathbf{8}, 6, \mathbf{4}, \mathbf{5}, 9\} &= \{\mathbf{7}, \mathbf{8}, \mathbf{9}, \mathbf{4}, \mathbf{5}, \mathbf{6}\} \end{aligned} \quad (3.32)$$

where boldface refer to elements where  $\sigma(a) \pmod a$  is in the correct position. The prescription dictates that, starting from the trivial element represented by

$$C_0 = \begin{pmatrix} 1 & 0 & 0 & 0 & 0 & 0 \\ 0 & 1 & 0 & 0 & 0 & 0 \\ 0 & 0 & 1 & 0 & 0 & 0 \end{pmatrix}. \quad (3.33)$$

<sup>2</sup>Not unique since the flip and square moves can relate different graphs to the same orientation.

For each element exchange in (the reverse ordering of) (3.3),  $(ab)$ , we shift the columns of  $C_0$  according to  $c_b \mapsto c_b + (-1)^q \alpha_i c_a$ , where  $\alpha_i$  is called a canonical coordinate and  $q$  counts the number of columns between  $c_a$  and  $c_b$ . Since it took 9 exchanges to reach the trivial element  $\sigma_0$ , we label  $\alpha_1, \dots, \alpha_9$  according to the reverse ordering of (3.3), e.g. (35) :  $c_5 \mapsto c_5 - \alpha_1 c_3$ . We build up the matrix

$$C_0 = \begin{pmatrix} 1 & 0 & 0 & 0 & 0 & 0 \\ 0 & 1 & 0 & 0 & 0 & 0 \\ 0 & 0 & 1 & 0 & 0 & 0 \end{pmatrix} \xrightarrow{(36)} \begin{pmatrix} 1 & 0 & 0 & 0 & 0 & 0 \\ 0 & 1 & 0 & 0 & 0 & 0 \\ 0 & 0 & 1 & 0 & 0 & \alpha_1 \end{pmatrix} \xrightarrow{(23)} \begin{pmatrix} 1 & 0 & 0 & 0 & 0 & 0 \\ 0 & 1 & \alpha_2 & 0 & 0 & 0 \\ 0 & 0 & 1 & 0 & 0 & \alpha_1 \end{pmatrix} \xrightarrow{(35)} \begin{pmatrix} 1 & 0 & 0 & 0 & 0 & 0 \\ 0 & 1 & \alpha_2 & 0 & -\alpha_2 \alpha_3 & 0 \\ 0 & 0 & 1 & 0 & -\alpha_3 & \alpha_1 \end{pmatrix} \xrightarrow{(12)} \dots \xrightarrow{(12)} \begin{pmatrix} 1 & \alpha_4 + \alpha_7 + \alpha_9 & \alpha_4(\alpha_5 + \alpha_8) + \alpha_7 \alpha_8 & \alpha_4 \alpha_5 \alpha_6 & 0 & 0 \\ 0 & 1 & \alpha_2 + \alpha_5 + \alpha_8 & \alpha_6(\alpha_2 + \alpha_5) & -\alpha_2 \alpha_3 & 0 \\ 0 & 0 & 1 & \alpha_6 & -\alpha_3 & \alpha_1 \end{pmatrix}, \quad (3.34)$$

which is a representation of the generic point in  $G(3, 6)$ .

It can be shown that the amalgamation procedure discussed in the final section, preserves positivity. If two on-shell diagrams, representing planes in positive Grassmannians, their amalgamation will also be an element of the positive Grassmannian [72].

### 3.3.1 Boundary Stratification

The positroid stratification of the Grassmannian  $G(k, n)$  partitions the space by matrices whose columns fulfill certain linear relations dictated by Cramer's rule (3.14). Earlier in this section, in the  $G_+(1, n)$  example, we discussed how the vanishing of certain Plücker coordinates of the *positive* Grassmannian are understood as the boundaries of the projective simplex. We interpret the positroid stratification of the positive Grassmannian as representing *boundaries* of the positive Grassmannian, which are themselves bounded regions in the Grassmannian called positroid cells. Let us consider an example for  $G_+(3, 6)$ . The top-dimensional cell  $C \in G_+(3, 6)$  with all positive Plücker coordinates can be represented by a  $(3 \times 6)$  matrix with columns  $c_a$ . We can scale each columns to be on the form  $c_a \sim (\hat{c}_a \ 1)^T$ , where  $\hat{c}_a \in \mathbb{R}^2$ . In this case, the statement of consecutive positivity is simply the statement that the points  $\hat{c}_a$  must span a convex polygon sketched on Figure 3.11. The codimension-1 boundaries of  $G_+(3, 6)$  simply occur when the consecutive minors become collinear. We can only let non-consecutive points become collinear by 1) breaking the convexity of the hexagon or 2) letting additional consecutive points become collinear, distinguishing boundaries of different dimensions. We can therefore infer that there must be  $n$  codimension-1 boundaries associated with consecutive Plücker coordinates vanishing; or equivalently, on the certain zero locus of a polynomial in canonical coordinates,  $\alpha$ .

An algorithm for finding the boundary stratification of the positive Grassmannian for all  $n$  and  $k$  was presented in [73] in the Mathematica™ package `positroids`, which we make use of extensively throughout this work.

Returning to the naturally defined top-form for the Grassmannian discussed in section 3.2 in (3.16), we define a natural top-form of the positive Grassmannian in

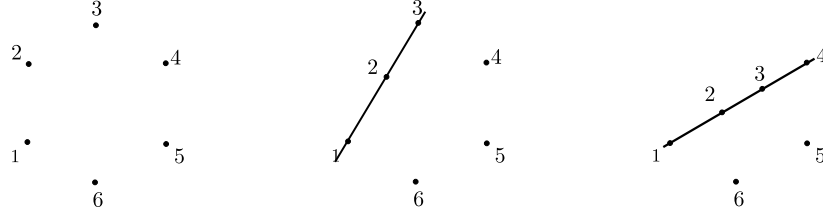


Figure 3.11: The geometry of  $G(3,6)$  sketched in the chart where  $c_a \sim (\hat{c}_a \ 1)^T$ . Therefore the geometry is embedded in two dimensions. In order to reach the cell where  $(124) = 0$  while still preserving convexity, we first go to the configuration  $(123) = 0$  and subsequently take  $(234) = 0$ . We take the configuration on the right as a codimension-1 boundary of the middle configuration, which is, in turn, a codimension-1 boundary of the configuration on the left.

the same manner

$$\Omega = \frac{d^{k \times n} C}{\text{vol}(GL(k))} \frac{1}{f(C)}. \quad (3.35)$$

As before,  $f(C)$  must be a function of the Plücker coordinates and must scale uniformly under  $GL(k)$ . This scaling is naturally carried by the  $n$  consecutive Plücker coordinates representing the codimension-1 boundaries as follows

$$f(C) = (1 \cdots k)(2 \cdots k+1) \cdots (n \cdots k-1) f'(C), \quad (3.36)$$

where  $f'(C)$  is now a scaleless function of the Plücker coordinates. The differential form with  $f(C)$  is a logarithmic differential form, with only single poles, and its singularities are exactly on the boundaries of the positive Grassmannian. Since  $f'(C)$  must be a scaleless function it will be a rational function of Plücker coordinates. In order to ensure that  $f'(C)$  does not introduce additional poles, it is natural to take  $f'(C) = 1$ . We will discuss these types of forms in details in chapter 4. Writing  $\Omega$  in terms of canonical coordinates by choosing a particular coordinate chart for  $C$  [72], we obtain

$$\Omega = \frac{d\alpha_1}{\alpha_1} \wedge \dots \wedge \frac{d\alpha_{k(n-k)}}{\alpha_{k(n-k)}}. \quad (3.37)$$

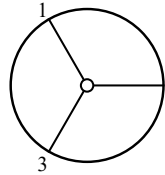
### 3.4 Scattering Amplitudes from the Grassmannian

The Grassmannian and its positive part are deeply connected to scattering amplitudes. Recall that the three-particle amplitudes in mSYM can be written as

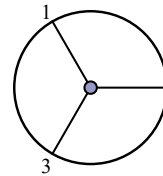
$$A_{3,1} = \frac{\delta^{1 \times 4} ([23]\eta_1 + [31]\eta_2 + [12]\eta_3)}{[12][23][31]} \delta^{2 \times 2}(\lambda_i \cdot \tilde{\lambda}_i), \quad (3.38)$$

$$A_{3,2} = \frac{\delta^{2 \times 4} (\sum_{i=1}^3 \lambda_i \eta_i)}{\langle 12 \rangle \langle 23 \rangle \langle 31 \rangle} \delta^{2 \times 2}(\lambda_i \cdot \tilde{\lambda}_i). \quad (3.39)$$

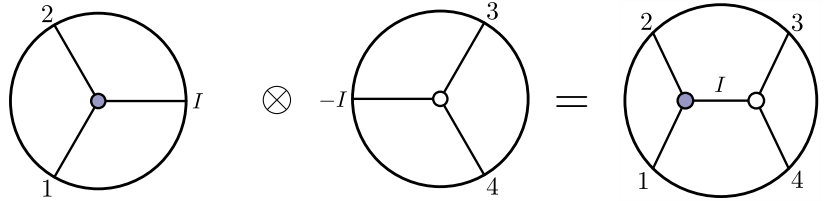
We encode these amplitudes as integrals over Grassmannian differential forms: taking  $W \in G(1, 3)$  and  $B \in G(2, 3)$ , we can cast these as

$$A_{3,1} = \int \frac{d^{1 \times 3} W}{\text{vol}(GL(1))} \frac{\delta^{1 \times 4}(W \cdot \eta) \delta^{1 \times 2}(W \cdot \tilde{\lambda}) \delta^{2 \times 2}(\lambda \cdot W^\perp)}{(1)(2)(3)} \sim \text{Diagram} \quad (3.40)$$


and

$$A_{3,2} = \int \frac{d^{2 \times 3} B}{\text{vol}(GL(2))} \frac{\delta^{2 \times 4}(B \cdot \eta) \delta^{2 \times 2}(B \cdot \tilde{\lambda}) \delta^{2 \times 1}(\lambda \cdot B^\perp)}{(12)(23)(31)} \sim \text{Diagram} \quad (3.41)$$


where we have associated a plabic graph to each three particle amplitude. We can glue these graphs together to generate a class of graph called on-shell diagrams (which are no longer necessarily planar) as follows

$$\text{Diagram}_1 \otimes -I \text{Diagram}_2 = \text{Diagram}_3 \quad (3.42)$$


To each on-shell diagram  $\Gamma$ , we associate an *on-shell function*,  $f_\Gamma$ , found from gluing together three point plabic graphs according to (3.40) and (3.41), and integrating over the internal leg

$$f_\Gamma = \prod_{i=I_\Gamma} \sum_{h_i} \int \frac{d^2 \lambda_i d^2 \tilde{\lambda}_i}{\text{vol}(GL(1))} \prod_{v \in V_\Gamma} A_v, \quad (3.43)$$

where  $I_\Gamma$  counts the internal lines and  $V_\Gamma$  counts the vertices in the on-shell diagram  $\Gamma$ . Each vertex is either associated with  $A_{3,1}$  or  $A_{3,2}$  scattering amplitude and we can construct a large class of functions relevant to physics by gluing different 3 point on-shell diagrams together. Let us discuss these functions in their generality. For any on-shell diagram  $\Gamma$ , we can count the number of integrations and  $\delta$ -functions by counting internal lines, and shaded and empty vertices [72]. The number of unfixed bosonic  $\delta$ -functions is found as

$$n_\delta \equiv 4n_V - 3n_I - 4, \quad (3.44)$$

where  $n_V$  is the number of vertices, each contributing four bosonic  $\delta$ -functions,  $n_I$  counts the internal integration, each localizing three  $\delta$ -functions. We subtract 4  $\delta$ -functions to account for overall momentum conservation. This means, we have three classes of on-shell diagrams:

- I  $n_\delta > 0$ . When there are unfixed  $\delta$ -functions, the on-shell function imposes additional constraints on the external kinematics beyond overall momentum conservation. Some on-shell functions of this type can be associated with *cuts* on scattering amplitudes, to be discussed in section 2.9.
- II  $n_\delta = 0$ . In this case, the integrations are completely localized by  $\delta$ -functions. This means that the on-shell function is simply a rational function of the external kinematics. Scattering amplitudes at tree-level are examples of these types of on-shell functions.
- III  $n_\delta < 0$ . The last class of on-shell diagrams is the one where there are additional integrations to perform after localizing all possible integrals using  $\delta$ -functions. The remaining integration has to be specified by an integration contour, and under an appropriate choice, can produce loop-level scattering amplitudes.

We can identify exactly which on-shell diagrams are related to scattering amplitudes by the BCFW construction, which we will review presently.

### 3.4.1 BCFW Bridge Construction

The BCFW recursion discussed in section 2.4 can be employed to find the specific on-shell diagrams associated with scattering amplitudes. We can attach a certain “BCFW” bridge to an on-shell diagram as depicted in Figure 3.12. Here we can

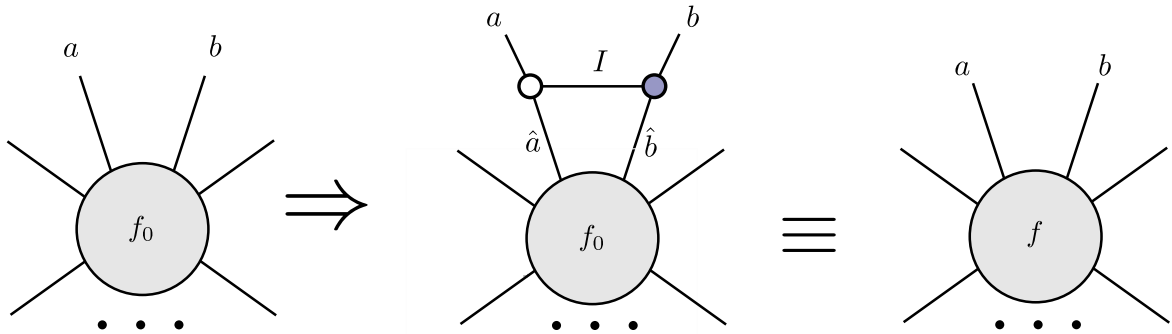


Figure 3.12: We can build more complex on-shell functions by recursively adding “BCFW” bridges to on-shell diagrams.

glue the three-point amplitudes together using the prescription described above. The on-shell function of the resulting diagram is simply

$$f = \int \prod_{i \in \{\hat{a}, \hat{b}, I\}} \frac{d^2 \lambda_i d^2 \tilde{\lambda}_i}{\text{vol}(GL(1))} d^4 \eta_i A_{3,1}(a, I, \hat{a}) A_{3,2}(b, \hat{b}, I) f_0(\dots, \hat{a}, \hat{b}, \dots). \quad (3.45)$$

Following the analysis of integrations and  $\delta$ -functions around (3.44), we see that this prescription introduces exactly one additional integration, once all  $\delta$ -functions have been localized. This remaining degree of freedom can be found by solving the  $\delta$  functions in (3.45) as follows

$$\lambda_{\hat{a}} = \lambda_a, \quad \tilde{\lambda}_{\hat{a}} = \tilde{\lambda}_a - \alpha \tilde{\lambda}_b, \quad \eta_{\hat{a}} = \eta_a - \alpha \eta_b, \quad (3.46)$$

$$\lambda_I = \alpha \lambda_a, \quad \tilde{\lambda}_I = \tilde{\lambda}_b, \quad \eta_I = \eta_b \quad (3.47)$$

$$\lambda_{\hat{b}} = \lambda_b + \alpha \lambda_a, \quad \tilde{\lambda}_{\hat{b}} = \tilde{\lambda}_b, \quad \eta_{\hat{b}} = \eta_b. \quad (3.48)$$

Resolving the  $\delta$  functions in (3.45) yields a Jacobian and evaluating the three point contributions  $A_3^1$  and  $A_3^2$  simply yields [72]

$$f(\dots, \lambda_a, \tilde{\lambda}_a, \eta_a, \lambda_b, \tilde{\lambda}_b, \eta_b, \dots) \Rightarrow \frac{d\alpha}{\alpha} f_0(\dots, \lambda_{\hat{a}}, \tilde{\lambda}_{\hat{a}}, \eta_{\hat{a}}, \lambda_{\hat{b}}, \tilde{\lambda}_{\hat{b}}, \eta_{\hat{b}}). \quad (3.49)$$

The BCFW bridge thus attaches a simple pole to the on-shell function  $f_0$ , the residue on which just returns  $f_0$ .

The specific on-shell diagrams related to scattering amplitudes were found in [72]. We present the resulting recursion relation and refer to chapter 17 of the book for its proof. The tree-level  $n$ -point scattering amplitude for msYM can be represented by attaching a BCFW bridge to the on-shell diagrams associated with  $n' < n$  external legs, in all possible ways. For loop-level amplitudes, we associate the on-shell diagram for the  $\ell$ -loop  $n$ -point amplitudes with an on-shell diagram associated with the  $\ell - 1$ -loop  $n + 2$ -point scattering amplitude with an internal loop associated with the 4 unfixed integrations. We sketch the recursion as follows in Figure 3.13. Let us make this explicit by way of a few examples.

### $n = 4$ Tree-Level BCFW Construction

First, taking the three-particle functions (3.26) and (3.25) as given, the next relevant tree-scattering amplitude is the  $n = 4$  MHV amplitude. In that case, the  $L$  and  $R$  functions defined using Figure 3.13 are just given by (3.26) and (3.25), and there is only one contributing on-shell diagram, namely Figure 3.14. We obtain the decorated permutation for this diagram using the LR paths defined earlier in this chapter. The decorated permutation is found to be  $\{3, 4, 5, 6\}$  associated with a top-dimensional element of the positive Grassmannian  $G_+(2, 4)$ . The on-shell function associated with

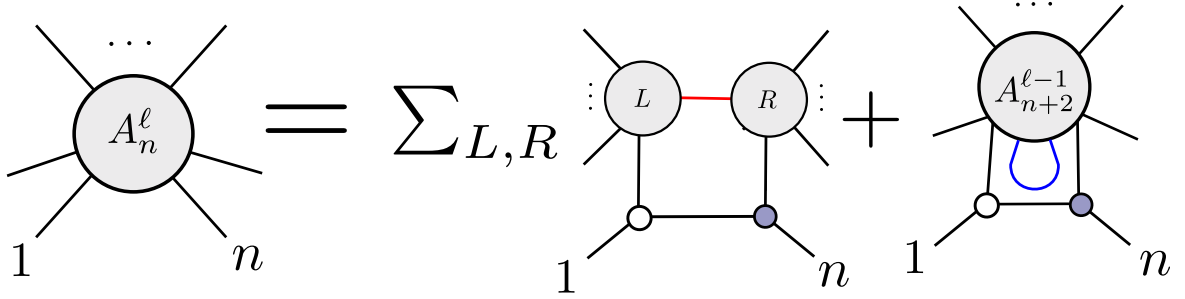


Figure 3.13: The on-shell function relevant to scattering amplitudes can be recursively constructed from the primitives according to the diagrammatic rules. Here the sum over  $L$  and  $R$  are chosen such that the sum of legs  $n_L + n_R = n + 2$  and  $k_L + k_R = k + 1$ , and the red line connecting the two subamplitudes on the left term is related to an internal unfixed momenta  $\lambda_I \tilde{\lambda}_I$  which is integrated over. In the right term, the internal loop, marked in blue, introduces exactly four unfixed momenta associated to the loop momenta, to be integrated over.

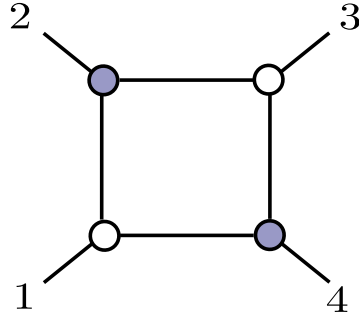


Figure 3.14: The on-shell graph whose associated on-shell function is associated to the  $n = 4$ ,  $k = 2$  scattering amplitudes in sYM as constructed from gluing the three point primitives in (3.26) and (3.25).

this diagram is completely localized and therefore a rational function of the external kinematics:

$$A_{4,2} = \int \prod_{i \in \{A,B,C,D\}} \frac{d^2 \lambda_i d^2 \tilde{\lambda}_i}{\text{vol}(GL(1))} d\eta_i A_{3,1}(1, A, -D) A_{3,2}(-A, 2, B) A_{3,1}(-B, 3, C) A_{3,2}(-C, 4, D), \quad (3.50)$$

which we can evaluate using (3.40) and (3.41), to the function

$$A_{4,2} = \frac{\delta^{2 \times 4}(\sum_i \lambda_i \eta_i)}{\langle 12 \rangle \langle 23 \rangle \langle 34 \rangle \langle 41 \rangle}, \quad (3.51)$$

which is exactly the four-point MHV scattering amplitude.

### $n = 5$ Tree-Level BCFW Construction

For  $n = 5$ , we can obtain the MHV scattering amplitude from the BCFW construction. In this case, we can start from the four point on-shell diagram and glue to it a three point according to Figure 3.13. There is only one way of combining  $A_{4,2}$  and  $A_{1,3}$  to form the on-shell diagram associated with  $A_{5,2}$ , namely the one sketched on (3.52).

$$A_{5,2} = A_{4,2} \otimes A_{3,1} = \text{Diagram} \quad (3.52)$$

Similarly for the  $n = 5$ ,  $k = 3$  there is also just a single contribution in the BCFW recursion, namely the one sketched on (3.53).

$$A_{5,3} = A_{3,2} \otimes A_{4,2} = \text{Diagram} \quad (3.53)$$

Both scattering amplitudes can be obtained by gluing three point functions together according to (3.42).

### $n = 6$ tree-level BCFW Construction

For  $n = 6$ , we have three distinct helicity sectors contributing to the scattering amplitude,  $k = 2$ ,  $k = 3$ , and  $k = 4$ . The  $k = 2$  and  $k = 4$  on-shell diagrams are easy to obtain, by attaching a  $A_{1,3}$  diagram to the  $A_{5,2}$  diagram on (3.52), or attaching a  $A_{2,3}$  diagram to the  $A_{5,3}$  diagram on (3.53) according to the BCFW prescription.

The resulting diagrams are recorded below

$$A_{6,2} = A_{5,2} \otimes A_{3,1} = \text{Diagram} \quad (3.54)$$

$$A_{6,4} = A_{5,3} \otimes A_{3,2} = \text{Diagram} \quad (3.55)$$

both of which are related to the respective top-dimensional elements of the positive Grassmannian  $C \in G_+(2, 6)$  and  $C \in G_+(4, 6)$ . The  $k = 3$  sector is the first case where we have more than one on-shell diagram contributing to the scattering amplitudes. The BCFW prescription requires the following three diagrams

$$A_{6,3} = A_{5,3} \otimes A_{3,1} + A_{4,2} \oplus A_{4,2} + A_{3,2} \otimes A_{5,2} =$$

$$= \text{Diagram 1} + \text{Diagram 2} + \text{Diagram 3} \quad (3.56)$$

$\{4, 5, 6, 8, 7, 9\}$ 
 $\{3, 5, 6, 7, 8, 10\}$ 
 $\{4, 6, 5, 7, 8, 9\}$

We have written the decorated permutation found from each on-shell diagram using the LR path. We notice that these are three particular codimension-1 boundaries of

$G_+(3, 6)$ , which can be related under cyclic rotation of the external legs

$$(3.57)$$

Having obtained a prescription to obtain the specific decorated permutations associated with a given scattering amplitude through the BCFW construction, we briefly review how to extract the scattering amplitude from the given permutations.

### 3.5 Scattering Amplitudes from Grassmannian Integrals

An arbitrary on-shell diagram associated with a cell,  $\Gamma_\sigma \in G(k, n)$  can be labeled by a given decorated permutation using the LR path as discussed in section 3.2. The corresponding cell in the Grassmannian can then be labeled by its canonical coordinates and we can construct a differential form on these variables. We obtain a differential form by solving

$$\sum_{i=1}^n C_{i\alpha} \eta_i^A = 0, \quad \sum_{i=1}^n C_{i\alpha} \tilde{\lambda}_i^{\dot{a}} = 0, \quad \sum_{i=1}^n \lambda_i^a C_{i\alpha'}^\perp = 0, \quad (3.58)$$

where  $\alpha = 1, \dots, k$  and  $\alpha' = 1, \dots, n-k$ . Given a  $d$  dimensional cell of the Grassmannian, labeled by its canonical coordinates  $\alpha_1, \dots, \alpha_d$ , the resulting on-shell function [72] is simply given by

$$f_\sigma^{(k)} = \int \frac{d\alpha_1}{\alpha_1} \wedge \dots \wedge \frac{d\alpha_d}{\alpha_d} \delta^{k \times 4}(C \cdot \eta) \delta^{k \times 2}(C \cdot \tilde{\lambda}) \delta^{2 \times (n-k)}(\lambda \cdot C^\perp), \quad (3.59)$$

where  $C = C(\alpha_1, \dots, \alpha_d) \subset \Gamma_\sigma \in G_+(k, n)$ . This differential form can also be written as the residue of the following top-dimensional form on  $G_+(k, n)$ ,

$$f_\sigma^{(k)} = \oint_{C \subset \Gamma_\sigma} \frac{d^{k \times n} C}{\text{vol}(GL(k))} \delta^{k \times 2}(C \cdot \eta) \frac{\delta^{k \times 2}(C \cdot \tilde{\lambda}) \delta^{2 \times (n-k)}(\lambda \cdot C^\perp)}{(1 \dots k) \dots (n \dots k-1)}, \quad (3.60)$$

where we have made the  $GL(k)$  redundancy explicit. Due to the  $\delta$ -functions  $\delta^{k \times 2}(C \cdot \tilde{\lambda}) \delta^{2 \times (n-k)}(\lambda \cdot C^\perp)$ , we have the interpretation that the plane  $C$  contains  $\lambda$

and is orthogonal to  $\tilde{\lambda}$ . Therefore an overall  $\delta$ -function  $\delta^{2 \times 2}(\lambda \cdot \tilde{\lambda})$ , associated with overall momentum conservation, can be extracted from the bosonic  $\delta$ -functions. The cells where the remaining  $(2n - 4)$  degrees of freedom can be fixed are precisely those associated with the scattering amplitudes of msYM. For instance, the 8 dimensional cell in the Grassmannian  $G(3, 6)$  labeled by  $\{3, 5, 6, 7, 8, 10\}$  discussed near equation (3.57) can be represented by a matrix (up to  $GL(3)$  transformations),  $C^*$ , subject to the following kinematic constraints

$$C^* = \begin{pmatrix} \lambda_1^1 & \lambda_2^1 & \lambda_3^1 & \lambda_4^1 & \lambda_5^1 & \lambda_6^1 \\ \lambda_1^2 & \lambda_2^2 & \lambda_3^2 & \lambda_4^2 & \lambda_5^2 & \lambda_6^2 \\ 0 & 0 & 0 & [56] & [64] & [45] \end{pmatrix}, \quad (3.61)$$

ensuring that the Plücker (123) = 0. Evaluating (3.60) on this point, we simply obtain the following on-shell function

$$f_{\{3,5,6,7,8,10\}}^{(3)} = \frac{\delta^{3 \times 4}(C^* \cdot \eta) \delta^{2 \times 2}(\lambda \cdot \tilde{\lambda})}{\langle 23 \rangle [56] \langle 3|4 + 5|6 \rangle_{S_{456}} \langle 1|5 + 6|4 \rangle \langle 12 \rangle [45]}, \quad (3.62)$$

by evaluating the minors of  $C^*$ . Note that we can easily write the on-shell functions in terms of the twistors defined in section 2.8. Recall the supertwistors defined on (2.167). We describe the on-shell function  $f(\lambda)$  in terms of  $\mu_i^{\dot{a}}$  by the following Fourier transform

$$f(\mu) = \int d^{2 \times n} \lambda e^{i\lambda \cdot \mu} f(\lambda), \quad (3.63)$$

and collect the supertwistor variables

$$\mathcal{W}_i^\alpha = (\lambda^a \quad \mu^{\dot{a}} \quad \eta^A). \quad (3.64)$$

We can easily write the Fourier transform of (3.60), which only acts on the following  $\delta$ -function

$$\int d^{2 \times n} \lambda e^{i\lambda \cdot \mu} \delta^{2 \times (n-k)}(\lambda \cdot C^\perp). \quad (3.65)$$

The  $\delta$ -function can be expressed as the integration over an auxiliary matrix,  $\rho$

$$(\lambda \cdot C^\perp) = \int d^{2 \times k} \rho \delta^{2 \times n}(\rho \cdot C - \lambda), \quad (3.66)$$

which, when applied to (3.65), just evaluates to

$$\int d^{2 \times n} \lambda e^{i\lambda \cdot \mu} \int d^{2 \times k} \rho \delta^{2 \times n}(\rho \cdot C - \lambda) = \int d^{2 \times k} \rho e^{i(\rho \cdot C) \cdot \mu} = \delta^{k \times 2}(C \cdot \mu). \quad (3.67)$$

The Fourier transform allows us to write a given on-shell function on a very succinct form in terms of supertwistors [74], as follows

$$f_{\sigma}^{(k)} = \oint_{C \in \Gamma_{\sigma}} \frac{d^{k \times n} C}{\text{vol}(GL(k))} \frac{\delta^{4k \times 4k}(C \cdot \mathcal{W})}{(1 \cdots k) \cdots (n \cdots k - 1)}, \quad (3.68)$$

known as the ACCK integral due to Arkani-Hamed, Cachazo, Cheung, and Kaplan [74]. It is clear, that only  $(2n - 4)$  of the  $4k$  bosonic  $\delta$ -functions are required to fix the cells  $\Gamma_{\sigma} \in G(k, n)$  in (3.68). The remaining  $\delta$ -functions serve to constrain the supertwistors, since the Fourier transformation (3.65), does not yield non-vanishing functions for generic external twistors.

There exists a similar representation of the scattering amplitudes from a Grassmannian integral due to Mason and Skinner [69], defined on the supermomentum twistors. Taking  $k' = k - 2$ , we have the integral

$$\hat{f}_{\hat{\sigma}}^{k'} = \oint_{\hat{C} \in \Gamma_{\hat{\sigma}}} \frac{d^{k' \times n} \hat{C}}{\text{vol}(Gl(k'))} \frac{\delta^{4k' \times 4k'}(\hat{C} \cdot \mathcal{Z})}{(1 \cdots k') \cdots (n \cdots k' - 1)}, \quad (3.69)$$

for any generic set of momentum twistors  $\mathcal{Z}$ , defined in (2.188). These two integrals (3.68) and (3.69) are related through the following Jacobian

$$f_{\sigma}^{(k)}(\mathcal{W}) = \frac{\delta^{2 \times 2}(\lambda \cdot \tilde{\lambda}) \delta^{2 \times 4}(\lambda \cdot \eta)}{\langle 12 \rangle \langle 23 \rangle \cdots \langle n1 \rangle} \hat{f}_{\hat{\sigma}}^{(k-2)}, \quad (3.70)$$

which is exactly the Parke-Taylor amplitude, hinting that the integral  $\hat{f}_{\hat{\sigma}}^k$  is related to the  $R$ -invariants of the  $2 < k < n - 2$  helicity scattering amplitudes.



# Chapter 4

## Positive Geometries

In this section we shall review the positive geometries [38], a class of geometries with a notion of orientation and a unique differential form associated with them. For certain positive geometries, these forms are physically relevant, e.g. they are related to scattering amplitude. We call such positive geometries physically relevant. Positive geometries are defined recursively, such that their boundaries are themselves positive geometries, and their unique differential form, labeled canonical form, has logarithmic singularities on and only on its boundaries. We review morphisms and triangulations of these geometries and we introduce the notion of oriented sums of positive geometries. We then proceed to introduce and review the prime example of positive geometries, the amplituhedron. The amplituhedron was first introduced in [1] and encodes the scattering amplitudes in the planar sector of msYM in momentum twistor space, discussed in section 2.8.

### 4.1 Positive Geometries and Canonical Forms

Positive geometries are a specific class of geometries defined as follows: let  $X$  be a complex projective algebraic variety of complex dimension  $D$  and let  $X_{\geq 0} \subset X(\mathbb{R})$  be an oriented set of real dimension  $D$ . A  $D$ -dimensional positive geometry [38] is then the pair  $(X, X_{\geq 0})$  equipped with a unique non-zero  $D$ -dimensional form  $\Omega(X, X_{\geq 0})$ , which we refer to as the *canonical form* of the positive geometry  $(X, X_{\geq 0})$ . The positive geometry is defined such that its differential form fulfills the following recursive definitions

- For  $D = 0$ :  $X = X_{\geq 0}$  and is a single real point. Its canonical form is simply  $\Omega(X, X_{\geq 0}) = \pm 1$  depending on the orientation of  $X_{\geq 0}$ .
- For  $D > 0$ : every boundary component  $(C, C_{\geq 0})$  of  $(X, X_{\geq 0})$  is a positive geometry of dimension  $D - 1$  and the form  $\Omega(X, X_{\geq 0})$  has logarithmic singularities along every boundary component  $C$ . The residues upon  $C$  is just

the canonical form on the boundary component, as follows

$$\text{Res}_C \Omega(X, X_{\geq 0}) = \Omega(C, C_{\geq 0}), \quad (4.1)$$

and no other singularities.

The residue operation in (4.1) is defined in the following manner: for a subvariety  $C$  of  $X$ , parameterized by the zero set of the holomorphic coordinate  $z$  on  $X$  with remaining coordinates  $u$ , we denote the singularity of a given form  $\omega$  on  $X$  in the neighborhood of  $C$  as the simple pole

$$\omega(u, z) = \omega'(u) \wedge d \log z + \dots \quad (4.2)$$

where (...) denotes smooth terms in the limit  $z \rightarrow 0$  and  $\omega'(u)$  is a non-zero differential form on the boundary component. We define the residue operation

$$\text{Res}_C \omega \equiv \omega'. \quad (4.3)$$

In the following, we will list some fundamental properties and aspects of positive geometries. The list is by no means exhaustive and we refer to [38] for more details.

## Reversing Orientation and Direct Products

Positive geometries admit a natural orientation. If a certain geometry  $(X, X_{\geq 0})$  is a positive geometry, then so is the geometry  $(X, X_{\leq 0}^-)$ , where  $X_{\leq 0}^-$  is the same positive region with opposite, or flipped orientation. The canonical form changes sign under reversing orientation such that

$$\Omega(X, X_{\geq 0}) = -\Omega(X, X_{\leq 0}^-). \quad (4.4)$$

Furthermore, we can take unions of positive geometries. We will encounter a more expanded version of unions of positive geometries in section 4.3. Here, we present the notion of union for disjoint positive geometries, such that for two positive geometries on the same complex variety,  $(X, X_{\geq 0})$  and  $(X, Y_{\geq 0})$  with

$$X_{\geq 0} \cap Y_{\geq 0} = \emptyset, \quad (4.5)$$

we have that the union  $(X, X_{\geq 0} \cup Y_{\geq 0})$  is also a positive geometry with orientation inherited from the two geometries  $(X, X_{\geq 0})$  and  $(X, Y_{\geq 0})$ . The boundary components of  $(X, X_{\geq 0} \cup Y_{\geq 0})$  are either boundary components of one of its constituting geometries or a disjoint union of such boundaries. The canonical form of the resulting geometry  $(X, X_{\geq 0} \cup Y_{\geq 0})$  is simply identified as

$$\Omega(X, X_{\geq 0} \cup Y_{\geq 0}) = \Omega(X, X_{\geq 0}) + \Omega(X, Y_{\geq 0}). \quad (4.6)$$

In the next section, we shall extend this notion to the *oriented sum*, also valid for overlapping geometries, however, it is not guaranteed that the resulting geometry is itself a positive geometry.

Positive geometries also incorporate a natural notion of *direct product*. Here, two positive geometries  $(X, X_{\geq 0})$  and  $(Y, Y_{\geq 0})$ , can be multiplied in the following manner: since the direct product of  $X \times Y$  naturally describes another affine variety, with

$$X_{\geq 0} \times Y_{\geq 0} \subset X \times Y, \quad (4.7)$$

then it is natural to define

$$(Z, Z_{\geq 0}) := (X \times Y, X_{\geq 0} \times Y_{\geq 0}), \quad (4.8)$$

with canonical form

$$\Omega(Z, Z_{\geq 0}) = \Omega(X, X_{\geq 0}) \wedge \Omega(Y, Y_{\geq 0}). \quad (4.9)$$

The boundary components of the product geometry  $\Omega(Z, Z_{\geq 0})$  can be found from the boundary components  $(C, C_{\geq 0})$  of  $(X, X_{\geq 0})$  and  $(D, D_{\geq 0})$  of  $(Y, Y_{\geq 0})$  as simply  $(C \times Y, C_{\geq 0} \times Y_{\geq 0})$  and  $(X \times D, X_{\geq 0} \times D_{\geq 0})$ .

## Triangulations

An important feature of positive geometries is the notion of triangulation. For a given positive geometry  $(X, X_{\geq 0})$  it is possible to find a set of positive geometries  $\mathcal{T} = \{(X, X_{i, \geq 0})\}_{i=1}^{|\mathcal{T}|}$  that tiles  $(X, X_{\geq 0})$ , if the following properties hold

- Each  $X_{i, \geq 0} \subset X_{\geq 0}$  and their orientations agree.
- The interiors  $X_{i, \geq 0}$  are mutually disjoint.
- If  $\bigcup_{i=1}^{|\mathcal{T}|} (X, X_{i, \geq 0}) = (X, X_{\geq 0})$ .

If these properties are fulfilled, we say that  $\mathcal{T}$  *triangulates*  $(X, X_{\geq 0})$ . We note, that this nomenclature has nothing to do with triangles and the tiling geometries  $(X, X_{i, \geq 0})$  can be various types of positive geometries and not just simplices. If a positive geometry  $(X, X_{\geq 0})$  is triangulated by  $(X, X_{i, \geq 0})$ , then the canonical form  $\Omega(X, X_{\geq 0})$  is simply

$$\Omega(X, X_{\geq 0}) = \sum_{i=1}^{|\mathcal{T}|} \Omega(X, X_{i, \geq 0}). \quad (4.10)$$

A given triangulation often introduces *spurious boundaries*, i.e. boundaries of  $(X, X_{i, \geq 0})$  that do not appear as boundaries of  $(X, X_{\geq 0})$  and thus  $\Omega(X, X_{i, \geq 0})$  may have singularities that are not singularities of the sum of canonical forms in the triangulation. The spurious boundaries are therefore required to cancel in the sum.



Figure 4.1: The positive geometry that is the line element between two point  $x = a$  and  $x = b$ . Its associated canonical form is given in (4.11) and it is oriented in the positive  $x$  direction.

## Types of Positive Geometries

Here we classify some important classes of positive geometries along with some simple examples.

### Example 1: The Line Element

The line element between  $a$  and  $b$  is a 1-dimensional object defined as the set of points  $\{(1, x) | x \in [a, b]\} \subset \mathbb{RP}^1$ , with  $a < b$ . The canonical form is

$$\Omega^{(1)} = \frac{dx}{x-a} - \frac{dx}{x-b} = \frac{(b-a)}{(b-x)(x-a)} dx, \quad (4.11)$$

with the orientation is along increasing  $x$ . We have sketched the line element in Figure 4.1

### Example 2: The Standard Simplex

We generalize the construction above to the standard projective  $m$ -simplex  $(\mathbb{RP}^m, \Delta)$ , with  $\Delta^m := \mathbb{RP}_{>0}^m$  which is cut out by exactly  $m+1$  linear inequalities. These are very simple geometries represented by a certain set of positive coordinates, with canonical form

$$\Omega(\Delta^m) = \prod_{i=1}^m \frac{d\alpha_i}{\alpha_i} = \prod_{i=1}^m d \log \alpha_i, \quad (4.12)$$

for  $(\alpha_0, \alpha_1, \dots, \alpha_m) \in \mathbb{P}^m$  where we can use projectivity to set  $\alpha_0 = 1$ , then the interior  $\Delta_{>0}^m$  is simply  $\mathbb{R}_{>0}^m$ . Here the choice  $\alpha_0 = 1$  implies the boundary represented by  $\alpha_0 \rightarrow 0$  is no longer manifestly visible as a singularity of the canonical form. We can make this boundary manifest again by changing the choice of chart  $\alpha_0 = 0$  into another chart, say represented by  $\alpha_1 = 1$ . This is a common feature of positive geometries and we refer to the choice of chart as a gauge choice<sup>1</sup>. Consider the top-form on  $\mathbb{RP}^2$ ,

$$\omega = \frac{dx \wedge dy}{(x+1)(y+1)}. \quad (4.13)$$

<sup>1</sup>Gauge choice is not understood here in the context of quantum field theory e.g. as in  $SU(N)$ ,  $U(N)$ ,  $SO(N)$  etc., rather it is in the context of having to choose a specific chart to study the features of a system, here represented by the canonical form.

Here  $\omega$  is represented in the chart  $\{(1, x, y)\} \subset \mathbb{RP}^2$ . This form can be seen to have three poles along  $x = -1$ ,  $y = -1$  and the line at infinity. This can be seen by changing the chart into  $\{(1, x, y)\} \rightarrow \{\alpha, 1, \beta\} = \{x^{-1}, 1, yx^{-1}\}$ , then the form becomes

$$\omega = \frac{d\alpha \wedge d\beta}{\alpha(\alpha + 1)(\alpha + \beta)}, \quad (4.14)$$

where we now find a boundary at  $\alpha = x^{-1} = 0$ , which in the previous chart was represented by  $x \rightarrow \infty$ .

## Integration of Canonical Forms

A natural thing to do with differential forms is to integrate them over some space. For two positive geometries  $(X, X_{\geq 0})$  and  $(Y, Y_{\geq 0})$  we introduce the notion of integration of canonical forms of  $(X, X_{\geq 0})$  with respect to  $(Y, Y_{\geq 0})$  [38]

$$\omega_{Y,X} := \int_{(Y, Y_{\geq 0})} \Omega(X, X_{\geq 0}). \quad (4.15)$$

Unless the intersection of  $(Y, Y_{\geq 0})$  and  $(X, X_{\geq 0})$  only consists of disjoint points, the integrals diverges, due to the logarithmic nature of  $\Omega(X, X_{\geq 0})$ . As an example, let us consider the integration of the canonical form associated with the line element  $\{(x \in \mathbb{R}^1) : 0 \leq x \leq 1\}$ , with respect to another line element  $\{z \in \mathbb{R}^1 : 1 - x \leq z \leq 1\}$

$$\int_{1-z}^1 \frac{dx}{x} = -\log(1-z) = Li_1(z). \quad (4.16)$$

It is possible to recursively construct di-logarithms of higher degree by integrating over higher-dimensional simplices against each other.

## 4.2 Morphisms of Positive Geometries

An important feature of positive geometries and their canonical forms is the notion of *push-forwards* and *pull-backs*. We will review their construction for differential forms of arbitrary degree [40].

### Pull-back

Consider a map  $\phi$  between two positive geometries,  $X$  of dimension  $n$ , and  $Y$  of dimension  $m$ ;

$$\phi : X \rightarrow Y. \quad (4.17)$$

Given a  $k$ -form  $\eta$  on  $Y$ , there is a notion of pulling back to a form  $\omega$  on  $X$  using the map  $\phi$ . Assuming the coordinate basis for  $X$  is  $(x_1, \dots, x_n)$  and the coordinate basis for  $Y$  is  $(y_1, \dots, y_m)$ , we write the map as  $\phi = (\phi_1, \dots, \phi_m)$ . Consider the  $k$ -form (not necessarily top-dimensional)  $\eta$  written in the coordinate basis of  $Y$

$$\eta = \sum_{i_1 \leq \dots \leq i_k \leq m} \beta_{i_1, \dots, i_k}(y_1, \dots, y_m) dy_{i_1} \wedge \dots \wedge dy_{i_k}. \quad (4.18)$$

The *pull-back* of  $\eta$  through the map  $\phi$  is simply

$$\omega = \phi^*(\eta) := \sum_{i_1 \leq \dots \leq i_k \leq m} \beta_{i_1, \dots, i_k}(\phi(x_1, \dots, x_n)) d\phi_{i_1} \wedge \dots \wedge d\phi_{i_k}. \quad (4.19)$$

This is tantamount to substituting the explicit expressions  $y_i = \phi_i(x)$  in the form  $\beta$ . The differential form (4.19) is now a differential  $k$ -form on  $X$ .

### Push-forward

The push-forward is the operation that, in some sense, is the reverse of the pull-back: starting from a differential form on  $X$  and the map  $\phi$ , we can find the corresponding differential form on  $Y$ . For each point  $b \in Y$ , we can find its pre-image under  $\phi$ , the collection of points  $a_i \in X$ , for which  $\phi(a_i) = b$ . In the neighborhood  $U_i$  of each point  $a_i$ , and in the neighborhood  $V$  of  $b$ , we can define the *inverse map* as follows

$$\psi_i = \phi^{-1}|_{U_i} : V \mapsto U_i. \quad (4.20)$$

The *push forward* of a differential form  $\omega$  on  $X$  through the map  $\phi$  is a differential form  $\eta$  on  $Y$  given as the sum over the pull-backs of  $\omega$  through the inverse maps  $\psi_i$

$$\eta = \phi_*\omega = \sum_i \psi_i^*\omega. \quad (4.21)$$

This amounts to solving the equation  $y = \phi(x)$  and for each solution set  $x = \psi_i(y)$  performing the pull-back of  $\omega$  and adding the resulting differential forms. We note, that canonical forms are preserved under a push-forward: if  $\omega$  has only unit residues, then  $\eta$  has also only unit residues, as long as they are top-forms on their respective spaces. Let us review these two constructions, pull-back and push-forward in some minimal examples to familiarize ourselves with such operations.

### Example 1: Pull-Back

Consider the following differential form on  $\mathbb{R}^3$  given by

$$\omega = d \log(a_1) \wedge d \log(a_2) - d \log a_1 \wedge d \log(a_3 + a_1) + d \log a_2 \wedge d \log a_3. \quad (4.22)$$

Consider also a map

$$\phi : \mathbb{R}^2 \mapsto \mathbb{R}^3, \quad (4.23)$$

with

$$(a_1, a_2, a_3) = \phi(x_1, x_2) = (e^{-(x_1+x_2)}, \frac{1}{x_1^2}, 2x_1x_2). \quad (4.24)$$

We pull the form  $\omega$  back through the map  $\phi$  as follows

$$\phi^*\omega = (x_1 - 3x_2 - 2)d\log x_1 \wedge d\log x_2, \quad (4.25)$$

found from inserting replacing the map  $a_i = \phi(x_j)$ , and evaluating the resulting form.

### Example 2: Push-Forward

On the other hand, consider the one-form on  $\mathbb{R}^1$  given by

$$\eta = d\log x, \quad (4.26)$$

and this time consider the map  $\chi : \mathbb{R}^1 \mapsto \mathbb{R}^1$  with  $a = \chi(x) = x^2$ . In order to find the push-forward, we first note that the map  $\chi$  is not invertible and has two local solutions  $x = \xi_1(a) = \sqrt{a}$  and  $x = \xi_2(a) = -\sqrt{a}$ . We pull the form back through these inverse maps

$$\omega = \chi_*\eta = \xi_1^*\eta + \xi_2^*\eta = \frac{d\sqrt{a}}{\sqrt{a}} + \frac{d(-\sqrt{a})}{-\sqrt{a}} = \frac{d\log a}{2} + \frac{d\log a}{2} = d\log a. \quad (4.27)$$

We see that both  $\eta$  and  $\omega$  are logarithmic top forms on  $\mathbb{R}^1$  as expected.

## 4.3 Adding Positive Geometries

As discussed in section 4.1, disjoint positive geometries  $(X, X_{i,\geq 0})$ ,  $(X, X_{j,\geq 0})$  can be readily added together

$$(X, X_{i,\geq 0}) \cup (X, X_{j,\geq 0}) = (X, X_{i,\geq 0} \cup X_{j,\geq 0}), \quad (4.28)$$

$$\Omega((X, X_{i,\geq 0}) \cup (X, X_{j,\geq 0})) = \Omega((X, X_{i,\geq 0})) + \Omega((X, X_{j,\geq 0})), \quad (4.29)$$

with orientation inherited from the two geometries  $(X, X_{i,\geq 0})$ ,  $(X, X_{j,\geq 0})$ . We take the first steps in generalizing this to positive geometries that do intersect in [41]. Here the notion of *oriented sum* of positive geometries is introduced to account for the relative orientations of the intersecting geometries. We assign the symbol  $\oplus$  to this operation.

We are interested in positive geometries that intersect in two ways: when two or more geometries intersect only on their boundaries, as in the familiar case of

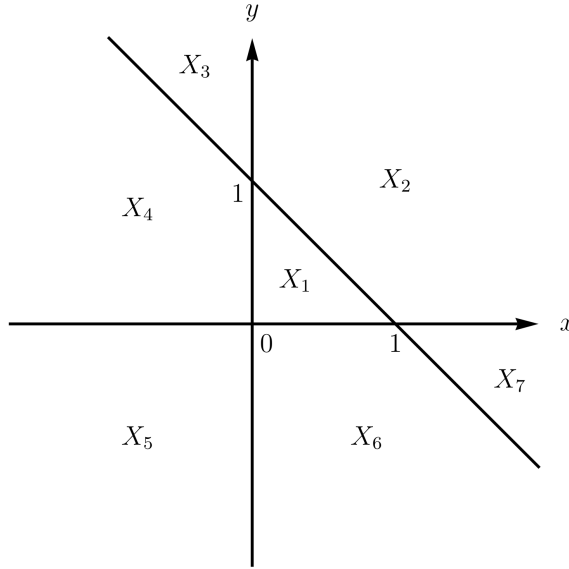


Figure 4.2: The decomposition of the two dimensional planes into 7 regions  $\{X_i\}_{i=1}^7$ . Along with  $X_8$  and  $X_9$ , denoting the left and right part of the upper half planes, they are the regions considered in illustrating the notion of oriented sums in the text. The figure is from [41].

triangulations of positive geometries, and when one geometry is a subset of another. We visualize both examples by considering the two-plane split into 9 regions denoted by  $\{X_i\}_{i=1}^9$ , where the regions  $X_1 \dots X_7$  are indicated in Figure 4.2, and  $X_8$  and  $X_9$  describe the upper quadrants such that  $X_8 = \{(x, y) : x \geq 0, y \geq 0\}$ , and  $X_9 = \{(x, y) : x \leq 0, y \geq 0\}$ . Each region  $\{X_i\}_{i=1}^9$  in Figure 4.2 is endowed with an orientation, either clockwise or counter-clockwise, denoted by  $X_i^-$  and  $X_i^+$ , respectively. Each region is a candidate for being a positive geometry, having boundaries of dimension 1 and 0 in all cases, and we can associate a canonical form to each of them,  $\Omega_i^\pm$ . Changing orientation with respect to the plane in which they are embedded, returns the same canonical form up to a sign  $\Omega_i^+ = -\Omega_i^-$  [38]. We consider two scenarios one can encounter when taking oriented sums of the different regions  $X_i$ . The first scenario (I) contains the cases where, under the oriented sum of two or more geometries, the resulting geometry is itself a positive geometry. The second scenario (II) contains the cases for which the oriented sum of two or more positive geometries violates the definition of positive geometries. We sketch a few examples

### I Oriented sum of two positive geometries giving rise to a positive geometry

- $X_1^+ \oplus X_2^+ = X_8^+$ . This geometry is nothing but the positive quadrant. We obtain the canonical form for this region as

$$\begin{aligned} \Omega = \Omega_1^+ + \Omega_2^+ &= \underbrace{\frac{dx \wedge dy}{xy} + d \log \frac{x}{y} \wedge d \log(1 - x - y)}_{\Omega_1^+} \\ &\quad + \underbrace{d \log \frac{x}{y} \wedge d \log(1 - x - y)}_{\Omega_2^+} = d \log x \wedge d \log y. \end{aligned} \quad (4.30)$$

While the two geometries share a common boundary, it is oppositely oriented in the two geometries. This results in a cancellation of that boundary in the final geometry similarly to triangulations, where shared boundaries cancel.

- $X_1^+ \oplus X_5^-$ . We sketch this geometry in Figure 4.3 and note its canonical form

$$\begin{aligned} \Omega = \Omega_1^+ + \Omega_5^- &= \frac{dx \wedge dy}{xy(1 - x - y)} - d \log x \wedge d \log y = \\ &= \frac{x + y}{(1 - x - y)xy} dx \wedge dy. \end{aligned} \quad (4.31)$$

This canonical form does not have a singularity on the point  $(x, y) = (0, 0)$ , since the singularities at this point of its constituent geometries have opposite sign. Direct inspection reveals

$$\text{Res}_{y=0} \text{Res}_{x=0} \Omega_5^- = -1, \quad \text{Res}_{y=0} \text{Res}_{x=0} \Omega_1^+ = +1, \quad (4.32)$$

and thus  $\text{Res}_{y=0} \text{Res}_{x=0} (\Omega_5^- + \Omega_1^+) = 0$ . The remaining vertices at  $(1, 0)$  and  $(0, 1)$  have residues  $\pm 1$ . We stress that the point  $(0, 0)$  is an element in the geometry  $X_1^+ \oplus X_5^-$ , but is not a boundary of the resulting geometry.

- $X_1^+ \oplus X_8^- = X_2^+$  the geometry  $X_1^+$  is a subset of  $X_8^-$  and share common boundaries. The boundaries are oriented in opposite directions, resulting in a geometry, where the shared boundaries are no longer boundaries. The remaining geometry can be identified as  $X_2^+$ , which is the intersection of the two geometries.

### II Oriented sum of two positive geometries giving rise to a geometry that is not a positive geometry

- $X_1^+ \oplus X_5^+$ . The geometries  $X_1^+$  and  $X_5^+$  intersect only on the vertex  $(0, 0)$ . The canonical form is found as the sum the two participating canonical form

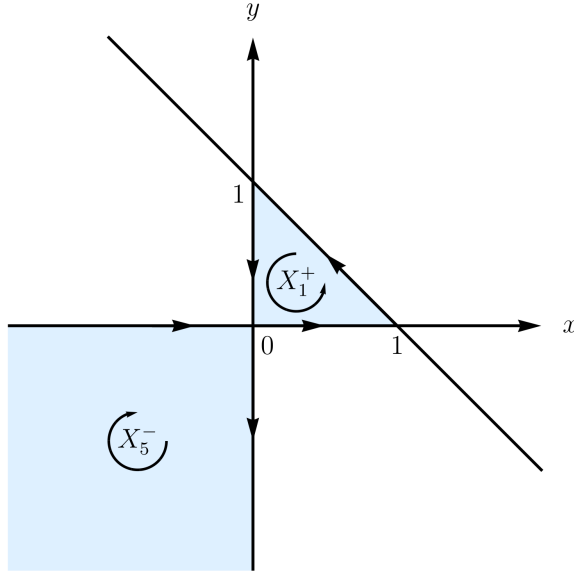


Figure 4.3: The oriented sum of  $X_1^+$  and  $X_5^-$  giving rise to a positive geometry. Note that point at the origin is a part of the resulting geometry, however it is not a boundary of said geometry as can be seen from taking residues on the sum of canonical forms. The figure is from [41].

as follows

$$\Omega = \Omega_1^+ + \Omega_5^+ = \frac{dx \wedge dy}{xy(1-x-y)} + d \log x \wedge d \log y = \frac{2+x+y}{(1-x-y)xy} dx \wedge dy. \quad (4.33)$$

We can evaluate the residue on both canonical forms

$$\text{Res}_{y=0} \text{Res}_{x=0} \Omega_5^+ = +1, \quad \text{Res}_{y=0} \text{Res}_{x=0} \Omega_1^+ = +1, \quad (4.34)$$

and we see the resulting canonical form has residue  $+2$  on the  $(0, 0)$  boundary and since the canonical form has residues of  $\pm 1$  on its remaining vertices (those in particular belonging to  $X_1^+$ ), the resulting geometry *cannot be said to be a positive geometry*, since we can no longer associate a logarithmic canonical form to the geometry.

- $X_8^+ \oplus X_5^-$ : This geometry is sketched in Figure 4.4 and is the union of two quadrants ( $x > 0, y > 0$ ) and ( $x < 0, y < 0$ ). Their canonical forms are therefore indistinguishable due to the negative orientation of  $X_5$ . The canonical form is therefore simply 0.
- $X_8^+ \oplus X_9^+$ : This geometry is sketched in Figure 4.5 and is the union of the two quadrants ( $x > 0, y > 0$ ) and ( $x < 0, y > 0$ ). This union is nothing but the upper half plane, which does not have the point  $(0, 0)$  as a 0-dimensional boundary.

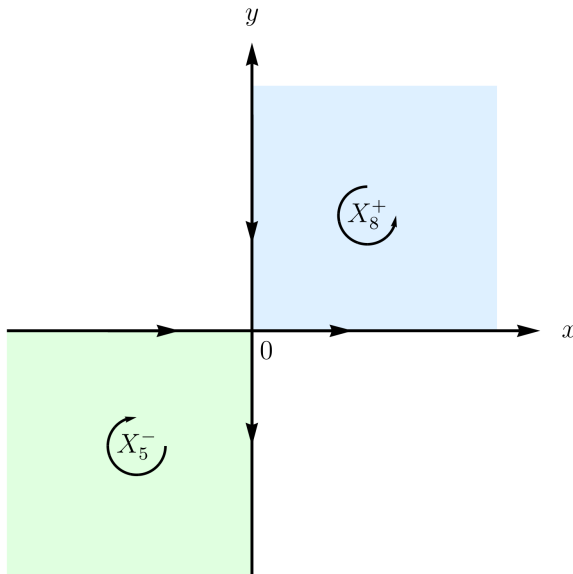


Figure 4.4: The oriented sum of  $X_8^+$  and  $X_5^-$  giving rise to a geometry that is not a positive geometry. This is due to the fact that the resulting geometry has no 0 dimensional boundaries (vertices) in its boundary stratification.

In the examples described above, the orientation of geometries is inherited from their embedding in an orientable plane and therefore defined with respect to this plane. While we leave a full definition of the oriented sum as an open problem, we expect the orientability of the embedded space  $X$  to be crucial in the construction of such a definition.

## 4.4 The Amplituhedron

The amplituhedron was the first example of a positive geometry and is physically relevant. In particular, the canonical form of the amplituhedron is related to  $R$ -invariants (2.157), and thus to the  $N^{k'}$ MHV scattering amplitudes in planar msYM in momentum twistor space as discussed in section 2.8. Remarkably the standard notions of locality and unitarity of scattering amplitudes are replaced with the positivity condition and become emergent properties. We review the construction of the amplituhedron in two frameworks: the original construction introduced in [1], where the amplituhedron is defined on an auxiliary Grassmann space, and another more recent construction where the amplituhedron is defined directly in the kinematic space of bosonized momentum twistors [75]. We then proceed to discuss how to extract scattering amplitudes or  $R$ -invariants from canonical forms on amplituhedra. Finally, we provide a brief discussion on how locality and causality appear as derived notions from the statement of positivity for the amplituhedron.

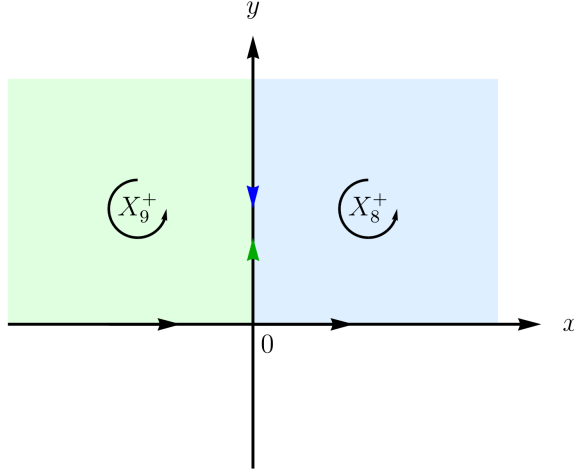


Figure 4.5: The oriented sum of  $X_8^+$  and  $X_9^+$  giving rise to a geometry which is lacking any zero-dimensional boundary and therefore not a positive geometry.

#### 4.4.1 Tree Amplituhedron

The amplituhedron [1] is a positive geometry belonging to the class of Grassmannian polytopes [38]. The starting point for the definition of the amplituhedron is the set of  $n$  momentum twistor variables defined in (2.188). These contain both bosonic  $(\lambda, \mu)$  and fermionic data  $\chi$ . In the following, we will *bosonize* [1] the supermomentum-twistors by introducing  $k'$  auxiliary Grassmann variables  $\phi_A$ ,  $A = 1, \dots, k'$ , and define the *bosonized* supermomentum-twistors as

$$Z_i^A = \begin{pmatrix} \lambda_i^a \\ \mu_i^a \\ \phi_1 \cdot \chi_i \\ \vdots \\ \phi_{k'} \cdot \chi_i \end{pmatrix}. \quad (4.35)$$

In the following, we shall assume that this matrix is a positive matrix<sup>2</sup>. We refer to the matrix (4.35) as “positive external data”,  $Z \in M_+(m + k', n)$ , interpreted as a map. The amplituhedron is the image of the positive Grassmannian, as defined in section 3.3, through positive external data  $Z$  as follows

$$\Phi_Z : G_+(k', n) \rightarrow G(k', k' + m), \quad (4.36)$$

<sup>2</sup>This seemingly innocuous restriction to positive data turns out to be of utmost consequence. In particular, the fact that the amplituhedron encodes unitarity and locality is a direct consequence of insisting on positive external data [1].

where to each element in the positive Grassmannian  $C \in G_+(k', n)$  we have associated a matrix  $Y \in G(k', k' + m)$  by

$$Y_\alpha^A = \sum_i C_{i\alpha} \cdot Z_i^A. \quad (4.37)$$

The notion of “positivity” completely encodes the co-dimension 1 boundaries [1], by identifying the  $k' + m$ - invariants

$$\langle Y^1 \dots Y^{k'} Z_{i_1} \dots Z_{i_m} \rangle = (C_{a_1} \dots C_{a_{k'}}) \langle Z_{a_1} \dots Z_{a_k} Z_{i_1} \dots Z_{i_m} \rangle \quad (4.38)$$

which are strictly positive for a given element of the positive Grassmannian  $C$  and under assumption of positivity of  $Z$  for the first few cases of  $m$ , we have the boundaries

$$m = 1 : \quad \langle Y i \rangle = 0, \quad (4.39)$$

$$m = 2 : \quad \langle Y i i + 1 \rangle = 0, \quad (4.40)$$

$$m = 4 : \quad \langle Y i i + 1 j j + 1 \rangle = 0. \quad (4.41)$$

In the last case,  $m = 4$ , the boundaries appearing are similar to the poles of the  $R$  invariants associated with (dual) propagators going on-shell in (2.154). It is exactly this case we call *physically relevant* and is related to scattering amplitudes<sup>3</sup>, since the bosonic part of the momentum twistors has  $m = 4$  entries. The scattering amplitude can be extracted from the canonical form of the amplituhedron, dubbed the “volume form”, with logarithmic singularities on its boundaries. The volume form of the amplituhedron is a top-form on  $G(k', m + k')$  and therefore of degree  $(m \times k')$ . We find the *volume function*,  $\Omega_{n,k}^{(m)}(Y, Z)$  by stripping off the canonical top form of  $\Omega_{n,k'}^{(m)}(Y, Z)$  as follows

$$\Omega_{n,k'}^{(m)}(Y, Z) = \prod_{\alpha=1}^{k'} \langle Y_1 \dots Y_{k'} d^m Y_\alpha \rangle \Omega_{n,k}^{(m)}(Y, Z). \quad (4.42)$$

We find the scattering amplitude (up to a  $A_n^{\text{MHV}}$ ) from the volume function by integrating out the bosonized auxiliary variables. It is conjectured that for all  $(n, k', m)$ , the amplituhedron is a positive geometry [38].

The amplituhedron can conveniently be found from the Grassmannian by considering positroid cells  $C \in G_+(k', n)$  of dimension  $(m \times k')$ . Then the image of the map  $Y = C \cdot Z$  carves out a region in  $G(k', m + k')$  and we can completely determine the amplituhedron by triangulation in terms of a collection of positroid cells, which are non-overlapping and dense in  $G(k', m + k')$ . The amplituhedron volume form is then found as the push-forward on these cells:

$$\Omega_{n,k'}^{(m)} = \sum_{\sigma \in \mathcal{T}} (\Phi_Z)_* \omega_\sigma, \quad (4.43)$$

---

<sup>3</sup>Rather, the amplituhedron is related to the polygonal Wilson loop dual to the scattering amplitude [76].

where  $\omega_\sigma$  refers to the canonical form on the  $m \times k'$  dimensional positroid cell in the triangulation of  $G_+(k, n)$  labeled by the decorated permutation  $\sigma$ . Parameterizing the correct  $(m \times k')$  dimensional cell in  $G_+(k', m+k')$  by the canonical positive coordinates  $\alpha_i$ , we simply obtain

$$\Omega_{n,k'}^{(m)} = \sum_{\sigma} d \log \alpha_1^\sigma(Y, Z) \wedge d \log \alpha_2^\sigma(Y, Z) \wedge \dots \wedge d \log \alpha_{mk'}^\sigma(Y, Z). \quad (4.44)$$

## Sign Flip Conditions

In [75] it was shown that the amplituhedron admits topological conditions, the sign-flip conditions. It was found by studying the sign patterns of certain brackets evaluated on points inside the amplituhedron. Here  $Y$  is taken to be a point in momentum twistor space for  $m = 4$ , then  $Y$  is inside the amplituhedron iff

$$[Yii + 1jj + 1] > 0, \quad \text{and the sequence } \{[Y1234], \dots, [Y123n]\} \text{ has exactly } k' \text{ sign-flips} \quad (4.45)$$

while for  $m = 2$ , the sign flip conditions states that the point  $Y$  is inside the amplituhedron iff

$$[Yii + 1] > 0, \quad \text{and the sequence } \{[Y12], \dots, [Y1n]\} \text{ has exactly } k' \text{ sign-flips} \quad (4.46)$$

This observation led to a definition of the amplituhedron based on intersections of certain subspaces [75]. First, we note that each element  $Y \in G(k', k' + m)$  defines an  $m$ -dimensional surface in  $n$  dimensions, in the following manner

$$z_i^a = (Y^\perp)_A^a Z_i^A, \quad (4.47)$$

where  $Y^\perp$  is the orthogonal complement of  $Y$  and  $Z$  is the bosonized momentum twistor defined in (4.35). This provides a map  $\Xi : G(k', k' + m) \rightarrow \mathcal{Z}_n$  from the auxiliary Grassmannian space  $G(k', k' + m)$  of the amplituhedron to the kinematic space of the bosonic parts of  $n$  momentum twistors,  $\mathcal{Z}_n \in (z)$  (4.47). We can compose this map with  $\Phi_Z$  and obtain a definition of the amplituhedron directly in the space of momentum twistors, as the image of the positive Grassmannian

$$\mathcal{A}_{n,k'}^{(m),z} := \Xi(\Phi_Z(G_+(k', n))). \quad (4.48)$$

The canonical form on the space  $\mathcal{Z}(n)$  can be obtained from the push-forward  $\Xi_*$  on the standard volume form  $\Omega_{n,k'}^{(m)}$  defined in (4.42)

$$\Omega_{n,k'}^{(m),z} = \Xi_* \Omega_{n,k'}^{(m)}, \quad (4.49)$$

which is an  $m \times k'$  form that is on differentials  $dz_i^a$ . This allows us to circumvent the space of auxiliary variables  $Y$ . We write  $Y$  in the following coordinate patch of  $G(k', k' + m)$

$$Y_\alpha^A = \begin{pmatrix} -y_\alpha^a \\ \mathbb{1}_{k' \times k'} \end{pmatrix}, \quad (4.50)$$

then decompose the positive matrix  $Z$  as follows

$$Z_i^A = \begin{pmatrix} z_i^{*a} \\ \Delta_i^\alpha \end{pmatrix}. \quad (4.51)$$

We denote by  $(z^*)$ , a fixed  $m$ -plane in  $n$  dimensions and  $\Delta$  as a fixed  $k'$ -plane in  $n$  dimension. We can then write (4.47) as

$$z_i^a = z_i^{*a} + y_\alpha^a \Delta_i^\alpha, \quad (4.52)$$

allowing us to define the space

$$\mathcal{V}_{n,k'}^{(m)} := \{z_i^a : z_i^a = z_i^{*a} + y_\alpha^a \Delta_i^\alpha\}. \quad (4.53)$$

This is referred to as the *affine subspace*. We also define the *winding space*  $\mathcal{W}_{n,k'}^{(m)}$  using the conditions in (4.45) projected down to  $z_i^a$  as follows

$$\begin{aligned} \mathcal{W}_{n,k'}^{(4)} &:= \{(z) : \langle ii + 1jj + 1 \rangle > 0, \\ &\text{and the sequence } \{\langle 1234 \rangle, \dots, \langle 123n \rangle\} \text{ has exactly } k' \text{ sign-flips } \}, \end{aligned} \quad (4.54)$$

where  $\langle ijkl \rangle = \epsilon_{abcd} z_i^a z_j^b z_k^c z_l^d$ . The amplituhedron can then be expressed in the kinematic space of bosonic momentum twistor space as the intersection

$$\mathcal{A}_{n,k'}^{(m),z} := \mathcal{V}_{n,k'}^{(m)} \cap \mathcal{W}_{n,k'}^{(m)}. \quad (4.55)$$

#### 4.4.2 Extracting scattering amplitudes

As discussed in this section on (4.41), the boundaries of the amplituhedron,  $\langle Yii + 1jj + 1 \rangle \rightarrow 0$ , are similar to the singularities of the tree level scattering  $R$ -invariants in msYM (2.195), which appear when the minor  $\langle ii + 1jj + 1 \rangle \rightarrow 0$  vanish. However  $\langle Yii + jj + 1 \rangle$  and  $\langle ii + 1jj + 1 \rangle$  are not completely equivalent. First and foremost,  $\langle Yii + jj + 1 \rangle$  is a  $(k' + 4)$ -bracket, including the  $k'$ -plane,  $Y$ , defined in (4.37), while the singularity  $\langle ii + 1jj + 1 \rangle$  is a four bracket. Second, the matrix  $Z_i^A$  consists of the bosonized supermomentum twistors depending on the auxiliary Grassmann variables  $\phi$ . We relate the two brackets in two steps. First, we localize  $Y$  on a reference plane [1]  $Y^*$  as follows

$$Y^* = \begin{pmatrix} \mathbb{0}_{m \times k'} \\ \mathbb{1}_{k' \times k'} \end{pmatrix}. \quad (4.56)$$

Second, we integrate the remaining auxiliary Grassmann variables as follows

$$A_{n,k'} = \int d^{\mathcal{N}=4} \phi_1 \dots d^{\mathcal{N}=4} \phi_{k'} \Omega_{n,k'}(Y^*, Z), \quad (4.57)$$

where  $\Omega_{n,k'}(Y^*, Z)$  is the volume function of the amplituhedron with  $Y$  evaluated on the reference plane  $Y^*$ . Let us consider a simple example.

We consider the amplituhedron for  $A_{5,1}^{(4)}$  related to the tree level scattering amplitude for the NMHV sector of planar  $\mathcal{N} = 4$  sYM. We bosonize the external momentum twistor data by taking  $Z_i^A = (\lambda_i^a, \mu_i^{\dot{a}}, \phi_\alpha \chi_i^\alpha)$  – in this case a square matrix – to be positive. An element of the positive Grassmannian,  $G_+(1, 5)$ , in this case is just  $C = (1, \alpha_2, \dots, \alpha_5)$ , with all  $\alpha_i > 0$  and its dimension coincides with that of  $Y \in G(1, m+1)$  defined in (4.37). This means there is no need to triangulate the amplituhedron and we can write (4.37) as follows

$$Y = Z_1 + \alpha_2 Z_2 + \dots + \alpha_5 Z_5. \quad (4.58)$$

Performing the push-forward as in (4.43) amounts to solving (4.58) with respect to the canonical coordinates  $\alpha_i$  and plugging in to

$$\omega_{5,1} = \bigwedge_{i=2}^5 d \log \alpha_i. \quad (4.59)$$

We handily obtain

$$\alpha_2 = \frac{\langle Y1345 \rangle}{\langle 12345 \rangle}, \quad \alpha_3 = \frac{\langle Y1245 \rangle}{\langle 12345 \rangle}, \quad \alpha_4 = \frac{\langle Y1235 \rangle}{\langle 12345 \rangle}, \quad \alpha_5 = \frac{\langle Y1234 \rangle}{\langle 12345 \rangle}, \quad (4.60)$$

and the push-forward of (4.59) through this map is simply

$$\Omega_{5,1} = \Phi_* \left( \bigwedge_{i=2}^5 \alpha_i \right) = \langle 12345 \rangle^4 \frac{\langle Y d^4 Y \rangle}{\langle Y1345 \rangle \langle Y1245 \rangle \langle Y1235 \rangle \langle Y1234 \rangle}. \quad (4.61)$$

The volume function can easily be extracted from this form. Two key differences between the volume function and the  $R$ -invariant from (2.195) of section 2.8, are the  $k'$ -planes,  $Y$ , and the auxiliary variables,  $\phi^A$ . We can take care of these in two steps: first, the  $k'$ -planes,  $Y$ , should be set to a fixed plane,  $Y \rightarrow Y^*$

$$Y^* = \begin{pmatrix} \mathbb{0}_{m \times k'} \\ \mathbb{1}_{k' \times k'} \end{pmatrix}. \quad (4.62)$$

In that case, the brackets in the denominator of (4.61) just become  $\langle Yijkl \rangle \rightarrow \langle ijkl \rangle$ . Further, the Grassmann integral should be performed over the remaining auxiliary

variables,  $\phi$ : in this case, we obtain e.g. that the 5-bracket in (4.61) can be expanded as

$$\begin{aligned} \langle 12345 \rangle &= \langle 1234 \rangle Z_5^5 - \langle 1235 \rangle Z_4^5 + \langle 1245 \rangle Z_3^5 - \langle 1345 \rangle Z_2^5 + \langle 2345 \rangle Z_1^5 \\ &= \phi_A (\langle 1234 \rangle \chi_5^A - \langle 1235 \rangle \chi_4^A + \langle 1245 \rangle \chi_3^A - \langle 1345 \rangle \chi_2^A + \langle 2345 \rangle \chi_1^A), \end{aligned} \quad (4.63)$$

and we are left with

$$A_{5,1} = \int d^{N=4} \phi \Omega_{5,1}(Y^*, Z) = \frac{\delta^{1 \times 4} (\langle 1234 \rangle \chi_4^A + \text{cyclic})}{\langle 1234 \rangle \langle 2345 \rangle \langle 3451 \rangle \langle 4512 \rangle \langle 5123 \rangle}, \quad (4.64)$$

which is exactly the  $R$ -invariant found in (2.195) for  $n = 5$ .

We can also extract scattering amplitudes directly from the canonical form on the kinematic space of bosonic momentum twistors,  $\Omega_{n,k'}^{(4),z}$  defined in (4.49) [77]. We relate the canonical form with scattering amplitudes by replacing the differentials  $dz_i^a \rightarrow \eta_i^a$  with the Grassmann variables parameterizing the on-shell chiral superspace.

### 4.4.3 The Loop Amplituhedron

We can extend the definition of the amplituhedron to also encode loop-integrands, by the notion of hiding particles. The general approach for constructing  $\ell$ -loop amplituhedra involves stacking two-planes in the  $(n - k)$  dimensional complement of  $C$ ,  $C^\perp$  on top of  $C$ . This space can be considered as a generalization of the Grassmannian,  $G(k', n, \ell)$ , with  $G(k', n) = G(k', n, 0)$ . A point in  $G(k', n, \ell)$  can be represented as a  $(k' + 2\ell) \times n$  matrix

$$\mathcal{C} = \begin{pmatrix} D^{(l_1)} \\ \vdots \\ D^{(l_\ell)} \\ C \end{pmatrix}. \quad (4.65)$$

We can define a positive version of  $G(k', n, \ell)$ ,  $G_+(k', n, \ell)$  by enforcing positivity conditions on  $C$  as well as any number of copies of  $D^{(l_i)}$  stacked on top of  $C$ . Then, we can obtain the image of the map

$$\mathcal{A}_{n,k'}^{\ell\text{-loop}} = \{\mathcal{Y} \in G(k', 4 + k', \ell); \mathcal{Y} = \mathcal{C} \cdot Z, \mathcal{C} \in G_+(k', n, \ell), Z \in M_+(4 + k', n)\}, \quad (4.66)$$

where  $\mathcal{Y}$  is a  $k'$ -plane in  $(4 + k')$  dimensions, with  $\ell$  two-planes  $\mathcal{L}^{l=1, \dots, \ell}$  stacked on top. The two-planes  $\mathcal{L}^{(l)}$  live in the orthogonal complement of  $Y$ . We define the map

$$\mathcal{Y} = \mathcal{C} \cdot Z = \begin{cases} Y = C \cdot Z \\ \mathcal{L}^{(1)} = D^{(l_1)} \cdot Z \\ \vdots \\ \mathcal{L}^{(\ell)} = D^{l_n} \cdot Z \end{cases}. \quad (4.67)$$

This definition implies the following positivity conditions in addition to the tree-level conditions (4.45):

$$[Y\mathcal{L}^{(l)}ii + 1] > 0, \quad (4.68)$$

$$\{[Y\mathcal{L}^{(l)}12], \dots, [Y\mathcal{L}^{(l)}1n]\} \text{ has } k' + 2 \text{ sign flips}, \quad (4.69)$$

$$[Y\mathcal{L}^{(l_i)}\mathcal{L}^{(l_j)}] > 0, \quad (4.70)$$

the last statement implies *mutual positivity* between any two pairs of loops. We observe that the one-loop MHV  $m = 4$  amplituhedron and the  $k = 2$ ,  $m = 2$  tree-level amplituhedron are formally identical [1].

#### 4.4.4 Emergent Unitarity and Locality

Scattering amplitudes in planar  $\mathcal{N} = 4$  in momentum twistor space should have singularities on and only on the following configurations of momentum twistors [1]

$$\langle ii + 1jj + 1 \rangle \rightarrow 0, \quad (4.71)$$

$$\langle ABii + 1 \rangle \rightarrow 0, \quad (4.72)$$

$$\langle (AB)_{l_i}(AB)_{l_j} \rangle \rightarrow 0. \quad (4.73)$$

This dictates locality, as it implies that particle  $i$  can only be affected by particle  $i + 1$  and particle  $i - 1$ , its immediate neighbors. Unitarity on the other hand reflects what happens when taking residues on these singularities [1, 78]. On the residues of these singularities, the  $n$ -point  $\ell$ -loop scattering amplitude factorizes into a product of scattering amplitudes with fewer external legs or amounts to the scattering amplitude with one fewer loop and two extra external legs, known as the forward limit as explored in terms of on-shell diagrams on Figure 3.12.

The tree amplituhedron naturally encodes the singularity structure of scattering amplitudes in its co-dimension-1 boundaries, which are precisely characterized when  $\langle Yii + 1jj + 1 \rangle \rightarrow 0$ , meaning that  $Y$  completely lies in the plane containing the points  $Z_i$ ,  $Z_{i+1}$ ,  $Z_j$ , and  $Z_{j+1}$ . This is a consequence of positivity coming from (4.37) and is precisely the statement of locality: that the amplitude has singularities when a certain internal momentum transfer goes on-shell.

Since we are interested how unitarity is encoded in the amplituhedron, let us review what occurs on the boundary of the amplituhedron associated with  $\langle Yii + 1jj + 1 \rangle \rightarrow 0$ . On this boundary we can parameterize  $Y_1$  as a linear combination of  $Z_i$ ,  $Z_{i+1}$ ,  $Z_j$ , and  $Z_{j+1}$ , implying the element of the positive Grassmannian  $C \in G_+(k', n)$ , can be parameterized by having only non-zero elements in the first row in the columns  $(c_i, c_{i+1}, c_j, c_{j+1})$ . Invoking positivity of the Grassmannian  $G_+(k', n)$  then forces the matrix  $C$  to factorize into two parts, denoted  $L$  and  $R$ , as can be seen on Figure 4.6. The two submatrices of Figure 4.6 can be seen as elements of the positive Grassmannian  $G_+(k'_L, n_L)$  and the positive Grassmannian  $G_+(k'_R, n_R)$ , where  $k'_L + k'_R = k' - 1$  and  $n_L + n_R = n - 2$  [1].

$$\begin{array}{c} \uparrow \\ k'_L \\ \downarrow \end{array} \left( \begin{array}{cccccccccccc} 0 & \dots & 0 & * & * & 0 & \dots & 0 & * & * & 0 & \dots & 0 \\ & & & \boxed{L} & & & & & & & \vdots & \ddots & \vdots \\ & & & & & & & & & & 0 & \dots & 0 \\ \vdots & \ddots & \vdots & & & & & & & & & & \\ & & & \boxed{R} & 0 & \dots & 0 & & \boxed{R} & & & & \\ & & & & \vdots & \ddots & \vdots & & & & & & \\ 0 & \dots & 0 & & 0 & \dots & 0 & & & & & & \end{array} \right) \begin{array}{c} \uparrow \\ k'_R \\ \downarrow \end{array}$$

Figure 4.6: When taking the limit  $\langle Y_{ii+1} j_{j+1} \rangle \rightarrow 0$  the matrix  $C \in G_+(k', n)$  factorizes into two matrices  $L$  and  $R$  which are relevant for lower dimensional amplituhedra. This implies, that the co-dimension one boundary of an amplituhedron is a product of two lower dimensional amplituhedra.



# Chapter 5

## Kinematic Associahedron

In this chapter, we discuss the “amplituhedron” relevant for bi-adjoint scalar theory discussed in section 2.5, known as the kinematic associahedron. This geometry was first studied in [43], where Arkani-Hamed, Bai, He, and Yan (ABHY) argued that the positive geometry naturally associated with *kinematic space* of planar Mandelstam variables, and whose canonical form naturally encodes the scattering amplitudes in bi-adjoint  $\phi^3$  theory, is nothing but the *associahedron* [79, 80]. The associahedron is also known as the Stasheff-polytope and is a well-described object in mathematics with particular relevance in combinatorics. We refer to the construction of the associahedron due to ABHY as the *kinematic* associahedron. In this chapter, we review the ABHY construction and provide a few examples of kinematic associahedra. We also show how the factorization properties are beautifully encoded in associahedron geometry. Finally, we will discuss how to construct the kinematic associahedron for different color orderings.

### 5.1 Kinematic Space

Consider the very simple theory of (massless) bi-adjoint scalars with cubic interactions discussed in section 2.5. Such a theory admits a color decomposition in which partial amplitudes can be found by a Feynman diagram expansion or various other methods, such as the CHY formalism also discussed in section 2.5. These partial amplitudes are rational functions of Mandelstam variables (2.26). To ensure that the construction of section 2.5 holds in arbitrary dimension, we can define the *kinematic space*,  $\mathcal{K}_n$ , for  $n$  massless momenta in  $D$  dimensions  $p_i \in \mathbb{R}^D$  with  $i = 1, \dots, n$ , as the space spanned by linearly independent Mandelstam variables in  $D \geq n - 1$ , given by

$$s_{ij} = (p_i + p_j)^2 = 2p_i \cdot p_j. \quad (5.1)$$

If  $D < n - 1$  we have further constraints on the space, the so-called Gram conditions. We will return to a discussion of Gram conditions in chapter 7 and for now assume

that  $D \geq n - 1$ . Momentum conservation of external momenta enforces  $n$  linearly independent constraints on the form

$$\sum_{j=1, j \neq i}^n s_{ij} = 0. \quad (5.2)$$

The linear independent space of Mandelstam variables can then be understood as the space of

$$\dim \mathcal{K}_n = \binom{n}{2} - n = n(n-3)/2, \quad (5.3)$$

independent variables. We can also define the set of multiparticle Mandelstam variables labeled by a subset  $I \subset \{1, \dots, n\}$  as follows

$$s_I = \sum_{i, j \in I: i < j} s_{ij}. \quad (5.4)$$

It turns out that there exists a more natural basis of this space, namely the set of planar Mandelstam variables. These can be realized by considering a graph consisting of edges and vertices where each edge is labeled by the momenta of the external particles  $\{1, \dots, n\}$ . On support of momentum conservation, each consecutive momentum vector begins at the end of the previous momentum vector. This carves out an  $n$ -gon in two dimensions. By definition, this object has as many edges as vertices and thus we label each vertex to be the one having to the  $i^{\text{th}}$  momentum edge incoming. In that case, we can realize the Euclidean distance between two vertices

$$X_{ij} = x_{ij}^2 = \left( \sum_{a=i}^{j-1} p_a \right)^2 = s_{i, i+1, \dots, j-1}, \quad (5.5)$$

where the lower case  $x$ 's are the dual momentum variables defined in (2.169). Naturally these variables have manifest cyclic symmetry and the number of  $X$  variables is exactly equal to the dimensionality of the kinematic space. Returning to the  $n$ -gon, it is easy to see that when the object is completely triangulated by non-overlapping triangles with internal edges  $X_{ij}$ . The triangulation is dual to a Feynman diagram contributing to the scattering amplitude  $m_n(12\dots n|12\dots n)$ , with the triangulating edges  $X$  as propagators, as illustrated on Figure 5.1.

## 5.2 The Planar Scattering Form

In the following, we define the planar scattering form naturally associated with the kinematic space of Mandelstam variables. Consider a complete triangulation of the



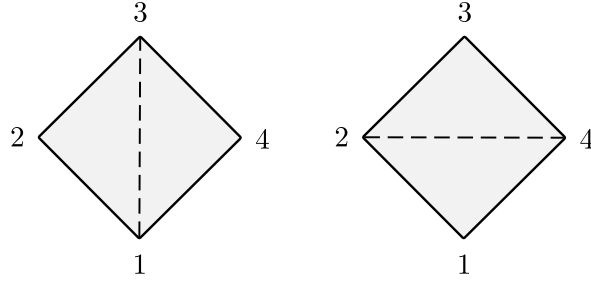


Figure 5.2: The two possible triangulations of the quadrilateral associated with the planar Mandelstam variables  $X_{13}$  on the left, and  $X_{24}$  on the right.

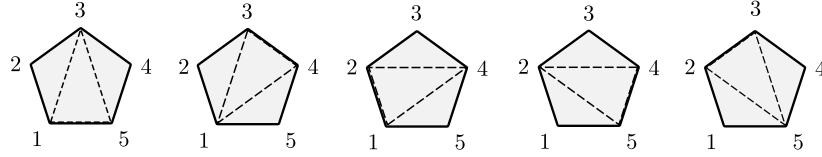


Figure 5.3: The five different ways to triangulate a pentagon fully in terms of simplices. The associated planar Mandelstam variables associated with a given triangulation are given in order  $\{X_{13}X_{35}, X_{13}X_{14}, X_{14}X_{24}, X_{24}X_{25}, X_{25}X_{35}\}$ .

The only projectively meaningful one-form we can obtain from these two variables is the following [43]

$$\omega_4 = d \log X_{13} - d \log X_{24} = d \log \frac{X_{13}}{X_{24}}. \quad (5.8)$$

Similarly, we can define the projectively meaningful two-form associated with triangulations of the pentagon. We draw the pentagon and realize that there are 5 ways of triangulating it with simplices, as sketched in Figure 5.3. The planar scattering form for  $n = 5$  is therefore

$$\begin{aligned} \omega_5 &= d \log X_{13} \wedge d \log X_{14} - d \log X_{14} \wedge d \log X_{24} + \\ &\quad + d \log X_{24} \wedge d \log X_{25} - d \log X_{25} \wedge d \log X_{35} + d \log X_{35} \wedge d \log X_{13} = \\ &= d \log \frac{X_{13}}{X_{24}} \wedge d \log \frac{X_{13}}{X_{14}} \wedge d \log \frac{X_{13}}{X_{25}} \wedge d \log \frac{X_{35}}{X_{24}}. \end{aligned} \quad (5.9)$$

### 5.3 The Kinematic Associahedron

We define the kinematic associahedron as the positive geometry associated with the planar scattering form, by first restricting to positive kinematic variables. We call this the *positive region*, given by

$$\Delta_n : X_{ij} > 0, \quad (5.10)$$

for all  $1 \leq i < i+1 < j \leq n$ , since  $X_{ii+1} = 0$ . This is a simplex with a facet at infinity when taking  $X_{ij} \in \mathbb{RP}^{|\mathcal{K}_n|}$ , where  $|\mathcal{K}_n|$  is  $n(n-3)/2$ , the number of linearly independent Mandelstam variables. We then consider the subspace of the kinematic space defined by the following set of constraints

$$\mathcal{H}_n : c_{ij} = X_{ij} + X_{i+1j+1} - X_{ij+1} - X_{i+1,j} > 0. \quad (5.11)$$

Where  $c_{ij}$  are positive constants for every non-adjacent pair of indices and  $j \neq n$ . The kinematic associahedron can be written as the intersection between the positive region and the space of constraints (5.11), namely

$$\mathcal{A}_n = \Delta_n \cap \mathcal{H}_n. \quad (5.12)$$

The kinematic associahedron is closely related to the  $n$ -gon. Each full triangulation of an  $n$ -gon corresponds to a vertex of the kinematic associahedron and each edge in the kinematic associahedron corresponds to a partial triangulation of the  $n$ -gon with 1 diagonal removed and each face corresponds to a partial triangulation with 2 diagonals removed. This pattern continues and can be summed up by the following

*The codimension- $d$  facet of the associahedron corresponds to the partial triangulation of the  $n$ -gon with  $d$  diagonals removed.*

In the following, we make this discussion explicit by considering a few examples of kinematic associahedra.

## 5.4 Examples

In the following, we review some examples of kinematic associahedra in order to illustrate the discussion of section 5.3.

### $n = 4$ Kinematic Associahedron

The kinematic space for the  $n = 4$  kinematic associahedron is 2-dimensional and can be parameterized by the kinematic variables  $\{X_{13}, X_{24}\} = \{s, t\}$ . The positive region is simply taking these two variables positive

$$\Delta_4 : \quad \{s > 0\} \cap \{t > 0\} \quad (5.13)$$

If we take  $s$  and  $t$  independent, the space of constraints  $\mathcal{H}_4$  is then the inequality

$$\mathcal{H}_4 : \quad c_{13} = s + t > 0 \quad \Rightarrow \quad 0 < s < c_{13}. \quad (5.14)$$

The kinematic associahedron for  $n = 4$  is then simply

$$\mathcal{A}_4 = \Delta_4 \cap \mathcal{H}_4, \quad (5.15)$$

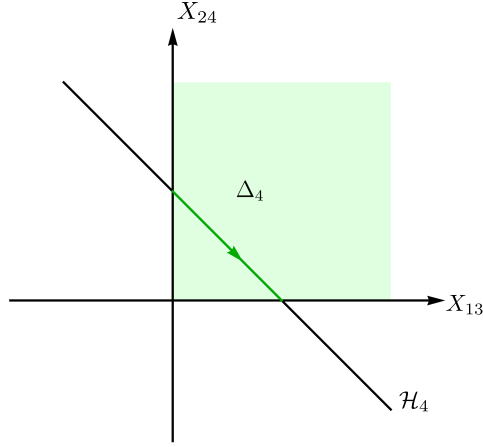


Figure 5.4: The  $n = 4$  kinematic association,  $\mathcal{A}_4$  (green line), as the intersection of a positive regions given by  $\Delta$ , the positive quadrant, and the  $\mathcal{H}_4$  space of constraints. In this graph we take  $s = X_{13}$  and  $t = X_{24}$  and we take the orientation along increasing  $s$ .

which is the line element with end points  $s = 0$  and  $s = c_{13}$  sketched in Figure 5.4. The canonical form for the line element was described in the last chapter in (4.11) and is given by

$$\Omega(\mathcal{A}_4) = \left( \frac{1}{s} - \frac{1}{s - c_{13}} \right) ds = \left( \frac{1}{s} + \frac{1}{t} \right) ds, \quad (5.16)$$

which is exactly the planar scattering form for  $n = 4$  (5.8) pulled back to  $\mathcal{H}_4$  using

$$dc_{13} = ds + dt = 0 \Rightarrow ds = -dt, \quad (5.17)$$

inserting in the planar scattering form just yields

$$\Omega(\mathcal{A}_4) = \omega_4|_{\mathcal{H}_\Delta} = \left( \frac{ds}{s} - \frac{dt}{t} \right) |_{\mathcal{H}_4} = \left( \frac{1}{s} + \frac{1}{t} \right) ds. \quad (5.18)$$

which is exactly the four-point scattering amplitude,  $m_4(1234|1234)$ , times the differential  $ds$ .

### $n = 5$ Kinematic Associahedron

For  $n = 5$ , the kinematic space  $\mathcal{K}_n$  is 5-dimensional and can be parameterized by the following set of variables  $\{X_{13}, X_{14}, X_{24}, X_{25}, X_{35}\}$  and we define the positive region as the following intersection

$$\Delta_5 : \quad \{X_{13} > 0\} \cap \{X_{14} > 0\} \cap \{X_{24} > 0\} \cap \{X_{25} > 0\} \cap \{X_{35} > 0\}, \quad (5.19)$$

which is a simplex in  $\mathbb{RP}^5$  with one facet at infinity. The  $\mathcal{H}_5$  space of constraints (5.11) can be obtained as

$$\mathcal{H}_5 : X_{13} + X_{24} - X_{14} = c_{13} \geq 0, \quad (5.20)$$

$$X_{24} + X_{35} - X_{25} = c_{24} \geq 0, \quad (5.21)$$

$$X_{14} + X_{25} - X_{24} = c_{14} \geq 0. \quad (5.22)$$

Taking the kinematic associahedron for  $n = 5$  as the intersection

$$\mathcal{A}_5 = \Delta_5 \cap \mathcal{H}_5. \quad (5.23)$$

We can visualize the kinematic associahedron for  $n = 5$  by solving the equations defining  $\mathcal{H}_5$  (5.20) choosing, e.g.  $\{X_{13}, X_{14}\}$  as our basis coordinates as follows

$$\begin{aligned} X_{13} &\geq 0, \\ X_{14} &\geq 0, \\ X_{24} = c_{13} - X_{13} + X_{14} &\geq 0, \\ X_{35} = c_{24} + c_{14} - X_{14} &\geq 0, \\ X_{25} = c_{14} + c_{13} - x_{13} &\geq 0. \end{aligned} \quad (5.24)$$

We have sketched this region in Figure 5.5 . The inequalities of (5.24) just cut out a pentagon. We could also realize the associahedron by considering the triangulations of the pentagon, whose associated geometry is itself a pentagon. This realization is visualized in Figure 5.6 . The canonical form on this space is just the canonical form on the kinematic space  $\mathcal{K}_5$ :

$$\begin{aligned} \Omega(\mathcal{K}_5) &= d \log X_{14} \wedge d \log X_{13} + d \log X_{13} \wedge d \log X_{35} + d \log X_{35} \wedge d \log X_{25} + \\ &\quad + d \log X_{25} \wedge d \log X_{24} + d \log X_{24} \wedge d \log X_{14}. \end{aligned} \quad (5.25)$$

pulled back to the subspace  $\mathcal{H}_5$  (5.20). The pull-back to  $\mathcal{H}_5$  just amounts to equating the numerators in (5.25) as follows

$$dX_{14} \wedge dX_{13} = dX_{13} \wedge dX_{35} = \dots = dX_{24} \wedge dX_{14} := d^2 X. \quad (5.26)$$

The pull-back to  $\mathcal{H}_5$  is just

$$\Omega(\mathcal{K}_5)|_{\mathcal{H}_5} = \left( \frac{1}{X_{13}X_{14}} + \frac{1}{X_{14}X_{24}} + \dots \frac{1}{X_{24}X_{14}} \right) d^2 X, \quad (5.27)$$

where the function multiplied by the differential  $d^2 X$  is identified as

$$\Omega(\mathcal{K}_5)|_{\mathcal{H}_5} = m(12345|12345)d^2 X, \quad (5.28)$$

namely, the scattering amplitude for bi-adjoint  $\phi^3$  theory for  $n = 5$  in the standard double color-ordering.

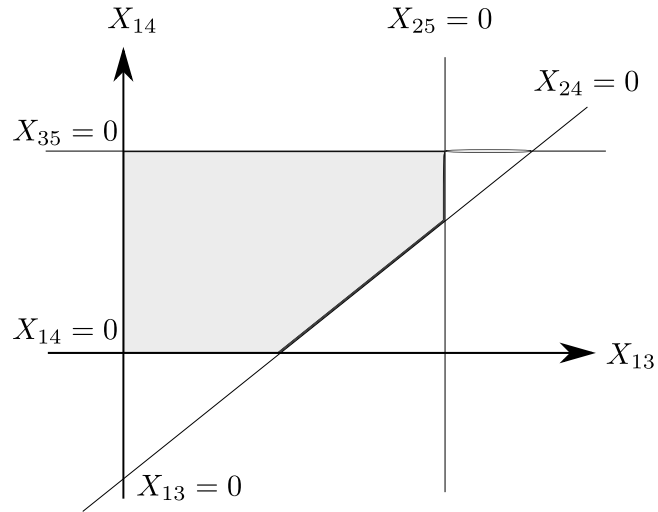


Figure 5.5: The kinematic associahedron for  $n = 5$ . The positive region is given by  $X_{13} > 0 \cup X_{14} > 0$ . The  $\mathcal{H}_5$  space is encoded in, e.g.  $X_{25} = X_{14} + c$ , the line  $X_{25} = 0$  is parallel to the line  $X_{14} = 0$  with separation  $c$ .

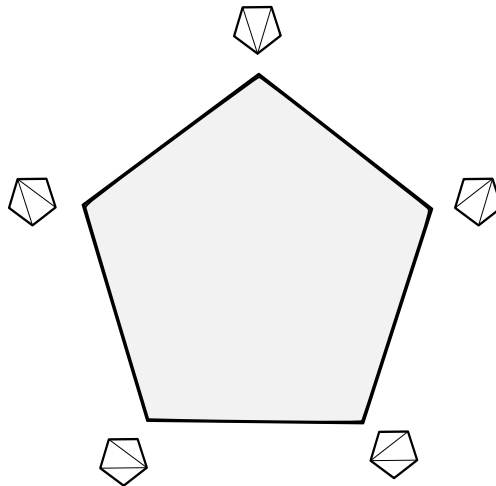


Figure 5.6: The associahedron, as realized by the triangulation of the pentagon, is itself a pentagon. This is unique for the  $n = 5$  associahedron.

### $n = 6$ Kinematic Associahedron

For  $n = 6$  the kinematic space of Mandelstam variables is 9 dimensional. We parameterize the kinematic space using the following variables  $\{X_{13}, X_{14}, X_{15}, X_{24}, X_{25}, X_{26}, X_{35}, X_{36}, X_{46}\}$ , taking the positive region as follows

$$\Delta_6 : \quad \{X_{13} > 0\} \cap \{X_{14} > 0\} \cap \dots \cap \{X_{46} > 0\}, \quad (5.29)$$

which is a simplex in  $\mathbb{RP}^9$  with one facet at infinity. We write the  $\mathcal{H}_6$  space of constraints according to (5.11) as follows

$$\begin{aligned} X_{13} + X_{24} - X_{14} &= c_{13} > 0, \\ X_{14} + X_{25} - X_{15} - X_{24} &= c_{14} > 0, \\ X_{15} + X_{26} - X_{25} &= c_{15} > 0, \\ X_{24} + X_{35} - X_{25} &= c_{24} > 0, \\ X_{25} + X_{36} - X_{26} - X_{35} &= c_{25} > 0, \\ X_{35} + X_{46} - X_{36} &= c_{35} > 0. \end{aligned} \quad (5.30)$$

The kinematic associahedron for  $n = 6$  is the intersection

$$\mathcal{A}_6 = \Delta_6 \cap \mathcal{H}_6. \quad (5.31)$$

Solving the constraints in (5.4) in the basis of  $(X_{13}, X_{14}, X_{46})$  yields a three dimensional subspace sketched on Figure 5.7. We do not quote the canonical form of the kinematic associahedron here, but refer to the paper [43].

## 5.5 Kinematic Associahedron for Arbitrary Color Orderings

As reviewed in section 2.5, the bi-adjoint  $\phi^3$  theory amplitudes admit a color decomposition with respect to two external orderings. The partial amplitudes  $m_n(\alpha|\beta)$  are rational functions of the planar Mandelstam variables, and in particular the planar Mandelstam variables that are *planar with respect to the two color orderings  $\alpha$  and  $\beta$* . This means, that we can fix one color ordering  $\alpha = \{1, 2, \dots, n\}$  to the standard ordering and discuss partial amplitudes on the form  $m_n(\beta) = m_n(1, 2, \dots, n|\beta)$ . For non-standard orderings  $\beta$ , the partial amplitudes are rational functions of a subset of the planar Mandelstam variables that are planar with respect to  $\beta$ . On the level of the kinematic associahedron, this is obtained by pushing certain boundaries associated with the planar Mandelstam variables not compatible with  $\beta$  to infinity. This can be done in two ways: 1) modifying the affine subspace,  $\mathcal{H}_n \rightarrow \mathcal{H}_n(\beta)$  in (5.11) as was done in [43], or 2) modifying our definition of the positive region (5.10) as was done in [41]. We will in this section explore the

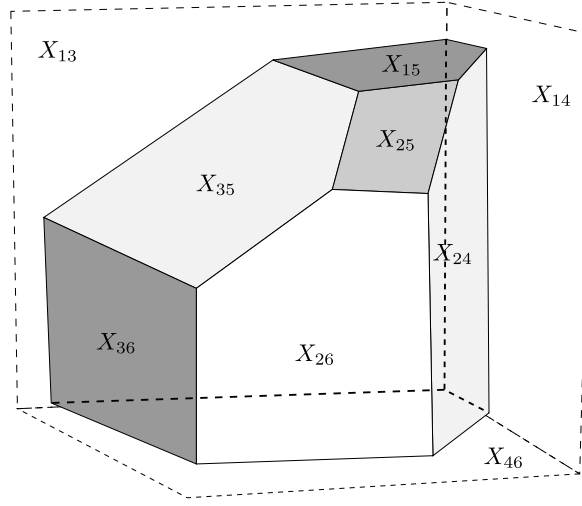


Figure 5.7: The kinematic associahedron for  $n = 6$  is three dimensional. We sketch it here and verify that the codimension-1 boundaries of the  $n = 6$  associahedron are pentagons ( $n = 5$  associahedra) and quadrilaterals (direct products of  $n = 4$  associahedra)

latter choice and we define the kinematic associahedron for a given color ordering  $\beta$  as follows

$$\mathcal{A}_n(\beta) = \Delta_n(\beta) \cap \mathcal{H}_n. \quad (5.32)$$

We define the positive region  $\Delta_n(\beta)$  in a way similar to the construction of double-partial amplitudes in  $m_n(\alpha|\beta)$  in section 2.5. In particular it reuses the polygon decomposition algorithm discussed in that section. The construction of  $\Delta_n(\beta)$  proceeds as follows: draw the circle of section 2.5 with external ordering  $\{1, 2, \dots, n\}$ , and connect the nodes on the boundary according to the ordering  $\beta$  in the interior. Then locate a set  $\{i, i+1, \dots, i+r\}$  of at least two consecutive external labels,  $r > 1$ , which are consecutive in both the standard- and the  $\beta$ -ordering. Thereafter, move all nodes in the set close together on the boundary and denote the intersection point of the two lines emanating from the nodes  $i$  and  $i+r$  by a new node,  $R$ . The nodes  $\{i, i+1, \dots, i+r, R\}$  then form a convex polygon. We remove this polygon from the circle by moving the node  $R$  to the boundary and repeat the procedure, with the nodes  $\{i, i+1, \dots, i+r\}$  replaced by the single node  $R$ . This procedure is sketched in Figure 2.2. In the case where there one fails to find a consecutive set with  $r > 1$  at any point in the algorithm, we set  $\Delta_n(\beta) = \emptyset$ . Each time we remove a polygon we denote the pair of labels  $(i_j, i_j + r_j + 1)$  following the decomposition to its conclusion, we are left with a set of labels corresponding to a partial triangulation of a regular  $n$ -gon with the following diagonals

$$\mathcal{D}(\beta) = \{(i_1, i_1 + r_1 + 1), (i_2, i_2 + r_2 + 1), \dots, (i_q, i_q + r_q + 1)\}, \quad (5.33)$$

where  $q$  denotes the number of iterations of the algorithm before it concludes. The positive region,  $\Delta_n(\beta)$ , is then defined as follows: for each diagonal  $(i, j) \in \mathcal{D}(\beta)$  we take  $X_{ij} \geq 0$  and furthermore for each diagonal  $(a, b)$  not crossing any diagonal in  $\mathcal{D}(\beta)$ , we take  $X_{ab} \geq 0$ . The definition of  $\mathcal{D}(\beta)$  is symmetric under reflection of  $\beta$  and therefore we have  $\Delta_n(\beta) = \Delta_n(\beta^{-1})$ , and similarly for the kinematic associahedron  $\mathcal{A}_n(\beta) = \mathcal{A}_n(\beta^{-1})$ . The kinematic associahedron of different orderings are overlapping geometries as can be seen already for the  $n = 4$  example, where the positive regions are

$$\Delta_4(1234) = X_{13} \geq 0 \cap X_{24} \geq 0, \quad (5.34)$$

$$\Delta_4(1243) = X_{13} \geq 0, \quad (5.35)$$

$$\Delta_4(1423) = X_{24} \geq 0. \quad (5.36)$$

The canonical form of  $\mathcal{A}_n(\beta)$  can be extracted from the canonical form of the standard ordered kinematic associahedron as follows

$$\Omega(\mathcal{A}_n(\beta)) = (-1)^{n_{\text{flip}}(\beta)} \Omega(\mathcal{A}_n(1, 2, \dots, n)) \Big|_{d \log X_{ij} \rightarrow 0 \text{ if } X_{ij}=0 \text{ is not a boundary of } \Delta_n(\beta)}. \quad (5.37)$$

Here  $n_{\text{flip}}(\beta) = n_{\text{flip}}(1, 2, \dots, n|\beta)$  and was introduced in section 2.5 and the prefactor  $(-1)^{n_{\text{flip}}(\beta)}$  determines the orientation of the kinematic associahedron  $\mathcal{A}_n(\beta)$  relative to the standard ordered kinematic associahedron. This orientation is chosen such that the double-partial amplitudes  $m_n(\beta)$  can be consistently extracted from the canonical forms  $\Omega(\mathcal{A}_n(\beta))$  by pulling back to the affine subspace  $\mathcal{H}_n$  as follows

$$\Omega_n(\mathcal{A}_n(\beta)) \Big|_{\mathcal{H}_n} = m_n(\beta) \bigwedge_{j=3}^{n-1} dX_{1j}. \quad (5.38)$$

Interestingly, since the definition of positive regions  $\Delta_n(\beta)$  allows for empty regions, not all orderings  $\beta \in \mathcal{O}_n = S_n/Z_n$  have a corresponding non-zero amplitude. We call such orderings *incompatible* orderings. By direct enumeration, we find the number of non-empty regions,  $p_n$ , for  $n \leq 8$  particles in the following Table 5.1. The sequence  $p_n$

$n$	4	5	6	7	8
$p_n$	6	22	90	394	1806

Table 5.1: The number of non-zero positive regions  $p_n$  for  $n = 4, \dots, 8$  particles. The sequence is known as the Large Schröder numbers.

is called the *Large Schröder Numbers* [82]. The Large Schröder Numbers have been studied in the context of positive geometries in [83], where they appear in the context of generalized triangles for the  $m = 2$  amplituhedron  $\mathcal{A}_{n,k}^{(2)}$ . In particular, the partial triangulations corresponding to the positive regions  $\Delta_n(\beta)$  correspond to graphical labels for the generalized triangles of  $\mathcal{A}_{n,k}^{(2)}$  [41, 83].

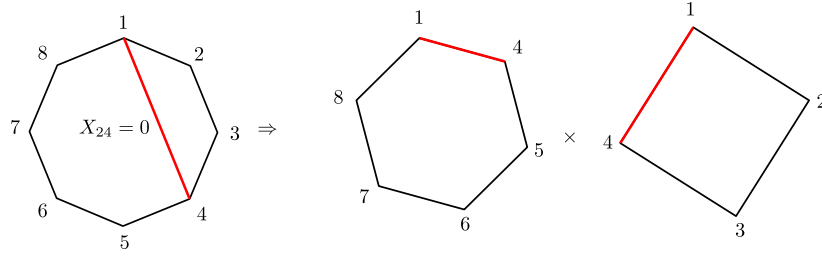


Figure 5.8: The factorization of the  $n = 8$  associahedron into the product geometry of the  $n = 6$  associahedron and the  $n = 4$  associahedron visualized as partitions of the octagon into a hexagon and a quadrilateral. The internal line is highlighted in red. The resulting 4-dimensional geometry is the direct product of the  $n = 6$  kinematic associahedron sketched in Figure 5.7 and the line element associated with the  $n = 4$  kinematic associahedron sketched on 5.4.

## 5.6 Factorization and Boundaries of the Kinematic Associahedron

The associahedron factorizes geometrically. Taking the associahedron for  $n = 3$ ,  $\mathcal{A}_3 := 1$  as the unit element, we see that each facet is the direct product:

$$\mathcal{A}_n|_{X_{ij}=0} \simeq \mathcal{A}_m \times \mathcal{A}_{n-m+2}, \quad (5.39)$$

as can be seen from the dissection of the  $n$ -gon displayed in Figure 5.8. This can be seen already in the  $n = 5$  kinematic associahedron example. Here each boundary, associated with  $X_{ij} \rightarrow 0$ , is the product of a line-element associated with the  $n = 4$  associahedron and a single point, or the unit element, associated with the  $n = 3$  associahedron, which, of course, is trivial. The factorization is even clearer for the 3-dimensional  $n = 6$  kinematic associahedron on Figure 5.7, where each codimension-1 boundary is either the direct product of the pentagon, that is the  $n = 5$  kinematic associahedron, and the unit element, or the direct product of two line elements, the  $n = 4$  kinematic associahedra, reflecting the factorization channels of scattering amplitudes as indicated in (2.51).

# Chapter 6

## The Momentum Amplituhedron

The momentum amplituhedron was first described in 2019 by the author, Ferro, Lukowski, and Parisi in [39]. Like its cousin the amplituhedron, reviewed in section 4.4, it is a positive geometry associated with scattering amplitudes in  $\mathcal{N} = 4$  sYM, however, the momentum amplituhedron makes use of spinor helicity variables instead of momentum twistors. While the momentum amplituhedron is, at first glance, a more complicated geometry compared to the ordinary amplituhedron, its definition opens an avenue of investigation of geometries associated with scattering amplitudes for which momentum twistors are not suitable variables. In particular, this is the case beyond the planar sector of msYM and in theories with less-than-maximal supersymmetry.

In the first case, the momentum amplituhedron is easily extendable to partial amplitudes planar with respect to arbitrary orderings of external legs, which is the closest to *non-planar* we can come for tree-level amplitudes. We postpone this discussion until chapter 8. As for the second case, we leave a generalization of the momentum amplituhedron for theories with  $\mathcal{N} < 4$  as an open problem. For now, we will introduce the momentum amplituhedron following its original proposal in [39] after having reviewed how scattering amplitudes in msYM can be expressed as differential forms. The original definition of the momentum amplituhedron can be seen as parallel to the original definition of the amplituhedron [1], where we bosonize the spinor helicity variables similarly to the momentum twistors of section 4.4. We then construct an auxiliary Grassmannian space from these variables and check that it fulfills certain conjectures for a candidate geometry put forward in [84]. Furthermore, we proceed to discuss how to extract the canonical form from the momentum amplituhedron and in turn, scattering amplitudes. Lastly, we review the factorization properties of the momentum amplituhedron and provide basic examples of momentum amplituhedra.

## 6.1 Scattering Amplitudes as Differential Forms

Scattering amplitudes in msYM have a natural interpretation as differential forms on the kinematic space of spinor-helicity variables. Before introducing the momentum amplituhedron in details, we discuss how to interpret scattering amplitudes in (ms)YM as differential forms, as explored by He and Zhang in [84]. We are interested in the differential forms on the kinematic space of spinor-helicity variables, which as we have seen extensively in section 3.2, can be represented as two  $(2 \times n)$  matrices,  $\lambda$  and  $\tilde{\lambda}$  subject to an orthogonality constraint:

$$(\lambda, \tilde{\lambda}) := \{\lambda_i^a \in M(2, n), \tilde{\lambda}_i^{\dot{a}} \in M(2, n) \mid \sum_{i=1}^n \lambda_i^a \tilde{\lambda}_i^{\dot{a}} = 0\}. \quad (6.1)$$

Since all particle states in msYM transform under a particular little group scaling (see the discussion in section 2.2), we wish to dress each external state of helicity  $h$  with a differential on  $(\lambda, \tilde{\lambda})$  such that the little group scaling of the state is canceled. This is possible for all theories with  $|h| \leq 1$ , as each helicity state scales

$$|(\lambda, \tilde{\lambda})^h\rangle \rightarrow |(t\lambda, t^{-1}\tilde{\lambda})^h\rangle = t^{-2h}|(\lambda, \tilde{\lambda})^h\rangle. \quad (6.2)$$

For  $h = \pm 1$  we can have at most  $(d\lambda)^2 = d\lambda^1 \wedge d\lambda^2$  or  $(d\tilde{\lambda})^2 = d\tilde{\lambda}^{\dot{1}} \wedge d\tilde{\lambda}^{\dot{2}}$ . Since we are interested in dressing external states such that they have trivial little group scaling, we associate these differentials to massless gluon states  $h = +1$  and  $h = -1$ , as follows

$$h = +1 : \quad g^+ \rightarrow (d\lambda)^2 g^+, \quad (6.3)$$

$$h = -1 : \quad g^- \rightarrow (d\tilde{\lambda})^2 g^-. \quad (6.4)$$

We can similarly dress fermionic states,  $\Gamma_a$  and  $\bar{\Gamma}_{\dot{a}}$  of (2.122) with  $h = \pm \frac{1}{2}$ . For each fermionic helicity state we have two choices

$$h = +\frac{1}{2} : \quad \bar{\Gamma}_a \rightarrow d\lambda^a \bar{\Gamma}_a \quad \text{or} \quad \bar{\Gamma}_{\dot{a}} \rightarrow (d\lambda)^2 d\tilde{\lambda}^{\dot{a}} \bar{\Gamma}_{\dot{a}}, \quad (6.5)$$

$$h = -\frac{1}{2} : \quad \Gamma_{\dot{a}} \rightarrow d\tilde{\lambda}^{\dot{a}} \Gamma_{\dot{a}} \quad \text{or} \quad \Gamma_a \rightarrow (d\tilde{\lambda})^2 d\lambda^a \Gamma_a. \quad (6.6)$$

In general, we ensure that when we have pairs of fermions of different helicities in a scattering process  $(\bar{f}_i^-, f_j^+)$ , we obtain either of the following four-forms

$$\epsilon_{\dot{a}\dot{b}} d\tilde{\lambda}_i^{\dot{a}} \wedge d\tilde{\lambda}_j^{\dot{b}} (d\lambda_j)^2, \quad \text{or} \quad (d\tilde{\lambda}_i)^2 \epsilon_{ab} d\lambda_i^a \wedge d\lambda_j^b, \quad (6.7)$$

where we have associated the spinor indices of the differentials with the flavour indices of the fermions [84].

This construction is universal for any theory with helicity states. However as we are interested in msYM, let us review the construction for this theory. As discussed in

section 2.6, the chiral superamplitude lives in the on-shell superspace  $(\lambda^a, \tilde{\lambda}^{\dot{a}}|\eta^A)$  with  $a, \dot{a} = 1, 2$  and  $A = 1, \dots, 4$ . However, as mentioned in the end of section 2.6, there also exists a non-chiral on-shell superspace related to the chiral on-shell superspace by Fourier transforms on half of the Grassmann variables. This leads to a representation where the  $R$ -symmetry is  $SU(2|2)$  and we can naturally associate the spinor indices of the  $R$ -symmetry indices [85] to  $(a, \dot{a})$ . We dress the states in the supermultiplet with differentials as follows [84]

$$\begin{aligned} \Phi(\lambda, \tilde{\lambda}, d\lambda, d\tilde{\lambda}) &= (d\lambda)^2 g^+ + (d\tilde{\lambda})^2 g^- + \phi + d\lambda^a \wedge d\tilde{\lambda}^{\dot{a}} \phi'_{a\dot{a}} + (d\lambda)^2 (d\tilde{\lambda})^2 \phi'' \\ &\quad + d\lambda^a \Gamma_a + (d\lambda)^2 d\tilde{\lambda}^{\dot{a}} \bar{\Gamma}_{\dot{a}} + d\tilde{\lambda}^{\dot{a}} \bar{\Gamma}'_{\dot{a}} + (d\tilde{\lambda})^2 d\lambda^a \Gamma'_a, \end{aligned} \quad (6.8)$$

where we distinguish between the  $6 = 1 + 4 + 1$  scalars  $\{\phi, \phi'_{a\dot{a}}, \phi''\}$  dressed with the forms  $\{1, d\lambda^a \wedge d\tilde{\lambda}^{\dot{a}}, (d\lambda)^2 (d\tilde{\lambda})^2\}$ , and the  $2 + 2$   $h = -\frac{1}{2}$  gluinos  $\{\psi_{\dot{a}}, \psi'_a\}$  dressed with the forms  $\{\tilde{\lambda}^{\dot{a}}, (d\tilde{\lambda})^2 \lambda^a\}$ , and similarly with the positive gluino states  $\bar{\psi}_a$  and  $\bar{\psi}'_{\dot{a}}$  which we dress with  $\{d\lambda^a, (d\lambda)^2 d\tilde{\lambda}^{\dot{a}}\}$ . This representation of the supermultiplet realizes an  $n$ -point superamplitude as a differential form of degree  $2n$ , which can be obtained directly from the scattering amplitude by the replacement

$$\eta^a \rightarrow d\lambda^a, \quad \tilde{\eta}^{\dot{a}} \rightarrow d\tilde{\lambda}^{\dot{a}}. \quad (6.9)$$

These replacements transform all superamplitudes into differential forms of degree  $2n = 2(n - k) + 2k$  on  $d\lambda$  and  $d\tilde{\lambda}$ . We can easily express the supercharges<sup>1</sup> as forms as follows

$$d\tilde{q}^{\dot{a}a} = \sum_i \tilde{\lambda}_i^{\dot{a}} d\lambda_i^a, \quad dq^{a\dot{a}} = \sum_i \lambda_i^a d\tilde{\lambda}_i^{\dot{a}}, \quad (6.10)$$

Since any superamplitude must respect overall supermomentum conservation, the  $2n$ -form for  $n > 3$  superamplitudes must contain overall factor  $(dq)^4 \wedge (d\tilde{q})^4$ . However this differential form vanish on support of supermomentum conservation, since for all superamplitudes, we have

$$0 = p^{a\dot{a}} = \sum_{i=1}^n \lambda_i^a \tilde{\lambda}_i^{\dot{a}} \Rightarrow (dp)^4 = (dq)^4 + (d\tilde{q})^4 \Rightarrow (dq)^4 \wedge (d\tilde{q})^4 = 0. \quad (6.11)$$

We can resolve this by stripping off a copy of either  $(d\tilde{q}^{\dot{a}a})^4$  or  $(dq^{a\dot{a}})^4$  from the canonical form [84], such that we obtain a form of degree  $(2n - 4)$ . Defining the vanishing  $2n$ -form for msYM, denoted by  $\mathcal{F}_n$ , we obtain a  $2n - 4$  form  $\Omega_{n,k}$ , by stripping off an overall factor of  $(dq)^4$ , or equivalently (up to a potential sign)  $(d\tilde{q})^4$ , as follows

$$\mathcal{F}_n := (dq)^4 \wedge \Omega_n, \quad (6.12)$$

---

<sup>1</sup>These are not the same supercharges of section 2.6. We will not encounter the chiral superspace anymore in this dissertation, so we should be free to redefine them here without cause for misunderstanding.

or equivalently, we can strip off both a factor of  $(dq)^4$  and  $(d\tilde{q})^4$  for  $n > 3$ , to obtain a form  $\hat{\Omega}$  of degree  $2n - 8$  as follows

$$\mathcal{F}_n := (dq)^4 \wedge (d\tilde{q})^4 \wedge \hat{\Omega}_n. \quad (6.13)$$

We define the differential two-forms for the  $n = 3$  scattering amplitudes (2.137) and (2.138) as follows

$$\mathcal{F}_{3,2} = (dq)^4 \wedge \Omega_{3,2} = (dq)^4 \wedge \frac{(d\lambda_1 \langle 23 \rangle + d\lambda_2 \langle 31 \rangle + d\lambda_3 \langle 12 \rangle)^2}{\langle 12 \rangle \langle 23 \rangle \langle 31 \rangle}, \quad (6.14)$$

$$\mathcal{F}_{3,1} = (d\tilde{q})^4 \wedge \Omega_{3,1} = (d\tilde{q})^4 \wedge \frac{(d\tilde{\lambda}_1 [23] + d\tilde{\lambda}_2 [31] + d\tilde{\lambda}_3 [12])^2}{[12][23][31]}. \quad (6.15)$$

The two-forms,  $\Omega_{3,k}$ , can be readily extracted using

$$d\lambda_i \langle jk \rangle + d\lambda_j \langle ki \rangle + d\lambda_k \langle ij \rangle = -(\lambda_i d \langle jk \rangle + \lambda_j d \langle ki \rangle + \lambda_k d \langle ij \rangle), \quad (6.16)$$

and similarly for  $\tilde{\lambda}$ , we are left with the following two-forms for  $n = 3$ :

$$\Omega_{3,2} = d \log \frac{\langle 12 \rangle}{\langle 31 \rangle} \wedge d \log \frac{\langle 23 \rangle}{\langle 31 \rangle}, \quad \Omega_{3,1} = d \log \frac{[12]}{[31]} \wedge d \log \frac{[23]}{[31]}. \quad (6.17)$$

We have found a logarithmic differential form for  $n = 3$  scattering amplitudes in msYM. It is not initially clear that such a form exists for all  $n > 3$ , however as it was argued in [84], all scattering amplitude forms  $\Omega_{n,k}^{(\gamma)}$  on the space of spinor-helicity variables  $(\lambda, \tilde{\lambda})$  can be found as the push-forward of the canonical form of a cell in the positive Grassmannian (3.35),  $\omega_{n,k}^{(\gamma)}$ . This can be done by identifying the first elements of the matrix  $C_{\alpha i} \in G_+(k, n)$  with  $\lambda_i^a$ , leading to the form

$$\Omega_{n,k}^{(\gamma)} = \int \omega_{n,k}^{(\gamma)} \prod_{\alpha'} \delta^2(C_{\alpha'} \cdot \tilde{\lambda}) \delta^2(C_{\alpha'}^\perp) \wedge_{\alpha'} (C_{\alpha'} \cdot d\tilde{\lambda})^2 \wedge_{\alpha'} (C_{\alpha'}^\perp \cdot d\lambda)^2, \quad (6.18)$$

where  $\alpha' = 3, \dots, k$  counts the remaining unfixed columns, when fixing  $C_{a=1,2i} \rightarrow C_{a=1,2i}^* = \lambda_i^a$ .

We review a few examples: for  $n = 4$  the associated positive Grassmannian is  $G_+(2, 4)$  and we represent an element  $C \in G_+(2, 4)$  as a  $2 \times 4$  matrix up to  $GL(2)$  transformations. The canonical top-form on  $G_+(2, 4)$  can then be written following the discussion in section 3.3 as

$$\omega_{4,2} = \frac{d^{2 \times 4} C}{\text{vol}(GL(2))(12)(23)(34)(41)}. \quad (6.19)$$

Taking  $C_{ia} = C_{ia}^* = \lambda_i^a$ , we can  $GL(2)$  transform using a particular  $2 \times 2$  matrix, to obtain a representation of  $C^*$  on the form

$$\begin{aligned} C^* &= \frac{1}{\langle 12 \rangle} \begin{pmatrix} \lambda_2^2 & -\lambda_2^1 \\ -\lambda_1^2 & \lambda_1^1 \end{pmatrix} \begin{pmatrix} \lambda_1^1 & \lambda_2^1 & \cdots & \lambda_n^1 \\ \lambda_1^2 & \lambda_2^2 & \cdots & \lambda_n^2 \end{pmatrix} = \\ &= \frac{1}{\langle 12 \rangle} \begin{pmatrix} \langle 12 \rangle & 0 & \langle 32 \rangle & \langle 42 \rangle \\ 0 & \langle 12 \rangle & \langle 13 \rangle & \langle 14 \rangle \end{pmatrix}. \end{aligned} \quad (6.20)$$

Pushing the form  $\omega_{4,2}$  forward using this map  $C^*$ , we obtain

$$\Omega_{4,2} = d \log \frac{\langle 12 \rangle}{\langle 13 \rangle} \wedge d \log \frac{\langle 23 \rangle}{\langle 13 \rangle} \wedge d \log \frac{\langle 34 \rangle}{\langle 13 \rangle} \wedge d \log \frac{\langle 41 \rangle}{\langle 13 \rangle}, \quad (6.21)$$

which is a logarithmic four-form. We could just as well have localized the map  $C \rightarrow C^* = \tilde{\lambda}$ , leading to the form

$$\Omega_{4,2} = d \log \frac{[12]}{[13]} \wedge d \log \frac{[23]}{[13]} \wedge d \log \frac{[34]}{[13]} \wedge d \log \frac{[41]}{[13]} \quad (6.22)$$

which is exactly equal to the above form on (6.21) due to momentum conservation  $\delta^{2 \times 2}(\lambda \cdot \tilde{\lambda})$ . We can write this differential form as the scattering amplitude for msYM with a factor of  $(d\tilde{q})^4$  or  $(dq)^4$  stripped off, either

$$\Omega_{4,2} = \frac{(d\tilde{q})^4}{\langle 12 \rangle [12] \langle 23 \rangle [23]}, \quad (6.23)$$

giving rise to (6.21), or

$$\Omega_{4,2} = \frac{(dq)^4}{\langle 12 \rangle [12] \langle 23 \rangle [23]} \quad (6.24)$$

giving rise to the form (6.22). The map  $C^*$  can be generalized to all  $n$  in the MHV sector, leading to the following logarithmic differential form for all MHV amplitudes at tree level [84]

$$\Omega_{n,2} = \prod_{i=2}^{n-1} d \log \frac{\langle ii+1 \rangle}{\langle 1i+1 \rangle} \wedge d \log \frac{\langle 1i+1 \rangle}{\langle 12 \rangle}. \quad (6.25)$$

The NMHV example is slightly more involved, but also more interesting, since the Grassmannian cell corresponding to the scattering amplitude is no longer the top-cell for  $n \geq 6$  and instead the scattering amplitude is related to a sum of  $(2n-4)$  dimensional cells found from BCFW recursion discussed in section 3.4. The first example of this is the  $n=6, k=3$  scattering amplitude, which can be found as the sum over three 8-dimensional cells of  $G_+(3,6)$ . We label the cells by  $\gamma_i$ , representing points in  $G_+(3,6)$  where the Plücker coordinate  $(ii+1i+2)$  vanish. Following the analysis

of section 3.4, we find two sums of cells relevant to the  $n = 6$ ,  $k = 3$  superamplitude, related by parity symmetry. We obtain a logarithmic form for the  $n = 6$ ,  $k = 3$  superamplitude as follows

$$\Omega_{6,3} = \Omega_{6,3}^{\gamma_1} + \Omega_{6,3}^{\gamma_3} + \Omega_{6,3}^{\gamma_5} = \Omega_{6,3}^{\gamma_2} + \Omega_{6,3}^{\gamma_4} + \Omega_{6,3}^{\gamma_6}, \quad (6.26)$$

where the form  $\Omega_{6,3}^{\gamma_1}$  on the cell  $\gamma_1$  is obtained by choosing the solution for  $C^*$  as follows

$$C^* = \begin{pmatrix} \lambda_1^a & \lambda_2^a & \lambda_3^a & \lambda_4^a & \lambda_5^a & \lambda_6^a \\ 0 & 0 & 0 & [56] & [64] & [45] \end{pmatrix}, \quad (6.27)$$

and pushing the Grassmannian form forward using this matrix  $C^*$  leading to the following form

$$\Omega_{6,3}^{\gamma_1} = \frac{(d\tilde{q})^4 (d\lambda_1 \langle 23 \rangle + \text{cyclic})^2 (d\tilde{\lambda}_4 [56] + \text{cyclic})}{s_{123} \langle 12 \rangle \langle 23 \rangle [45] [56] \langle 1|5+6|4 \rangle \langle 3|4+5|6 \rangle}, \quad (6.28)$$

where cyclic refer to summing over all cyclic permutations of the labels  $\{1, 2, 3\}$  in the first term and  $\{4, 5, 6\}$  in the second term. The denominator of this form appears exactly as the five non-zero Plücker coordinates of the matrix  $C^*$ , and the numerators stem from  $(C^* \cdot d\tilde{\lambda})^2$  and  $(C^* \cdot d\lambda)^2$ . This differential form can equivalently be cast on a manifestly logarithmic form on 8 canonical coordinates defined as follows

$$\begin{aligned} \Omega_{6,3}^{\gamma_i} = d \log \frac{\langle 12 \rangle}{\langle 31 \rangle} \wedge d \log \frac{\langle 23 \rangle}{\langle 31 \rangle} \wedge d \log \frac{[34]}{[\hat{3}1]} \wedge d \log \frac{[46]}{[\hat{3}1]} \wedge \\ \wedge d \log \frac{[61]}{[\hat{3}1]} \wedge d \log \frac{[14]}{[\hat{3}1]} \wedge d \log \frac{[54]}{[64]} \wedge d \log \frac{[65]}{[64]}, \end{aligned} \quad (6.29)$$

with the shifted spinor helicity variables defined by the following

$$\hat{\lambda}_1 = \tilde{\lambda}_1 + \frac{\langle 12 \rangle}{\langle 13 \rangle} \tilde{\lambda}_2, \quad \hat{\lambda}_3 = \tilde{\lambda}_3 + \frac{\langle 23 \rangle}{\langle 13 \rangle} \tilde{\lambda}_2. \quad (6.30)$$

In the following, we will review the underlying positive geometry to which these logarithmic forms are canonical forms, the momentum amplituhedron.

## 6.2 The Momentum Amplituhedron

Having found a  $(2n-4)$ -form on  $(\lambda, \tilde{\lambda})$  associated with each superamplitude in msYM, a natural question arises about whether there exists a positive geometry to which the  $(2n-4)$ -form is the canonical form. The answer is yes and the positive geometry is the momentum amplituhedron [39]. The momentum amplituhedron  $\mathcal{A}_{n,k}$  encodes

superamplitudes,  $A_{n,k}$ , for  $n$  particles with helicity<sup>2</sup>  $k = (2, \dots, n-2)$  in msYM directly in terms of spinor helicity variables. The momentum amplituhedron is defined on the space of *bosonized* spinor helicity variables which we define by introducing  $2(n-k)$  auxiliary Grassmann variables  $\phi_a^\alpha$  and  $2k$  auxiliary Grassmann variables  $\tilde{\phi}_a^{\dot{\alpha}}$  where  $\alpha = 1, \dots, n-k$ ,  $\dot{\alpha} = 1, \dots, k$ , and  $a, \dot{a} = 1, 2$ . The bosonized spinor helicity variables are then defined as follows

$$\begin{aligned}\Lambda_i^A &= \begin{pmatrix} \lambda_i^a \\ \phi_a^\alpha \eta_i^a \end{pmatrix}, & A = (a, \alpha) = 1, \dots, n-k+2 \\ \tilde{\Lambda}_i^{\dot{A}} &= \begin{pmatrix} \lambda_i^{\dot{a}} \\ \tilde{\phi}_a^{\dot{\alpha}} \tilde{\eta}_i^{\dot{a}} \end{pmatrix} & \dot{A} = (\dot{a}, \dot{\alpha}) = 1, \dots, k+2.\end{aligned}\quad (6.31)$$

The bosonized spinor helicity variables are organized into matrices:

$$\Lambda = (\Lambda_1^A, \Lambda_2^A, \dots, \Lambda_n^A) \in M(n-k+2, n), \quad \tilde{\Lambda} = (\tilde{\Lambda}_1^{\dot{A}}, \tilde{\Lambda}_2^{\dot{A}}, \dots, \tilde{\Lambda}_n^{\dot{A}}) \in M(k+2, n)\quad (6.32)$$

Interpreting these matrices as linear subspaces of dimension  $(n-k+2)$  and  $(k+2)$  in  $n$ -dimensional space, we can define their orthogonal complements as  $\Lambda^\perp \in M(k-2, n)$  and  $\tilde{\Lambda}^\perp \in M(n-k-2, n)$  as the orthogonal subspaces in  $n$  dimensions, defined up to  $GL$ -transformations. We generalize the spinor products ( $\langle ij \rangle, [ij]$ ), defined in section 2.1, to  $(n-k+2)$ -brackets

$$\langle i_1 i_2 \dots i_{n-k+2} \rangle = \det(\Lambda_{i_1}^A \Lambda_{i_2}^A \dots \Lambda_{i_{n-k+2}}^A),\quad (6.33)$$

denoting the  $GL(n-k+2)$  invariant information of  $\Lambda$ , and  $(k+2)$ -brackets

$$[i_1 i_2 \dots i_{k+2}] = \det(\tilde{\Lambda}_{i_1}^{\dot{A}} \tilde{\Lambda}_{i_2}^{\dot{A}} \dots \tilde{\Lambda}_{i_{k+2}}^{\dot{A}}),\quad (6.34)$$

denoting the  $GL(k+2)$  invariant information of  $\tilde{\Lambda}$ .

Breaking the symmetry between  $\Lambda$  and  $\tilde{\Lambda}$ , we impose our notion of positivity on  $\tilde{\Lambda}$  and *twisted positivity* on  $\Lambda$ . The condition of twisted positivity is equivalent to stating that the orthogonal complement  $\Lambda^\perp$  is a positive matrix. The result of imposing positivity restricts  $(\Lambda, \tilde{\Lambda})$  to  $\tilde{\Lambda} \in M_+(k+2, n)$  and  $\Lambda \in M_{t,+}(n-k+2, n)$ . Note that this choice of taking  $\Lambda^\perp$  positive does not imply that  $\Lambda$  is positive<sup>3</sup>.

Having organized the external data in  $(\Lambda, \tilde{\Lambda})$ , we define the momentum amplituhedron,  $\mathcal{M}_{n,k}$ , as the image of the positive Grassmannian, defined in section 3.3, through the map [39]:

$$\Phi_{(\Lambda, \tilde{\Lambda})} : G_+(k, n) \rightarrow G(k, k+2) \times G(n-k, n-k+2),\quad (6.35)$$

<sup>2</sup>Here and in the following we take  $k = k' + 2$  in comparison to the ordinary amplituhedron, since the momentum amplituhedron geometry is related to the full superamplitude and not just the  $R$ -invariants.

<sup>3</sup>We could just as well have chosen  $\Lambda$  to be positive and  $\tilde{\Lambda}$  to be twisted positive. This would provide an alternative, but equivalent, definition for the momentum amplituhedron.

We associate an element of the positive Grassmannian  $C = \{c_{\dot{\alpha}i}\} \in G_+(k, n)$  to a pair of Grassmannian elements  $(Y, \tilde{Y}) \in G(k, k+2) \times G(n-k, n-k+2)$  as follows

$$\tilde{Y}_{\dot{\alpha}}^A = \sum_{i=1}^n c_{\dot{\alpha}i} \tilde{\Lambda}_i^A, \quad Y_{\alpha}^A = \sum_{i=1}^n c_{\alpha i}^{\perp} \Lambda_i^A, \quad (6.36)$$

where we have defined  $c_{\alpha i}^{\perp}$  as an element of the orthogonal complement of the positive Grassmannian, such that  $C^{\perp} \cdot C = 0$ . This map is well defined, since  $Y$  has rank  $(n-k)$  and is an element of  $G(n-k, n-k+2)$ . We claim that the momentum amplituhedron is a positive geometry and its canonical form encodes the  $n$ -particle  $\mathbb{N}^{k-2}$ MHV tree-level scattering amplitude. We notice that the dimension of this map is

$$\dim G(k, k+2) + \dim G(n-k, n-k+2) = 2k + 2(n-k) = 2n. \quad (6.37)$$

This means that a given top-form on this space will have degree  $(2n)$ : the image of the positive Grassmannian is lower-dimensional. The momentum amplituhedron is restricted to the following codimension-4 subspace

$$P^{a\dot{a}} = \sum_{i=1}^n (Y^{\perp} \cdot \Lambda)_i^a \left( \tilde{Y}^{\perp} \cdot \tilde{\Lambda} \right)_i^{\dot{a}} = 0. \quad (6.38)$$

with orthogonal complements  $Y^{\perp} \in G(2, n-k+2)$  and  $\tilde{Y}^{\perp} \in G(2, k+2)$ .

In the paper [84], the authors conjecture two criteria that must be imposed if a certain geometry is to be considered a positive geometry for sYM in spinor helicity space. The criteria reads:

1. Positive planar Mandelstam variables:  $s_{i, i+1, \dots, i+p} > 0$  for  $i = 1, \dots, n$  and  $p = 1, \dots, n-3$ .
2. Correct sign flips: let  $N$  count the sign flips of the list  $\{\langle 12 \rangle, \langle 13 \rangle, \dots, \langle 1n \rangle\}$  and let  $\tilde{N}$  count the sign flips of the list  $\{[12], [13], \dots, [1n]\}$  then either  $(N, \tilde{N}) = (k-2, k)$  or  $(N, \tilde{N}) = (n-k-2, n-k)$ .

As we will see, momentum amplituhedron fulfills these conditions when projecting through fixed  $Y$  and  $\tilde{Y}$ , such that

$$(Y^{\perp} \cdot \Lambda)_i^a \rightarrow \lambda_i^a, \quad \left( \tilde{Y}^{\perp} \cdot \tilde{\Lambda} \right)_i^{\dot{a}} \rightarrow \tilde{\lambda}_i^{\dot{a}}, \quad (6.39)$$

then the condition (6.38) reduces to the familiar statement of momentum conservation

$$0 = \sum_{i=1}^n (Y^{\perp} \cdot \Lambda)_i^a \left( \tilde{Y}^{\perp} \cdot \tilde{\Lambda} \right)_i^{\dot{a}} \rightarrow \sum_{i=1}^n \lambda_i^a \tilde{\lambda}_i^{\dot{a}}. \quad (6.40)$$

The first criterion concerning positive planar multiparticle Mandelstam variables appears to be fulfilled by our geometry “out of the box” for the MHV and  $\overline{\text{MHV}}$  cases for all  $n$ , but is not guaranteed beyond  $k = 2$ . Therefore, we impose an additional set of constraints on  $\Lambda$  and  $\tilde{\Lambda}$  ensuring Mandelstam positivity. These relations are simple, but currently fail to reveal a physical interpretation [39]. We will investigate the case specifically for  $n = 6$ ,  $k = 3$  in the examples of section 6.3.

The second check is automatically fulfilled by our geometry. We prove this by making identifications of  $Y$  and  $\tilde{Y}$  as elements in ordinary amplituhedra with different  $m$  and  $k'$ , whose sign flip conditions are known. We can check that our geometry fulfills the sign flip condition by performing a similar projection through fixed  $(Y, \tilde{Y})$  yielding only the bosonic part of kinematic space

$$\langle Yij \rangle \rightarrow \langle ij \rangle, \quad [\tilde{Y}ij] \rightarrow [ij]. \quad (6.41)$$

Taking the sequences

$$\{\langle Y12 \rangle, \langle Y13 \rangle, \dots, \langle Y1n \rangle\}, \quad (6.42)$$

$$\{[\tilde{Y}12], [\tilde{Y}13], \dots, [\tilde{Y}1n]\}, \quad (6.43)$$

it is easy to see that the sequence in (6.42) has  $k - 2$  sign flips and the sequence (6.43) has  $k$  sign flips. For the latter case, we identify the ordinary amplituhedron [1] for  $m = 2$  and  $k' = k$  and simply quote its number of sign flips obtained in [75], as  $k$ . The former case relies on a similar observation, but the proof is slightly more involved. Here we first consider a different object. Let us define  $X \in G(k - 2, k)$  as follows

$$X_{\dot{\alpha}}^{\bar{A}} = (\Lambda^{\perp})_i^{\bar{A}} c_{\dot{\alpha}}. \quad (6.44)$$

Here the roles of  $\Lambda$  and  $c$  has been reversed. Since both  $\Lambda^{\perp}$  and  $c$  are positive matrices, this construction is similar to the ordinary amplituhedron with  $m = 2$  and  $k' = k - 2$  and the sign-flip conditions of this object is simply that

$$\{(X12), (X13), \dots, (X1n)\}, \quad (6.45)$$

has  $(k - 2)$  sign flips using  $(Xab) = \epsilon_{\dot{\alpha}_1 \dots \dot{\alpha}_k} X_{\dot{\alpha}_1}^1 \dots X_{\dot{\alpha}_k}^k c_{\dot{\alpha}_{k-1}, a} c_{\dot{\alpha}_k, b}$ . We further identify

$$(Xab) = \sum_{i_1 < \dots < i_{k-2}} (i_1 \dots i_{k-2} ab) \langle i_1 \dots i_{k-2} \rangle^{\perp}, \quad (6.46)$$

using the results of Appendix A, we can rewrite this in two steps

$$\begin{aligned} (Xab) &= \sum_{i_1 < \dots < i_{k-2}} (i_1 \dots i_{k-2} ab) \langle i_1 \dots i_{k-2} \rangle^{\perp} = \\ &= \sum_{j_1 < \dots < j_{n-k}} \epsilon_{i_1 \dots i_{k-2} a b j_1 \dots j_{n-k}} (j_1 \dots j_{n-k})^{\perp} \epsilon_{i_1 \dots i_{k-2} j_1 \dots j_{n-k} a b} \langle j_1 \dots j_{n-k} ab \rangle = \\ &= \sum_{j_1 < \dots < j_{n-k}} (j_1 \dots j_{n-k})^{\perp} \langle j_1 \dots j_{n-k} ab \rangle = \langle Yab \rangle, \end{aligned} \quad (6.47)$$

thus proving the sequence  $\{Y1i\}$  has exactly  $(k - 2)$  sign flips.

Before moving on we stress that the momentum amplituhedron admits a natural generalization [86] away from the setting strictly relevant to scattering amplitudes. In particular, we can define the momentum amplituhedron through *any* pair of matrices subject to positivity and twisted positivity constraints. We define the momentum amplituhedron,  $\mathcal{M}_{n,k}^{(m)}$  for all even  $m$  as follows. Let  $\tilde{\Lambda} \in M_+(k + \frac{m}{2}, n)$  be a positive matrix, and let  $\Lambda \in M_{t,+}(n - k + \frac{m}{2}, n)$  be a twisted positive matrix, where  $m$  is a positive, even integer and  $k + m < n$ . This pair  $(\tilde{\Lambda}, \Lambda)$  induces a map from the positive Grassmannian

$$\Phi_{(\tilde{\Lambda}, \Lambda)}^{(m)} : G_+(k, n) \rightarrow G(k, k + \frac{m}{2}) \times G(n - k, n - k + \frac{m}{2}), \quad (6.48)$$

by associating the pair  $(\tilde{Y}, Y)$  to each element in the positive Grassmannian  $C \in G_+(k, n)$ , as follows

$$\tilde{Y}_{\dot{\alpha}}^{\dot{A}} = \sum_{i=1}^n c_{\dot{\alpha}i} \Lambda_i^{\dot{A}}, \quad Y_{\alpha}^A = \sum_{i=1}^n c_{\alpha i}^{\perp} \tilde{\Lambda}_i^A. \quad (6.49)$$

We identify  $\mathcal{M}_{n,k}^{(4)} = \mathcal{M}_{n,k}$  as the *physical* momentum amplituhedron. We notice the dimensionality of  $G(k, k + \frac{m}{2}) \times G(n - k, n - k + \frac{m}{2})$  is

$$\dim G(k, k + \frac{m}{2}) \times G(n - k, n - k + \frac{m}{2}) = \frac{m}{2}k + \frac{m}{2}(n - \frac{m}{2}) = \frac{m}{2}n. \quad (6.50)$$

As was shown in the paper [86], the momentum amplituhedron  $\mathcal{M}_{n,k}^{(m)}$  lives inside the co-dimension  $\frac{m^2}{4}$  surface, constrained by

$$P^{a\dot{a}} = (Y^{\perp} \cdot \Lambda)_i^a \left( \tilde{Y}^{\perp} \cdot \tilde{\Lambda} \right)_i^{\dot{a}} = 0. \quad (6.51)$$

The simplest momentum amplituhedron  $\mathcal{M}_{n,k}^{(2)}$  can provide a setting in which to study the mathematical properties of the geometry in general, and in the papers [86, 87] it was observed that the  $m = 2$  momentum amplituhedron is closely related to the so-called hypersimplex, which we will not review here.

### 6.3 The Momentum Amplituhedron Boundaries and Volume Form

There are several ways to obtain the canonical form for the momentum amplituhedron for the physical case,  $\mathcal{M}_{n,k}^{(4)}$ . Before discussing these methods, let us review the boundary structure of momentum amplituhedron, as this will provide important checks that the candidate forms are indeed canonical forms with the correct recursive singularity structure as discussed in section 4.1.

### 6.3.1 Boundaries of the Momentum Amplituhedron

We consider the three types of codimension-1 boundaries of the momentum amplituhedron,

$$\langle Y ii + 1 \rangle \rightarrow 0, \quad [\tilde{Y} ii + 1] \rightarrow 0, \quad S_{ii+1\dots i+j} \rightarrow 0. \quad (6.52)$$

The planar Mandelstam variables,  $S_{ij\dots k}$ , are the uplift of the usual planar Mandelstam variables we have encountered throughout this dissertation:

$$S_{ii+1\dots j} = \sum_{a=i}^{j-1} \sum_{b=a+1}^j \langle Y ab \rangle [\tilde{Y} ab]. \quad (6.53)$$

The first two boundaries in (6.52) correspond to collinear limits of scattering amplitudes, while the vanishing of the Mandelstams (6.53) correspond to the factorization channels as discussed in section 2.4, that is, the boundaries of the momentum amplituhedron correspond to all singularities of tree-level amplitudes in msYM. It is possible to obtain the full boundary stratification of the momentum amplituhedron as done in the papers [88, 89] through careful study of images of the relevant positroid cells. An important result of these papers was that the Euler characteristic for all momentum amplituhedra  $n < 10$  for all  $k$  is equal to

$$\chi = \sum_{i=0}^{2n-4} (-1)^i |\Delta^i \mathcal{M}_{n,k}^{(4)}| = 1, \quad (6.54)$$

where  $|\Delta^i \mathcal{M}_{n,k}^{(4)}|$  represents the number of codimension- $i$  boundaries of the momentum amplituhedron. This statement suggests that the momentum amplituhedron has a boundary structure similar to a ball [89]. The study of the boundary structure of the momentum amplituhedron, along with other relevant geometries is facilitated through the Mathematica package `amplituhedronBoundaries` developed by Łukowski and Moerman [88].

### 6.3.2 The Momentum Amplituhedron Canonical Form

The canonical form for the momentum amplituhedron is a differential form of degree  $(2n - 4)$  which is finite inside the momentum amplituhedron and has logarithmic singularities on all of its boundaries. We shall restrict ourselves to the physical momentum amplituhedron for  $m = 4$  in the following.

First and foremost, the momentum amplituhedron  $\mathcal{M}_{n,k}^{(4)}$  is a geometry of dimension  $(2n - 4)$  and therefore we need to study its triangulation through images of the dimension  $(2n - 4)$  cells of the positive Grassmannian through the map  $\Phi_{\Lambda, \tilde{\Lambda}}$ . The correct choice of positroid cells,  $\mathcal{T}$ , can be found using the Mathematica package `positroid` [73] via the function `treeContour[n,k]`. Having chosen a correct set of

positroid cells, which are non-overlapping and dense inside the momentum amplituhedron, the volume form can be found as the sum over push-forwards of the canonical forms of these cells

$$\Omega_{n,k}^{(m)} = \sum_{\sigma \in \mathcal{T}} (\Phi_{(\Lambda, \tilde{\Lambda})})_* \omega_{n,k}^\sigma. \quad (6.55)$$

This approach, based on the push-forward of Grassmannian cells will in general introduce spurious boundaries canceling in the sum. We obtain the canonical form of degree  $(2n - 4)$  whose explicit representation is not invariant under momentum conservation and we obtain an invariant top-form by wedging with  $1 = \delta^4(P)d^4P$ , with  $P$  defined in (6.38), as follows

$$\Omega_{n,k}^{(m)} \wedge d^4P \delta^4(P) = \delta^4(P) \prod_{\alpha=1}^{n-k} \langle Y_1 \dots Y_{n-k} d^2 Y_\alpha \rangle \prod_{\dot{\alpha}=1}^k [\tilde{Y}_1 \dots \tilde{Y}_k d^2 \tilde{Y}_{\dot{\alpha}}] \Omega_{n,k}, \quad (6.56)$$

where  $\Omega_{n,k}^{(m)} \wedge d^4P$  is a top-form and independent of the particular representation of the canonical form of the momentum amplituhedron due to momentum conservation and independent of triangulation choice [39]. We extract the *volume* function by stripping off the overall gauge invariant differential forms  $\langle Y_1 \dots Y_{n-k} d^2 Y_\alpha \rangle$  and  $[\tilde{Y}_1 \dots \tilde{Y}_k d^2 \tilde{Y}_{\dot{\alpha}}]$  and momentum conservation. This volume function is exactly what encodes the scattering amplitude.

Alternatively, we can obtain the invariant volume function as the Grassmannian integral

$$\begin{aligned} \delta^4(P) \Omega_{n,k} = \int \frac{d^{(n-k) \cdot (n-k)} g}{(\det g)^{n-k}} \int_{\gamma} \omega_{n,k} \prod_{\alpha=1}^{n-k} \delta^{(n-k+2)}(Y_\alpha^A - g_\alpha^\beta (c^\perp)_{\beta i} \Lambda_i^A) \\ \times \prod_{\dot{\alpha}=1}^k \delta^{(k+2)}(\tilde{Y}_{\dot{\alpha}}^{\dot{A}} - c_{\dot{\alpha} i} \tilde{\Lambda}_i^{\dot{A}}), \end{aligned} \quad (6.57)$$

where we integrate over the matrix  $g$  encoding the  $GL(n-k)$  redundancy when defining the orthogonal complement of  $C \in G_+(k, n)$ . The specific integration contour  $\gamma$  can be obtained from the BCFW construction for the Grassmannian discussed in section 3.4. The measure  $\omega_{n,k}$  is the standard Grassmannian integration measure discussed in section 3.3:

$$\omega_{n,k} = \frac{d^{n \times k} c_{\dot{\alpha} i}}{(12 \dots k)(23 \dots k+1) \dots (n1 \dots k-1)}. \quad (6.58)$$

Both methods of extracting  $\Omega_{n,k}$  defines a volume function from which scattering amplitudes can be obtained.

### 6.3.3 Scattering Amplitudes from the Volume Function

Once the invariant volume function has been obtained, we can extract the scattering amplitude. We fix the  $Y$  and  $\tilde{Y}$  matrices by

$$Y^* = \begin{pmatrix} \mathbb{0}_{2 \times (n-k)} \\ \mathbb{1}_{(n-k) \times (n-k)} \end{pmatrix}, \quad \tilde{Y}^* = \begin{pmatrix} \mathbb{0}_{2 \times k} \\ \mathbb{1}_{k \times k} \end{pmatrix}. \quad (6.59)$$

Evaluating the volume function on these reference planes and integrating out the auxiliary Grassmann variables, the scattering amplitude is extracted from  $\Omega_{n,k}$  as follows

$$A_{n,k}[1, 2, \dots, n] = \delta^4(p) \int d\phi_a^1 \dots d\phi_a^{n-k} \int d\tilde{\phi}_a^1 \dots d\tilde{\phi}_a^k \Omega_{n,k}(Y^*, \tilde{Y}^*, \Lambda, \tilde{\Lambda}), \quad (6.60)$$

which is precisely the partial amplitude in msYM for all  $n$  and  $k$  in spinor-helicity variables in the standard color ordering, with  $\delta^4(p)$  coming from the localization of  $\delta^4(P)$  on  $Y^*$  and  $\tilde{Y}^*$ . We will postpone a discussion of how to extract partial amplitudes for non-standard orderings from the momentum amplituhedron to chapter 8.

## 6.4 Factorization Properties

As we have seen throughout this work, the factorization properties are fundamental features of scattering amplitudes and we will in the following discuss how these features emerge from the momentum amplituhedron geometry.

When planar multi-particle Mandelstam variables vanish, amplitudes generally factor into products of lower point amplitudes, as we have discussed extensively in chapter 2 and chapter 3. As discussed in section 4.4, the amplituhedron too factorizes into direct products of lower-dimensional geometries and thus features the factorization properties of scattering amplitudes directly. This is also true for the momentum amplituhedron, however, the factorization properties here are slightly more involved than for the amplituhedron. This is because the factorization properties of the momentum amplituhedron are related to amalgamations of on-shell diagrams inside the positive Grassmannian as discussed in section 3.2 and in [72].

Consider two planes  $C_L \in G_+(k_L, n_L)$  and  $C_R \in G_+(k_R, n_R)$ , where  $n_L$  and  $n_R$  are the number of particles on a left and right diagram, respectively, and  $k_L$  and  $k_R$  denote their helicity. We take their direct product, bringing us to  $\hat{C} \in G(k_L + k_R, n_L + n_R)$ , and subsequently project the matrix down to  $C \in G(k_L + k_R - 1, n_L + n_R - 2)$ . Thus, the matrix  $C$ , parameterizing the cell of the Grassmannian where the factorization takes place, can be described as two overlapping matrices describing the left and right planes.

To see how this works for the momentum amplituhedron, we focus on the  $n = 6$ ,  $k = 3$  case. Here, we encounter three distinct types of amalgamations, depending on which boundary we are in the vicinity of. First, we consider the momentum

amplituhedron near the boundary  $S_{123} \rightarrow 0$ . This boundary is parametrized by a seven-dimensional positroid cell for which  $(123) = (456) = 0$ . This cell can be written in terms of positive coordinates as

$$C_{6,3}|_{S_{123}=0} = \left( \begin{array}{ccc|cc} 1 & \alpha_5 + \alpha_7 & \alpha_5\alpha_6 & 0 & 0 & 0 \\ 0 & 1 & \alpha_6 & \alpha_2 + \alpha_4 & \alpha_2\alpha_3 & 0 \\ 0 & 0 & 0 & 1 & \alpha_3 & \alpha_1 \end{array} \right). \quad (6.61)$$

This matrix can be regarded as coming from the amalgamation of the two positive matrices corresponding to four-point MHV amplitudes as follows

$$C_{4,2} \otimes C'_{4,2} = \begin{pmatrix} 1 & \alpha_2 + \alpha_4 & \alpha_2\alpha_3 & 0 & 0 & 0 & 0 & 0 \\ 0 & 1 & \alpha_3 & \alpha_1 & 0 & 0 & 0 & 0 \\ 0 & 0 & 0 & 0 & 1 & \beta_2 + \beta_4 & \beta_2\beta_3 & 0 \\ 0 & 0 & 0 & 0 & 0 & 1 & \beta_3 & \beta_1 \end{pmatrix}. \quad (6.62)$$

Projecting this matrix by the 4th and 5th column, yields the matrix

$$C_{6,3} = \begin{pmatrix} 1 & \alpha_2 + \alpha_4 & \alpha_2 & 0 & 0 & 0 \\ 0 & 1 & \frac{\alpha_3}{\alpha_1} & (\beta_2 + \beta_4)\alpha_1 & \alpha_1\beta_2\beta_3 & 0 \\ 0 & 0 & 0 & 1 & \beta_3 & \beta_1 \end{pmatrix}, \quad (6.63)$$

which can be brought to the form of  $C_{6,3}|_{S_{123}=0}$  by fixing  $\alpha_1 = 1$  and relabeling the remaining variables.

The second type of boundaries we consider is  $[\tilde{Y}ii + 1] \rightarrow 0$ . We specifically focus on  $[\tilde{Y}56] \rightarrow 0$ . On the level of scattering amplitudes,  $[56] \rightarrow 0$  describes the limit where particles 5 and 6 become collinear, and the scattering amplitude  $A_{6,3}[1, 2, 3, 4, 5, 6]$  reduces to  $A_{5,2}[1, 2, 3, 4, 5]$ . We expect this to also be the case for the momentum amplituhedron. Studying the seven-dimensional cell parameterizing the boundary  $[\tilde{Y}56] \rightarrow 0$ :

$$C_{6,3}|_{[\tilde{Y}56]=0} = \left( \begin{array}{ccccc|c} 1 & \alpha_3 + \alpha_5 + \alpha_7 & (\alpha_3 + \alpha_5)\alpha_6 & \alpha_3\alpha_4 & 0 & 0 \\ 0 & 1 & \alpha_6 & \alpha_4 & \alpha_2 & 0 \\ 0 & 0 & 0 & 0 & 1 & \alpha_1 \end{array} \right). \quad (6.64)$$

We identify this as the projection of the matrix constructed from  $C_{5,2} \otimes C_{3,2}$  up to a  $GL(1)$  transformation. We note that the value of  $k$  reduces by one in this limit. Finally, we consider the limit  $\langle Yii + 1 \rangle \rightarrow 0$  which should correspond to a collinear limit with  $k$  preserved. Indeed, the boundary with  $\langle Y56 \rangle = 0$ , corresponds to the following seven-dimensional cell in the positive Grassmannian:

$$C_{6,3}|_{\langle Y56 \rangle=0} = \left( \begin{array}{ccccc|c} 1 & \alpha_5 + \alpha_7 & \alpha_5\alpha_6 & 0 & 0 & 0 \\ 0 & 1 & \alpha_3 + \alpha_6 & \alpha_3\alpha_4 & 0 & 0 \\ 0 & 0 & 1 & \alpha_4 & \alpha_2 & \alpha_1 \end{array} \right), \quad (6.65)$$

which again can be considered as a projection operation on the matrix constructed from  $C_{5,3} \otimes C_{1,3}$ .

## 6.5 Extra positivity conditions

While the sign-flip conditions are automatically fulfilled under the map (6.35), the positivity of generalized Mandelstam variables (6.53) is not automatically guaranteed in all cases. Indeed if we consider the generalized Mandelstam variable  $S_{123}$  for  $n = 6$ ,  $k = 3$ , we have

$$S_{123} = \langle Y12 \rangle [\tilde{Y}12] + \langle Y23 \rangle [\tilde{Y}23] + \langle Y13 \rangle [\tilde{Y}13] \geq 0. \quad (6.66)$$

The first two terms are always positive, but the last term can be either positive or negative. Expanding using (6.36), we get

$$\begin{aligned} S_{123} = (123) & \left[ \langle 1 \rangle^\perp [(145)[12345] + (146)[12346] + (156)[12356] + (456)[23456]] \right. \\ & + \langle 2 \rangle^\perp [(245)[12345] + (246)[12346] + (256)[12356] - (456)[13456]] \\ & \left. + \langle 3 \rangle^\perp [(345)[12345] + (346)[12346] + (356)[12356] + (456)[12456]] \right] \\ + (456) & \left[ \langle 4 \rangle^\perp [(124)[12456] + (234)[23456] + (134)[13456] + (123)[12356]] \right. \\ & + \langle 5 \rangle^\perp [(125)[12456] + (235)[23456] + (135)[13456] - (123)[12346]] \\ & \left. + \langle 6 \rangle^\perp [(126)[12456] + (236)[23456] + (136)[13456] + (123)[12345]] \right], \end{aligned} \quad (6.67)$$

where  $\langle i \rangle^\perp$  is defined in (A.11) of Appendix A. We note the two negative terms, which in principle could dominate over the remaining terms in certain kinematic configurations, given by

$$(123)(456)[13456] \quad \text{and} \quad (456)(123)[12346]. \quad (6.68)$$

We can ensure total positivity of  $S_{123}$  by introducing extra positivity conditions on the condensed form

$$\langle 1 \rangle^\perp [\check{1}] - \langle 2 \rangle^\perp [\check{2}] + \langle 3 \rangle^\perp [\check{3}] + \langle 4 \rangle^\perp [\check{4}] - \langle 5 \rangle^\perp [\check{5}] + \langle 6 \rangle^\perp [\check{6}] > 0, \quad (6.69)$$

where the brackets  $[\check{i}]$  is shorthand for  $[12\dots\hat{i}\dots 6]$ , the five-bracket with the index  $i$  omitted. Together with the three remaining independent Mandelstam variables  $S_{234}$  and  $S_{345}$ , whose positivity conditions can be cast on the same form but with the signs shifted one or two places, respectively, we obtain a set of mutually inclusive positivity conditions on the external data [39]. It is conjectured, that for all external data respecting these conditions the geometry  $\mathcal{M}_{6,3}$  is a positive geometry. This structure appears to generalize to higher  $n$ . For all  $k = 3$  cases we can introduce the collection of brackets

$$\mathcal{P}_{i_1 i_2 i_3; j_1 j_2 j_3} = \langle i_1 \rangle^\perp [i_2 i_3 j_1 j_2 j_3] - \langle i_2 \rangle^\perp [i_1 i_3 j_1 j_2 j_3] + \langle i_3 \rangle^\perp [i_1 i_2 j_1 j_2 j_3]. \quad (6.70)$$

For any  $n$  we can obtain the necessary positivity conditions on the external data from a three-particle Mandelstam variable,  $S_{ii+1\dots i_p}$ ,

$$\mathcal{P}_{i_1 i_2 i_3; j_1 j_2 j_3} + \mathcal{P}_{j_1 j_2 j_3; i_1 i_2 i_3} > 0, \quad i_1 i_2 i_3 \in I_{i,p}, \quad j_1 j_2 j_3 \in \bar{I}_{i,p}, \quad (6.71)$$

having defined  $I_{i,p} := \{i, i+1, \dots, i+p\}$  and  $\bar{I}_{i,p} = \{1, \dots, n\} \setminus I_{i,p}$ . Similar relations have been found for higher  $k$  sectors. A geometric interpretation of these inequalities between external data remains elusive. Through careful numerical analysis it has been established that the kinematic region where the inequalities are not fulfilled corresponds to a very small region of the full kinematic space [39] and thus only a very small number of kinematic configurations leads to cases where the consecutive generalized planar Mandelstam variables are not strictly positive.

## 6.6 Examples

In this section, we explore the momentum amplituhedron by considering a few examples.

### $n = 4$ MHV Momentum Amplituhedron

In the  $n = 4$ ,  $k = 2$  case the momentum amplituhedron,  $\mathcal{M}_{4,2}^{(4)}$  is isomorphic to the positive Grassmannian  $G_+(2, 4)$  [39]. This can be seen from the fact that the dimensionality of the momentum amplituhedron is  $(2n - 4) = 4$  and coincides with the dimension of the positive Grassmannian,  $k(n - k) = 4$ . Choosing a patch in the positive Grassmannian

$$C = \begin{pmatrix} 1 & \alpha_2 & 0 & -\alpha_3 \\ 0 & \alpha_1 & 1 & \alpha_4 \end{pmatrix}, \quad (6.72)$$

and solving  $Y = C^\perp \cdot \Lambda$ , we obtain

$$\alpha_1 = \frac{\langle Y12 \rangle}{\langle Y13 \rangle}, \quad \alpha_2 = \frac{\langle Y23 \rangle}{\langle Y13 \rangle}, \quad \alpha_3 = \frac{\langle Y34 \rangle}{\langle Y13 \rangle}, \quad \alpha_4 = \frac{\langle Y14 \rangle}{\langle Y13 \rangle}. \quad (6.73)$$

Pushing the Grassmannian top-form forward through this map yields the volume form:

$$\Omega_{4,2} = \bigwedge_{i=1}^4 \frac{d\alpha_i}{\alpha_i} = \frac{[1234]^2}{\langle Y12 \rangle \langle Y23 \rangle \langle Y34 \rangle \langle Y14 \rangle} \langle Y d^2 Y_1 \rangle \langle Y d^2 Y_2 \rangle. \quad (6.74)$$

We could just as well have resolved the map in terms of  $\tilde{\Lambda}$ . In that case, we would have obtained

$$\Omega_{4,2} = \frac{[1234]^2}{[\tilde{Y}12][\tilde{Y}23][\tilde{Y}34][\tilde{Y}14]} [\tilde{Y} d^2 \tilde{Y}_1][\tilde{Y} d^2 \tilde{Y}_2], \quad (6.75)$$

which is related to (6.74) through momentum conservation. Evaluating the volume function using (6.56), we obtain in both cases

$$\Omega_{4,2} = \frac{\langle 1234 \rangle^2 [1234]^2}{\langle Y12 \rangle [Y12] \langle Y23 \rangle [Y23]}, \quad (6.76)$$

which is manifestly parity symmetric. Extracting the scattering amplitude using (6.60), we are simply left with

$$A_{4,2}[1, 2, 3, 4] = \frac{\delta^4(p)\delta^4(q)\delta^4(\tilde{q})}{\langle 12 \rangle [12] \langle 23 \rangle [23]}, \quad (6.77)$$

where  $\langle ij \rangle$  and  $[ij]$  are now nothing but the usual spinor-helicity contractions and agrees with [84]. This representation of  $A_{4,2}[1, 2, 3, 4]$  might appear slightly different from the equation (2.145), taking  $n = 4$ . However, we can easily see that

$$\frac{\delta^4(p)\delta^4(q)\delta^4(\tilde{q})}{\langle 12 \rangle [12] \langle 23 \rangle [23]} = \frac{\langle 34 \rangle \langle 41 \rangle}{[12] [23]} \times \frac{\delta^4(p)\delta^4(q)\delta^4(\tilde{q})}{\langle 12 \rangle \langle 23 \rangle \langle 34 \rangle \langle 41 \rangle}, \quad (6.78)$$

where the factor  $\langle 34 \rangle \langle 41 \rangle / [12] [23] = 1$  since momentum conservation  $\delta^4(p) = \delta^{2 \times 2}(\lambda \cdot \tilde{\lambda})$  restricts  $\lambda^\perp = \tilde{\lambda}$  for  $n = 4$ ,  $k = 2$  and we can use the results of Appendix A to relate  $\langle \rangle \rightarrow \langle \rangle^\perp = []$ .

### All $n$ MHV Momentum Amplituhedra

The calculation from the previous section can be generalized to any  $n$ . A suitable representation of the volume form is

$$\begin{aligned} \Omega_{n,2} &= \bigwedge_{i=2}^{n-1} \left( d \log \left( \frac{\langle Yii+1 \rangle}{\langle Y1i+1 \rangle} \right) \wedge d \log \left( \frac{\langle Y1i+1 \rangle}{\langle Y12 \rangle} \right) \right) \\ &= \frac{\langle 12 \dots n \rangle^2}{\langle Y12 \rangle \langle Y23 \rangle \dots \langle Y1n \rangle} \langle Yd^2Y_1 \rangle \langle Yd^2Y_2 \rangle \dots \langle Yd^2Y_{n-2} \rangle \end{aligned} \quad (6.79)$$

This is similar to the volume form for all  $n$  for the  $m = 2$  amplituhedron  $\mathcal{A}_{n,n-2}^{(2)}$  found in [38]. We get the MHV volume function when projecting through momentum conservation (6.56), namely

$$\Omega_{n,2} = \frac{\langle 1 \dots n \rangle^2 \left( \sum_{i < j} [12ij] \langle Yij \rangle \right)^2}{[\tilde{Y}12]^2 \langle Y12 \rangle \langle Y23 \rangle \dots \langle Y1n \rangle}. \quad (6.80)$$

We could just as well have focused on the  $\tilde{\Lambda}$  sector and found the  $\overline{\text{MHV}}$  formula, which would have been the parity conjugate of (6.80). In both cases, the momentum amplituhedron is  $(2n - 4)$  dimensional and there is no need to triangulate  $\mathcal{M}_{n,2}$  or  $\mathcal{M}_{n,n-2}$ . The boundaries are easily found and take the form  $[\tilde{Y}ii+1] = 0$  and  $\langle Yii+1 \rangle = 0$ , respectively.

### $n = 6$ NMHV Momentum Amplituhedron

In the MHV examples described above the momentum amplituhedron was isomorphic to the positive Grassmannian  $G_+(2, n)$ . This behavior does not extend beyond MHV and we see the first example of this at the NMHV sector of  $n = 6$ . This can be seen from the fact that the dimensionality of the positive Grassmannian is  $\dim G_+(3, 6) = (6 - 3)3 = 9$ , while the momentum amplituhedron has dimensionality  $\dim \mathcal{M}_{6,3} = (2 \times 6 - 4) = 8$ . The discrepancy between the dimensionality of the image and the pre-image indicates that the map  $\Phi_{(\Lambda, \tilde{\Lambda})}$  is not injective. This means that we are required to triangulate the momentum amplituhedron in order to find the volume form. We choose a combination of eight-dimensional cells in the positive Grassmannian that overlap only on boundaries. Using the `treeContour` $[n, k]$  function of the Mathematica<sup>TM</sup> package `positroid` [73], we find two options for triangulation

$$\mathcal{T}_1 = \{(123) = 0, (345) = 0, (561) = 0\}, \quad \mathcal{T}_2 = \{(234) = 0, (456) = 0, (612) = 0\}, \quad (6.81)$$

whereby  $(ijk) = 0$  we mean the cell in  $G_+(3, 6)$  for which the minor  $(ijk)$  vanishes. The volume form can be written as

$$\Omega_{6,3} = \Omega_{6,3}^{(612)} + \Omega_{6,3}^{(234)} + \Omega_{6,3}^{(456)} = \Omega_{6,3}^{(123)} + \Omega_{6,3}^{(345)} + \Omega_{6,3}^{(561)}, \quad (6.82)$$

where  $\Omega_{6,3}^{(ijk)}$  is the push-forward of the canonical form on the cell  $(ijk) = 0$ . We can parameterize this cell using canonical coordinates for the positive Grassmannian, and solve for them using (6.36), yielding

$$\alpha_1 = \frac{\langle Y12 \rangle}{\langle Y13 \rangle}, \quad \alpha_2 = \frac{\langle Y23 \rangle}{\langle Y13 \rangle}, \quad \alpha_3 = \frac{[\tilde{Y}\hat{3}4]}{[\tilde{Y}\hat{1}\hat{3}]}, \quad \alpha_4 = \frac{[\tilde{Y}\hat{6}4]}{[\tilde{Y}\hat{1}\hat{3}]}, \quad (6.83)$$

$$\alpha_5 = \frac{[\tilde{Y}\hat{6}\hat{1}]}{[\tilde{Y}\hat{1}\hat{3}]}, \quad \alpha_6 = \frac{[\tilde{Y}\hat{4}\hat{1}]}{[\tilde{Y}\hat{1}\hat{3}]}, \quad \alpha_7 = \frac{[\tilde{Y}45]}{[\tilde{Y}64]}, \quad \alpha_8 = \frac{[\tilde{Y}56]}{[\tilde{Y}64]}, \quad (6.84)$$

where we have denoted the following shifted variables

$$\hat{\Lambda}_1 = \tilde{\Lambda}_1 + \frac{\langle Y23 \rangle}{\langle Y13 \rangle} \tilde{\Lambda}_2, \quad \hat{\Lambda}_3 = \tilde{\Lambda}_3 + \frac{\langle Y12 \rangle}{\langle Y13 \rangle} \tilde{\Lambda}_2, \quad (6.85)$$

which is the uplift of an analogous formula in (6.30) up to a sign discrepancy due to a convention choice. The push-forward is simply

$$\Omega_{6,3}^{(123)} = \bigwedge_{i=1}^8 d \log \alpha_i. \quad (6.86)$$

Extracting the volume function using (6.56) leads to the following volume function of the “triangle” in the momentum amplituhedron triangulation

$$\Omega_{6,3}^{(123)} = \frac{(\langle Y12 \rangle [\check{3}] + \langle Y13 \rangle [\check{2}] + \langle Y23 \rangle [\check{1}])^2 ([\check{Y}45] \langle \check{6} \rangle + [\check{Y}46] \langle \check{5} \rangle + [\check{Y}56] \langle \check{4} \rangle)^2}{S_{123} \langle Y12 \rangle \langle Y23 \rangle [\check{Y}45] [\check{Y}56] \langle Y1|5+6|4\check{Y} \rangle \langle Y3|4+5|6\check{Y} \rangle}, \quad (6.87)$$

where as before  $\langle \check{5} \rangle = \langle 12346 \rangle$ ,  $[\check{3}] = [12456]$ , etc.. This expression is completely equivalent to the expression (6.28). We identify the numerator proportional to “ $d^6 \tilde{\lambda}$ ”, namely

$$(\langle Y12 \rangle [\check{3}] + \langle Y13 \rangle [\check{2}] + \langle Y23 \rangle [\check{1}])^2 \rightarrow \delta^4(q) (\tilde{\eta}_4 [56]_{\tilde{\lambda}} + \tilde{\eta}_5 [64]_{\tilde{\lambda}} + \tilde{\eta}_6 [45]_{\tilde{\lambda}})^2, \quad (6.88)$$

and the numerator proportional to “ $d^6 \lambda$ ” to be

$$([\check{Y}45] \langle \check{6} \rangle + [\check{Y}46] \langle \check{5} \rangle + [\check{Y}56] \langle \check{4} \rangle)^2 \rightarrow \delta^4(\tilde{q}) (\eta_1 \langle 23 \rangle_{\lambda} + \eta_2 \langle 31 \rangle_{\lambda} + \eta_3 \langle 12 \rangle_{\lambda})^2. \quad (6.89)$$

Clearly (6.87) contains spurious poles on  $\langle Y1|5+6|4\check{Y} \rangle = 0$  and  $\langle Y3|4+5|6\check{Y} \rangle = 0$ , but when taken together with the other two terms in the triangulation, they cancel in the sum

$$\Omega_{6,3} = \Omega_{6,3}^{(123)} + \Omega_{6,3}^{(345)} + \Omega_{6,3}^{(561)} = \Omega_{6,3}^{(123)} + \Omega_{6,3}^{(123)} \Big|_{i \rightarrow i+2} + \Omega_{6,3}^{(123)} \Big|_{i \rightarrow i+4}, \quad (6.90)$$

where the remaining volume forms are found from  $\Omega_{6,3}^{(123)}$  by shifting the labels of  $\Lambda$  and  $\tilde{\Lambda}$  in (6.87). Here, explicitly taking residues on the sum (6.90) on the spurious poles, we obtain 0, thus verifying that the poles are indeed spurious and the remaining 15 boundaries of the momentum amplituhedron are equivalent to the 15 physical singularities of the 6-point NMHV scattering amplitude in msYM. The boundaries of  $\mathcal{M}_{6,3}$  are on the form

$$\langle Yii+1 \rangle = 0, \quad i = 1, \dots, 6, \quad [\check{Y}ii+1] = 0, \quad i = 1, \dots, 6, \quad S_{i,i+1,i+2} = 0, \quad (6.91)$$

when imposing the additional positivity condition discussed in section 6.5.



# Chapter 7

## Momentum Amplituhedron & Kinematic Associahedron Map

In this chapter, we consider the interesting map between the canonical forms of the momentum amplituhedron and the kinematic associahedron as presented in [40]. We will open the chapter with an alternative definition of the momentum amplituhedron through fixed planes in the kinematic space. We will follow with a discussion of the different kinematic spaces related to the momentum amplituhedron and the kinematic associahedron as well as how they map on to each other. We shall then discuss how these maps between the kinematic spaces act on the canonical forms for the two geometries. We close the chapter with a few examples of this construction and a discussion of how to extract the “reduced volume forms” for the momentum amplituhedron using the inverse-soft construction.

### 7.1 Momentum Amplituhedron in Kinematic Space

An alternative definition of the momentum amplituhedron inspired by a similar construction for the amplituhedron (proposed in [75] and reviewed in section 4.4), was found and employed in [40]. This definition is very powerful, as we shall see, since it naturally extends to external orderings other than the standard, though we will postpone the discussion of different color-orderings to the next chapter. The definition is based on the notion of projecting through fixed external data. We start by defining the following  $(2n - 4)$  dimensional subspace of the kinematic space of spinor helicity variables:

$$\mathcal{V}_n := \{(\lambda_i^a, \tilde{\lambda}_i^{\dot{a}}) : \lambda_i^a = \lambda_i^{*a} + y_\alpha^a \Delta_i^\alpha, \tilde{\lambda}_i^{\dot{a}} = \tilde{\lambda}_i^{*\dot{a}} + \tilde{y}_{\dot{\alpha}}^{\dot{a}} \tilde{\Delta}_i^{\dot{\alpha}}, \sum_{i=1}^n \lambda_i^a \tilde{\lambda}_i^{\dot{a}} = 0\}. \quad (7.1)$$

Here,  $(\lambda^*, \tilde{\lambda}^*)$  are two fixed two-planes in  $n$  dimensions, while  $\Delta$  and  $\tilde{\Delta}$  are fixed planes of dimension  $(n - k)$  and  $k$  in  $n$  dimensions, respectively. We also assume that when we organize the planes into the matrices as follows

$$\Lambda_i^A = \begin{pmatrix} \lambda_i^{*a} \\ \Delta_i^\alpha \end{pmatrix}, \quad \tilde{\Lambda}_i^A = \begin{pmatrix} \tilde{\lambda}_i^{*a} \\ \tilde{\Delta}_i^{\dot{\alpha}} \end{pmatrix}, \quad (7.2)$$

then  $\Lambda$  is a twisted positive matrix (see section 6.2) and  $\tilde{\Lambda}$  is a positive matrix. We also define the *winding space* fulfilling the conjectures of [84] described in section 6.2 as follows

$$\begin{aligned} \mathcal{W}_{n,k} := & \{(\lambda_i^a, \tilde{\lambda}_i^{\dot{a}}) : s_{ii+1\dots i+j} > 0, \\ & \text{the sequence } \{\langle 12 \rangle, \langle 13 \rangle, \dots, \langle 1n \rangle\} \text{ has } k - 2 \text{ sign flips} \\ & \text{the sequence } \{[12], [13], \dots, [1n]\} \text{ has } k \text{ sign flips}\}, \end{aligned} \quad (7.3)$$

where  $s_{ii+1\dots i+j}$  are the multiparticle Mandelstam variables,  $\langle ij \rangle = \lambda_i^a \lambda_j^b \epsilon_{ab}$ , and  $[ij] = \tilde{\lambda}_i^{\dot{a}} \tilde{\lambda}_j^{\dot{b}} \epsilon_{\dot{a}\dot{b}}$ . The  $m = 4$  momentum amplituhedron  $\mathcal{M}_{n,k}^{(\lambda, \tilde{\lambda})}$  is then defined as the intersection

$$\mathcal{M}_{n,k}^{(\lambda, \tilde{\lambda})} := \mathcal{V}_n \cap \mathcal{W}_{n,k}. \quad (7.4)$$

This definition is consistent with the one described in section 6.2 and we can obtain the canonical form on this space by pulling back the volume form  $\Omega_{n,k}$ , found in chapter 6, using  $(\lambda, \tilde{\lambda})$  defined above. We note, that this definition of the momentum amplituhedron can be seen as analogous to the kinematic associahedron definition from chapter 5, where the geometry is defined as the intersection of two spaces (5.10) and (5.11).

## 7.2 Kinematic Spaces and their Maps

The momentum amplituhedron lives in the space of bosonized spinor helicity variables, while the kinematic associahedron lives in the kinematic space of planar Mandelstam variables, as discussed at length in chapter 5. In this section, we discuss some various kinematic spaces related to these two and show how they are connected through maps.

### 7.2.1 Kinematic spaces

**The on-shell space  $\mathcal{O}_n$**

The momentum amplituhedron is defined on the bosonic part of the on-shell superspace parameterized by two  $(2 \times n)$  matrices denoted by  $\lambda$  and  $\tilde{\lambda}$  as described in the previous chapter 6. The canonical forms associated with momentum amplituhedra are written in terms of  $SL(2) \times SL(2)$  invariants on this space, each fixing 3 degrees of freedom

while imposing momentum conservation fixes 4 degrees freedom. The dimensionality of the space is simply

$$\dim \mathcal{O}_n = 4n - 10. \quad (7.5)$$

### The little group invariant space $\mathcal{L}_n$

As reviewed in section 2.2, scattering amplitudes in (super) Yang-Mills amplitudes respect little group scaling invariance. Little group scaling, as seen from the point of view of the non-chiral superspace are a subgroup of Poincare' group transformations of scattering amplitudes of the form

$$\begin{aligned} \lambda_i &\rightarrow t_i \lambda_i, & \tilde{\lambda}_i &\rightarrow t_i^{-1} \tilde{\lambda}_i, \\ \eta_i &\rightarrow t_i \eta_i, & \tilde{\eta}_i &\rightarrow t_i^{-1} \tilde{\eta}_i. \end{aligned} \quad (7.6)$$

We parameterize  $(\lambda, \tilde{\lambda})$  of  $\mathcal{O}_n$  using an explicit set of  $n$  parameters denoted  $t_i$  and the remaining variables  $\mathbf{a}$ . There are exactly  $(3n - 10)$  independent variables left over once we have removed the  $t_i$  variables and we write the *little group invariant space*,  $\mathcal{L}_n$  as the on-shell space modulo the little group torus,  $T$ , identified by  $T = \mathbb{R}_+^n$  (see for instance [90]), as follows  $\mathcal{L}_n = \mathcal{O}_n/T$ . The parameterization of the  $(3n - 10)$  dimensional space  $\mathcal{L}_n$  is by no means unique. We will make use of the parameterization obtained by considering the  $\lambda$  matrix and introducing variables  $t_i$  as per (7.6). The remaining matrix is of dimension  $(2n - 3 - n) = (n - 3)$ , and spans the modulo space of the  $n$ -punctured Riemann sphere, naturally parameterized by the Fock-Goncharov parameterization [91]:

$$\lambda = \begin{pmatrix} 0 & 1 & 1 & 1 & 1 & \dots & 1 \\ -1 & 0 & 1 & 1 + a_1 & 1 + a_1(1 + a_2) & \dots & 1 + a_1 + \dots + a_1 a_2 \dots a_{n-3} \end{pmatrix}. \quad (7.7)$$

The  $\tilde{\lambda}$  matrix is then fixed by imposing  $\lambda \cdot \tilde{\lambda} = 0$  and fixing the remaining  $SL(2)$  invariance. This parameterization of  $(\lambda, \tilde{\lambda})$  is referred to as the *extended Fock-Goncharov parameterization*. We might as well have chosen to parameterize  $\tilde{\lambda}$  and then fix  $\lambda$  instead and therefore the parity symmetry between  $\lambda$  and  $\tilde{\lambda}$  is broken. A parameterization keeping the parity symmetry would be in terms of the following cross-ratios

$$R_{ijkl} = \frac{\langle ij \rangle \langle kl \rangle}{\langle il \rangle \langle jk \rangle}, \quad \bar{R}_{ijkl} = \frac{[ij][kl]}{[il][jk]}. \quad (7.8)$$

Note, we can write  $a_i$  of (7.7) in terms of the cross-ratios by  $a_i = R_{ii+1i+2i+3}$ . Since there are  $(n - 3)$  independent  $R$  cross-ratios and  $(n - 3)$  independent  $\bar{R}$  cross-ratios, we need to introduce  $(n - 4)$  additional parameters to cover the  $(3n - 10)$  dimensional space  $\mathcal{L}_n$ . The Mandelstam variables are an obvious choice ensuring all variables are little group scaling invariant and the parity symmetry is conserved<sup>1</sup>.

<sup>1</sup>at the expense of cyclic symmetry, which is no longer manifest.

### The space of Mandelstam variables $\mathcal{K}_n$ and Gram determinant surface $\mathcal{G}_n$

The kinematic space of Mandelstam variables,  $\mathcal{K}_n$  was discussed previously in chapter 5 and is the natural space to describe scalar bi-adjoint  $\phi^3$  scattering amplitudes discussed in section 2.5. It is parameterized by  $X_{ij}$  and is  $\frac{n(n-3)}{2}$  dimensional. However, since the Mandelstam variables are constructed from four-momentum, when the space-time dimension  $D$  is smaller than the number of otherwise independent massless momenta  $n-1$ ,  $D < n-1$ , not all of the planar Mandelstam variables are independent: we need to impose the so-called *Gram determinant condition*. At fixed space-time dimension,  $D$ , the Gram matrices are  $(D+1) \times (D+1)$  matrices depending on  $(D+1)$  momenta as follows

$$G(p_{i_1}, p_{i_2}, \dots, p_{i_{d+1}}) = (s_{ij})_{i,j \in \{i_1, i_2, \dots, i_{d+1}\}}, \quad (7.9)$$

build from the two particle Mandelstam variables  $s_{ij} = 2p_i \cdot p_j$ . For  $D < n-1$ , we must have

$$\det G(p_{i_1}, p_{i_2}, \dots, p_{i_{d+1}}) = 0, \quad (7.10)$$

imposing further constraints between the Mandelstam variables. In four-dimensional theories the Gram determinants are non-trivial for  $n > 5$  and we must therefore impose Gram determinant conditions for  $n \geq 6$ . Not all the Gram determinant conditions are independent, however, and after resolving them, we find the resulting dimensionality of the *Gram determinant surface*,  $\dim \mathcal{G}_n = (3n-10)$  is congruent with the dimensionality of the little group invariant space. We denote the coordinates on the Gram determinant surface by the collective label  $\mathbf{x}$ .

### 7.2.2 Maps between kinematic spaces

We can relate the spaces defined in the previous subsection to each other using maps which will be defined momentarily. We assemble the maps and their relations in Figure 7.1. Later we shall provide these maps explicitly for the first few values of  $n$ .

As stated earlier, we can remove the little group scaling by parameterizing the  $\lambda$ -matrix of the on-shell space  $\mathcal{O}_n$  by  $t_i$  and the Fock-Goncharov variables  $\mathbf{a}$  according to (7.6), we define the map

$$\mathbf{f}_n : \mathcal{L}_n \rightarrow \mathcal{O}_n, \quad \begin{matrix} (t_i, \mathbf{a}) \\ n+(3n-10) \end{matrix} \mapsto \begin{matrix} (\lambda, \tilde{\lambda}) \\ 4n-10 \end{matrix}. \quad (7.11)$$

We note that if we take  $t_i \in \mathbb{R}_+^n$  as positive, the map  $\mathbf{f}_n$  is invertible. Since the Mandelstam variables can straight forwardly be written in terms of spinor-helicity brackets

$$s_{ij} = \langle ij \rangle [ij], \quad (7.12)$$

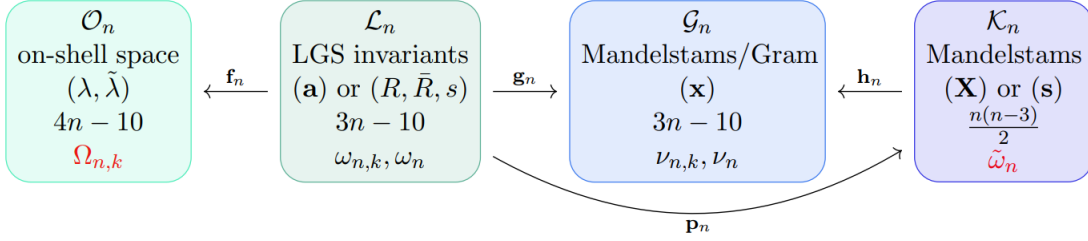


Figure 7.1: Summary of the kinematic spaces and relations between them, together with the differential forms defined on these spaces. We highlight the canonical forms of the momentum amplituhedron  $\Omega_{n,k}$  and of the associahedron  $\tilde{\omega}_n$  in red.

there is a natural map between the little group invariant space  $\mathcal{L}_n$  and the space of Mandelstam variables,  $\mathcal{K}_n$ , or the Gram determinant surface  $\mathcal{G}_n$ . We label the latter as  $\mathbf{g}_n$ , defined as

$$\mathbf{g}_n : \mathcal{L}_n \rightarrow \mathcal{G}_n, \quad \mathbf{a}_{3n-10} \mapsto \mathbf{x}_{3n-10}, \quad (7.13)$$

and the former as  $\mathbf{p}_n$ , defined as

$$\mathbf{p}_n : \mathcal{L}_n \rightarrow \mathcal{K}_n, \quad \mathbf{a}_{3n-10} \mapsto \mathbf{X}_{\frac{n(n-3)}{2}}. \quad (7.14)$$

Importantly, these maps are rational and for  $n \geq 5$ , they are generally not invertible. Instead, one can find that the number of local inverses increases with increasing  $n$ . Finally, the Gram conditions provide a map between the space of all planar Mandelstam variables and the  $(3n - 10)$ -dimensional Gram determinant surface. We denote this map by  $\mathbf{h}_n$

$$\mathbf{h}_n : \mathcal{K}_n \rightarrow \mathcal{G}_n, \quad \mathbf{X}_{\frac{n(n-3)}{2}} \mapsto \mathbf{x}_{3n-10}. \quad (7.15)$$

This map is defined by imposing a certain number of Gram conditions and therefore we are unable to write  $\mathbf{h}_n$  explicitly. That being said, the solutions to these constraints define possible inverse functions, which we can use to perform push-forwards of differential forms from  $\mathcal{K}_n$  to  $\mathcal{G}_n$ .

### 7.2.3 Comparing canonical forms

We can compare the canonical forms of momentum amplituhedra and kinematic associahedra on these spaces. We start by comparing the forms on the little group

invariant space,  $\mathcal{L}_n$ , by pulling the canonical forms of our positive geometries back to this space. Following this, we push the differential forms forward to the Gram determinant surface,  $\mathcal{G}_n$ , inside of  $\mathcal{K}_n$ . Starting from the canonical form of the momentum amplituhedron  $\Omega_{n,k}$ <sup>2</sup>, defined on  $\mathcal{O}_n$ , we pull it back through the map  $\mathbf{f}_n$  defining a differential form on the little group invariant space  $\mathcal{L}_n$ . We observe in the examples we have studied, that the differential form has the common property that the term with the highest degree in  $dt_i$  is independent of our parameterization of  $\mathcal{L}_n$ . In particular it takes the form

$$\mathbf{f}_n^* \Omega_{n,k} = \mu_n \wedge \omega_{n,k} + \dots, \quad (7.16)$$

where

$$\mu_n = \mu(\mathbb{P}^{n-1}) = \sum_{i=1}^n (-1)^{n-i} d \log t_1 \wedge d \log t_2 \wedge \dots \wedge \overline{d \log t_i} \wedge \dots \wedge d \log t_n, \quad (7.17)$$

is the canonical form on projective space  $\mathbb{R}\mathbb{P}^{n-1}$ . Here the overline means that the term is absent and the ellipses in (7.16) denotes terms of lower form-degree in  $dt_i$ . These terms depend on how we parameterize  $\mathcal{L}_n$  and not projectively well defined. We therefore disregard those terms in the following<sup>3</sup>. We note, that since the  $\deg \Omega_{n,k} = (2n - 4)$  (as discussed in details in chapter 6) and  $\deg \mu_n = (n - 1)$ , the degree of  $\omega_{n,k}$  is simply  $\deg \omega_{n,k} = (n - 3)$ . We refer to  $\omega_{n,k}$  as the *reduced momentum amplituhedron form* and it is manifestly little group invariant. At the end of this chapter in section 7.4, we discuss a recursive method for obtaining the reduced momentum amplituhedron form, based on the inverse-soft construction of [84]. Bringing our attention to the kinematic associahedron form (5.7), here denoted  $\tilde{\omega}_n$ , we can pull  $\tilde{\omega}_n$  back to the little group invariant space  $\mathcal{L}_n$  using the map  $\mathbf{p}_n$ , which defines the following form:

$$\omega_n = \mathbf{p}_n^* \tilde{\omega}_n. \quad (7.18)$$

After performing this pull-back of the associahedron form we find that the resulting form  $\omega_n$  on  $\mathcal{L}_n$  is equal to the sum over all  $k$ -sectors of the reduced momentum amplituhedron form, as follows

$$\omega_n = \sum_{k=2}^{n-2} \omega_{n,k}. \quad (7.19)$$

Therefore we can write that on the little group invariant space  $\mathcal{L}_n$ : the (pull-back of the) differential form for the full msYM scattering amplitude  $\Omega_n$  and the (pull-back of

<sup>2</sup>Note, that since we will not make use of the *volume function* of the previous chapter, so we will in the following denote the non-boldface  $\Omega_{n,k}$  as the volume form of the momentum amplituhedron.

<sup>3</sup>This choice represents a loss of information about the momentum amplituhedron form.

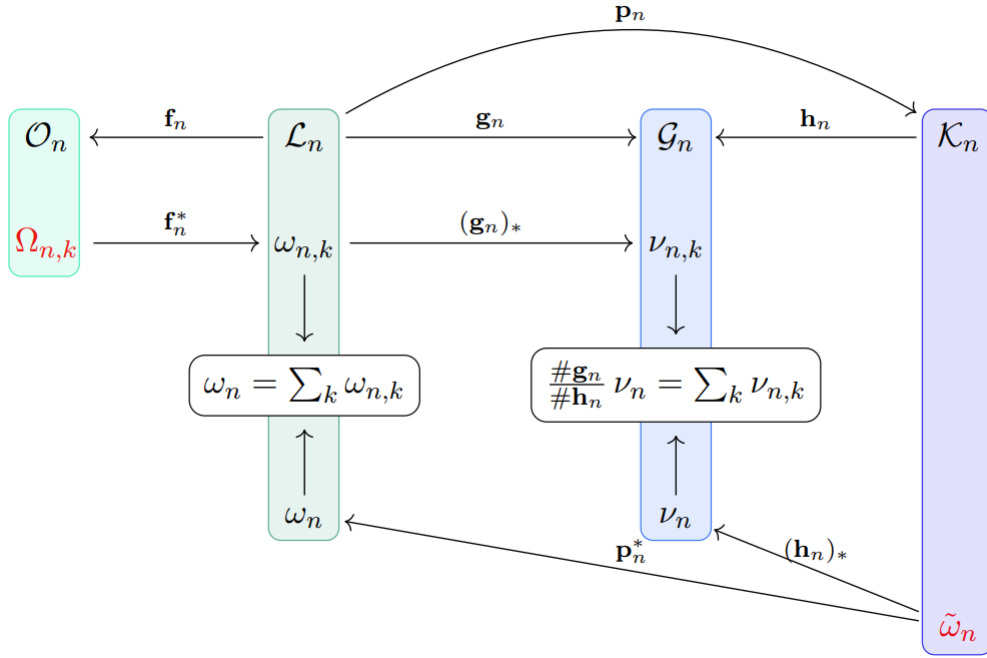


Figure 7.2: Relations between the kinematic spaces and the various differential forms on them defined in this section. We highlight the canonical forms of the momentum amplituhedron  $\Omega_{n,k}$  and of the associahedron  $\tilde{\omega}_n$ .

the) differential form for the bi-adjoint  $\phi^3$  scattering amplitude,  $\tilde{\omega}_n$  are related in the following way

$$\Omega_n = \sum_{k=2}^{n-2} \Omega_{n,k} \xrightarrow{f_n^*} \mu_n \wedge \sum_{k=2}^{n-2} \omega_{n,k} = \mu_n \wedge \omega_n \xleftarrow{P_n^*} \mu_n \wedge \tilde{\omega}_n. \quad (7.20)$$

This relation is illustrated in a diagrammatic form on Figure 7.2, where we have denoted the canonical form for the momentum amplituhedron and for the kinematic associahedron in red. As will be illustrated in explicit examples in the following, the relation (7.20) tells us how the singularity structure of the momentum amplituhedron and the kinematic associahedron are related. In particular, the factorization channels given by the vanishing of planar Mandelstam variables are the same, as can be seen from the discussions of section 5.6 and section 6.3.

The reduced momentum amplituhedron form  $\omega_{n,k}$  defined in (7.19) can be pushed forward to  $\mathcal{G}_n$  using the map  $\mathbf{g}_n$  as follows

$$\nu_{n,k} = (\mathbf{g}_n)_* \omega_{n,k}. \quad (7.21)$$

The same is true for the kinematic associahedron form  $\tilde{\omega}_n$ , which is pushed forward using the Gram determinant map  $\mathbf{h}_n$  to define

$$\nu_n = (\mathbf{h}_n)_* \tilde{\omega}_n, \quad (7.22)$$

which is also illustrated in Figure 7.2. In all the examples we have checked, we observe the following

$$\sum_{k=2}^{n-2} \nu_{n,k} = \begin{cases} \nu_n & \text{for } n = 4 \\ 2\nu_n & \text{for } n > 4. \end{cases} \quad (7.23)$$

The intriguing factor of 2 in (7.23) can be explained as follows: let  $\#\mathbf{g}_n$  and  $\#\mathbf{h}_n$  be the degree of the maps  $\mathbf{g}_n$  (7.13) and  $\mathbf{h}_n$  (7.15), respectively, i.e. the number of solutions to the equations  $y = \mathbf{g}_n(x)$  and  $y = \mathbf{h}_n(x)$ . Then the formula (7.23) can be rewritten as

$$\sum_{k=2}^{n-2} \nu_{n,k} = \frac{\#\mathbf{g}_n}{\#\mathbf{h}_n} \nu_n. \quad (7.24)$$

We have explicitly checked for  $n = 4, 5, 6, 7$ , where we get<sup>4</sup>:  $(\#\mathbf{g}_4, \#\mathbf{h}_4) = (1, 1)$ ,  $(\#\mathbf{g}_5, \#\mathbf{h}_5) = (2, 1)$ ,  $(\#\mathbf{g}_6, \#\mathbf{h}_6) = (4, 2)$  and  $(\#\mathbf{g}_7, \#\mathbf{h}_7) = (8, 4)$ . We believe that this pattern extends beyond  $n = 7$ . We postpone a more detailed discussion on (7.24) until the next section when we consider explicit examples.

## 7.3 Examples

To illustrate the discussion of the previous section we work out some examples for low  $n$  and provide explicit definitions of maps and forms where applicable.

### 7.3.1 Four-point amplitudes

As we have seen, the simplest kinematic associahedron and momentum amplituhedron are the  $n = 4$  cases. The momentum amplituhedron has only one  $k$  sector for  $n = 4$ , and therefore there is only one momentum amplituhedron geometry to consider. The canonical form of  $\mathcal{M}_{4,2}^{(4)}$  found in (6.74), written explicitly on  $\mathcal{O}_4$ , is simply

$$\Omega_{4,2} = d \log \frac{\langle 12 \rangle}{\langle 13 \rangle} \wedge d \log \frac{\langle 23 \rangle}{\langle 13 \rangle} \wedge d \log \frac{\langle 34 \rangle}{\langle 13 \rangle} \wedge d \log \frac{\langle 14 \rangle}{\langle 13 \rangle}. \quad (7.25)$$

<sup>4</sup>Depending on the choice of basis for  $\mathcal{G}_7$  we also find  $(\#\mathbf{g}_7, \#\mathbf{h}_7) = (16, 8)$ , but their ratio is still 2.

The kinematic associahedron, discussed in section 5.3, has the following canonical form defined on  $\mathcal{K}_4$

$$\tilde{\omega}_4 = d \log \frac{X_{13}}{X_{24}} = d \log \frac{s_{12}}{s_{23}}. \quad (7.26)$$

We have defined the map  $\mathbf{f}_4 : \mathcal{L}_4 \mapsto \mathcal{O}_4$  by removing the little group scaling and we parameterize the remaining  $\lambda$  and  $\tilde{\lambda}$  matrices using the extended Fock-Goncharov variables as follows

$$\lambda = \begin{pmatrix} 0 & t_2 & t_3 & t_4 \\ -t_1 & 0 & t_3 & t_4(1+a_1) \end{pmatrix}, \quad \tilde{\lambda} = \begin{pmatrix} t_1^{-1}a_2 & -t_2^{-1}a_2 & t_3^{-1}a_2 & 0 \\ t_1^{-1}(1+a_1) & -t_2^{-1} & 0 & t_4^{-1} \end{pmatrix}, \quad (7.27)$$

where we have fixed  $\tilde{\lambda}$  by a particular choice of  $SL(2)$  in (7.27). We define the map  $\mathbf{p} : \mathcal{L}_4 \mapsto \mathcal{K}_4$ , taking the form

$$\mathbf{p}_4 : s_{12} = \langle 12 \rangle [12] = a_1 a_2, \quad s_{23} = \langle 23 \rangle [23] = a_2. \quad (7.28)$$

Finally, since there is no Gram matrix for  $n = 4$ , we have  $\mathcal{G}_4 = \mathcal{K}_4$  and  $\mathbf{h}_4 = \mathbf{I}_4$  is trivial, implying that  $\mathbf{g}_4 = \mathbf{p}_4$  and  $\nu_4 = \tilde{\omega}_4$ . We pull  $\Omega_{4,2}$  back to  $\mathcal{L}_4$  through the map  $\mathbf{f}_4$  as follows

$$\mathbf{f}_4^* \Omega_{4,2} = \mu_4 \wedge d \log a_1 \longleftrightarrow \omega_{4,2} = d \log a_1 = d \log R_{1234}, \quad (7.29)$$

where  $\mu_4$  is defined in (7.17) and the cross-ratio  $R_{1234}$  in (7.8). We compare the above differential form to the pull-back of  $\tilde{\omega}_4$  using the map  $\mathbf{p}_4$  and observe that

$$\omega_4 = \mathbf{p}_4^* \tilde{\omega}_4 = d \log R_{1234}, \quad (7.30)$$

on the little group invariant space  $\mathcal{L}_4$ . Here we verify the result (7.20) for  $n = 4$

$$\omega_4 = \omega_{4,2}. \quad (7.31)$$

We can also compare on the space  $\mathcal{G}_4 = \mathcal{K}_4$ . Since the map  $\mathbf{p}_4$  is invertible, pushing the form  $\omega_{4,2}$  forward via  $\mathbf{p}_4$ , simply returns the kinematic associahedron form as follows

$$\nu_{4,2} = (p_4)_* d \log R_{1234} = d \log \frac{s_{12}}{s_{23}} = \nu_4. \quad (7.32)$$

### 7.3.2 Five-point amplitudes

There are two distinct momentum amplituhedron geometries for  $n = 5$  labeled  $k = 2$  and  $k = 3$ . Their canonical forms are

$$\Omega_{5,2} = -d \log \frac{\langle 13 \rangle}{\langle 14 \rangle} \wedge d \log \frac{\langle 34 \rangle}{\langle 14 \rangle} \wedge d \log \frac{\langle 45 \rangle}{\langle 14 \rangle} \wedge d \log \frac{\langle 51 \rangle}{\langle 14 \rangle} \wedge d \log \frac{\langle 12 \rangle}{\langle 13 \rangle} \wedge d \log \frac{\langle 23 \rangle}{\langle 13 \rangle}, \quad (7.33)$$

and

$$\Omega_{5,3} = -d \log \frac{[13]}{[14]} \wedge d \log \frac{[34]}{[14]} \wedge d \log \frac{[45]}{[14]} \wedge d \log \frac{[51]}{[14]} \wedge d \log \frac{[12]}{[13]} \wedge d \log \frac{[23]}{[13]}. \quad (7.34)$$

On the other hand, the canonical form for the kinematic associahedron is found in (5.9) to be

$$\tilde{\omega}_5 = d \log \frac{X_{13}}{X_{24}} \wedge d \log \frac{X_{13}}{X_{14}} + d \log \frac{X_{13}}{X_{25}} \wedge d \log \frac{X_{35}}{X_{24}}. \quad (7.35)$$

We define the map  $\mathbf{f}_5 : \mathcal{L}_5 \mapsto \mathcal{O}_5$  by removing the little group scaling and choosing an extended Fock-Goncharov parameterization of  $\mathcal{L}_5$  depending on  $(3 \times 5 - 10) = 5$  variables. We choose the manifestly parity symmetric parameterization of cross-ratios and Mandelstam variables with the parameters  $\{R_{1234}, R_{1345}, \bar{R}_{1234}, \bar{R}_{1345}, s_{12}\}$  allowing us to write

$$\lambda = \begin{pmatrix} 0 & t_2 & t_3 & t_4 & t_5 \\ -t_1 & 0 & t_3 & t_4(1 + R_{1234}) & t_5(1 + R_{1234} + R_{1234}R_{1345}) \end{pmatrix}, \quad (7.36)$$

and the parameterization of  $\tilde{\lambda}$  can be found in (B.1) in Appendix B.

The map  $\mathbf{p}_5 : \mathcal{L}_5 \rightarrow \mathcal{K}_5$  can be found by calculating the minors of the matrices (7.36) and (B.1). The map  $\mathbf{p}_5$  is rational and not invertible. Instead, we can find two local inverses taking the form

$$\mathbf{p}_{5,\pm}^{-1} : \begin{aligned} R_{1234} &= \frac{s_{12} s_{23} + s_{34} s_{23} - s_{34} s_{45} - s_{12} s_{51} + s_{45} s_{51} \pm \sqrt{\Delta}}{2s_{23}(s_{23} - s_{45} - s_{51})}, \\ R_{1345} &= \frac{s_{12} s_{23} - s_{34} s_{23} + s_{34} s_{45} - s_{12} s_{51} + s_{45} s_{51} \mp \sqrt{\Delta}}{2s_{34} s_{51}}, \\ \bar{R}_{1234} &= \frac{s_{12} s_{23} + s_{34} s_{23} - s_{34} s_{45} - s_{12} s_{51} + s_{45} s_{51} \mp \sqrt{\Delta}}{2s_{23}(s_{23} - s_{45} - s_{51})}, \\ \bar{R}_{1345} &= \frac{s_{12} s_{23} - s_{34} s_{23} + s_{34} s_{45} - s_{12} s_{51} + s_{45} s_{51} \pm \sqrt{\Delta}}{2s_{34} s_{51}}, \end{aligned} \quad (7.37)$$

where the two solutions are distinguished by the sign in front of the square root of

$$\Delta = (s_{23} s_{34} + s_{12}(s_{23} - s_{51}) + s_{45}(s_{51} - s_{34}))^2 - 4s_{12} s_{23} s_{34}(s_{23} - s_{45} - s_{51}). \quad (7.38)$$

Interestingly the conjugation operation, interchanging  $R$  and  $\bar{R}$ , exchanges the sign in front of the  $\sqrt{\Delta}$ :

$$\bar{R}_{ijkl} = R_{ijkl}|_{\sqrt{\Delta} \rightarrow -\sqrt{\Delta}}. \quad (7.39)$$

As in the  $n = 4$  case, no Gram determinant conditions arise for  $n = 5$  and we have that  $\mathcal{G}_5 = \mathcal{K}_5$ ,  $\mathbf{g}_5 = \mathbf{p}_5$ , and  $\mathbf{h}_5 = \mathbf{I}_5$  is the identity map. This implies that  $\nu_5 = \tilde{\omega}_5$ .

Starting from the kinematic associahedron  $\mathcal{A}_5$ , we pull the canonical form  $\tilde{\omega}$  (7.35) back to  $\mathcal{L}_5$  using the map  $\mathbf{p}_5$  to obtain

$$\omega_5 = \mathbf{p}_5^* \tilde{\omega}_5 = d \log R_{1234} \wedge d \log R_{1345} + d \log \bar{R}_{1234} \wedge d \log \bar{R}_{1345}. \quad (7.40)$$

We pull the momentum amplituhedron canonical forms  $\Omega_{5,2}$  (7.33) and  $\Omega_{5,3}$  (found in (7.34)) back to  $\mathcal{L}_5$  as well using  $\mathbf{f}_5$  to obtain

$$\mathbf{f}_5^* \Omega_{5,2} = \mu_5 \wedge d \log R_{1234} \wedge d \log R_{1345} \quad \rightarrow \quad \omega_{5,2} = d \log R_{1234} \wedge d \log R_{1345}, \quad (7.41)$$

$$\mathbf{f}_5^* \Omega_{5,3} = \mu_5 \wedge d \log \bar{R}_{1234} \wedge d \log \bar{R}_{1345} + \mathcal{O}(d^3 t) \quad \rightarrow \quad \omega_{5,3} = d \log \bar{R}_{1234} \wedge d \log \bar{R}_{1345}. \quad (7.42)$$

We note, that when pulling  $\Omega_{5,3}$  (found in (7.34)) back to  $\mathcal{L}_5$  the resulting form contains several terms of lower form degree in  $dt_i$ , which we have neglected, while the pull-back of  $\Omega_{5,2}$  (7.33) contains only the top-degree form in  $dt_i$ .

When comparing the momentum amplituhedron forms to the kinematic associahedron form on  $\mathcal{L}_5$ , we observe

$$\omega_5 = \omega_{5,2} + \omega_{5,3}, \quad (7.43)$$

which is exactly the structure we expect from (7.20).

We can only construct one Gram matrix for  $n = 5$  whose determinant is trivially 0 on support of momentum conservation. This means, that there are no non-trivial Gram determinant conditions. We therefore push the forms  $\omega_{5,k}$  forward directly to the space of Mandelstam variables,  $\mathcal{K}_5$ , the native space of the kinematic associahedron, using the map  $\mathbf{p}_5$ . As per the definition of the push-forward in section 4.2, we need to pull  $\omega_{5,k}$  back using the two solutions (7.37) and add the resulting forms. Here, the square roots present in the inverse maps cancel in the sum and we get the answer

$$\nu_{5,2} = (\mathbf{p}_5)_* \omega_{5,2} = \tilde{\omega}_5 \nu_{5,3} = (\mathbf{p}_5)_* \omega_{5,3} = \tilde{\omega}_5. \quad (7.44)$$

verifying the statement of (7.23) since

$$\nu_{5,2} + \nu_{5,3} = 2\tilde{\omega}_5 = 2\nu_5. \quad (7.45)$$

### 7.3.3 Six-point amplitudes

The momentum amplituhedron for  $n = 6$  has three distinct  $k$  sectors, each contributing the superamplitude, namely  $k = 2$ ,  $k = 3$ , and  $k = 4$ . The two sectors  $k = 2$  and  $k = 4$  are particularly simple and can be written on  $\mathcal{O}_6$  as follows

$$\Omega_{6,2} = -d \log \frac{\langle 14 \rangle}{\langle 15 \rangle} \wedge d \log \frac{\langle 45 \rangle}{\langle 15 \rangle} \wedge d \log \frac{\langle 56 \rangle}{\langle 15 \rangle} \wedge d \log \frac{\langle 61 \rangle}{\langle 15 \rangle} \wedge d \log \frac{\langle 13 \rangle}{\langle 14 \rangle} \wedge d \log \frac{\langle 34 \rangle}{\langle 14 \rangle} \\ \wedge d \log \frac{\langle 12 \rangle}{\langle 13 \rangle} \wedge d \log \frac{\langle 23 \rangle}{\langle 13 \rangle}, \quad (7.46)$$

and

$$\begin{aligned} \Omega_{6,4} = & -d \log \frac{[14]}{[15]} \wedge d \log \frac{[45]}{[15]} \wedge d \log \frac{[56]}{[15]} \wedge d \log \frac{[61]}{[15]} \wedge d \log \frac{[13]}{[14]} \wedge d \log \frac{[34]}{[14]} \\ & \wedge d \log \frac{[12]}{[13]} \wedge d \log \frac{[23]}{[13]}. \end{aligned} \quad (7.47)$$

The momentum amplituhedron form in the  $k = 3$  sector is significantly more involved, consisting of the sum of three BCFW terms [92, 93]. The explicit expression can be found in [84] and we provide a method to construct the BCFW differential forms using the inverse-soft construction in the very end of this chapter in section 7.4. For now, it will be sufficient to recall that  $\Omega_{6,3}$  can be constructed as follows

$$\Omega_{6,3} = \Omega_{6,3}^{\gamma_2} + \Omega_{6,3}^{\gamma_4} + \Omega_{6,3}^{\gamma_6} = \Omega_{6,3}^{\gamma_1} + \Omega_{6,3}^{\gamma_3} + \Omega_{6,3}^{\gamma_5}, \quad (7.48)$$

where  $\Omega_{6,3}^{\gamma_i}$  is the BCFW term with vanishing minor  $\gamma_i := (i, i+1, i+2)$  as in (6.87) of section 6.6, when projected through constant  $(Y, \tilde{Y})$ .

The canonical form of the kinematic associahedron  $\mathcal{A}_6$  on  $\mathcal{K}_5$  is found in [43] to be

$$\begin{aligned} \tilde{\omega}_6 = & d \log \frac{X_{24}}{X_{13}} \wedge d \log \frac{X_{14}}{X_{46}} \wedge d \log \frac{X_{15}}{X_{46}} + d \log \frac{X_{26}}{X_{13}} \wedge d \log \frac{X_{36}}{X_{13}} \wedge d \log \frac{X_{46}}{X_{35}} - \\ & - d \log \frac{X_{26}}{X_{15}} \wedge d \log \frac{X_{25}}{X_{35}} \wedge d \log \frac{X_{24}}{X_{35}} + d \log \frac{X_{24}}{X_{13}} \wedge d \log \frac{X_{46}}{X_{35}} \wedge d \log \frac{X_{26}}{X_{15}}. \end{aligned} \quad (7.49)$$

In order to define the map  $\mathbf{f}_6 : \mathcal{L}_6 \mapsto \mathcal{O}_6$  we employ the extended Fock-Goncharov parameterization for  $(\lambda, \tilde{\lambda})$ , choosing  $3 \times 6 - 10 = 8$  parameters to be the cross-ratios  $\{R_{1234}, R_{1345}, R_{1456}\}$ , the cross-ratios  $\{\bar{R}_{1234}, \bar{R}_{1345}, \bar{R}_{1456}\}$ , together with the two Mandelstam variables  $\{s_{12}, s_{23}\}$ . We obtain the following representation for  $\lambda$  as per (7.7):

$$\lambda = \left( \begin{array}{cccccc} 0 & 1 & 1 & 1 & 1 & 1 \\ -1 & 0 & 1 & 1 + R_{1234} & 1 + R_{1234}(1 + R_{1345}) & 1 + R_{1234}(1 + R_{1345}(1 + R_{1456})) \end{array} \right). \quad (7.50)$$

The representation for  $\tilde{\lambda}$  is too cumbersome to quote explicitly, but it is found by imposing orthogonality on  $\lambda$  and fixing the  $SL(2)$  invariance similarly to the two previous examples. With the extended Fock-Goncharov representation at hand, it is a straight forward exercise to construct the maps  $\mathbf{g}_6 : \mathcal{L}_6 \mapsto \mathcal{G}_6$  and  $\mathbf{p}_6 : \mathcal{L}_6 \mapsto \mathcal{K}_6$  using  $s_{ij} = \langle ij \rangle [ij]$  and substituting the explicit forms of  $\lambda$  and  $\tilde{\lambda}$ .

For  $n = 6$  the Gram determinant surface is no longer trivial and we are required to choose a set of Mandelstam variables to parameterize the surface  $\mathcal{G}_6$ . our choice is  $\{s_{12}, s_{23}, s_{34}, s_{45}, s_{56}, s_{61}, s_{123}, s_{234}\}$ . To define the push-forward through the map  $\mathbf{g}_6$ , we need to first invert it, leading to four local solutions, a single of which is quoted

here and the rest can be reconstructed by changing signs in the expression

$$\mathbf{g}_{6,1}^{-1} : \begin{aligned} R_{1234}^{(1)} &= \frac{s_{12}s_{23}+s_{23}s_{34}-s_{23}s_{56}-s_{34}s_{123}-s_{12}s_{234}+s_{123}s_{234}-\sqrt{\Delta_1}}{2s_{23}(s_{23}+s_{56}-s_{123}-s_{234})} \\ R_{1345}^{(1)} &= \frac{-s_{12}s_{23}+s_{23}s_{34}+s_{23}s_{56}-s_{34}s_{123}+s_{12}s_{234}-s_{123}s_{234}-\sqrt{\Delta_1}}{2s_{34}(s_{56}+s_{61}-s_{234})} \times \\ &\quad \times \frac{s_{23}s_{56}+s_{45}s_{56}-s_{56}s_{61}+s_{61}s_{123}-s_{45}s_{234}-s_{123}s_{234}-\sqrt{\Delta_2}}{2(s_{23}s_{56}-s_{123}s_{234})}, \\ R_{1456}^{(1)} &= \frac{-s_{23}s_{56}+s_{45}s_{56}+s_{56}s_{61}-s_{61}s_{123}-s_{45}s_{234}+s_{123}s_{234}-\sqrt{\Delta_2}}{2s_{45}s_{61}}, \end{aligned} \quad (7.51)$$

with

$$\bar{R}_{ijkl}^{(1)} = R_{ijkl}^{(1)}|_{\sqrt{\Delta_1} \leftrightarrow -\sqrt{\Delta_1}, \sqrt{\Delta_2} \leftrightarrow -\sqrt{\Delta_2}}, \quad (7.52)$$

where the arguments of the square roots,  $\Delta_1$  and  $\Delta_2$ , are written explicitly in Appendix C. The three remaining inverses of  $\mathbf{g}_6$  can be obtained by exchanging the signs in front of the square roots

$$R_{ijkl}^{(2)} = R_{ijkl}^{(1)}|_{\sqrt{\Delta_1} \leftrightarrow -\sqrt{\Delta_1}}, \quad R_{ijkl}^{(3)} = R_{ijkl}^{(1)}|_{\sqrt{\Delta_2} \leftrightarrow -\sqrt{\Delta_2}}, \quad (7.53)$$

$$R_{ijkl}^{(4)} = R_{ijkl}^{(1)}|_{\sqrt{\Delta_1} \leftrightarrow -\sqrt{\Delta_1}, \sqrt{\Delta_2} \leftrightarrow -\sqrt{\Delta_2}}. \quad (7.54)$$

When solving the Gram conditions in order to define the map  $\mathbf{h}_6$ , we reduce the nine-dimensional space  $\mathcal{K}_6$  to the eight-dimensional surface  $\mathcal{G}_6$ . There is exactly one Gram determinant condition in four dimensions and we choose to solve for the variables  $s_{345}$ , which would leave us with the set of variables defined above. The map has two local inverses

$$\mathbf{h}_{6,\pm}^{-1} : \quad s_{345} = \frac{\Gamma \pm \sqrt{\Delta_1 \Delta_2}}{2s_{14}Q}, \quad (7.55)$$

where  $\Delta_1$  and  $\Delta_2$  are the same as before,  $s_{14} = s_{23} + s_{56} - s_{123} - s_{234}$  and  $Q = s_{23}s_{56} - s_{123}s_{234}$ . The explicit form for  $\Gamma$  can be found in Appendix C in (C.3).

We are now ready to compare forms on the little groups scaling invariant space  $\mathcal{L}_6$ : for the  $k = 2$  and  $k = 4$  sectors the pull-backs of  $\Omega_{6,2}$  and  $\Omega_{6,4}$  on  $\mathcal{L}_6$  takes the very simple form

$$\mathbf{f}_6^* \Omega_{6,2} = \mu_6 \wedge \omega_{6,2} \quad \longrightarrow \quad \omega_{6,2} = d \log R_{1234} \wedge d \log R_{1345} \wedge d \log R_{1456}, \quad (7.56)$$

$$\mathbf{f}_6^* \Omega_{6,4} = \mu_6 \wedge \omega_{6,4} + \mathcal{O}(d^4 t) \quad \longrightarrow \quad \omega_{6,4} = d \log \bar{R}_{1234} \wedge d \log \bar{R}_{1345} \wedge d \log \bar{R}_{1456}. \quad (7.57)$$

For  $k = 3$ , we can use the inverse-soft construction, to be reviewed in the next section, to find the following compact expression for  $\omega_{6,3}$

$$\begin{aligned} \mathbf{f}_6^* \Omega_{6,3} = \mu_6 \wedge \omega_{6,3} + \mathcal{O}(d^4 t) \quad \longrightarrow \quad \omega_{6,3} &= d \log R_{5612}^{(234)} \wedge d \log R_{1524}^{(234)} \wedge d \log R_{1234}^{(234)} \\ &\quad + d \log R_{1236}^{(456)} \wedge d \log R_{3146}^{(456)} \wedge d \log R_{1456}^{(456)} \\ &\quad + d \log R_{3456}^{(612)} \wedge d \log R_{5462}^{(612)} \wedge d \log R_{5612}^{(612)}, \end{aligned} \quad (7.58)$$

where  $R_{ijkl}^\gamma$  are the cross-ratios of angle brackets, defined in (7.8). The label  $\gamma$  refers to the particular BCFW triangulation cell in the positive Grassmannian (see (7.48) for details), and hatted particle labels  $\hat{i}$  in  $R^\gamma$  are defined by  $\lambda_{\hat{i}}^\alpha = \sum_{j \in \gamma} \lambda_j^\alpha [ji]$ . When pulling the kinematic associahedron form (7.49) back to the little group space,  $\mathcal{L}_6$  using the map  $\mathbf{p}_6$  we obtain

$$\omega_6 = \mathbf{p}_6^* \tilde{\omega}_6 = \omega_{6,2} + \omega_{6,3} + \omega_{6,4}. \quad (7.59)$$

The space of Gram conditions,  $\mathcal{G}_n$ , is in the case of  $n = 6$  not equal to the full space of Mandelstam variables, and therefore the map  $\mathbf{h}_6$  is no longer trivial. There are two solutions to the inverse of the map  $\mathbf{h}_6$  as recorded in (7.55). We push the kinematic associahedron form forward to surface  $\mathcal{G}_6$

$$\nu_6 = (\mathbf{h}_6)_* \tilde{\omega}_6. \quad (7.60)$$

While for the  $\mathbf{g}_6$  map, we find four local inverses in (7.51). We push the reduced momentum amplituhedron form  $\omega_{6,k}$  forward to the Gram determinant surface  $\mathcal{G}_6$ , as follows

$$\nu_{6,k} = (\mathbf{g}_6)_* \omega_{6,k}, \quad k = (2, 3, 4). \quad (7.61)$$

Intriguingly, the differential forms  $\nu_{6,k}$  have non-canonical behavior, that is, they have certain residues on zero-dimensional boundaries that no longer yield  $\pm 1$ . We write the explicit form of  $\nu_{6,2}$ , as well as provide a more detailed discussion of its non-logarithmic behavior in Appendix D. Summing the reduced momentum amplituhedron forms for the three  $k$  sectors pushed forward to  $\mathcal{G}_6$ , we verify the full reduced momentum amplituhedron form to be proportional to the push-forward of the kinematic associahedron form to the same surface, as follows

$$\nu_{6,2} + \nu_{6,3} + \nu_{6,4} = 2\nu_6. \quad (7.62)$$

The factor of 2 above stems from a property of the push-forwards and not of the specific differential forms involved. To make this fact clear, we rewrite (7.62) as

$$(\mathbf{g}_6)_* \mathbf{p}_6^* \tilde{\omega}_6 = 2(\mathbf{h}_6)_* \tilde{\omega}_6. \quad (7.63)$$

Since  $\mathcal{G}_6$  is a subspace of  $\mathcal{K}_6$  found by solving a particular Gram determinant condition with respect to the Mandelstam variable  $s_{345}$ , if we take  $\beta$  to be an *arbitrary* differential form on  $\mathcal{K}_6$  which does **not** depend on  $s_{345}$ , we see that trivially

$$(\mathbf{h}_6)_* \beta = \# \mathbf{h}_6 \beta, \quad (7.64)$$

and

$$(\mathbf{g}_6)_* \mathbf{p}_6^* \beta = \# \mathbf{g}_6 \beta, \quad (7.65)$$

where  $\#\mathbf{g}_6 = 4$  and  $\#\mathbf{h}_6 = 2$  counts the degree of  $\mathbf{g}_6$  and  $\mathbf{h}_6$ , respectively. Combining the equations (7.64) and (7.65) we obtain

$$(\mathbf{g}_6)_* \mathbf{p}_6^* \beta = \frac{\#\mathbf{g}_6}{\#\mathbf{h}_6} (\mathbf{h}_6)_* \beta = 2(\mathbf{h}_6)_* \beta. \quad (7.66)$$

The statement (7.66) hold in general for all differential forms, including those that **do** depend on  $s_{345}$ . We can verify this by first observing that the four solutions  $\mathbf{g}_{6,i}^{-1}$  are related by a  $\mathbb{Z}_2 \times \mathbb{Z}_2$  symmetry, where each discrete  $\mathbb{Z}_2$  changes the sign of one of the square roots, and the symmetry group double-covers the two solutions  $\mathbf{h}_{6,\pm}^{-1}$ . Since the Gram determinant condition is automatically satisfied on  $\mathcal{L}_6$ , the double-covering of  $\mathbf{h}_{6,\pm}^{-1}$  implies that one of the local inverses  $\mathbf{h}_{6,\pm}^{-1}$  corresponds to the composition  $\mathbf{p}_6 \circ \mathbf{g}_{6,1}^{-1} = \mathbf{p}_6 \circ \mathbf{g}_{6,4}^{-1}$  and the other to  $\mathbf{p}_6 \circ \mathbf{g}_{6,2}^{-1} = \mathbf{p}_6 \circ \mathbf{g}_{6,3}^{-1}$ . This then implies that (7.66) must hold for all differential forms  $\beta$  on  $\mathcal{K}_6$ .

### 7.3.4 Beyond $n = 6$

We have verified that (7.20) and (7.23) is satisfied for  $n = 7$ . In particular, we obtain

$$\omega_7 = \omega_{7,2} + \omega_{7,3} + \omega_{7,4} + \omega_{7,5}, \quad (7.67)$$

$$\nu_{7,2} + \nu_{7,3} + \nu_{7,4} + \nu_{7,5} = 2\nu_7. \quad (7.68)$$

Since the explicit forms of the differential forms present in these relations are very involved, and not very illuminating on their own, we refrain from representing them directly. We conjecture that (7.20) and (7.23) extends to all  $n$ .

We observe the following for the reduced momentum amplituhedron forms: for all  $n$ , the  $k = 2$  and  $k = n - 2$  reduced momentum amplituhedron form have very simple structure, namely

$$\omega_{n,2} = \bigwedge_{i=2}^{n-3} d\log R_{1ii+1i+2}, \quad \omega_{n,n-2} = \bigwedge_{i=2}^{n-3} d\log \bar{R}_{1ii+1i+2}. \quad (7.69)$$

These formulae are easily proven using the inverse-soft construction which we will review presently wherein both cases particle 2 is taken to be the inverse-soft particle.

## 7.4 The Inverse-Soft Construction for $\omega_{n,k}$

In [40], we propose that the inverse soft construction described in [84] can be applied to obtain the reduced momentum amplituhedron form. Starting from the reduced form  $\omega_{4,2}$  defined in (7.16), we recursively add inverse-soft particles to obtain reduced forms for higher  $n$  and  $k$ . We review the inverse-soft construction in the following. The BCFW construction of scattering amplitudes discussed in chapter 2 indicates that a scattering amplitude can be written as a sum of BCFW terms, each of which

can be represented by an affine permutation corresponding to a cell in the positive Grassmannian as reviewed in section 3.3; see also [72]. A BCFW term for  $n \geq 4$  is labeled by an affine permutation  $\sigma$  and is said to be *inverse-soft (IS) constructable* if there exists an  $i \in [n] = \{1, 2, \dots, n\}$  such that

$$\sigma(i-1) = i+1 \pmod n, \quad \text{or} \quad \sigma(i+1) = i-1 \pmod n, \quad (7.70)$$

In the first case, we say  $i$  label a *helicity-preserving IS particle* and in the second a *helicity-increasing IS particle*, we will discuss the former case first. In [84] it was argued that the canonical form can be decomposed as

$$\Omega_\sigma(1, \dots, i, \dots, n) = \Omega_{\hat{\sigma}}(1, \dots, \widehat{i-1}, \widehat{i+1}, \dots, n) \wedge \Omega_{3,2}(i-1, i, i+1), \quad (7.71)$$

where we shift the two particles adjacent to the IS particle by

$$\tilde{\lambda}_{\widehat{i-1}} = \tilde{\lambda}_{i-1} + \frac{\langle i i+1 \rangle}{\langle i-1 i+1 \rangle} \tilde{\lambda}_i, \quad \tilde{\lambda}_{\widehat{i+1}} = \tilde{\lambda}_{i+1} + \frac{\langle i-1 i \rangle}{\langle i-1 i+1 \rangle} \tilde{\lambda}_i, \quad (7.72)$$

leaving  $\lambda$ 's unshifted and taking

$$\Omega_{3,2}(i-1, i, i+1) = d \log \frac{\langle i-1 i \rangle}{\langle i-1 i+1 \rangle} \wedge d \log \frac{\langle i i+1 \rangle}{\langle i-1 i+1 \rangle}. \quad (7.73)$$

Alternatively, if  $\sigma(i+1) = i-1$  in (7.70), then  $i$  is said to be *helicity-increasing IS particle* and the canonical form is decomposed as follows

$$\Omega_\sigma(1, \dots, i, \dots, n) = \Omega_{\hat{\sigma}}(1, \dots, \widehat{i-1}, \widehat{i+1}, \dots, n) \wedge \Omega_{3,1}(i-1, i, i+1), \quad (7.74)$$

where

$$\lambda_{\widehat{i-1}} = \lambda_{i-1} + \frac{[i i+1]}{[i-1 i+1]} \lambda_i, \quad \lambda_{\widehat{i+1}} = \lambda_{i+1} + \frac{[i-1 i]}{[i-1 i+1]} \lambda_i, \quad (7.75)$$

where we leave  $\tilde{\lambda}$  unshifted and take

$$\Omega_{3,1}(i-1, i, i+1) = d \log \frac{[i-1 i]}{[i-1 i+1]} \wedge d \log \frac{[i i+1]}{[i-1 i+1]}. \quad (7.76)$$

In both cases,  $\hat{\sigma}$  is an affine permutation on  $[n]$  not containing  $i$ , whose precise definition depends on whether it is helicity preserving or increasing and quoted in [72]. By construction, we can write an expression for  $\Omega_\sigma$  as a logarithmic differential form on canonical coordinates of the positroid cell associated with the particular permutation as follows

$$\Omega_\sigma(1, 2, \dots, n) = \bigwedge_{j=1}^{2n-4} d \log \alpha_j. \quad (7.77)$$

The arguments of the  $d\log$ 's,  $\alpha_j$ , are simply the canonical coordinates for the particular positroid cell  $\Gamma_\sigma$  labeled by  $\sigma$  discussed in section 3.3. Let us study the little group action on the canonical coordinates. Recall the representation of the momentum amplituhedron for  $n = 4$ ,  $k = 2$  in (7.25). Here, we identify the canonical coordinates as scaling according to

$$\alpha_1 = \frac{\langle 12 \rangle}{\langle 13 \rangle} \sim \frac{t_2}{t_3}, \quad \alpha_2 = \frac{\langle 23 \rangle}{\langle 13 \rangle} \sim \frac{t_2}{t_1}, \quad \alpha_3 = \frac{\langle 34 \rangle}{\langle 13 \rangle} \sim \frac{t_4}{t_1}, \quad \alpha_4 = \frac{\langle 14 \rangle}{\langle 13 \rangle} \sim \frac{t_4}{t_3}. \quad (7.78)$$

It is clear in the above that for all  $i \in [4]$ , there is a canonical variable  $\alpha_j$  such that either  $\alpha_j$  or  $1/\alpha_j$  scales like  $t_i/t_{i+1}$  (where  $t_{4+1} = t_1$ ). For instance, for  $i = 1$ , the canonical coordinate scaling as  $t_1/t_2$  is  $\alpha_2^{-1}$ . This is a general property of IS-constructible canonical forms, which extends beyond  $n = 4$ . In particular, for any canonical form  $\Omega_\sigma$  with canonical variables  $\{\alpha_j\}_j^{2n-4}$  there exists for all  $i \in [n]$  at least one canonical variable  $\tilde{\alpha}_i \in \{\alpha_j\}_{j=1}^{2n-4}$  such that either  $\tilde{\alpha}_i$  or  $\tilde{\alpha}_i^{-1}$  scales as  $t_i/t_{i+1}$ . Using this fact, we construct the reduced momentum amplituhedron forms by combining (7.76), (7.74) and (7.71) into a single equation as follows

$$\Omega_\sigma(1, \dots, i, \dots, n) = \Omega_{\hat{\sigma}}(1, \dots, \widehat{i-1}, \widehat{i+1}, \dots, n) \wedge \Omega_{3,\hat{k}}(1-i, i, i+1), \quad (7.79)$$

where  $\hat{k} = 1$  or  $\hat{k} = 2$ , and we define

$$\Omega_{3,\hat{k}} = d\log x_i \wedge d\log y_i, \quad (7.80)$$

where we take  $x_i$  and  $y_i$  as follows

$$\begin{cases} x_i = \frac{[i-1\ i]}{[i-1\ i+1]} \text{ and } y_i = \frac{[i\ i+1]}{[i-1\ i+1]}, & \text{for } \hat{k} = 1, \\ x_i = \frac{\langle i-1\ i \rangle}{\langle i-1\ i+1 \rangle} \text{ and } y_i = \frac{\langle i\ i+1 \rangle}{\langle i-1\ i+1 \rangle}, & \text{for } \hat{k} = 2. \end{cases} \quad (7.81)$$

The form  $\Omega_{\hat{\sigma}}$  can be represented as a wedge product of canonical coordinates. We denote the canonical coordinates for  $\Omega_{\hat{\sigma}}$  as  $\{\beta_j\}_{j=1}^{2n-6}$ , and there exists a coordinate  $\tilde{\beta} \in \{\beta_j\}_{j=1}^{2n-6}$  such that

$$\omega_\sigma(1, \dots, i, \dots, n) = (-1)^{n+i+k'} d\log \left( \frac{x_i}{y_i} \tilde{\beta}^s \right) \wedge \omega_{\hat{\sigma}}(1, \dots, \widehat{i-1}, \widehat{i+1}, \dots, n). \quad (7.82)$$

We fix  $\tilde{\beta}$  and  $s \in \{\pm 1\}$  in (7.82) by the requirement that the argument of the first logarithm,  $\left( \frac{x_i}{y_i} \tilde{\beta}^s \right)$ , is little group scaling invariant. In particular, due to the fact that  $\frac{x_i}{y_i} \sim \frac{t_{i+1}}{t_{i-1}}$  for  $k' = 1$  and  $\frac{x_i}{y_i} \sim \frac{t_{i-1}}{t_{i+1}}$  for  $k' = 2$ , we know from the discussion laid out above that it is always possible to find such a  $\tilde{\beta}$  that cancels the scaling of  $\frac{x_i}{y_i}$ <sup>5</sup>.

<sup>5</sup>Note that  $\Omega_{\hat{\sigma}}$  does not depend on particle  $i$  meaning that at least one canonical variable will scale as  $\frac{t_{i-1}}{t_{i+1}}$  or  $\frac{t_{i+1}}{t_{i-1}}$ .

We can fix all reduced momentum amplituhedron forms in the MHV sector to have +1 coefficient by choosing particle  $i = 2$  to be the IS particle and redefining  $\Omega_n$  to contain an additional factor of  $(-1)^n$ . This is the origin of the signs in (7.33) and (7.46) that distinguishes them from their counterparts in chapter 6. Fixing the sign of the MHV reduced form in this way also provides a useful prescription for fixing the sign ambiguity in the definition of the canonical form of the kinematic associahedron due to the map between them.

# Chapter 8

## Momentum Amplituhedron & Kleiss-Kuijf Relations

In this section we review how the Kleiss-Kuijf (KK) relations discussed in section 2.4 emerge geometrically from the momentum amplituhedron and the kinematic associahedron, respectively. We shall see how the KK relations emerge from purely geometrical statements about oriented sums of positive geometries, discussed in section 4.3. In the case of the momentum amplituhedron, we exploit the fact that it is defined on the space of spinor helicity variables and therefore is not restricted to a particular external ordering. We shall review how the KK relations emerge by way of homology, and in particular discuss two different approaches: one based on identifying boundaries along rays pointing in opposite directions, suitable for polytopal geometries such as the momentum amplituhedron in the MHV and  $\overline{\text{MHV}}$  sectors and kinematic associahedra, and another approach, based on poset intervals, which is relevant beyond the MHV/ $\overline{\text{MHV}}$  sectors.

### 8.1 Non-Standard Orderings of the Momentum Amplituhedron

In the previous chapters, when discussing the momentum amplituhedron we have restricted ourselves to standard ordering of external particle momenta. As we have stressed, this is not a necessary restriction as spinor-helicity variables have no preferred color ordering. At tree-level, the partial amplitudes in msYM for a given ordering, denoted by  $\sigma \in \mathcal{O}_n \simeq S_n/Z_n$ , can be obtained from the standard ordering by relabeling the external momenta, or as in our case, the spinor helicity variables

$$A_{n,k}[\sigma(1), \sigma(2), \dots, \sigma(n)] = A_{n,k}[1, 2, \dots, n] \Big|_{\lambda_i \rightarrow \lambda_{\sigma(i)}, \bar{\lambda}_i \rightarrow \bar{\lambda}_{\sigma(i)}}. \quad (8.1)$$

This relabeling can be performed on the momentum amplituhedron by modifying the winding space (7.3) according to

$$\mathcal{W}_{n,k}^{(\sigma)} = \{(\lambda_i, \tilde{\lambda}_i) : (\lambda_{\sigma(i)}, \tilde{\lambda}_{\sigma(i)}) \in \mathcal{W}_{n,k}\}, \quad (8.2)$$

while keeping the subspace  $\mathcal{V}_{n,k}$  fixed, leading to

$$\mathcal{M}_{n,k}^{(\sigma)} := \mathcal{V}_{n,k} \cap \mathcal{W}_{n,k}^{(\sigma)}. \quad (8.3)$$

Similarly, the canonical form of the momentum amplituhedron of a non-standard color ordering is just the canonical form of the momentum amplituhedron of the standard color ordering with spinor helicity variables relabeled according to the non-standard color ordering as follows

$$\Omega_{n,k}^{(\sigma)} = \Omega_{n,k}^{(12\dots n)} \Big|_{\lambda_i \rightarrow \lambda_{\sigma(i)}, \tilde{\lambda}_i \rightarrow \tilde{\lambda}_{\sigma(i)}}. \quad (8.4)$$

Having relabeled the external data according to the ordering of interest, it is straightforward to extract the partial color-ordered amplitude

$$A_{n,k}[\sigma(1), \sigma(2), \dots, \sigma(n)] = \delta^{(4)}(p) d^4 p \wedge \Omega_{n,k}^{(\sigma)} \Big|_{d\lambda \rightarrow \eta, d\tilde{\lambda} \rightarrow \tilde{\eta}}. \quad (8.5)$$

An interesting fact about momentum amplituhedra of different orderings, stemming from this definition, is that the boundary stratification of the momentum amplituhedron of a given ordering  $\mathcal{M}_{n,k}^{(\sigma)}$  is combinatorially isomorphic to the standard ordered momentum amplituhedron  $\mathcal{M}_{n,k}$ . In particular, the  $\binom{n}{k}$  vertices labeled by the positive Grassmannian are shared among all particle orderings. We can therefore focus on momentum amplituhedra around a single vertex when comparing different orderings.

## 8.2 Simplicial realization of KK relations for MHV Amplitudes

Armed with a definition of the momentum amplituhedron for non-standard orderings, we are equipped to interpret the KK relations as geometric identities. For MHV amplitudes the proper dimensional subspace  $\mathcal{V}_{n,2}$  (7.1) is defined in terms of  $(2n-4)$   $y$  variables and 4  $\tilde{y}$  variables. On support of momentum conservation, we can fix the four  $\tilde{y}$  variables in terms of the remaining  $y$  variables. This means that the subspace  $\mathcal{V}_{n,2}$  is only dependent on  $\lambda$ . We obtain the MHV momentum amplituhedra by intersecting this subspace with winding spaces of all different particle orderings,  $\mathcal{W}_{n,k}^\sigma$ . In the following we make use of the cyclic identity to bring all external orderings to the form where  $\sigma(1) = 1$ , ensuing that all winding spaces contain the condition that  $\langle 1i \rangle > 0$ ,

and we can parameterize  $\lambda$  as an element of  $G_+(2, n)$  in the coordinate patch where  $\langle 12 \rangle = 1$ . This provides a natural parameterization of  $\lambda$ , and therefore  $\mathcal{V}_{n,2}$ , using the canonical coordinates,  $\alpha_i$  of the positive Grassmannian  $G_+(2, n)$  as follows

$$\mathcal{V}_{n,2} : \lambda = \begin{pmatrix} 1 & \sum_{i=1}^{n-2} \alpha_{2i} & (\sum_{i=1}^{n-3} \alpha_{2i}) \alpha_{2(n-2)-1} & (\sum_{i=1}^{n-4} \alpha_{2i}) \alpha_{2(n-3)-1} & \cdots & \alpha_{2\alpha_3} & 0 \\ 0 & 1 & \alpha_{2(n-2)-1} & \alpha_{2(n-3)-1} & \cdots & \alpha_3 & \alpha_1 \end{pmatrix}, \quad (8.6)$$

which can be obtained from the Mathematica<sup>TM</sup> package `positroids` [73], as discussed in section 3.3. This choice ensures that for the collection  $\mathcal{O}_n = \{1, \sigma(2), \sigma(3), \dots, \sigma(n)\}$  for  $\sigma \in S_{n-1}$ , we have that  $\langle 1i \rangle \geq 0$  if the  $\alpha_{2m-1}$  are all positive for all  $m \in \mathbb{N}$ . Since we are interested in how the geometries of the different orderings compare, we can neglect the odd  $\alpha$ 's since they are all positive for all orderings. This cuts the dimensionality of the space we need to study in half and thus we can focus on  $\mathbb{R}^{n-2}$  of even  $\alpha$ 's. The boundaries of the  $k=2$  momentum amplituhedron are given by the equations  $\langle ij \rangle = 0$  for  $1 < i < j \leq n$  and define  $\binom{n-1}{2}$  co-dimension-one hyperplanes in  $\mathbb{R}^{n-2}$  passing through the origin of the space. The hyperplanes are simply

$$\langle ij \rangle = 0 \quad \Leftrightarrow \quad \sum_{l=n-j+1}^{n-i} \alpha_{2l} = 0 \quad (\text{for } 1 < i < j \leq n). \quad (8.7)$$

We denote this set of co-dimension-one hyperplanes by  $\mathcal{H}_n$ . The hyperplanes cut our  $\mathbb{R}^{(n-2)}$  space into  $(n-1)!$  distinct regions called *positive sectors*. These positive sectors can be interpreted as cones spanned by  $(n-2)$  rays and they have  $(n-2)$  hyperplane facets as their boundaries. Each positive sector is denoted by  $c[\sigma]$  for each  $\sigma \in \mathcal{O}_n$ . The set of all cones is the complete fan of  $\mathbb{R}^{(n-2)}$ . As a curious side note, we observe that the set of all positive sectors in  $\mathbb{R}^{(n-2)}$  are dual to the permutahedron of order  $(n-1)$  [94]: the  $(n-2)$  polytope whose vertices encode all the permutations of  $(n-1)$  symbols, and each edge corresponds to a transposition of two elements relating two permutations. Here each positive sector is dual to a permutation, i.e a vertex of the permutahedron and each ray is dual to an edge of the permutahedron. This means that constructing the positive sectors from the  $\alpha$ -parameterization of  $G_+(2, n)$  yields a new explicit realization of the permutahedron.

For  $n=4$  and  $n=5$ , the cones are 2 and 3 dimensional, respectively, and we can sketch them explicitly. This allows us to immediately identify the geometric interpretation of the KK relations as different combinations of positive sectors as we shall see in the following. We find that the KK relations appear as collections of positive sectors such that their oriented sums do not have any vertices in their boundary stratifications, and the resulting geometries are no longer positive geometries.

### Four particle MHV Amplitudes

For the  $n = 4$  momentum amplituhedron, only the MHV sector exists. We choose the parameterization of  $\mathcal{V}_{n,k}$  in terms of the canonical coordinates on  $G_+(4,2)$  as follows

$$\lambda = \begin{pmatrix} 1 & \alpha_2 + \alpha_4 & \alpha_2\alpha_3 & 0 \\ 0 & 1 & \alpha_3 & \alpha_1 \end{pmatrix}. \quad (8.8)$$

The intersection with winding spaces coming from different ordering yields the positivity conditions sketched in Table 8.1.

	(1234)	(1243)	(1324)	(1342)	(1423)	(1432)
$\langle 12 \rangle = 1$	+	+	+	+	+	+
$\langle 13 \rangle = \alpha_3$	+	+	+	+	+	+
$\langle 14 \rangle = \alpha_1$	+	+	+	+	+	+
$\langle 23 \rangle = \alpha_3\alpha_4$	+	+	-	-	+	-
$\langle 24 \rangle = \alpha_1(\alpha_2 + \alpha_4)$	+	+	+	-	-	-
$\langle 34 \rangle = \alpha_1\alpha_2\alpha_3$	+	-	+	+	-	-

Table 8.1: Positivity conditions coming from  $\mathcal{W}_{4,2}^{(\sigma)}$  for each ordering  $\sigma \in \mathcal{O}_4$ .

As can be seen from Table 8.1, all odd  $\alpha$ 's are positive for all orderings and are thus irrelevant when comparing the different orderings in the same space. We consider all momentum amplituhedra on the subspace parameterized by  $(\alpha_2, \alpha_4)$  defined by taking  $\alpha_1 = \alpha_3 = 1$ . The remaining positivity conditions are sketched in Table 8.2. The positivity conditions of Table 8.2 clearly subdivides the  $\mathbb{R}^2$ -plane into

	(1234)	(1243)	(1324)	(1342)	(1423)	(1432)
$\langle 23 \rangle \sim \alpha_4$	+	+	-	-	+	-
$\langle 24 \rangle \sim \alpha_2 + \alpha_4$	+	+	+	-	-	-
$\langle 34 \rangle \sim \alpha_2$	+	-	+	+	-	-

Table 8.2: Positivity conditions on even  $\alpha$ 's coming from  $\mathcal{W}_{4,2}^{(\sigma)}$  for each ordering  $\sigma \in \mathcal{O}_4$ .

six positive sectors as cones spanning from the shared vertex  $(\alpha_2, \alpha_4) = (0, 0)$ . We draw the cones in Figure 8.1. Before we embark on a discussion of how the KK relations are realized in this space, we note how the permutahedron appears in Figure 8.1. We identify a polytope dual to the fan of positive sectors associated with  $G_+(2,4)$ . This dual polytope is isomorphic to the permutahedron of order 3 and is sketched in Figure 8.2.

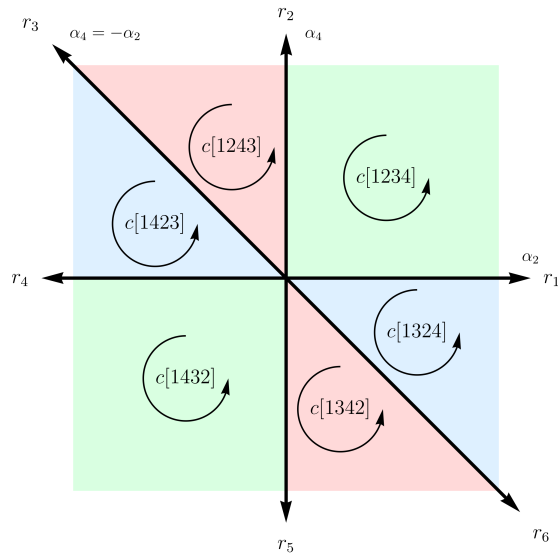


Figure 8.1: Positive sectors corresponding to four-particle MHV amplitudes for each ordering.

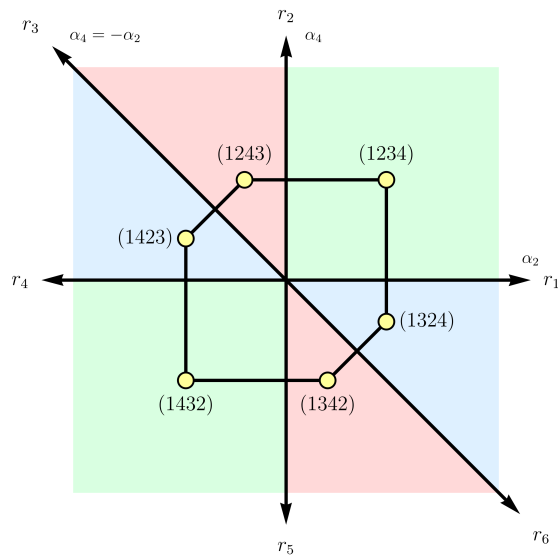


Figure 8.2: The permutahedron of order 3 is dual to the complete fan of positive sectors for the  $n = 4, k = 2$  momentum amplituhedron

From Figure 8.1, the KK relations appear in a clear manner. For instance, the

reflection identities (2.69) for  $n = 4$  can be written as follows

$$A_{4,2}[1, 4, 3, 2] = A_{4,2}[1, 2, 3, 4], \quad (8.9)$$

$$A_{4,2}[1, 4, 2, 3] = A_{4,2}[1, 3, 2, 4], \quad (8.10)$$

$$A_{4,2}[1, 2, 4, 3] = A_{4,2}[1, 3, 4, 2]. \quad (8.11)$$

From Figure 8.1, these identities emerge from the notion that the positive sectors with the same color-ordering define positive geometries with identical canonical differential forms as follows

$$\Omega(c[1432]) = \Omega(c[1234]) = d \log(\alpha_4) \wedge d \log(\alpha_2), \quad (8.12)$$

$$\Omega(c[1423]) = \Omega(c[1324]) = d \log(\alpha_2) \wedge d \log(\alpha_2 + \alpha_4), \quad (8.13)$$

$$\Omega(c[1243]) = \Omega(c[1342]) = d \log(\alpha_2 + \alpha_4) \wedge d \log(\alpha_4). \quad (8.14)$$

Following the discussion of section 4.3, we can identify the cone  $c^-[\sigma]$  with orientation opposite to the cone  $c[\sigma]$ . Then according to the standard operation of reversing the orientation of positive geometries (4.4), we have

$$\Omega(c^-[\sigma]) = -\Omega(c[\sigma]), \quad (8.15)$$

and we identify the oriented sums

$$c[1432] \oplus c^-[1234], \quad (8.16)$$

$$c[1423] \oplus c^-[1324], \quad (8.17)$$

$$c[1243] \oplus c^-[1342], \quad (8.18)$$

all of which have no zero-dimensional boundaries in their boundary stratifications. Therefore the sum of their canonical forms all vanishes as follows

$$0 = \Omega(c[1432]) + \Omega(c^-[1234]) = \Omega(c[1432]) - \Omega(c[1234]), \quad (8.19)$$

$$0 = \Omega(c[1432]) + \Omega(c^-[1324]) = \Omega(c[1432]) - \Omega(c[1324]), \quad (8.20)$$

$$0 = \Omega(c[1243]) + \Omega(c^-[1342]) = \Omega(c[1243]) - \Omega(c[1342]). \quad (8.21)$$

Following the same line of argument about other oriented sums of positive sectors we can generate the remaining KK relations, namely the  $U(1)$  relations. We combine the following positive sectors

$$c[1234] \oplus c[1324] \oplus c[1342], \quad (8.22)$$

with the corresponding geometry sketched in Figure 8.3. The oriented sum of positive sectors sketched in Figure 8.3 has no zero-dimensional boundaries and thus the sums of their canonical forms vanish. On the level of scattering amplitudes, we can translate this to

$$0 = \Omega(c[1234]) + \Omega(c[1324]) + \Omega(c[1342]) \Rightarrow \\ A_{4,2}[1, 2, 3, 4] + A_{4,2}[1, 3, 2, 4] + A_{4,2}[1, 3, 4, 2] = 0, \quad (8.23)$$

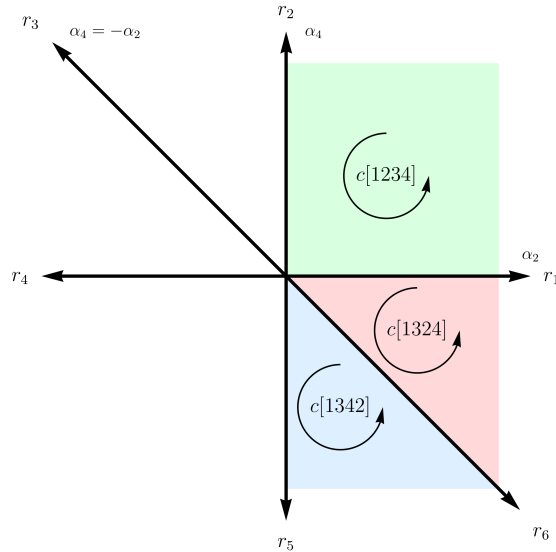


Figure 8.3: The three positive sectors  $c[1234]$ ,  $c[1324]$ ,  $c[1342]$  appearing in the  $U(1)$  decoupling relation (8.23).

which is nothing but one of the  $U(1)$  relations discussed in section 2.4. There are other choices of three sectors that together cancel the shared vertex that is not related to (8.22) through the reflection identity. For instance the geometry

$$c[1324] \oplus c[1234] \oplus c[1243], \quad (8.24)$$

which has been sketched in Figure 8.4, does not have the common vertex as a boundary and thus give rise to the  $U(1)$  identity

$$A_{4,2}[1, 3, 2, 4] + A_{4,2}[1, 2, 3, 4] + A_{4,2}[1, 2, 4, 3] = 0. \quad (8.25)$$

Another choice of three sectors giving rise to a  $U(1)$  relation is sketched on Figure 8.4 and given by

$$c[1234] \oplus c[1324] \oplus c[1243]. \quad (8.26)$$

Again, this geometry has no zero-dimensional boundary and therefore the sum of canonical forms just give rise to the other  $U(1)$  relation of section 2.4, namely

$$0 = \Omega(c[1234]) + \Omega(c[1324]) + \Omega(c[1243]) \Rightarrow \\ A_{4,2}[1, 2, 3, 4] + A_{4,2}[1, 3, 2, 4] + A_{4,2}[1, 2, 4, 3] = 0. \quad (8.27)$$

As a last example for  $n = 4$ , we consider a combination of three positive sectors which only intersect on the vertex, in such a way that it vanishes as a boundary of the full geometry. In Figure 8.5, we see the geometric realization of the  $U(1)$  relation

$$A_{4,2}[1, 2, 3, 4] + A_{4,2}[1, 3, 4, 2] + A_{4,2}[1, 4, 2, 3] = 0, \quad (8.28)$$

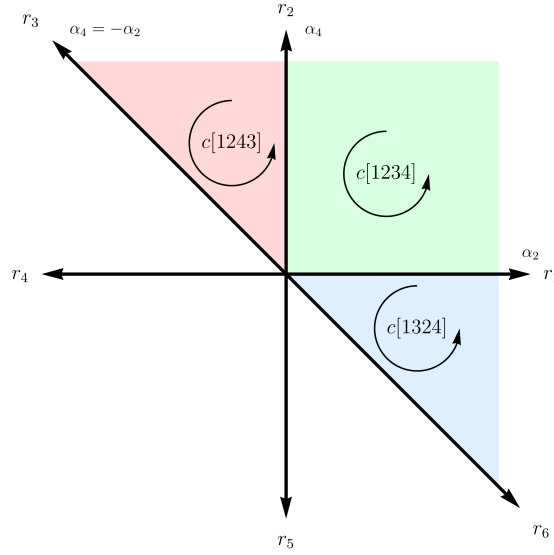


Figure 8.4: The three positive sectors  $c[1234]$ ,  $c[1324]$ ,  $c[1243]$  appearing in the  $U(1)$  decoupling relation (8.27).

as a consequence of the lack of zero dimensional boundaries in the oriented sum

$$c[1234] \oplus c[1342] \oplus c[1423]. \quad (8.29)$$

## Five particle MHV Amplitudes

The construction carries over naturally to the  $n = 5$  MHV sector. We parameterize the affine subspace  $\mathcal{V}_{5,2}$ , by

$$\lambda = \begin{pmatrix} 1 & \alpha_2 + \alpha_4 + \alpha_6 & (\alpha_2 + \alpha_4)\alpha_5 & \alpha_2\alpha_3 & 0 \\ 0 & 1 & \alpha_5 & \alpha_3 & \alpha_1 \end{pmatrix}. \quad (8.30)$$

Having chosen the parameterization of  $\lambda$  to be the canonical coordinates of  $G_+(5, 2)$  along with the cyclic invariance to fix leg 1 in position 1, all winding spaces for all relevant orderings in  $\mathcal{O}_5$  have  $\langle 1i \rangle > 0$ , as can be seen in the table in Appendix E. The remaining positivity conditions can be embedded in  $\mathbb{R}^3$ . As before, each positive sector associated with an ordering  $\sigma \in \mathcal{O}_5$  are cones. Here, it is of course slightly harder to see the cancellation by inspection, since the space is three dimensional. On Figure 8.6 we see how the reflection identity

$$A_{5,2}[1, 2, 3, 4, 5] - A_{5,2}[1, 5, 4, 3, 2] = 0, \quad (8.31)$$

is encoded in the oriented sum of the two geometries

$$c[12345] \oplus c^-[15432], \quad (8.32)$$

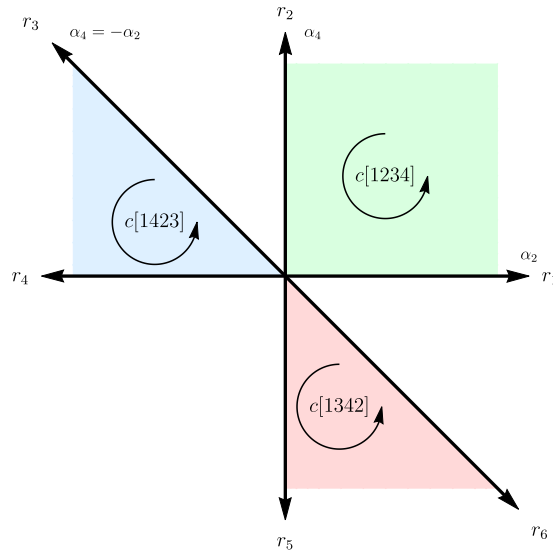


Figure 8.5: The three positive sectors  $c[1234]$ ,  $c[1342]$ ,  $c[1423]$  appearing in the  $U(1)$  decoupling relation (8.27).

which is a geometry lacking a zero-dimensional boundary. The reflection identity can be constructed from (2.72) by taking  $n_\beta = 4$ . Likewise on Figure 8.7 we see how the KK relation

$$A_{5,2}[1, 2, 5, 4, 3] - A_{5,2}[1, 2, 3, 4, 5] + A_{5,2}[1, 3, 2, 4, 5] + A_{5,2}[1, 3, 4, 2, 5] = 0, \quad (8.33)$$

found from (2.72) by setting  $n_\beta = 2$ , is obtained from the oriented sum

$$c^- [12543] \oplus c[12345] \oplus c[13245] \oplus c[13425], \quad (8.34)$$

which, again does not contain a zero-dimensional boundary. Analogously we can write oriented sums for the cases displayed in the figures Figure 8.8 and Figure 8.9, which encode  $U(1)$  decoupling relations found in (2.72) by setting  $n_\beta = 1$ .

As with the four particle case, we obtain a representation of the permutahedron of order 4, as dual to the complete fan of positive sectors of the  $n = 5$ ,  $k = 2$  momentum amplituhedra in Figure 8.10. By considering all combinations of sectors the remaining KK relations can be obtained, but they are slightly harder to see by inspection as we are attempting to sketch three dimensional regions in two dimensions. Due to this fact, and the fact that we cannot extend this analysis to KK relations for the  $n = 6$  momentum amplituhedra since we can not sketch four dimensional geometries, we need consider the geometries and vertex cancellation more abstractly.

### 8.3 Ray-based Homological Algorithm

In this section we develop the machinery to find all KK relations in the MHV sector of the momentum amplituhedron for all  $n$ . This method exploits the simplicial nature

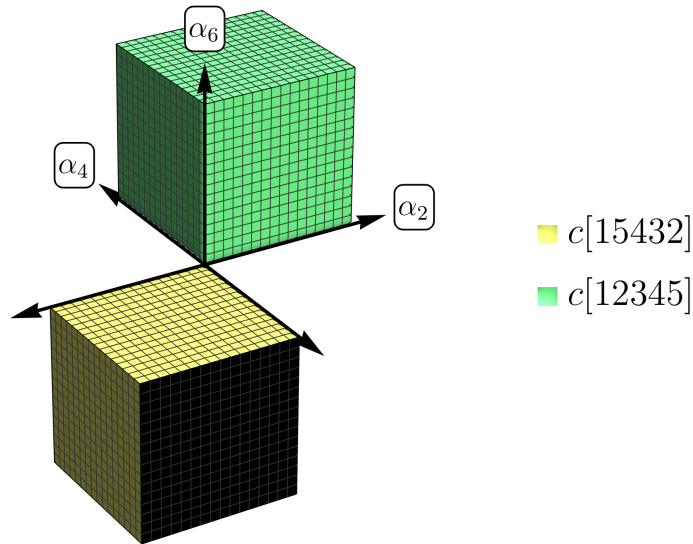


Figure 8.6: The momentum amplituhedron geometry associated with the reflection identity for five particle amplitudes. Here we obtain the geometry associated with the oriented sums of cones  $c[15432] \oplus c^-[12345]$ . Since this geometry do not have the vertex at  $(0, 0, 0)$  as a boundary of the combined geometry, we find the reflection identity  $A_5[12345] = A_5[15432]$ .

of the MHV sector and thus requires further generalization to encompass all helicity sectors. We shall return to this point later, but for now be content with the fact that the KK relations are independent of helicity and if we find the KK relations for one helicity sector, we have found all possible KK relations for the given particle number. The method is based on a generalization of the notions discussed in the previous section and relies on the same cone decomposition. However, the actual identification of regions without vertex-boundaries is generalized in such a way that it does not depend on being represented on two-dimensional paper.

So how did we identify regions that have no vertices as boundaries? In the two-dimensional examples sketched above in Figure 8.3, Figure 8.4, and Figure 8.5, if two or more regions conspire to no longer produce a vertex as a zero-dimensional boundary, that must imply that the one-dimensional dimensional boundaries add together to infinite lines. Since we know that the one-dimensional boundaries of the positive sectors are straight lines, this allows us to identify *pairs of rays pointing in opposite directions*. This will be the fundamental guide pole for deriving an algorithm to find KK relations, in the following.

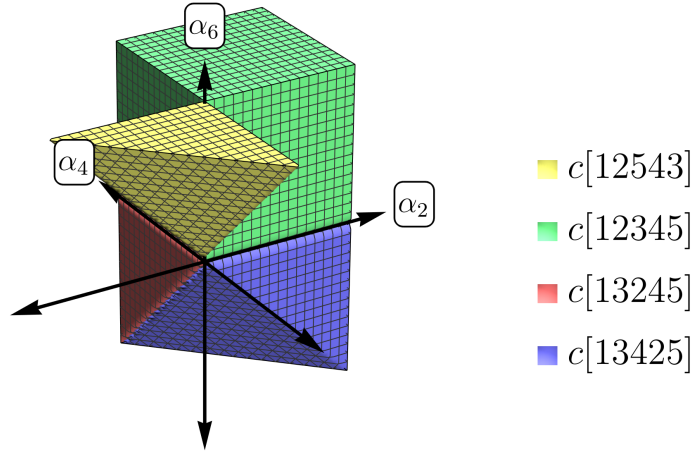


Figure 8.7: The momentum amplituhedron geometry associated with KK relation  $A[12534] = A[12345] + A[13245] + A[13245] + A[13425]$ . This is associated with the oriented sum of cones  $c^{-}[12543] \oplus c[12345] \oplus c[13245] \oplus c[13425]$  which generates a geometry which does not contain any zero-dimensional boundary.

### Rays Pointing in Opposite Directions

As described earlier, the set of  $\binom{n-1}{2}$  co-dimension-one hyperplanes in  $\mathbb{R}^{n-2}$  denoted by  $\mathcal{H}_n$  divides the space into  $(n-1)!$  positive sectors. We enumerate each hyperplane  $\mathcal{H}_n = \{h_i\}_{i=1}^{|\mathcal{H}_n|}$  with  $|\mathcal{H}_n| = \binom{n-1}{2}$ . The intersection of  $(n-3)$  hyperplanes defines lines (some at infinity) and some of these will intersect at the origin. On each of such lines, we define two unit vectors pointing in opposite directions along the line, starting from the origin and refer to these as *rays*. There are exactly  $(2^{n-1} - 2)$  of these rays defined by one-dimensional intersections of  $(n-3)$  hyperplanes, which as we have seen for four and five points, coincides with the number of facets for the  $(n-1)$  permutahedron. We label the set of rays by  $\mathcal{R}_n = \{r_j\}_{j=1}^{|\mathcal{R}_n|}$  with  $|\mathcal{R}_n| = (2^{n-1} - 2)$ . We cast each positive sector associated with an color-ordering  $\sigma$  as the positive span of  $(n-2)$  rays  $\{r_{j_1^\sigma} r_{j_2^\sigma}, \dots, r_{j_{(n-2)}^\sigma}\}$  as follows

$$c[\sigma] = \text{span}_{\mathbb{R}_{\geq 0}} \{r_{j_1^\sigma} r_{j_2^\sigma}, \dots, r_{j_{(n-2)}^\sigma}\}. \quad (8.35)$$

We are interested in defining a homological algorithm to find all KK relations, meaning that we should define proper homological operators and define our object by way of differential forms<sup>1</sup>. To this end, we associate a formal one-form to each ray,

<sup>1</sup>We stress that in the following, any differential forms associated to positive sectors are not the

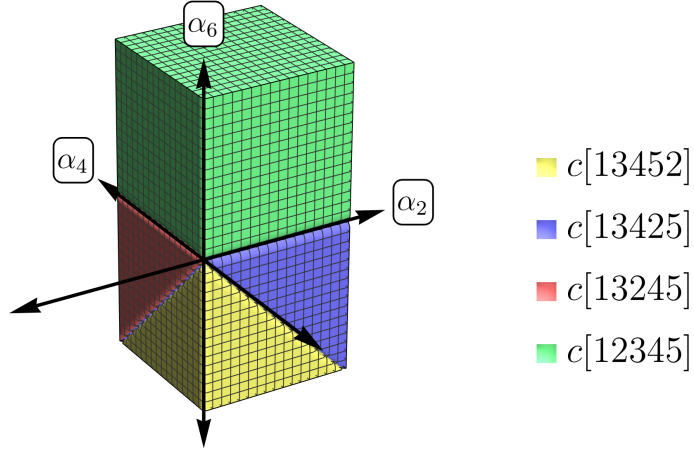


Figure 8.8: The momentum amplituhedron geometry associated with the  $U(1)$  decoupling identity  $A[13452] = -A[13425] - A[13245] - A[12345]$ . This is associated with the oriented sum of cones  $c[13425] \oplus c[13425] \oplus c[13245] \oplus c[12345]$  which generates a geometry which does not contain any zero-dimensional boundary

denoted *ray 1-forms*,  $\tilde{r}_i^\sigma$ , and a formal  $(n-2)$ -form to each positive sector as a wedge product of ray 1-forms. In particular, to each cone  $c[\sigma]$  we associate a formal  $(n-2)$  form as follows

$$\omega(c[\sigma]) = \frac{\det(r_{j_1^\sigma} r_{j_2^\sigma} \dots r_{j_{(n-2)}^\sigma})}{|\det(r_{j_1^\sigma} r_{j_2^\sigma} \dots r_{j_{(n-2)}^\sigma)|} \tilde{r}_{j_1^\sigma} \wedge \tilde{r}_{j_2^\sigma} \wedge \dots \wedge \tilde{r}_{j_{(n-2)}^\sigma}, \quad (8.36)$$

where  $\det(r_{j_1^\sigma} r_{j_2^\sigma} \dots r_{j_{(n-2)}^\sigma})$  is the determinant of the  $(n-2) \times (n-2)$  matrix constructed from the rays  $r_{j_1^\sigma} r_{j_2^\sigma} \dots r_{j_{(n-2)}^\sigma}$ . We refer to such forms, constructed from wedge products of ray 1-forms collectively as *ray  $p$ -forms*. Since a ray  $p$ -form is invariant under relabeling and rescaling of the rays in  $\mathcal{R}_n$ , it is manifestly well-defined. The next step requires the definition of a *boundary operator* with respect to each hyperplane  $h \in \mathcal{H}_n$ , which we will denote as  $\partial_h$ , acting recursively on ray  $p$ -forms as follows: for  $p = 1$ , we have

$$\partial_h \tilde{r} = \bar{\Theta}_h(r) \equiv \begin{cases} 0, & \text{if } r \in h \\ 1, & \text{else} \end{cases}, \quad (8.37)$$

where by  $r \in h$  we mean that  $r$  is contained in the hyperplane  $h$ , while if  $p > 1$ , we canonical forms of the momentum amplituhedra themselves.

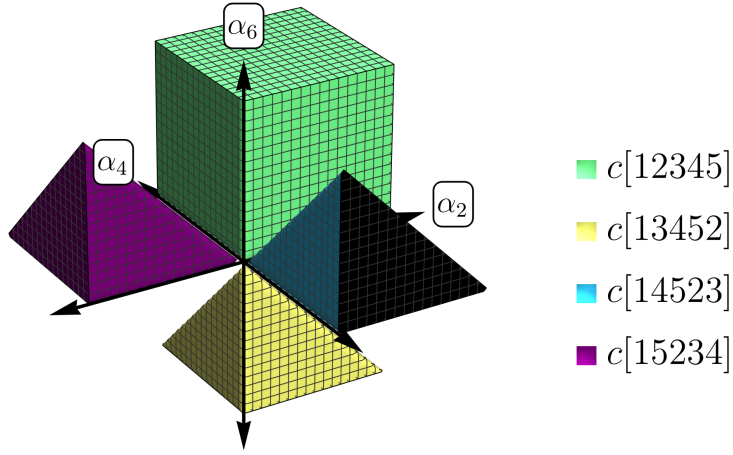


Figure 8.9: The momentum amplituhedron geometry associated with the  $U(1)$  decoupling identity  $A[12345] = -A[13452] - A[14523] - A[15234]$ . This is associated with the oriented sum of cones  $c[12345] \oplus c[13452] \oplus c[14523] \oplus c[15234]$  which generates a geometry which does not contain any zero-dimensional boundary

define the action of the boundary operator on a ray  $p$ -form as follows

$$\begin{aligned} \partial_h \left( \tilde{r}_{j_1}^\sigma \wedge \tilde{r}_{j_2}^\sigma \wedge \dots \wedge \tilde{r}_{j_{(n-2)}}^\sigma \right) &= \bar{\Theta}_h(r_{j_1}) \Theta_h(r_{j_2}, \dots, r_{j_p}) \tilde{r}_{j_2}^\sigma \wedge \dots \wedge \tilde{r}_{j_{(n-2)}}^\sigma \\ &\quad - \Theta_h(r_{j_1}) \tilde{r}_{j_1} \wedge \partial_h \left( \tilde{r}_{j_2}^\sigma \wedge \dots \wedge \tilde{r}_{j_{(n-2)}}^\sigma \right), \end{aligned} \quad (8.38)$$

where

$$\Theta_h(r_{j_2}, \dots, r_{j_p}) \equiv \Theta_h(r_{j_2}) \dots \Theta_h(r_{j_p}) \quad (8.39)$$

and

$$\Theta_h(r_j) \equiv 1 - \bar{\Theta}_h(r_j). \quad (8.40)$$

This boundary operator is manifestly nilpotent, that is  $\partial_h^2 = 0$ . This can be seen by applying the operator to any hyperplane  $h \in \mathcal{H}_n$  twice and notice the result is proportional to  $\bar{\Theta}_h(r) \Theta_h(r) = 0$ , for all rays  $r \in \mathcal{R}_n$ . Next we define a graded vector space combining all ray- $p$ -forms for positive sectors and their boundaries as follows

$$V_n \equiv \bigoplus_{i=0}^{n-2} V_n^{(i)}, \quad (8.41)$$

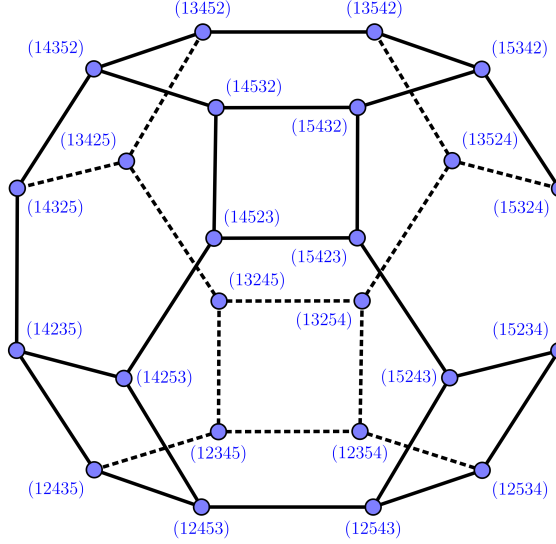


Figure 8.10: The permutahedron of order 4 is dual to the complete fan of positive sectors for the  $n = 5$ ,  $k = 2$  momentum amplituhedron

where

$$V_n^{(0)} \equiv \text{span}_{\mathbb{Z}}\{\omega(c[\sigma]) : \sigma \in \mathcal{O}_n\}, \quad (8.42)$$

is the vector space containing integer linear combinations of the ray  $(n - 2)$ -forms associated with each cone  $c[\sigma]$ . The remaining vector spaces are defined as follows

$$V_n^{(i)} \equiv \text{span}_{\mathbb{Z}} \left\{ \bigwedge_{j \in J} \tilde{r}_j : J \in \binom{[\![\mathcal{R}_n]\!] }{n - 2 - i} \right\}, \quad (8.43)$$

that is, the vector space,  $V_n^{(i)}$  denotes the space of integer linear combinations of all possible ray forms of degree  $(n - 2 - i)$ . Here by  $\binom{[\![\mathcal{R}_n]\!] }{n - 2 - i}$  we mean the collection of  $(n - 2 - i)$  element subsets of  $[\![\mathcal{R}_n]\!] \equiv \{1, 2, \dots, |\mathcal{R}_n|\}$ . Of course, with this definition the maximal vector space, that is  $V_n^{(n-2)}$ , is just the space of integers. For any hyperplane  $h \in \mathcal{H}_n$ , we can write the exact sequence:

$$V_n^{(0)} \xrightarrow{\partial_h} V_n^{(1)} \xrightarrow{\partial_h} \dots \xrightarrow{\partial_h} V_n^{(n-3)} \xrightarrow{\partial_h} V_n^{(n-2)} = \mathbb{Z} \xrightarrow{\partial_h} 0. \quad (8.44)$$

So what is all this machinery for? Clearly we can encode the formal ray  $p$ -forms associated to all positive sectors and their boundaries in the graded vector space, and the boundary operator naturally takes us from a vector space to a lower vector space. A KK relation can then be understood as a *vector*  $\nu \in V_n^{(0)}$ , the vector space of full cones in  $\mathbb{R}^{n-2}$ , such that for every  $(n - 2)$  element subset  $I$  of  $[\![\mathcal{H}_n]\!] = \{1, 2, \dots, |\mathcal{H}_n|\}$ , i.e.  $I \in \binom{[\![\mathcal{H}_n]\!] }{n-2}$ , we have that

$$\left( \prod_{i \in I} \partial_{h_i} \right) \nu = 0. \quad (8.45)$$

This is exactly the statement that the geometry corresponding to  $\nu$  has no boundary of dimension 0 at the origin of  $\mathbb{R}^{n-2}$ . The matter of finding such a vector can be cast as a simple linear algebra problem as follows. Consider the  $\binom{|\mathcal{H}_n|}{n-2} \times (n-2)!$  matrix  $M_n$  obtained by applying all combinations of boundary operators labeled by  $(n-2)$  element subsets of  $I$  of  $[\mathcal{H}_n]$  on each ray  $(n-2)$ -form associated with each positive sector with ordering  $\sigma \in \mathcal{O}_n$  as follows

$$(M_n)_\sigma^I = \left( \prod_{i \in I} \partial_{h_i} \right) \omega(c[\sigma]). \quad (8.46)$$

This *boundary matrix* is a map  $M_n : V_n^{(0)} \rightarrow V_n^{(n-2)}$  and its kernel is simply the list of all combinations of positive sectors that conspire to not have a boundary at the origin of  $\mathbb{R}^{n-2}$ , thus encoding the KK relations. We will illustrate this construction by considering a few examples at low  $n$ , but the construction completely generalizes to all  $n$  [41].

### Four-particle MHV Amplitudes

Taking as a starting point the cone decomposition of the momentum amplituhedra discussed in section 8.3, we identify the three hyperplanes intersecting the origin of  $\mathbb{R}^2$  as follows

$$h_1 : \alpha_4 = 0, \quad h_2 : \alpha_2 + \alpha_4 = 0, \quad h_3 : \alpha_2 = 0. \quad (8.47)$$

Along these hyperplanes we define six rays pointing in opposite directions

$$r_1 = (1, 0) = -r_4, \quad r_2 = (0, 1) = -r_5, \quad r_3 = \frac{1}{\sqrt{2}}(-1, 1) = -r_6. \quad (8.48)$$

These rays correspond to those drawn in Figure 8.1. Using the definition in (8.36), the ray forms for each positive sector are simply

$$\begin{aligned} \omega(c[1234]) &= \tilde{r}_1 \wedge \tilde{r}_2, & \omega(c[1243]) &= \tilde{r}_2 \wedge \tilde{r}_3, \\ \omega(c[1423]) &= \tilde{r}_3 \wedge \tilde{r}_4, & \omega(c[1432]) &= \tilde{r}_4 \wedge \tilde{r}_5, \\ \omega(c[1342]) &= \tilde{r}_5 \wedge \tilde{r}_6, & \omega(c[1324]) &= \tilde{r}_6 \wedge \tilde{r}_1. \end{aligned} \quad (8.49)$$

Using the labels from (8.47), we obtain the boundary matrix by continually applying the boundary operator (8.38) associated with each hyperplane labels to get

$$M_4 = \begin{array}{c} \{1, 2\} \\ \{1, 3\} \\ \{2, 3\} \end{array} \begin{array}{cccccc} (1234) & (1243) & (1324) & (1342) & (1423) & (1432) \\ \left( \begin{array}{cccccc} 0 & 1 & -1 & 1 & -1 & 0 \\ 1 & -1 & 0 & -1 & 0 & 1 \\ 1 & -1 & 0 & -1 & 0 & 1 \end{array} \right) \begin{array}{c} \partial_{h_1} \partial_{h_2} \\ \partial_{h_1} \partial_{h_3} \\ \partial_{h_2} \partial_{h_3} \end{array} \\ \tilde{r}_1 \wedge \tilde{r}_2 & \tilde{r}_2 \wedge \tilde{r}_3 & \tilde{r}_6 \wedge \tilde{r}_1 & \tilde{r}_5 \wedge \tilde{r}_6 & \tilde{r}_3 \wedge \tilde{r}_4 & \tilde{r}_4 \wedge \tilde{r}_5 \end{array} \cdot \quad (8.50)$$

We can obtain the kernel of this matrix by applying the Mathematica<sup>TM</sup> function `NullSpace` on the matrix, yielding the following set of null-vectors

$$\ker M_4 = \begin{pmatrix} -1 & 0 & 0 & 0 & 0 & 1 \\ 0 & 0 & -1 & 0 & 1 & 0 \\ 1 & 0 & 1 & 1 & 0 & 0 \\ 1 & 1 & 1 & 0 & 0 & 0 \end{pmatrix}. \quad (8.51)$$

The standard KK relations for  $n = 4$  are then obtained by multiplying

$$\ker M_4 \cdot A_4[\sigma] = 0, \quad (8.52)$$

leading to the relations

$$-A_{4,2}[1, 2, 3, 4] + A_{4,2}[1, 4, 3, 2] = 0, \quad (8.53)$$

$$-A_{4,2}[1, 3, 2, 4] + A_{4,2}[1, 3, 2, 4] = 0, \quad (8.54)$$

$$A_{4,2}[1, 2, 3, 4] + A_{4,2}[1, 3, 2, 4] + A_{4,2}[1, 3, 4, 2] = 0, \quad (8.55)$$

$$A_{4,2}[1, 2, 3, 4] + A_{4,2}[1, 2, 4, 3] + A_{4,2}[1, 3, 2, 4] = 0. \quad (8.56)$$

These relations are identical to the ones in (2.72) and found in section 8.2.

The approach described in this section was employed to find all the KK relations for  $n \leq 7$  in the MHV sector, and since the KK relations are identical for all  $k$ -sectors, we have effectively found all KK relations for all  $n \leq 7$ . We expect the algorithm to be valid for all  $n$ . The geometric interpretation is not applicable when discussing higher  $k$  sectors, however. This is because the momentum amplituhedron is a Grassmannian geometry and have boundaries that are “curvy” and no longer linear inequalities like in (8.47). This means that the higher  $k$  sectors can no longer be decomposed into simple, simplicial regions. Therefore more sophisticated machinery needs to be introduced in order to perform a similar analysis beyond the MHV sector. We will return to this point after a brief discussion on how the construction above works for the kinematic associahedron, discussed in chapter 5.

## 8.4 Kleiss-Kuijf Relations for the Kinematic Associahedron

We wish to reemploy the homological algorithm of the previous section to find KK relations for bi-adjoint  $\phi^3$  theory. That is, identify KK relations as oriented sums of kinematic associahedra with no vertices in their boundary stratification. The kinematic associahedron for arbitrary orderings is defined in section 5.5 and upon inspection of Figure 5.4 and Figure 5.5 we observe that the kinematic associahedra generally have several vertices in their boundary stratification. This requires us to

ensure cancellation around *each* vertex. This might appear different from the momentum amplituhedron case, but we remind the reader that the MHV momentum amplituhedron has  $\binom{n}{2} = \frac{n(n-1)}{2}$  vertices in its boundary stratification, which are shared among all orderings  $\sigma \in \mathcal{O}_n$  and the momentum amplituhedron for a given ordering around a single vertex is isomorphic to the momentum amplituhedron for another ordering around a different vertex [41]. Therefore, if we ensure vertex cancellation for one combination of orderings, all vertices are removed from the boundary stratification due to the isomorphism of the differently ordered momentum amplituhedra. Similarly for the kinematic associahedron, we zoom in on the neighborhood of a single vertex  $v \in \mathcal{V}_n$  of the kinematic associahedron and reproduce the homological algorithm above. Here every kinematic associahedron appears as a  $(n-3)$ -dimensional simplicial cone spanned by  $(n-3)$  rays. We apply the algorithm described in the previous section by zooming in on each vertex individually and find a boundary matrix corresponding to cancellation around said matrix, then we assemble each boundary matrix into a single common boundary matrix whose kernel exposes KK relations for the kinematic associahedron.

A single cone corresponding to a kinematic associahedron with a given ordering in the neighborhood of a single vertex  $v$  is denoted by

$$c^{(v)}[\beta] = \begin{cases} v + \text{span}_{\mathbb{R}_{\geq 0}} \left\{ r_{j_1^\beta}^v r_{j_2^\beta}^v \dots r_{j_{n-3}^\beta}^v \right\}, & \text{if } v \in \mathcal{A}_n(\beta), \\ 0, & \text{otherwise} \end{cases}, \quad (8.57)$$

where  $r_{j_i^\beta}^v$  are rays. As for the momentum amplituhedron case, we associate a ray  $(n-3)$ -form to each cone around the vertex  $v$  as follows

$$\omega(c^{(v)}[\beta]) = (-1)^{n_{\text{flip}}(\beta)} \frac{\det \begin{pmatrix} r_{j_1^\beta}^v & r_{j_2^\beta}^v & \dots & r_{j_{n-3}^\beta}^v \end{pmatrix}}{\left| \det \begin{pmatrix} r_{j_1^\beta}^v & r_{j_2^\beta}^v & \dots & r_{j_{n-3}^\beta}^v \end{pmatrix} \right|} \tilde{r}_{j_1^\beta}^v \wedge \tilde{r}_{j_2^\beta}^v \wedge \dots \wedge \tilde{r}_{j_{n-2}^\beta}^v. \quad (8.58)$$

We set  $\omega(c^{(v)}[\beta]) = 0$  if  $v \notin \mathcal{A}[\beta]$  and define the boundary operators in complete analogy with (8.3) and we then construct the boundary matrices. The KK relations appear as the common null space of all the boundary matrices associated with each vertex. We shall in the following give examples for  $n = 4$  and  $n = 5$  kinematic associahedra. We notice that there are exactly  $p_n - |\mathcal{V}_n|$  independent KK relations, with  $p_n$  is the number of non-empty positive regions of kinematic associahedra and  $|\mathcal{V}_n|$  is the combined number of vertices for all kinematic associahedra orderings which coincides with  $C_{n-2}$ , the  $(n-2)^{\text{nd}}$  Catalan number [81].

## Four Particle Amplitudes

For  $n = 4$  there are exactly six non-empty positive regions labeled by  $\beta \in \mathcal{O}_4$ . We remind ourselves that the positive regions admit reflection symmetry

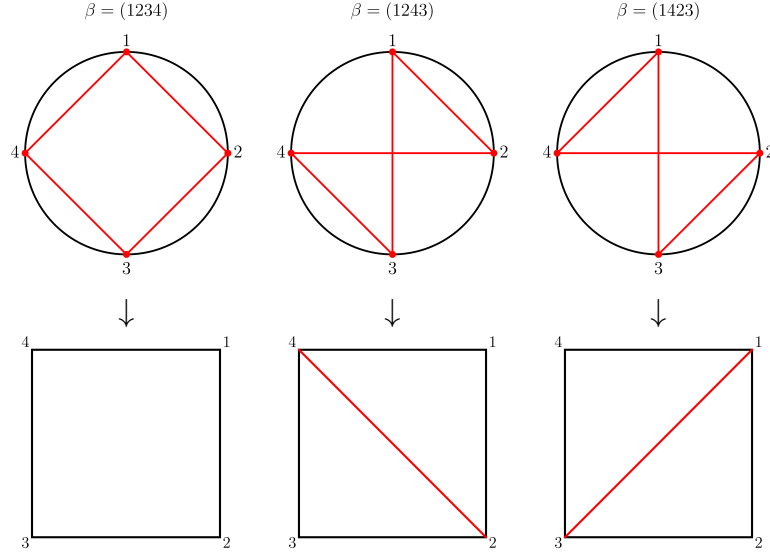


Figure 8.11: Partial triangulations in the definition of positive regions  $\Delta_4(\beta)$ . The regions give rise to the positive regions in (8.63)

$\Delta_n(\beta) = \Delta_n(\beta^{-1})$ , therefore we only get three distinct positive regions  $\Delta_4(1234) = \Delta_4(1432)$ ,  $\Delta_4(1243) = \Delta_4(1432)$ , and  $\Delta_4(1423) = \Delta_4(1324)$ . Using the definition of  $\Delta_n(\beta)$  in section 5.5, we express the regions as follows

$$\Delta_4(1234) = \{X_{13} \geq 0, X_{24} \geq 0\}, \quad (8.59)$$

$$\Delta_4(1243) = \{X_{13} \geq 0\}, \quad (8.60)$$

$$\Delta_4(1423) = \{X_{24} \geq 0\}. \quad (8.61)$$

These regions can be determined from the partial triangulation of the square, as can be seen in Figure 8.11. The two-dimensional space of constraints  $H_4$ , defined in (5.11) is the same for all orderings and is found to be

$$H_4 = \{(X_{13}, X_{24}) : X_{24} = c_{13} - X_{13}\}, \quad (8.62)$$

using the label  $H_n$  for the space of constraints for the kinematic associahedron to avoid confusion with  $\mathcal{H}_n$ , the collection of hyperplanes for a given positive sector. The intersection of the positive regions with the space of constraints simply yields the kinematic associahedra for each ordering  $\sigma$  as follows

$$\mathcal{A}_4[1234] = [0, c_{13}], \quad \mathcal{A}_4[1243] = [0, +\infty), \quad \mathcal{A}_4[1423] = (-\infty, c_{13}]. \quad (8.63)$$

The space of kinematic associahedra has two vertices,  $v_1 = (0)$  and  $v_2 = (c_{13})$ , which we organize in  $\mathcal{V}_4 = \{v_1, v_2\}$ . The kinematic associahedra for different orderings are then understood as lines, that is one-dimensional cones, emanating from each vertex and we organize the kinematic associahedra in Table 8.3. Here we take  $r^{v_1} = (1)$  and

$\beta$	$\mathcal{A}_4(\beta)$	around $v_1 = (0)$	around $v_2 = (c_{13})$
(1234)	$[0, c_{13}]$	$v_1 + \text{span}_{\mathbb{R}_{>0}}\{r^{v_1}\}$	$v_2 + \text{span}_{\mathbb{R}_{>0}}\{r^{v_2}\}$
(1243)	$[0, +\infty)$	$v_1 + \text{span}_{\mathbb{R}_{>0}}\{r^{v_1}\}$	$\emptyset$
(1423)	$(-\infty, c_{13}]$	$\emptyset$	$v_2 + \text{span}_{\mathbb{R}_{\geq 0}}\{r^{v_2}\}$

Table 8.3: Associahedra for  $n = 4$  in the neighbourhood of each vertex in  $\mathcal{V}_4$  as one-dimensional cones.

$\beta$	$\mathcal{A}_4(\beta)$	around $v_1 = (0)$	around $v_2 = (c_{13})$
(1234)	$[0, c_{13}]$	$\tilde{r}^{v_1}$	$-\tilde{r}^{v_2}$
(1243)	$[0, +\infty)$	$-\tilde{r}^{v_1}$	$0$
(1423)	$(-\infty, c_{13}]$	$0$	$\tilde{r}^{v_2}$

Table 8.4: Ray one-forms describing associahedra for  $n = 4$  in the neighbourhood of each vertex in  $\mathcal{V}_4$ .

$r^{v_2} = (-1)$ . We then associate a ray 1-form to each associahedra as given in Table 8.4. We obtain a boundary matrix for each vertex, namely

$$M_4^{(v_1)} = (1 \quad -1 \quad 0), \quad M_4^{(v_2)} = (-1 \quad 0 \quad 1). \quad (8.64)$$

We stack these matrices into  $M_4 = \begin{pmatrix} M_4^{(v_1)} & M_4^{(v_2)} \end{pmatrix}$ , the common space of null vectors spans

$$\ker M_4 = (1 \quad 1 \quad 1), \quad (8.65)$$

implying that the kinematic associahedron forms obey

$$\omega_4^{(1234)} + \omega_4^{(1243)} + \omega_4^{(1423)} = 0, \quad (8.66)$$

from which we extract the KK relation

$$m_4(1, 2, 3, 4) + m_4(1, 2, 4, 3) + m_4(1, 4, 2, 3) = 0. \quad (8.67)$$

We can visualize the relation (8.66) as in Figure 8.12 where the kinematic associahedra combines into a single, infinite line void of any vertices, and therefore encoding the KK relations.

## Five Particle Amplitudes

For  $n = 5$  we encounter two permutations  $\beta \in \mathcal{O}_n$  associated with empty positive regions, namely  $\Delta_5(13524) = \Delta_5(14253) = \emptyset$ . Therefore we count  $p_5 = 4! - 2 = 22$  non-trivial permutations and under the cyclic invariance we are left with 11 distinct

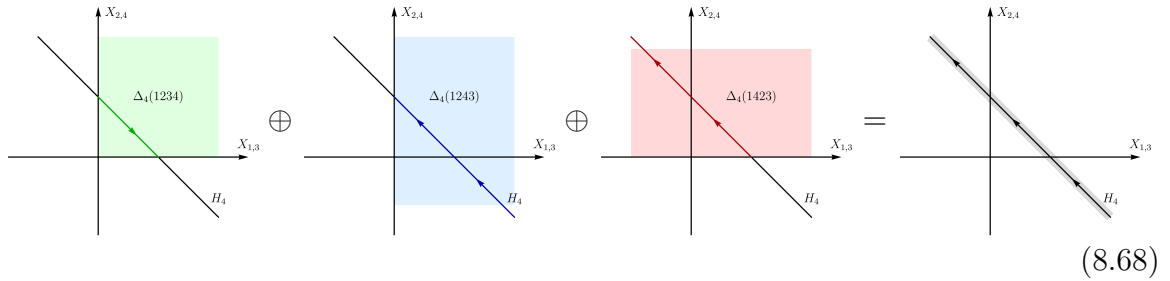


Figure 8.12: Oriented sum of three associahedra for  $n = 4$  producing an infinite line. We note that we fix the affine subspace  $X_{13} + X_{24} = c$  and intersect with different positive regions.

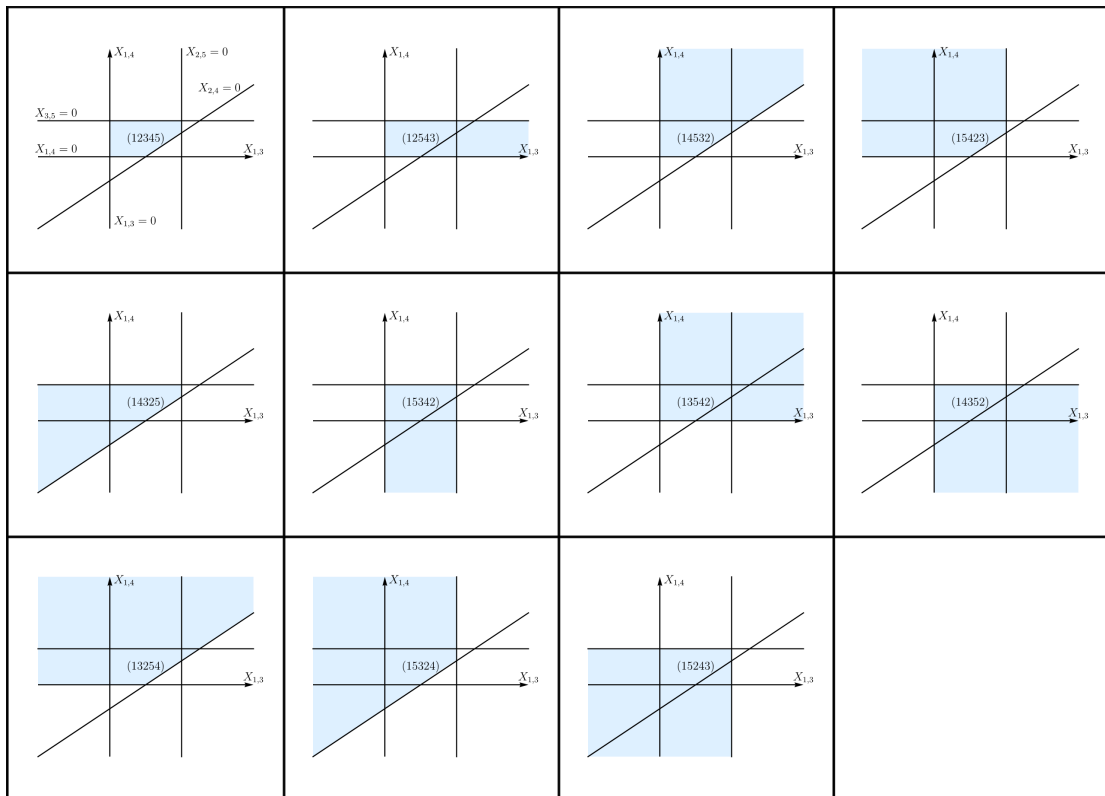


Figure 8.13: Kinematic associahedra for  $n = 5$ . The depicted geometries are all oriented counter-clockwise.

kinematic associahedra. The 11 positive sectors are sketched on Figure 8.13. As described in section 5.3 the standard ordered kinematic amplituhedron for  $n = 5$  is a pentagon. The five vertices are common to all positive sectors and found in  $(X_{13}, X_{14})$  coordinates to be

$$v_1 = (0, 0), \quad v_2 = (c_{13}, 0), \quad v_3 = (c_{13} + c_{14}, c_{14}), \quad (8.69)$$

$$v_4 = (c_{13} + c_{14}, c_{13} + c_{24}), \quad v_5 = (0, c_{14} + c_{24}), \quad (8.70)$$

which we organize into  $\mathcal{V}_5 = \{v_1, v_2, v_3, v_4, v_5\}$ . From the definition of the affine subspace, we identify the five hyperplanes (lines) by

$$\underbrace{X_{1,3} = 0}_{h_1}, \quad \underbrace{X_{1,4} = 0}_{h_2}, \quad \underbrace{X_{1,3} - c_{13} - c_{14} = 0}_{h_3}, \quad \underbrace{X_{1,4} - c_{14} - c_{24} = 0}_{h_4}, \quad \underbrace{X_{1,3} - X_{1,4} - c_{13} = 0}_{h_5}, \quad (8.71)$$

and organize them into  $\mathcal{H}_n = \{h_1, h_2, h_3, h_4\}$ . Around each vertex  $v \in \mathcal{V}_5$  we identify each positive region as: a) a two-dimensional cone spanning two rays pointing along the hyperplanes, if the region encompasses the vertex, or b) as the empty region otherwise. We can associate a ray 2-form to each positive region  $\omega(c^v[\beta])$  and define a boundary matrix using the boundary operator (8.38) for each vertex,  $M_5^{(v)}$ . Each boundary matrix  $M_5^{(v)}$  has size  $\binom{\mathcal{H}_5}{2} \times \frac{p_5}{2} = 10 \times 11$ . In order to find the common kernel, we stack the matrices as

$$M_5 = \left( M_5^{(v_1)}, M_5^{(v_2)}, M_5^{(v_3)}, M_5^{(v_4)}, M_5^{(v_5)} \right), \quad (8.72)$$

the kernel of which is six dimensional and gives rise to the following relations

$$\begin{aligned} \omega_5^{(12345)} + \omega_5^{(12354)} + \omega_5^{(12435)} + \omega_5^{(14235)} &= 0, \\ \omega_5^{(12345)} + \omega_5^{(12435)} + \omega_5^{(12453)} + \omega_5^{(13245)} &= 0, \\ \omega_5^{(12345)} + \omega_5^{(13245)} + \omega_5^{(13425)} + \omega_5^{(13452)} &= 0, \\ \omega_5^{(13425)} + \omega_5^{(14235)} + \omega_5^{(14325)} &= 0, \\ \omega_5^{(12435)} - \omega_5^{(13425)} + \omega_5^{(14352)} &= 0, \\ \omega_5^{(13245)} + \omega_5^{(13254)} - \omega_5^{(14235)} &= 0, \end{aligned} \quad (8.73)$$

for a certain choice of 11 basis orderings in  $\mathcal{O}_5$  labeling the distinct positive regions. The relations (8.73) together with the reflection identities gives rise to  $6 + 11 = 17$  distinct KK relations between canonical forms  $\omega_5^{(\beta)}$  and therefore also between the partial amplitudes  $m_5(\beta)$ . We illustrate one of these relations in Figure 8.14 where we take the oriented sum of the regions, which conspire to cancel all the zero-dimensional boundaries and therefore the sum of canonical forms vanish.

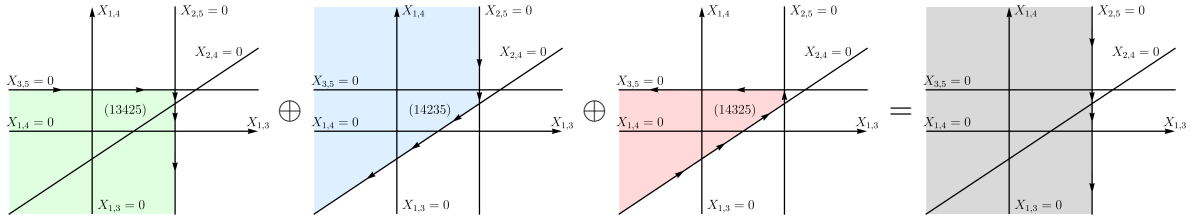


Figure 8.14: Oriented sum of three associahedra for  $n = 5$  giving rise to the KK relation  $\omega_5^{(13425)} + \omega_5^{(14235)} + \omega_5^{(14325)} = 0$ .

## 8.5 Poset-based Homological Algorithm

In section 8.2 we considered the geometric origins of the KK relations for the MHV momentum amplituhedron through its polytopal realization in terms of simplicial cones. There, we saw how certain positive sectors share boundaries which cancel in the boundary stratification of their oriented sum. While the positive sectors are not equivalent to the momentum amplituhedra geometries *per se*, they encode which momentum amplituhedra share boundaries. Exploiting this construction, we presented a homological algorithm to find KK relations for momentum amplituhedra in section 8.3 and kinematic associahedra in section 8.4.

When moving beyond the MHV sector, we find that this approach is limited by the fact that we cannot reduce the space of canonical coordinates,  $\{\alpha_i\}$  parameterizing the  $\lambda$  matrix by identifying a subset of sign-flip conditions respected by all color orderings. Furthermore, the inequalities coming from the sign-flip conditions – and therefore the boundaries of the momentum amplituhedra – are no longer linear: for  $2 < k < n - 2$ , momentum conservation between  $\lambda$  and  $\tilde{\lambda}$  produces rational inequalities for the canonical coordinates coming from the sign-flips. These complicated *curvy* boundaries in the neighborhood of each vertex makes the conical description unfeasible beyond the MHV sector. Fortunately, the conical description is not essential for the construction and upon introducing some more complicated machinery, we can derive KK relations from a strictly homological perspective for all  $k$  sectors. Indeed the only information the cones provided us in section 8.3 was

- which rays are shared by different color orderings
- which pairs of rays live in the same one-dimensional intersection of hyperplanes.

Using these two pieces of information, we can identify combinations of positive sectors containing rays pointing in opposite directions, therefore removing the common vertex from which the rays are emitted.

In the following, we abstract the derivation of KK relations for the  $k = 2$  sector: we will employ the *partially ordered set* as the positive sectors, which can in principle be

applied to any helicity sector. The construction will be parameterization independent as it takes as input the combinatorial structure of the boundaries of the momentum amplituhedra discussed in section 6.3 and found using the Mathematica<sup>TM</sup> package `amplituhedronBoundaries` [88]. The algorithm will first be considered for the positive sectors of the  $n = 4$ ,  $k = 2$  momentum amplituhedron and subsequently we proceed with a discussion on how to generalize to full momentum amplituhedron geometries for higher  $n$  and  $k$  sectors.

### 8.5.1 Revisiting MHV amplitudes

As described in section 8.3,  $\mathcal{O}_4$  is the set of four tuples describing the  $3! = 6$  different four-particles orderings. For each ordering  $\sigma \in \mathcal{O}_4$ , we associate a simplicial cone  $c[\sigma]$  in  $\mathbb{R}^2$  parameterized by  $(\alpha_2, \alpha_4)$  associated with the momentum amplituhedron for the given ordering. These regions are shown in Figure 8.1 and each cone has two one-dimensional boundaries which are semi-infinite lines spanned by rays and a single zero-dimensional boundary, the vertex  $v$  at the origin. We label the six rays as in section 8.3 by  $r_i$  for  $i = 1, \dots, 6$ . We collect all these structures into a set  $\mathcal{P}^{(\sigma)}$  containing the geometry itself along with all of its boundaries, e.g. for the standard ordering we have

$$\mathcal{P}^{(1234)} = \{c[1234], r_1, r_2, v\}. \quad (8.74)$$

This set admits a *partial ordering*, where the first element is 2 dimensional, the next two elements  $r_i$  are 1 dimensional and the last element  $v$  is 0 dimensional. We refer to  $\mathcal{P}^{(\sigma)}$  as a partial-ordered set or *poset*. Here *partial order*, denoted by  $\preceq$  is defined for any two boundaries<sup>2</sup>  $\mathcal{B}_1, \mathcal{B}_2 \in \mathcal{P}^{(\sigma)}$  such that

$$\mathcal{B}_1 \preceq \mathcal{B}_2 \text{ if } \mathcal{B}_1 = \mathcal{B}_2 \text{ or } \mathcal{B}_1 \text{ is a boundary (of any co-dimension) of } \mathcal{B}_2. \quad (8.75)$$

If  $\mathcal{B}_1 \preceq \mathcal{B}_2$  and if  $\mathcal{B}_1 \neq \mathcal{B}_2$  we write  $\mathcal{B}_1 \prec \mathcal{B}_2$ . Since each boundary  $\mathcal{B} \in \mathcal{P}^{(\sigma)}$  has a well-defined dimension,  $\mathcal{P}^{(\sigma)}$  is a graded poset.

This organization of geometries and their boundaries into a poset can be done for any positive geometry as follows. Consider a positive geometry  $(X, X_{\geq 0})$  and let  $\mathcal{P}[X_{\geq 0}]$  be the set consisting of  $X_{\geq 0}$  and its boundaries of all codimension. We refer to this graded poset as the *boundary stratification* of  $X_{\geq 0}$ . We will use shorthand  $\mathcal{P} = \mathcal{P}[X_{\geq 0}]$  for brevity in the following. We can encode the combinatorial relationship between boundaries in  $\mathcal{P}$  in *Hasse diagrams*. Hasse diagrams are graphs of nodes and edges, where each node refer to an element in  $\mathcal{P}$  and two nodes are connected by a directed edge if one node represents a boundary of the other node. Specifically, if  $\mathcal{B}_1$  is a codimension-1 boundary of  $\mathcal{B}_2$ , we draw a directed edge  $e = (\mathcal{B}_1, \mathcal{B}_2)$  from  $\mathcal{B}_2$  to  $\mathcal{B}_1$ . Here we refer to  $\mathcal{B}_2$  as the **source** node,  $\partial^-(e) = \mathcal{B}_2$  of  $e$ , and  $\mathcal{B}_1$  as the **target**

<sup>2</sup>We refer to each element, including  $c[\sigma]$ , in  $\mathcal{P}^{(\sigma)}$  as boundaries.

node,  $\partial^+(e) = \mathcal{B}_1$ , of  $e$ . We use a lower case  $e$  to denote a directed edge in a Hasse diagram and  $H[\mathcal{P}]$  to label the Hasse diagram associated with a poset  $\mathcal{P}$  and  $E$  as the collective set of all its directed edges  $e$ .

We sketch the Hasse diagrams for the six orderings  $\sigma \in \mathcal{O}_4$  in Figure 8.15. Here, we have labeled each edge by a subset of expressions  $\{\alpha_2, \alpha_4, \alpha_2 + \alpha_4\}$  which we refer to as the *edge labels*. Given a directed edge  $e = (\mathcal{B}_2, \mathcal{B}_1)$ , an expression  $l = l(\vec{\alpha})$  in the canonical coordinates is an *edge label* for  $e$  if one reaches  $\mathcal{B}_1$  in the limit  $l \rightarrow 0$  of  $\mathcal{B}_2$ . We use a lowercase  $l$  for the individual edge labels and the upper case  $L(e)$  for the collection of edge labels for a given edge. For instance, for the standard ordering  $H[\mathcal{P}^{(1234)}]$  we have edges

$$e_1 = (c[1234], r_1), \quad e_2 = (c[1234], r_2), \quad e_3 = (r_1, v), \quad e_4 = (r_2, v), \quad (8.76)$$

with edge labels

$$L(e_1) = \{\alpha_4\}, \quad L(e_2) = \{\alpha_2\}, \quad L(e_3) = \{\alpha_2, \alpha_2 + \alpha_4\}, \quad L(e_4) = \{\alpha_4, \alpha_2 + \alpha_4\}. \quad (8.77)$$

Fixing  $n$  and  $k$ , we can introduce *collections* of positive geometries which might be related through the KK relation. We label each relevant positive geometry by a permutation,  $\sigma \in \mathcal{O}_n$ . Then  $\{\mathcal{P}^\sigma\}_{\sigma \in \mathcal{O}_n}$  denotes an indexed set of boundary stratifications of positive geometries  $X_{\geq 0}^{(\sigma)}$ . Assigning edge labels to each edge in every Hasse diagram, we denote  $\mathcal{E}$  the set of all edges in the Hasse diagrams

$$\mathcal{E} \equiv \bigcup_{\sigma \in \mathcal{O}_n} E[\mathcal{P}^\sigma], \quad (8.78)$$

and given an edge label we define

$$\check{E} \equiv \{e \in \mathcal{E} : l \in L(e)\}, \quad (8.79)$$

to be the set of all edges which has  $l$  as an edge label. For  $n = 4$ , the posets  $\{\mathcal{P}^\sigma\}_{\sigma \in \mathcal{O}}$  are constructed such that  $\check{E}(\alpha_2)$ ,  $\check{E}(\alpha_4)$ , and  $\check{E}(\alpha_2 + \alpha_4)$  contain 12 edges each as can be seen in Figure 8.15. Having defined the Hasse diagrams and edge labels, we have effectively generalized our notion of positive sectors as we shall see later. In order to find KK relations, we also require a boundary operator in this setting. Here, we generalize “boundary operators with respect to hyperplanes” to “boundary operators with respect to edge labels” and in complete analogy with section 8.3, we will define a boundary matrix, the kernel of which will precisely span the KK relations. In order to define a boundary matrix, we require a homological boundary operator. In order to ensure a proper nilpotent boundary operator we assign certain signs to each edge in every Hasse diagram according to the criteria called the *diamond compatibility criteria* as we shall define in the following using the notions of *poset intervals* and *diamonds*.

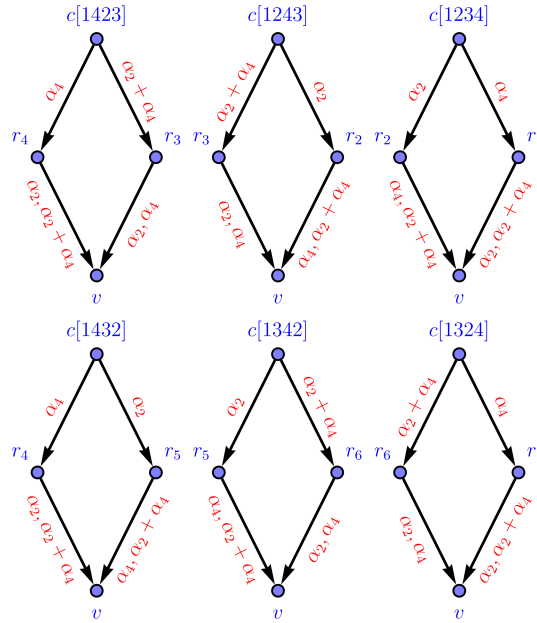


Figure 8.15: The Hasse diagrams  $H[\mathcal{P}^{(\sigma)}]$  for the simplicial cones (see section 8.2) all four-particle orderings relevant for the  $n = 4$ ,  $k = 2$  momentum amplituhedron.

## Intervals, the Diamond Compatibility Criteria and the Boundary Operator

We define the poset intervals for two boundaries  $\mathcal{B}_1 \prec \mathcal{B}_2$ ,  $[\mathcal{B}_1, \mathcal{B}_2]$  as the set of all boundaries,  $\mathcal{B}$ , in the poset,  $\mathcal{P}$ , such that  $\mathcal{B}_1 \preceq \mathcal{B} \preceq \mathcal{B}_2$  as follows

$$[\mathcal{B}_1, \mathcal{B}_2] \equiv \{\mathcal{B} \in \mathcal{P} : \mathcal{B}_1 \preceq \mathcal{B} \preceq \mathcal{B}_2\}. \quad (8.80)$$

Consider the poset interval between two boundaries  $\mathcal{I} = [\mathcal{B}_1, \mathcal{B}_2]$ , where  $\dim(\mathcal{B}_2) = \dim(\mathcal{B}_1) + 2$  and  $\mathcal{I} = \{\mathcal{B}_1, \mathcal{B}, \mathcal{B}', \mathcal{B}_2\}$ . Here we take  $\mathcal{B}$  and  $\mathcal{B}'$  as co-dimension-one boundaries of  $\mathcal{B}_2$ , we refer to such an interval as a *diamond*, reflecting the fact that the Hasse diagram for this interval is diamond shaped and we refer to any such subgraph with this structure as a diamond. The Hasse diagrams for the cones  $c[\sigma]$ , for  $\sigma \in \mathcal{O}_5$ , depicted in Figure 8.15 are all examples of diamonds. For a generic interval,  $\mathcal{I}$ , we assign a sign to each edge in the Hasse diagram of  $\mathcal{I}$ ,  $H(\mathcal{I})$  such that for every diamond subgraph,  $\mathcal{D}$ , we have

$$\prod_{e \in E[\mathcal{D}]} \text{sign } e = -1, \quad (8.81)$$

where the product is over every edge in the diamond  $\mathcal{D}$  and  $\text{sign } e$  is the sign assignment on  $e$ . Assigning signs in a Hasse diagram such that for every diamond subgraph the criteria is fulfilled is referred to as a diamond compatible assignment.

This condition ensures that the boundary operator, defined momentarily, will be nilpotent and therefore the algorithm will be homological. There are several choices of sign assignments and an example of a sign assignment for the Hasse diagrams in Figure 8.15 is given in Figure 8.16.

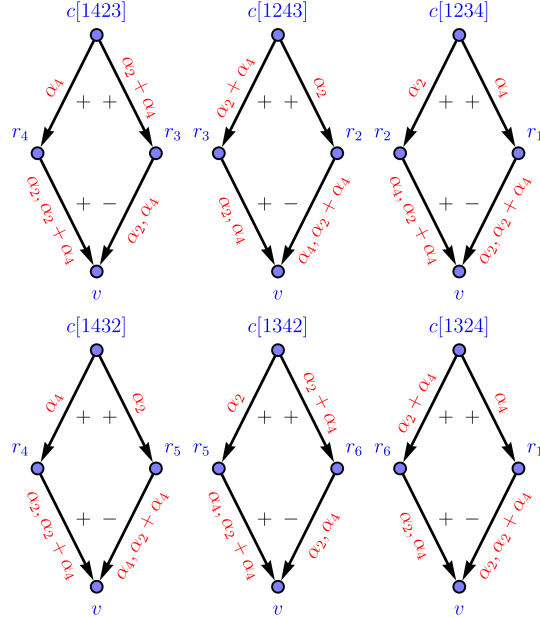


Figure 8.16: Example of diamond-compatible sign assignment for the Hasse diagrams  $H[\mathcal{P}^{(\sigma)}]$ ,  $\sigma \in \mathcal{O}_4$ .

We are now ready to define the boundary operator, denoted  $\partial_l$ , with respect to each edge label  $l$  as follows. Consider the boundary  $\mathcal{B} \in \mathcal{P}^{(\sigma)}$ , for a given  $\sigma \in \mathcal{O}_n$ , we set

$$\partial_l \mathcal{B} \equiv \sum_{e: \mathcal{B} \rightarrow \mathcal{B}' \in \check{E}(l)} \mathcal{B}', \tag{8.82}$$

that is, summing over all directed edges  $e$  with  $\mathcal{B}$  as its source node  $\partial^-(e) = \mathcal{B}$  with  $l$  as its edge label. As an example, consider the Hasse diagrams in Figure 8.16, we see that

$$\partial_{\alpha_4} \partial_{\alpha_2} c[1234] = \partial_{\alpha_4} r_2 = v, \quad \text{and} \quad \partial_{\alpha_2} \partial_{\alpha_4} c[1234] = \partial_{\alpha_2} r_1 = -v. \tag{8.83}$$

Due to the sign assignment of the edges in Figure 8.16 the boundary operator is nilpotent  $\partial_l^2 = 0$  for each edge label. This follows from the fact that for each pair of edges  $(e, e')$  connected to a single boundary, the sets of their edge labels are disjoint  $L(e) \cap L(e') = \emptyset$ . Defining the total boundary operator as the sum

$$\partial \equiv \sum_l \partial_l, \tag{8.84}$$

summing over all possible edge labels, counting each label once, it is easy to see that the boundary operator is nilpotent as follows

$$\partial^2 c[\sigma] = (\partial_{\alpha_2} + \partial_{\alpha_4} + \partial_{\alpha_2 + \alpha_4})^2 c[\sigma] = 0, \quad (8.85)$$

for all  $\sigma \in \mathcal{O}_4$  given that we have assigned diamond compatible signs as in Figure 8.16. Graphically, the boundary operators allows us to move from one *level*, that is the set of boundaries of the same dimension, to a lower level and therefore we can define chains of boundary operators all the way from the top of a Hasse diagram (the positive sector itself) to the bottom (its zero dimensional boundaries). We introduce the notion of *complete paths*, *complete path labels*, and boundary operators with respect to complete path labels in the following.

## Complete Path Labels and the Boundary Matrix

Consider the boundary stratification  $\mathcal{P}$  of a  $d$ -dimensional positive geometry  $(X, X_{\geq 0})$  and let  $v$  be one of its zero-dimensional boundaries. We denote by  $\mathcal{I}_v = [v, X_{\geq 0}]$  the interval between the lowest element  $\min \mathcal{I}_v = v$  and the top dimensional element  $\max \mathcal{I}_v = X_{\geq 0}$ , the positive sector itself. A *complete path*  $\gamma$  in  $\mathcal{I}_v$  is then defined as a path tracing edges in the Hasse diagram,  $H[\mathcal{I}_v]$  from  $X_{\geq 0}$  to  $v$ , expressed as a  $d$ -tuple of edges  $\gamma = (e_1, \dots, e_d)$  from a connected chain  $\partial^-(e_1) = X_{\geq 0}$  and  $\partial^+ e_d$  with every pair of adjacent edges  $(e_i, e_{i+1})$  in  $\gamma$  satisfying  $\partial^+(e_i) = \partial^-(e_{i+1})$ . In the following, we refer to  $\Gamma[\mathcal{I}_v]$  as the set of complete paths in  $\mathcal{I}_v$ . Let  $\{\mathcal{I}_v^{(\sigma)}\}_{\sigma \in \mathcal{O}_n} = \{[v, X_{\geq 0}^{(\sigma)}]\}_{\sigma \in \mathcal{O}_n}$  be an indexed family of intervals, sharing the vertex  $\min \mathcal{I}_v^{(\sigma)} = v$  as their minimal element. Furthermore, assume we have assigned compatible signs to each edge in the Hasse diagrams. We then take  $\Gamma_v$  to be the set of complete paths in all Hasse diagrams as follows

$$\Gamma_v \equiv \bigcup_{\sigma \in \mathcal{O}_n} \Gamma[\mathcal{I}_v^{(\sigma)}]. \quad (8.86)$$

Additionally, take  $\vec{l} = (l^{(1)}, \dots, l^{(d)})$  the  $d$ -tuple of all edge labels and

$$\check{\Gamma}(\vec{l}) = \bigcup_{\sigma \in \mathcal{O}_n} \{\gamma = (e_1, \dots, e_d) \in \Gamma[\mathcal{I}_v^{(\sigma)}] : e_i \in \check{E}(l^{(i)})\} \subseteq \Gamma_v, \quad (8.87)$$

the set of all complete paths in each interval which can be identified by  $\vec{l}$ . In the case where  $\check{\Gamma}(\vec{l}) \neq \emptyset$  we refer to  $\vec{l}$  as a *complete path label*. In the example of the  $n = 4$  simplicial cones we note there are 4 complete paths which can be labeled by  $\vec{l} = (\alpha_4, \alpha_2)$  and therefore  $(\alpha_4, \alpha_2)$  is a complete path label since  $\check{\Gamma}(\alpha_4, \alpha_2)$  has 4 elements.

In the following the complete path labels will be the equivalent of “rays pointing in opposite directions” which can be seen from the following. Consider a complete

path label  $\vec{l} = (l^{(1)}, \dots, l^{(d-1)}, l^{(d)})$ . The complete paths in  $\check{\Gamma}(\vec{l})$  allows us to identify all one-dimensional boundaries inhabiting the same one-dimensional variety defined by  $l^{(1)} = \dots = l^{(d-1)} = 0$ . The one dimensional boundaries are simply given by the source nodes  $\partial^- e_d$  of the final edges in each path  $\gamma \in \check{\Gamma}$ . This machinery allows us to identify different one dimensional boundaries which either

- are the same one-dimensional boundary or
- join together to form the one-dimensional variety  $l^{(1)} = \dots = l^{(d-1)} = 0$ ,

without solving any equations. We define the boundary operator with respect to a complete path label  $\vec{l} = (l^{(1)}, \dots, l^{(d)})$  as follows

$$\partial_{\vec{l}} \equiv \partial_{l^{(d)}} \dots \partial_{l^{(1)}}, \quad (8.88)$$

as the product, in the reverse order, of boundary operators with respect to each edge label in  $\vec{l}$ . E.g. for  $n = 4$  we have the two complete path labels  $\vec{l}_1 = (\alpha_w, \alpha_4)$  and  $\vec{l}_2 = (\alpha_4, \alpha_2)$  relevant for the boundary stratification of  $c[1234]$  as can be seen on 8.17, we take

$$\partial_{(\alpha_2, \alpha_4)} c[1234] = \partial_{\alpha_4} \partial_{\alpha_2} c[1234] = v \quad \text{and} \quad \partial_{(\alpha_4, \alpha_2)} c[1234] = \partial_{\alpha_2} \partial_{\alpha_4} c[1234] = -v. \quad (8.89)$$

Equipped with the boundary operators for all complete path label, we can now proceed to define the boundary matrix in this setup, in parallel to section 8.3. We do this in two steps: first we identify a *minimal collection of complete paths* needed in order for the kernel of the resulting boundary matrix to be congruent with the space of all KK relations and second, we define the boundary matrix with respect to a minimal collection of complete paths.

We define a *minimal collection* of complete path labels,  $\Gamma_{\min} \subset \Gamma_v$ , which is a collection of path labels  $\gamma$ , such that for all intervals between positive geometries for each ordering and a vertex element  $\mathcal{I}_v^{(\sigma)}$  all one dimensional boundaries are represented at least once. More accurately, there exists a complete path  $\gamma \in \bigcup_{\vec{l} \in \Gamma_{\min}} \check{\Gamma}(\vec{l})$  in a minimal collection of complete path labels such that  $\gamma$  passes through the one-dimensional boundary  $\mathcal{B}$  (i.e.  $\partial^- e_d = \mathcal{B}$ ) and all the complete paths in the minimal collection covers the entire collection of one-dimensional boundaries for all intervals  $\mathcal{I}_v^{(\sigma)}$ .

The minimal collections of complete paths  $\{\check{\Gamma}(\vec{l})\}_{\vec{l} \in \Gamma_{\min}}$  are generally not disjoint and their union is a strict subset of  $\Gamma_v$ . A minimal collection for  $n = 4$  is given by  $\{\vec{l}_1, \vec{l}_2, \vec{l}_3\}$  and we quote them in the following [41]

$$\vec{l}_1 \text{ (solid)} = (\alpha_4, \alpha_2), \quad (8.90a)$$

$$\vec{l}_2 \text{ (dashed)} = (\alpha_2, \alpha_4), \quad (8.90b)$$

$$\vec{l}_3 \text{ (dotted)} = (\alpha_2 + \alpha_4, \alpha_2), \quad (8.90c)$$

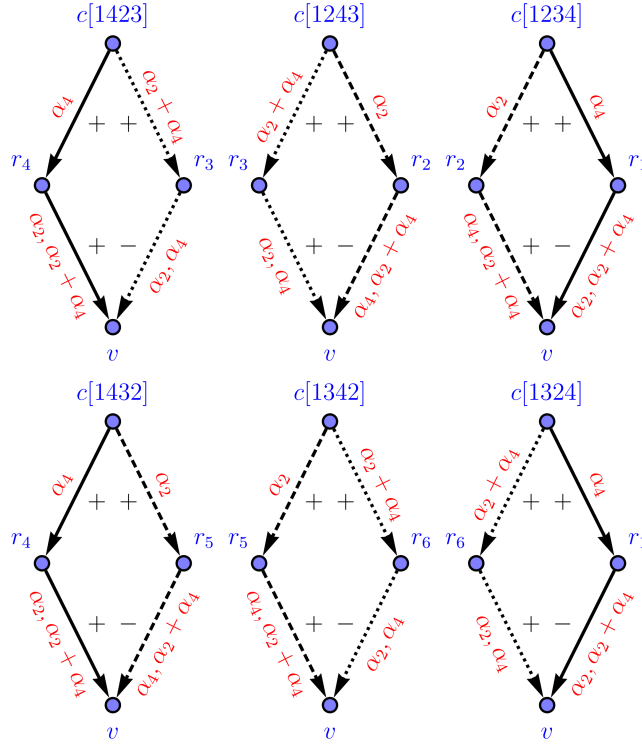


Figure 8.17: Complete paths for  $n = 4$  and the minimal collection of labels which identify them.

and sketch them in Figure 8.17 as solid, dashed, and dotted paths, respectively. Finally, we are ready to define the boundary matrix with respect to a minimal collection of complete paths, denoted  $M(\Gamma_{\min})$  as follows [41]

$$M_{j\sigma}(\Gamma_{\min}) = \partial_{\vec{l}_j} X_{\geq 0}^{(\sigma)} = \left[ \sum_{\gamma=(e_1, \dots, e_d) \in \vec{\Gamma}(\vec{l}_j) \cap \Gamma[\mathcal{I}_v^{(\sigma)}]} \left( \prod_{t=1}^d \text{sgn}(e_t) \right) \right] v, \quad (8.91)$$

where we take  $\vec{l}_j \in \Gamma_{\min}$ ,  $\sigma \in \mathcal{O}_n$  and  $v$  is the common minimal element of each interval – the common vertex.

We have expressed the boundary operator as a sum over all complete paths in  $H[\mathcal{I}_v^{(\sigma)}]$  labeled by  $\vec{l}_j$  and for each complete path we have taken the product of the signs along the edges as prescribed by the diamond compatibility condition. As in section 8.3, the null space of  $M_{j\sigma}(\Gamma_{\min})$  encodes all KK relations between the positive geometries  $\{X_{\geq 0}^{(\sigma)}\}_{\sigma \in \mathcal{O}_n}$ . This can be seen by the fact that any minimal collection of complete paths has the property that for each one-dimensional boundary  $\mathcal{B}$  in an interval  $\{\mathcal{I}_v^{(\sigma)}\}_{\sigma \in \mathcal{O}_n}$ , there is at least one complete path identified by one of the labels  $\Gamma_{\min}$  passing through  $\mathcal{B}$ . Having found the kernel, we label  $\nu_{\text{null}} \in \ker M_{j\sigma}(\Gamma_{\min})$  as a

non-trivial element of the null space of  $M_{j\sigma}(\Gamma_{\min})$ . We identify  $\nu_{\text{null}}$  as a linear combination of positive geometries  $\{X_{\geq 0}^{(\sigma)}\}$ , such that for every complete path label  $\vec{l} = (l^{(1)}, \dots, l^{(d-1)}, l^{(d)}) \in \Gamma_{\min}$ ,  $\partial_{\vec{l}} \nu_{\text{null}} = 0$ ; for every one-dimensional variety defined by  $l^{(1)} = \dots = l^{(d-1)} = 0$ , passing through the zero-dimensional boundary  $v$  which contains a non-empty subset of one-dimensional boundaries from the intervals in  $\{\mathcal{I}_v^{(\sigma)}\}$ , the one-dimensional boundaries inhabiting this variety conspire in  $\nu_{\text{null}}$  to completely remove the zero-dimensional boundary. Therefore the null vector  $\nu_{\text{null}}$  corresponds to an oriented sum of geometries without a zero-dimensional boundary in its boundary stratification. This means that the oriented sum cannot be a positive geometry and, therefore the corresponding linear combination of canonical differential forms must vanish, according to the analysis of section 4.3.

As an example, consider the minimal collection of complete path labels given in (8.90) for  $n = 4$ . We assemble the corresponding boundary matrix as follows

$$M = \begin{pmatrix} \partial_{\vec{l}_1} c[1234] & \cdots & \partial_{\vec{l}_1} c[1432] \\ \partial_{\vec{l}_2} c[1234] & \cdots & \partial_{\vec{l}_2} c[1432] \\ \partial_{\vec{l}_3} c[1234] & \cdots & \partial_{\vec{l}_3} c[1432] \end{pmatrix} = \begin{pmatrix} -1 & 0 & -1 & 0 & 1 & 1 \\ 1 & -1 & 0 & 1 & 0 & -1 \\ 0 & 1 & 1 & -1 & -1 & 0 \end{pmatrix}. \quad (8.92)$$

We find the following basis for the null space of  $M$ :

$$c[1234] \oplus c[1432], \quad (8.93)$$

$$c[1324] \oplus c[1423], \quad (8.94)$$

$$c[1234] \oplus c^- [1324] \oplus c^- [1342], \quad (8.95)$$

$$c[1234] \oplus c[1243] \oplus c^- [1324]. \quad (8.96)$$

We want to replace the cones in each of the four null vectors listed above by their corresponding canonical differential forms and set each linear combination to zero. However, we are required to multiply each canonical differential form by an appropriate sign to ensure its leading singularities – that is, its residues on zero-dimensional boundaries – are compatible with the signs we assigned to the edges of the corresponding Hasse diagram. To find these multiplicative weights, we begin by listing the canonical differential forms for each cone,

$$\Omega(c[1234]) = \Omega(c[1432]) = d \log \alpha_4 \wedge d \log \alpha_2, \quad (8.97)$$

$$\Omega(c[1243]) = \Omega(c[1342]) = d \log \alpha_2 \wedge d \log(\alpha_2 + \alpha_4), \quad (8.98)$$

$$\Omega(c[1324]) = \Omega(c[1423]) = d \log(\alpha_2 + \alpha_4) \wedge d \log \alpha_4, \quad (8.99)$$

which we can be read off directly from Figure 8.1. For every complete path label  $\vec{l} = (l^{(1)}, l^{(2)}) \in \{\vec{l}_1, \vec{l}_2, \vec{l}_3\}$  in (8.90), we define the *residue along  $\vec{l}$* ,  $\text{res}_{\vec{l}}$  as follows

$$\text{res}_{\vec{l}} = \text{res}_{l^{(2)}=0} \text{res}_{l^{(1)}=0}. \quad (8.100)$$

For each color ordering  $\sigma \in \mathcal{O}_4$ , the weight required to be multiplied by  $\Omega(c[\sigma])$ , denoted by  $w[\sigma]$ , can be obtained by taking a single complete path label  $\vec{l}$  with respect to  $\sigma$  (i.e.  $\check{\Gamma}(\vec{l}) \cap \Gamma[\mathcal{I}_v^{(\sigma)}] \neq \emptyset$ ) and computing the residue as follows

$$\text{res}_{\vec{l}} \Omega(c[\sigma]) \times v = w[\sigma] \times \partial_{\vec{l}} c[\sigma]. \quad (8.101)$$

We obtain the following weights for the  $n = 4$  case:

$$w[1234] = -1 = -w[1432], \quad w[1243] = -1 = -w[1342], \quad w[1324] = 1 = -w[1423]. \quad (8.102)$$

We make the replacements  $c[\sigma] \rightarrow w[\sigma]\Omega(c[\sigma])$  in (8.93) and set each null vector to zero. Then the KK relations for  $n = 4$  appear the canonical forms as follows

$$-\Omega(c[1234]) + \Omega(c[1432]) = 0, \quad (8.103)$$

$$-\Omega(c[1324]) + \Omega(c[1423]) = 0, \quad (8.104)$$

$$\Omega(c[1234]) + \Omega(c[1324]) + \Omega(c[1342]) = 0, \quad (8.105)$$

$$\Omega(c[1234]) + \Omega(c[1243]) + \Omega(c[1324]) = 0, \quad (8.106)$$

which is exactly the KK relations for four-particle MHV amplitudes discussed in (8.53).

This algorithm can be applied to the general  $n$  case by using the intervals  $\{\mathcal{I}_v^{(\sigma)}\}_{\sigma \in \mathcal{O}_n}$ . For all color orderings  $\sigma \in \mathcal{O}_n$ , we define the weight  $w[\sigma]$  by taking any complete path label  $\vec{l}$  for an interval  $\mathcal{I}_v^{(\sigma)}$  and computing the residue as follows

$$\text{res}_{\vec{l}} \Omega(X_{\geq 0}^{(\sigma)}) \times v = w[\sigma] \times \partial_{\vec{l}} X_{\geq 0}^{(\sigma)}, \quad (8.107)$$

where  $\Omega(X_{\geq 0}^{(\sigma)})$  is the canonical differential form for  $X_{\geq 0}^{(\sigma)}$ , while  $v$  is the zero-dimensional boundary common to each interval, and  $\text{res}_{\vec{l}}$  is residue operation along  $\vec{l}$ . Each vector in the null space of the boundary matrix (with respect to some minimal collection) can then be mapped to a KK relation by the replacement  $X_{\geq 0}^{(\sigma)} \rightarrow w[\sigma] \times \Omega(X_{\geq 0}^{(\sigma)})$  and setting the null vector to zero.

### 8.5.2 All Helicity Sectors

The homological algorithm described in the previous section was used to derive KK relations for “simplified” MHV momentum amplituhedra, where each geometry is just an oriented simplicial cone in  $(n - 2)$  dimensions. We recall that the actual, full momentum amplituhedra are of dimension  $(2n - 4)$ . However, since the only input of this algorithm was the boundary stratification of each positive sector, we can rederive the KK relations using the boundary stratifications of the momentum amplituhedra for all color orderings. While this is excessive for the MHV sector, it is crucial for deriving KK relations for all helicity sectors. Two steps in the procedure, however, require some elaboration. We need to specify

1. how to find the boundary stratification of the momentum amplituhedron for different orderings, and
2. how to generate edge labels for a given boundary stratification.

The first point can be treated as follows. For generic  $n$  and  $k$ , with  $2 \leq k \leq n-2$ , there are  $\binom{n}{k}$  zero-dimensional boundaries (or vertices) of the standard-ordering momentum amplituhedron  $\mathcal{M}_{n,k} = \mathcal{M}_{n,k}^{(12\dots n)}$  and each vertex is shared by all particle orderings [41]. These boundaries are in one-to-one correspondence with vertices of the positive Grassmannian  $G_+(k, n)$  via the linear map as discussed in section 6.2. Each vertex of  $\mathcal{M}_{n,k}$  can be labeled by a  $k$ -element subset  $I$  of  $[n] = \{1, 2, \dots, n\}$  representing the matrix in the positive Grassmannian with only non-zero entries in the  $k$  columns labeled by  $I$ , corresponding to a vertex in  $G_+(k, n)$ . Consider for instance the  $n = 6$ ,  $k = 3$  case: we take the subset (123) to refer to the matrix

$$C = \begin{pmatrix} 1 & 0 & 0 & 0 & 0 & 0 \\ 0 & 1 & 0 & 0 & 0 & 0 \\ 0 & 0 & 1 & 0 & 0 & 0 \end{pmatrix}. \quad (8.108)$$

We will denote the vertex of  $\mathcal{M}_{n,k}$  identified by  $I \in \binom{[n]}{k}$  as  $v_I$ . The poset interval between  $\mathcal{M}_{n,k}$  and  $v_I$ , denoted by  $[v_I, \mathcal{M}_{n,k}]$ , can be obtained using the function `momInterval` from the Mathematica<sup>TM</sup> package `amplituhedronBoundaries` [88]. Given an arbitrary ordering  $\sigma \in \mathcal{O}_n$ , the interval between  $\mathcal{M}_{n,k}^{(\sigma)}$  and  $v_I$  is isomorphic to the interval between the standard ordering momentum amplituhedron and the vertex  $v_{\sigma^{-1}(I)}$  labeled by  $\sigma^{-1}(I) \equiv \{\sigma^{-1}(i_1), \sigma^{-1}(i_2), \dots, \sigma^{-1}(i_k)\}$  [41];

$$[v_I, \mathcal{M}_{n,k}^{(\sigma)}] \cong [v_{\sigma^{-1}(I)}, \mathcal{M}_{n,k}^{(12\dots n)}]. \quad (8.109)$$

Consequently, `momInterval` allows us to obtain intervals for different orderings in the neighborhood of each vertex  $v_I$ . Two examples of such intervals for  $\mathcal{M}_{4,2}^{(\sigma)}$  for the orderings  $\sigma = (1234)$  and  $\sigma = (1324)$  can be found in Appendix F.

Regarding the question of generating edge label for a given boundary stratification, we find that for any boundary  $\mathcal{B}$  of the momentum amplituhedron  $\mathcal{M}_{n,k}^{(\sigma)}$ , we can identify the exact amplitude singularities associated with each boundary. That is, we can find which exact spinor brackets and multi-particle Mandelstam variables vanish for a given boundary,  $\mathcal{B}$ . Moreover, when analyzing the boundary structure of the  $n = 6$  and  $k = 3$  momentum amplituhedron, we find that some lower dimensional elements in the boundary poset of  $\mathcal{M}_{n,k}$  might have boundaries corresponding to a sum of several external momenta going soft. This will distinguish the multi-particle Mandelstam variables  $s_{i_1, \dots, i_m}$  from the multi-particle momenta  $p_{i_1} + \dots + p_{i_r}$  soft singularities, for  $r > 2$ . We will denote the set of vanishing spinor brackets, multi-particle Mandelstam variable factorization channels and the multi-particle momenta

$p_{i_1} + \dots + p_{i_r}$  by  $Z(\mathcal{B})$ . Now, given a directed edge  $e = (\mathcal{B}_2, \mathcal{B}_1)$  in the Hasse diagram for the interval  $[v_I, \mathcal{M}_{n,k}^{(\sigma)}]$  we fix the set of edge labels for  $e$  to be  $S(e) = Z(\mathcal{B}_1) \setminus Z(\mathcal{B}_2)$ . It contains all spinor brackets, Mandelstam variables and sums of momenta which vanish for  $\mathcal{B}_1$  but are not zero for  $\mathcal{B}_2$ .

Once we have generated all intervals and all edge labels have been assigned, the poset-based homological algorithm can be used to derive the KK relations in all helicity sectors and not just positive sectors as in the MHV case. Importantly, it is sufficient to consider momentum amplituhedra around a single vertex, say  $v_{\{1,2,\dots,k\}}$ , to derive all KK relations. This is due to the fact that all momentum amplituhedra share all vertices in their boundary stratification and the momentum amplituhedra in the neighborhood of a given vertex  $v_I$  are identical with the ones around  $v_{\{1,2,\dots,k\}}$ , after a relabeling the external particles. We have explicitly verified that our algorithm reproduces the correct KK relations for all  $2 \leq k \leq n - 2$  and for  $n \leq 7$ , and we conjecture that the algorithm is valid all  $n$  and  $k$  momentum amplituhedra.



# Chapter 9

## Conclusion and Outlook

The star player of this dissertation is the momentum amplituhedron, defined in chapter 6 and the latter three chapters are exclusively concerned with the developments on the ideas first presented in [39]. We have proposed an object encoding scattering amplitudes in  $\mathcal{N} = 4$  sYM as the image of the positive Grassmannian through a map of bosonized spinor helicity variables respecting some positivity conditions. The natural notion of the canonical form of the momentum amplituhedron is related to  $\mathcal{N} = 4$  scattering amplitudes with the Grassmann odd-parameters exchanged with differentials on spinor helicity variables, after stripping off a copy of supermomentum conservation.

Further study of the canonical forms of momentum amplituhedra has revealed a surprising relationship between the momentum amplituhedron and the kinematic associahedron [40]. Stripping off the highest degree of little group scaling from the canonical form of momentum amplituhedron produces the kinematic associahedron canonical form when pulled back or pushed forward to the proper space. This can be understood as a reflection of the common singularities of scattering amplitudes in  $\mathcal{N} = 4$  sYM and bi-adjoint  $\phi^3$  theory, specifically the common factorization channels.

A detailed investigation of the novel geometric structure continued to yield surprising results. In particular, after providing a second definition of the momentum amplituhedron directly in kinematic space, more suitable for describing momentum amplituhedra of various color orderings, the Kleiss-Kuijf relations [42] emerge naturally from studying geometries of different color orderings in the same space [41]. This is a luxury only available to the momentum amplituhedron since the space of spinor helicity variables allows for the direct comparison of momentum amplituhedra of differently color orderings in the same kinematic space. This was first observed for the MHV case where the momentum amplituhedron has a simplicial decomposition, and the boundary structure only consists of linear inequalities, which match up neatly as cones spanning the full fan of  $\mathbb{R}^{(n-2)}$ . The construction was further

generalized to all sectors of the momentum amplituhedron in an algorithm discussed in the latter part of chapter 8. This is a stunning result as the amplitudes relations stem from the color structure of  $\mathcal{N} = 4$  sYM which the momentum amplituhedron inherently does not carry information about. The construction also appeared to be applicable to the kinematic associahedron where similar relations were found as a consequence of the double color structure of scattering amplitudes in bi-adjoint  $\phi^3$  theory.

Obviously, the natural question of a generalization of the momentum amplituhedron to include loops is still at the time of writing left unanswered. Here, a few challenges bear mention: as explored in section 4.4, loop momentum has a very neat representation as “lines in momentum twistor space” and this representation was crucial to the original formulation of the loop amplituhedron in [1]. Here, the notion of “hiding particles” defines positivity conditions for the lines defining the loop variables, ensuring that the loop amplituhedron inherits the correct boundary structure as expected for scattering amplitudes. It appears, that not only does an obvious notion of hiding particles not generalize to the momentum amplituhedron, but a deeper question about defining loop-momenta in non-planar settings is raised: in non-planar sectors, it is not obvious how to actually define the loop-momenta at the integrand level [95]. Several strides have been made to circumvent this challenge, recently in 2019 by Bourjaily et al. [96], however the generalization to the momentum amplituhedron does not seem obvious at the time of writing. Another immediate open question directly related to the construction of the momentum amplituhedron concerns the extra positivity conditions mixing  $(\Lambda, \tilde{\Lambda})$  found in (6.71). The origins of these conditions are still unclear from a physical perspective.

Another interesting avenue of investigation would build upon the ideas presented in chapter 8 and in the paper [41]. Here, we studied the scattering amplitude relations described in section 2.4 in the context of the momentum amplituhedron, and surprisingly, the relations stemming from the gauge/color structure of  $\mathcal{N} = 4$  sYM appears naturally in the geometric framework, where gauge redundancy is not manifestly enforced and color is never introduced. There exists however, as detailed in section 2.4, a further set of scattering amplitudes relations reducing the basis of color ordered scattering amplitudes from  $(n - 2)!$  to  $(n - 3)!$  – the BCJ relations (2.77). Attempts have been made at generalizing the results of [41] to also include the BCJ relations. However, at the time of writing, there is no concrete evidence that the momentum amplituhedron encodes the BCJ relations geometrically. This question of BCJ relations for the momentum amplituhedron is a curious one, due to the relation between the BCJ relations and the double-copy construction [53], where it is possible to encode scattering amplitudes in gravity as the product of two Yang-Mills scattering amplitudes [97]. While the outstanding question of a positive geometry for gravity is an obvious avenue of investigation in its own right [98], understanding the BCJ relations for the momentum amplituhedron might give hints at an exotic geometry governing the scattering of gravitons through the double copy

construction.

Furthermore, there is also an outstanding question of a mathematically rigorous definition oriented sum proposed in section 4.3. A similar construction was considered by Dian and Heslop in [99] in their recent work on the correlahedron. We are leaving a rigorous mathematical definition of the oriented sum to future work.

These two directions, naturally following from the work described in this dissertation, forms a natural starting point for further research. However in the research program as a whole several fascinating avenues of research also arise: first, a generalization of the amplituhedron to encode more realistic theories, e.g. QCD. To this end, there is an immediate challenge in how to define a positive geometry related to the differential form associated with scattering amplitudes in theories with less-than-maximal supersymmetry, discussed by He and Zhang in [84]. We believe, that a starting point for such geometries might be the momentum amplituhedron since the spinor helicity variables are naturally suited to discuss scattering amplitudes in generic Yang-Mills theories including QCD.

Another promising direction of study involves going beyond the loop-level *integrand*s to loop-level *integrals*. Since loop integrands are rational functions and most of the phenomenologically relevant information is tied up with the full, integrated scattering amplitude, much effort has gone into developing techniques to evaluate scattering amplitude integrals, for instance, bootstrap methods [100], various representations, e.g. due to Baikov [101], differential equations [102]. These methods have revealed and benefited from the fact that there is a lot of structure in the transcendental functions appearing in loop integrals. Perhaps, these transcendental functions can be encoded geometrically [38] by integrating canonical forms with respect to each other as briefly discussed in section 4.1.

Throughout this work, we have taken steps towards a new framework for quantum field theory based on the notion of positive geometries. We have seen how the central axioms of quantum field theory, locality, and unitarity, have been replaced by the notion of positivity and appear as emergent qualities. This represents a new leap forward in the program of scattering amplitudes without reference to space-time and therefore makes a small step towards alleviating the great tension between quantum mechanics and gravity that has haunted theoretical physics for decades. This is an extremely lofty goal and requires, among other things, the rederivation of the great trove of known theorems and general results in quantum field theory from its around eighty years of history as was initiated in [48].



# Appendix A

## Orthogonal complement

Throughout the dissertation we make use of the notion of orthogonal complements, specifically in chapters 3 and 6. The orthogonal complement is naturally defined for the Grassmannian, the space of  $k$  planes in  $n$  dimensions. For a given  $k$  - plane in the Grassmannian  $c \in G(k, n)$  we can naturally associate an  $(n - k)$  plane,  $c^\perp$  defined as [72]

$$c \cdot c^\perp = 0. \quad (\text{A.1})$$

The matrix  $c^\perp$  defined up to  $GL(n - k)$  transformations and can therefore be associated with an element in  $G(n - k, n)$  and the minors can be determined precisely from the minors of  $c$  as we shall see in the following. We consider the matrix

$$B = \begin{pmatrix} b_{11} & b_{12} & \dots & b_{1n} \\ b_{21} & b_{22} & \dots & b_{2n} \\ \vdots & \vdots & \ddots & \vdots \\ b_{k1} & b_{k2} & \dots & b_{kn} \end{pmatrix}. \quad (\text{A.2})$$

Describing a  $k$ -plane  $\mathcal{B}$  in an  $n$ -dimensional space. We define its orthogonal complement  $\mathcal{B}^\perp$  as an  $(n - k)$ -plane in  $n$  dimensions. Such plane can be parametrized by an  $(n - k) \times n$  matrix

$$B^\perp = \begin{pmatrix} b_{11}^\perp & b_{12}^\perp & \dots & b_{1n}^\perp \\ b_{21}^\perp & b_{22}^\perp & \dots & b_{2n}^\perp \\ \vdots & \vdots & \ddots & \vdots \\ b_{n-k1}^\perp & b_{n-k2}^\perp & \dots & b_{n-kn}^\perp \end{pmatrix}. \quad (\text{A.3})$$

Acting on this matrix with a  $GL(n - k)$  transformation describes the same plane in a different basis. We can relate the maximal minors of  $\mathcal{B}$  and  $\mathcal{B}^\perp$

$$(i_1, \dots, i_{n-k})_B^\perp = g \epsilon_{i_1 \dots i_{n-k} j_1 \dots j_k} (j_1, \dots, j_k)_B \quad (\text{A.4})$$

Where the set  $\{j_1, \dots, j_k\} = \{i_1, \dots, i_{n-k}\}^c$  is the complementary set of the set  $\{i_1, \dots, i_{n-k}\}$  and  $g$  is an unfixed scalar global to all sets of minors. We describe  $B$  as a patch in the positive Grassmannian such that

$$B = (\mathbb{1}_{k \times k} | b) \quad (\text{A.5})$$

and the orthogonal complement

$$B^\perp = (-b^T | \mathbb{1}_{(n-k) \times (n-k)}). \quad (\text{A.6})$$

One can check, by taking  $\{j_1, \dots, j_k\} = \{1, \dots, k\}$ , that

$$g = (-1)^{k(n-k)}. \quad (\text{A.7})$$

Since (A.4) is not an involution, we can generally associate

$$(j_1, \dots, j_k) = \tilde{g} \epsilon_{j_1 \dots j_k i_1 \dots i_{n-k}} (i_1, \dots, i_{n-k})^\perp_B \quad (\text{A.8})$$

In order for this to agree with (A.4) we need to fix

$$\tilde{g} = (-1)^{k(n-k)} g = 1 \quad (\text{A.9})$$

In chapter 6 we let positive matrices play the role of  $B$  and twisted positive matrices play the role of  $B^\perp$  and find the following relations between minors of matrices

$$(j_1, \dots, j_k) = \epsilon_{j_1 \dots j_k i_1 \dots i_{n-k}} (i_1, \dots, i_{n-k})^\perp \quad (\text{A.10})$$

$$\langle j_1, \dots, j_{k-2} \rangle^\perp = \epsilon_{j_1 \dots j_{k-2} i_1 \dots i_{n-k+2}} \langle i_1, \dots, i_{n-k+2} \rangle \quad (\text{A.11})$$

$$[j_1, \dots, j_{k+2}] = \epsilon_{j_1 \dots j_{k+2} i_1 \dots i_{n-k+2}} [i_1, \dots, i_{n-k+2}]^\perp \quad (\text{A.12})$$

which are necessary for the claim that the momentum amplituhedron fulfills the proposed sign-flip conditions [84].

# Appendix B

## Extended Fock-Goncharov Parametrization for $n = 5$

The  $\tilde{\lambda}$  matrix in the extended Fock-Goncharov parametrization reads

$$\tilde{\lambda} = \begin{pmatrix} t_1^{-1} & 0 & t_3^{-1}\tilde{\lambda}_3^1 & t_4^{-1}\tilde{\lambda}_4^1 & t_5^{-1}\tilde{\lambda}_5^1 \\ 0 & t_2^{-1}s_{12} & t_3^{-1}\tilde{\lambda}_3^2 & t_4^{-1}\tilde{\lambda}_4^2 & t_5^{-1}\tilde{\lambda}_5^2 \end{pmatrix} \quad (\text{B.1})$$

with

$$\tilde{\lambda}_3^1 = \frac{R_{1234}(R_{1345}(\bar{R}_{1234} + 1) - \bar{R}_{1234}\bar{R}_{1345}) - \bar{R}_{1234}\bar{R}_{1345}}{R_{1234}\bar{R}_{1234}((R_{1234} + 1)\bar{R}_{1345} - R_{1345}(-R_{1234}\bar{R}_{1345} + \bar{R}_{1234}(\bar{R}_{1345} + 1) + 1))} \quad (\text{B.2})$$

$$\tilde{\lambda}_4^1 = \frac{(\bar{R}_{1234} + 1)(\bar{R}_{1234}(\bar{R}_{1345} + 1) - R_{1234}(R_{1345} + 1))}{R_{1234}\bar{R}_{1234}((R_{1234} + 1)\bar{R}_{1345} - R_{1345}(-R_{1234}\bar{R}_{1345} + \bar{R}_{1234}(\bar{R}_{1345} + 1) + 1))} \quad (\text{B.3})$$

$$\tilde{\lambda}_5^1 = \frac{(\bar{R}_{1234}(\bar{R}_{1345} + 1) + 1)(R_{1234} - \bar{R}_{1234})}{R_{1234}\bar{R}_{1234}((R_{1234} + 1)\bar{R}_{1345} - R_{1345}(-R_{1234}\bar{R}_{1345} + \bar{R}_{1234}(\bar{R}_{1345} + 1) + 1))} \quad (\text{B.4})$$

$$\tilde{\lambda}_3^2 = -\frac{s_{1,2}(R_{1234}(R_{1345}(\bar{R}_{1234} + 1) - \bar{R}_{1234}\bar{R}_{1345}) - \bar{R}_{1234}\bar{R}_{1345})}{R_{1234}\bar{R}_{1234}(R_{1345} - \bar{R}_{1345})} \quad (\text{B.5})$$

$$\tilde{\lambda}_4^2 = \frac{s_{1,2}(R_{1234}(R_{1345} + 1) - \bar{R}_{1234}(\bar{R}_{1345} + 1))}{R_{1234}\bar{R}_{1234}(R_{1345} - \bar{R}_{1345})} \quad (\text{B.6})$$

$$\tilde{\lambda}_5^2 = \frac{s_{1,2}(\bar{R}_{1234} - R_{1234})}{R_{1234}\bar{R}_{1234}(R_{1345} - \bar{R}_{1345})}. \quad (\text{B.7})$$



# Appendix C

## Formulae for Six-point Amplitudes

The arguments of the square roots,  $\Delta_1$  and  $\Delta_2$ , appearing when finding the inverse of the map  $\mathbf{g}_6$ , see (7.51) are found to be

$$\begin{aligned} \Delta_1 = & s_{12}^2 (s_{23} - s_{234})^2 + (s_{23}(s_{34} - s_{56}) + s_{123}(s_{234} - s_{34}))^2 + \\ & + 2s_{12} \left( -(s_{34} + s_{56})s_{23}^2 + (s_{34}(s_{123} - 2s_{56}) + (s_{34} + s_{56} + s_{123})s_{234})s_{23} + \right. \\ & \left. + s_{123}(s_{34} - s_{34})s_{234} \right), \end{aligned} \quad (\text{C.1})$$

$$\begin{aligned} \Delta_2 = & (s_{23}s_{56} - s_{61}s_{56} + s_{61}s_{123} - s_{123}s_{234} + s_{45}(s_{234} - s_{56}))^2 - \\ & - 4s_{45}s_{56}s_{61}(s_{23} + s_{56} - s_{123} - s_{234}), \end{aligned} \quad (\text{C.2})$$

while the explicit form for  $\Gamma$  appearing in the solutions for the inverse of the map  $\mathbf{h}_6$  in (7.55) is as follows

$$\begin{aligned} \Gamma = & (s_{34} - s_{56})s_{56}s_{23}^2 + \left( s_{56}(s_{56}s_{61} + s_{45}(s_{56} - s_{234}) - s_{123}(s_{61} - 2s_{234})) \right. \\ & \left. - s_{34}(s_{56}(s_{61} + s_{123}) + s_{45}(s_{56} - s_{234}) + s_{123}(s_{61} + s_{234})) \right) s_{23} \\ & + s_{123} \left( (s_{45} - s_{123})s_{234}^2 + (-s_{56}(s_{45} + s_{61}) + s_{61}s_{123}) \right. \\ & \left. + s_{34}(-s_{45} + 2s_{61} + s_{123}) \right) s_{234} + s_{34}(s_{45}s_{56} + s_{61}(s_{123} - s_{56})) \\ & + s_{12} \left( (s_{45} + s_{123})s_{234}^2 - (s_{56}(s_{45} - s_{61}) + (s_{61} - 2s_{45})s_{123}) \right. \\ & \left. + s_{23}(s_{45} + s_{56} + s_{123}) \right) s_{234} + s_{23}(s_{56}(s_{23} - s_{45} - s_{61}) + s_{61}s_{123}). \end{aligned} \quad (\text{C.3})$$



# Appendix D

## Geometry of the Differential Form

$\nu_{6,2}$

Pushing the differential form  $\omega_{6,2}$  forward to the differential form on  $\mathcal{G}_6(\mathbf{g}_6)_*$   $\omega_{6,2} = \nu_{6,2}$ , we find that the square-roots present in the individual solutions  $\mathbf{g}_{6,i}^{-1}$  cancel exactly when summing over all four solutions, and we are left with the following

$$\begin{aligned} \nu_{6,2} = & \nu_{6,2}^{(A)}(s_{12}, s_{23}, s_{34}; s_{45}, s_{56}, s_{61}) + \nu_{6,2}^{(B)}(s_{12}, s_{45}, s_{123}; s_{34}, s_{61}, s_{234}) \\ & - \nu_{6,2}^{(A)}(s_{45}, s_{56}, s_{61}; s_{1,2}, s_{23}, s_{34}) - \nu_{6,2}^{(B)}(s_{34}, s_{61}, s_{234}; s_{12}, s_{45}, s_{123}), \end{aligned} \quad (\text{D.1})$$

where

$$\begin{aligned} \nu_{6,2}^{(A)}(s_{12}, s_{23}, s_{34}; s_{45}, s_{56}, s_{61}) = & d \log s_{12} \wedge d \log s_{34} \wedge d \log \left( \frac{s_{45}s_{61}}{s_{14}s_{56}} \right) \\ & + \frac{s_{23}}{s_{123} - s_{234}} d \log \left( \frac{s_{12}s_{34}}{s_{23}^2} \right) \wedge d \log \left( \frac{s_{14}}{s_{23}} \right) \wedge d \log \left( \frac{Q}{s_{14}s_{56}} \right), \end{aligned} \quad (\text{D.2})$$

$$\begin{aligned} \nu_{6,2}^{(B)}(s_{12}, s_{45}, s_{123}; s_{34}, s_{61}, s_{234}) = & \frac{s_{123}}{s_{123} - s_{234}} \\ & \times \left\{ \left[ d \log \left( \frac{s_{45}}{s_{12}} \right) \wedge d \log (s_{14}s_{23}) - d \log \left( \frac{s_{12}}{s_{56}} \right) \wedge d \log \left( \frac{s_{56}}{s_{23}} \right) \right] \wedge d \log Q \right. \\ & \left. + \left[ d \log s_{56} \wedge d \log \left( \frac{s_{12}s_{34}}{s_{23}} \right) - d \log s_{23} \wedge d \log \left( \frac{s_{45}s_{61}}{s_{56}} \right) \right] \wedge d \log \left( \frac{s_{14}}{Q} \right) \right\} \\ & + d \log s_{12} \wedge d \log s_{45} \wedge d \log Q, \end{aligned} \quad (\text{D.3})$$

$s_{14} = s_{23} + s_{56} - s_{123} - s_{234}$  and  $Q = s_{23}s_{56} - s_{123}s_{234}$ . The above form,  $\nu_{6,2}$  has simple poles exactly on all planar two-particle Mandelstam variables, and additionally on  $s_{14}$  and on  $Q$ . These two remaining appear as a consequence of the Gram determinant condition for  $n = 6$  in four dimensions. They appear exactly as denominators in the two solutions to the Gram determinant in (7.55).

Taking subsequent residues of  $\nu_{6,2}$ , we not only obtain total residues of  $\pm 1$ , but also of  $\pm 2$  on zero-dimensional boundaries, in contradistinction to canonical forms which, by definition, can only have residues  $\pm 1$  on boundaries of zero dimension [38]. One might have expected  $\nu_{6,2}$  to be a canonical form, due to the fact that it is the push-forward of the canonical form  $\omega_{6,2}$ . However, since push-forwards only preserve top-dimensional canonical forms [38], and  $\omega_{6,2}$  is not top-dimensional (being defined on  $\mathcal{L}_6$ ), we anticipate that this is the explanation of the appearance of the  $\pm 2$  residues – the non-canonical behavior of  $\nu_{6,2}$ . In every solution, we have verified that  $\mathbf{g}_{6,i}^{-1}$ , given by  $\nu_{6,2}^{(i)} = (\mathbf{g}_{6,i}^{-1})^* \omega_{6,2}$  is indeed a positive geometry with residues  $\pm 1$ . This suggests that the geometry of  $\nu_{6,2}$  is a geometric sum of four positive geometries  $\nu_{6,2}^{(i)}$  and as was explored in section 4.3, the sum of positive geometries can give rise to geometries that are not positive geometries.

# Appendix E

## Positivity conditions on $\mathcal{V}_{5,2}$ from $\mathcal{W}_{5,2}^{(\sigma)}$

We find the positivity conditions for  $n = 5$  and  $k = 2$  by intersecting the affine subspace  $\mathcal{V}_5$  with the winding spaces of the  $4! = 24$  different color orderings of the  $n = 5$  scattering amplitude.

	$\langle 12 \rangle$	$\langle 13 \rangle$	$\langle 14 \rangle$	$\langle 15 \rangle$	$\langle 23 \rangle$	$\langle 24 \rangle$	$\langle 25 \rangle$	$\langle 34 \rangle$	$\langle 35 \rangle$	$\langle 45 \rangle$
(12345)	+	+	+	+	+	+	+	+	+	+
(12354)	+	+	+	+	+	+	+	+	+	-
(12435)	+	+	+	+	+	+	+	-	+	+
(12453)	+	+	+	+	+	+	+	-	-	+
(12534)	+	+	+	+	+	+	+	+	-	-
(12543)	+	+	+	+	+	+	+	-	-	-
(13245)	+	+	+	+	-	+	+	+	+	+
(13254)	+	+	+	+	-	+	+	+	+	-
(13425)	+	+	+	+	-	-	+	+	+	+
(13452)	+	+	+	+	-	-	-	+	+	+
(13524)	+	+	+	+	-	+	-	+	+	-
(13542)	+	+	+	+	-	-	-	+	+	-
(14235)	+	+	+	+	+	-	+	-	+	+
(14253)	+	+	+	+	+	-	+	-	-	+
(14325)	+	+	+	+	-	-	+	-	+	+
(14352)	+	+	+	+	-	-	-	-	+	+
(14523)	+	+	+	+	+	-	-	-	+	+
(14532)	+	+	+	+	-	-	-	-	-	+
(15234)	+	+	+	+	+	-	-	+	-	-
(15243)	+	+	+	+	+	+	-	-	-	-
(15324)	+	+	+	+	-	+	-	+	-	-
(15342)	+	+	+	+	-	-	-	+	-	-
(15423)	+	+	+	+	+	-	-	-	-	-
(15432)	+	+	+	+	-	-	-	-	-	-

Table E.1: The positivity conditions from  $\mathcal{W}_{5,2}^\sigma$  for all orderings  $\sigma \in \mathcal{O}_5$ . The positivity of  $\langle 1i \rangle > 0$  allows the remaining positivity conditions to be embedded in  $\mathbb{R}^3$

# Appendix F

## Poset Intervals for MHV Four-point Amplitudes

In this appendix we present in Fig. F.1 the Hasse diagrams of the intervals between the momentum amplituhedra  $\mathcal{M}_{4,2}^{(1234)}$ ,  $\mathcal{M}_{4,2}^{(1324)}$  and the zero-dimensional boundary, or vertex,  $v_{\{1,2\}}$ , representing the full boundary stratification. The intervals for the other orderings are topologically equivalent to the ones presented here. In the Hasse diagrams, we explicitly indicate the edge labels, i.e. the spinor brackets which vanish when approaching a specific boundary, and a diamond-compatible assignment of signs to every edge.

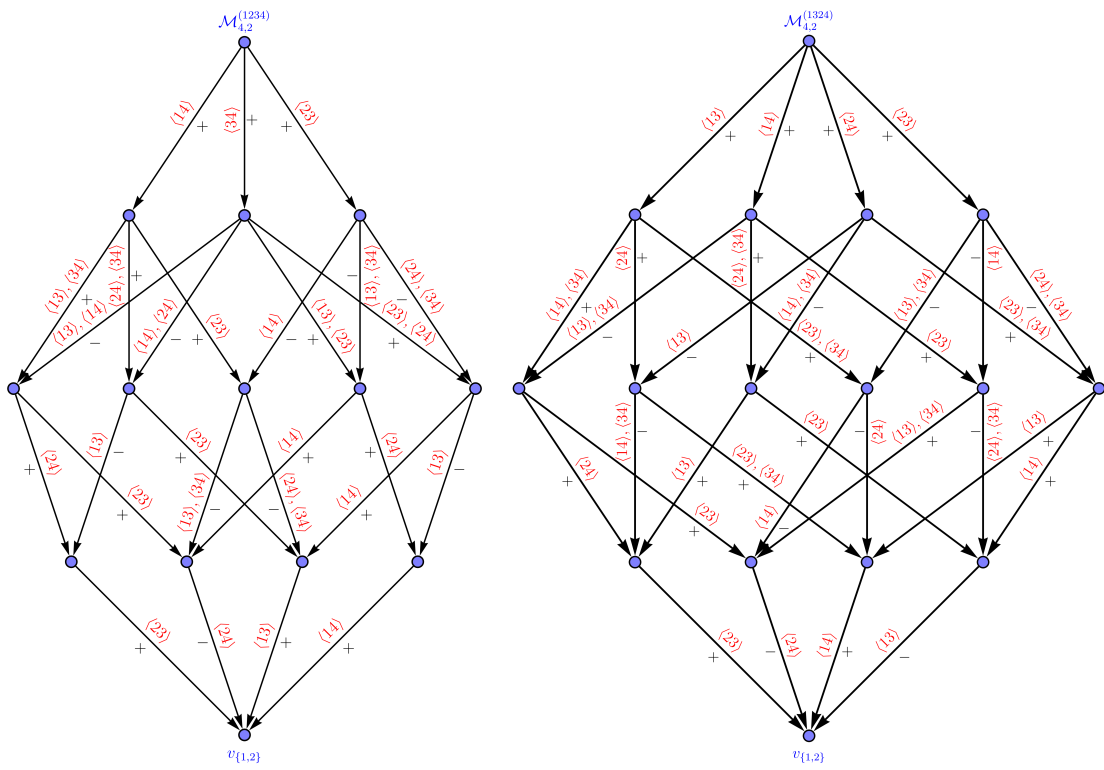


Figure F.1: Hasse diagrams of the interval between  $\mathcal{M}_{4,2}^{(1234)}$  (left) and  $\mathcal{M}_{4,2}^{(1324)}$  (right), and the vertex  $v_{\{1,2\}}$ .

# Bibliography

- [1] N. Arkani-Hamed and J. Trnka, “*The Amplituhedron*”, JHEP 1410, 030 (2014), [arxiv:1312.2007](#).
- [2] M. Ammon and J. Erdmenger, “*Gauge/gravity duality: Foundations and applications*”, Cambridge University Press (2015), Cambridge.
- [3] S. Weinberg, “*The Quantum theory of fields. Vol. 1: Foundations*”, Cambridge University Press (2005).
- [4] C. Hofer, “*Causal Determinism*”, in: “*The Stanford Encyclopedia of Philosophy*”, Spring 2016 edition, ed.: E. N. Zalta, Metaphysics Research Lab, Stanford University (2016).
- [5] P. de Laplace, F. Truscott and F. Emory, “*A Philosophical Essay on Probabilities*”, Wiley (1902).
- [6] P. de Laplace and N. Bowditch, “*Mecanique Céleste*”, Boston: Hillard, Gray, Little, and Wilkins (1839).
- [7] A. Einstein, “*On the electrodynamics of moving bodies*”, Annalen Phys. 17, 891 (1905).
- [8] A. Einstein, “*Über die vom Relativitätsprinzip geforderte Trägheit der Energie*”, Annalen Phys. 23, 371 (1907).
- [9] S. M. Carroll, “*Spacetime and Geometry*”, Cambridge University Press (2019).
- [10] A. Einstein, “*Concerning an heuristic point of view toward the emission and transformation of light*”, Annalen Phys. 17, 132 (1905).
- [11] M. Planck, “*On the Law of Distribution of Energy in the Normal Spectrum*”, Annalen Phys. 4, 553 (1901).
- [12] N. Bohr, “*On the Constitution of Atoms and Molecules*”, Phil. Mag. Ser. 6 26, 1 (1913).
- [13] J. J. Sakurai and J. Napolitano, “*Modern Quantum Mechanics*”, Cambridge University Press (2020).
- [14] M. E. Peskin and D. V. Schroeder, “*An Introduction to quantum field theory*”, Addison-Wesley (1995), Reading, USA.
- [15] M. Srednicki, “*Quantum field theory*”, Cambridge University Press (2007).

- [16] L. D. Landau and E. M. Lifshitz, “*Statistical Physics, Part 1*”, Butterworth-Heinemann (1980), Oxford.
- [17] D. Schroeder and H. Gould, “*An Introduction to Thermal Physics*”, *Physics Today* 53, 44 (2000).
- [18] A. Fetter and J. Walecka, “*Theoretical Mechanics of Particles and Continua*”, Dover Publications (2012).
- [19] I. Newton, “*Philosophiæ Naturalis Principia Mathematica*”, England.
- [20] R. P. Feynman, “*The Theory of Positrons*”, *Phys. Rev.* 76, 749 (1949), <https://link.aps.org/doi/10.1103/PhysRev.76.749>.
- [21] G. Altarelli, “*The Higgs and the Excessive Success of the Standard Model*”, [arxiv:1407.2122](https://arxiv.org/abs/1407.2122).
- [22] S. J. Parke and T. R. Taylor, “*An Amplitude for  $n$  Gluon Scattering*”, *Phys. Rev. Lett.* 56, 2459 (1986).
- [23] F. A. Berends and W. T. Giele, “*Recursive Calculations for Processes with  $n$  Gluons*”, *Nucl. Phys. B* 306, 759 (1988).
- [24] Z. Bern and D. A. Kosower, “*EFFICIENT COMPUTATION OF GAUGE THEORY LOOPS USING STRING THEORY*”.
- [25] Z. Bern and D. A. Kosower, “*The Computation of loop amplitudes in gauge theories*”, *Nucl. Phys. B* 379, 451 (1992).
- [26] Z. Bern, L. J. Dixon and D. A. Kosower, “*One loop corrections to five gluon amplitudes*”, *Phys. Rev. Lett.* 70, 2677 (1993), [hep-ph/9302280](https://arxiv.org/abs/hep-ph/9302280).
- [27] Z. Bern, L. J. Dixon, D. C. Dunbar and D. A. Kosower, “*One loop  $n$  point gauge theory amplitudes, unitarity and collinear limits*”, *Nucl. Phys. B* 425, 217 (1994), [hep-ph/9403226](https://arxiv.org/abs/hep-ph/9403226).
- [28] R. Britto, F. Cachazo and B. Feng, “*New recursion relations for tree amplitudes of gluons*”, *Nucl. Phys. B* 715, 499 (2005), [hep-th/0412308](https://arxiv.org/abs/hep-th/0412308).
- [29] R. Britto, F. Cachazo, B. Feng and E. Witten, “*Direct proof of tree-level recursion relation in Yang-Mills theory*”, *Phys. Rev. Lett.* 94, 181602 (2005), [hep-th/0501052](https://arxiv.org/abs/hep-th/0501052).
- [30] F. Cachazo, S. He and E. Y. Yuan, “*Scattering equations and Kawai-Lewellen-Tye orthogonality*”, *Phys. Rev. D* 90, 065001 (2014), [arxiv:1306.6575](https://arxiv.org/abs/1306.6575).
- [31] F. Cachazo, S. He and E. Y. Yuan, “*Scattering of Massless Particles in Arbitrary Dimensions*”, *Phys. Rev. Lett.* 113, 171601 (2014), [arxiv:1307.2199](https://arxiv.org/abs/1307.2199).
- [32] F. Cachazo, S. He and E. Y. Yuan, “*Scattering in Three Dimensions from Rational Maps*”, *JHEP* 1310, 141 (2013), [arxiv:1306.2962](https://arxiv.org/abs/1306.2962).
- [33] F. Cachazo, S. He and E. Y. Yuan, “*Scattering of Massless Particles: Scalars, Gluons and Gravitons*”, *JHEP* 1407, 033 (2014), [arxiv:1309.0885](https://arxiv.org/abs/1309.0885).
- [34] N. Arkani-Hamed, T.-C. Huang and Y.-t. Huang, “*Scattering Amplitudes For All Masses and Spins*”, [arxiv:1709.04891](https://arxiv.org/abs/1709.04891).

- [35] J. A. Wheeler, “*On the Mathematical Description of Light Nuclei by the Method of Resonating Group Structure*”, *Phys. Rev.* 52, 1107 (1937).
- [36] H. Lehmann, S. K. and W. Zimmerman, “*On the formulation of quantized field theories*”, *Nuovo Cim.* 1, 205 (1995).
- [37] N. Arkani-Hamed, F. Cachazo and J. Kaplan, “*What is the Simplest Quantum Field Theory?*”, *JHEP* 1009, 016 (2010), [arxiv:0808.1446](#).
- [38] N. Arkani-Hamed, Y. Bai and T. Lam, “*Positive Geometries and Canonical Forms*”, *JHEP* 1711, 039 (2017), [arxiv:1703.04541](#).
- [39] D. Damgaard, L. Ferro, T. Lukowski and M. Parisi, “*The Momentum Amplituhedron*”, *JHEP* 1908, 042 (2019), [arxiv:1905.04216](#).
- [40] D. Damgaard, L. Ferro, T. Lukowski and R. Moerman, “*Momentum amplituhedron meets kinematic associahedron*”, *JHEP* 2102, 041 (2021), [arxiv:2010.15858](#).
- [41] D. Damgaard, L. Ferro, T. Lukowski and R. Moerman, “*Kleiss-Kuijf Relations from Momentum Amplituhedron Geometry*”, [arxiv:2103.13908](#).
- [42] R. Kleiss and H. Kuijf, “*Multi - Gluon Cross-sections and Five Jet Production at Hadron Colliders*”, *Nucl. Phys. B* 312, 616 (1989).
- [43] N. Arkani-Hamed, Y. Bai, S. He and G. Yan, “*Scattering Forms and the Positive Geometry of Kinematics, Color and the Worldsheet*”, *JHEP* 1805, 096 (2018), [arxiv:1711.09102](#).
- [44] E. P. Wigner, “*On Unitary Representations of the Inhomogeneous Lorentz Group*”, *Annals Math.* 40, 149 (1939).
- [45] H. Elvang and Y.-t. Huang, “*Scattering Amplitudes in Gauge Theory and Gravity*”, Cambridge University Press (2015).
- [46] L. J. Dixon, “*Calculating scattering amplitudes efficiently*”, [hep-ph/9601359](#), in: “*Theoretical Advanced Study Institute in Elementary Particle Physics (TASI 95): QCD and Beyond*”.
- [47] L. J. Dixon, “*A brief introduction to modern amplitude methods*”, [arxiv:1310.5353](#), in: “*Theoretical Advanced Study Institute in Elementary Particle Physics: Particle Physics: The Higgs Boson and Beyond*”.
- [48] P. Benincasa and F. Cachazo, “*Consistency Conditions on the S-Matrix of Massless Particles*”, [arxiv:0705.4305](#).
- [49] T. Adamo, “*Lectures on twistor theory*”, [arxiv:1712.02196](#).
- [50] N. Arkani-Hamed and J. Kaplan, “*On Tree Amplitudes in Gauge Theory and Gravity*”, *JHEP* 0804, 076 (2008), [arxiv:0801.2385](#).
- [51] V. Del Duca, L. J. Dixon and F. Maltoni, “*New color decompositions for gauge amplitudes at tree and loop level*”, *Nucl. Phys. B* 571, 51 (2000), [hep-ph/9910563](#).
- [52] Z. Bern, J. J. M. Carrasco and H. Johansson, “*New Relations for Gauge-Theory Amplitudes*”, *Phys. Rev. D* 78, 085011 (2008), [arxiv:0805.3993](#).

- [53] Z. Bern, J. J. Carrasco, M. Chiodaroli, H. Johansson and R. Roiban, “*The Duality Between Color and Kinematics and its Applications*”, arxiv:1909.01358.
- [54] N. E. J. Bjerrum-Bohr, P. H. Damgaard and P. Vanhove, “*Minimal Basis for Gauge Theory Amplitudes*”, Phys. Rev. Lett. 103, 161602 (2009), arxiv:0907.1425.
- [55] N. Arkani-Hamed and J. Kaplan, “*On Tree Amplitudes in Gauge Theory and Gravity*”, JHEP 0804, 076 (2008), arxiv:0801.2385.
- [56] M. Spradlin, A. Volovich and C. Wen, “*Three Applications of a Bonus Relation for Gravity Amplitudes*”, Phys. Lett. B 674, 69 (2009), arxiv:0812.4767.
- [57] B. Feng, R. Huang and Y. Jia, “*Gauge Amplitude Identities by On-shell Recursion Relation in S-matrix Program*”, Phys. Lett. B 695, 350 (2011), arxiv:1004.3417.
- [58] J. M. Henn and J. C. Plefka, “*Scattering Amplitudes in Gauge Theories*”, Springer (2014), Berlin.
- [59] E. Witten, “*Perturbative gauge theory as a string theory in twistor space*”, Commun. Math. Phys. 252, 189 (2004), hep-th/0312171.
- [60] D. J. Gross and P. F. Mende, “*String Theory Beyond the Planck Scale*”, Nucl. Phys. B 303, 407 (1988).
- [61] S. Mizera, “*Inverse of the String Theory KLT Kernel*”, JHEP 1706, 084 (2017), arxiv:1610.04230.
- [62] Particle Data Group Collaboration, P. Zyla et al., “*Review of Particle Physics*”, PTEP 2020, 083C01 (2020).
- [63] J. M. Drummond, J. Henn, G. P. Korchemsky and E. Sokatchev, “*Generalized unitarity for  $N=4$  super-amplitudes*”, Nucl. Phys. B 869, 452 (2013), arxiv:0808.0491.
- [64] A. Herderschee, S. Koren and T. Trott, “*Constructing  $\mathcal{N} = 4$  Coulomb branch superamplitudes*”, JHEP 1908, 107 (2019), arxiv:1902.07205.
- [65] J. M. Drummond and J. M. Henn, “*All tree-level amplitudes in  $N=4$  SYM*”, JHEP 0904, 018 (2009), arxiv:0808.2475.
- [66] J. M. Drummond, J. M. Henn and J. Plefka, “*Yangian symmetry of scattering amplitudes in  $N=4$  super Yang-Mills theory*”, JHEP 0905, 046 (2009), arxiv:0902.2987.
- [67] R. Penrose, “*Twistor algebra*”, J. Math. Phys. 8, 345 (1967).
- [68] A. P. Hodges and S. Huggett, “*TWISTOR DIAGRAMS*”, Surveys High Energy Phys. 1, 333 (1980).
- [69] L. J. Mason and D. Skinner, “*Dual Superconformal Invariance, Momentum Twistors and Grassmannians*”, JHEP 0911, 045 (2009), arxiv:0909.0250.
- [70] Z. Bern and D. A. Kosower, “*Color decomposition of one loop amplitudes in gauge theories*”, Nucl. Phys. B 362, 389 (1991).
- [71] G. 't Hooft, “*A Planar Diagram Theory for Strong Interactions*”, Nucl. Phys. B 72, 461 (1974).

- [72] N. Arkani-Hamed, J. L. Bourjaily, F. Cachazo, A. B. Goncharov, A. Postnikov and J. Trnka, “*Grassmannian Geometry of Scattering Amplitudes*”, Cambridge University Press (2016).
- [73] J. L. Bourjaily, “*Positroids, Plabic Graphs, and Scattering Amplitudes in Mathematica*”, arxiv:1212.6974.
- [74] N. Arkani-Hamed, F. Cachazo, C. Cheung and J. Kaplan, “*A Duality For The S Matrix*”, JHEP 1003, 020 (2010), arxiv:0907.5418.
- [75] N. Arkani-Hamed, H. Thomas and J. Trnka, “*Unwinding the Amplituhedron in Binary*”, JHEP 1801, 016 (2018), arxiv:1704.05069.
- [76] S. Caron-Huot, “*Notes on the scattering amplitude / Wilson loop duality*”, JHEP 1107, 058 (2011), arxiv:1010.1167.
- [77] L. Ferro and T. Lukowski, “*Amplituhedra, and beyond*”, J. Phys. A 54, 033001 (2021), arxiv:2007.04342.
- [78] A. Yelleshpur Srikant, “*Emergent unitarity from the amplituhedron*”, JHEP 2001, 069 (2020), arxiv:1906.10700.
- [79] J. D. Stasheff, “*Homotopy Associativity of H-Spaces. I*”, Transactions of the American Mathematical Society 108, 275 (1963), <http://www.jstor.org/stable/1993608>.
- [80] J. D. Stasheff, “*Homotopy Associativity of H-Spaces. II*”, Transactions of the American Mathematical Society 108, 293 (1963), <http://www.jstor.org/stable/1993609>.
- [81] The OEIS Foundation, “*The Online Encyclopedia of Integer Sequences (accessed 15/10/21)*”, <https://oeis.org/A000108>.
- [82] N. J. A. Sloane and T. O. F. Inc., “*The on-line encyclopedia of integer sequences*”, <https://oeis.org/A006318>.
- [83] T. Lukowski, M. Parisi, M. Spradlin and A. Volovich, “*Cluster Adjacency for  $m = 2$  Yangian Invariants*”, JHEP 1910, 158 (2019), arxiv:1908.07618.
- [84] S. He and C. Zhang, “*Notes on Scattering Amplitudes as Differential Forms*”, JHEP 1810, 054 (2018), arxiv:1807.11051.
- [85] Y.-t. Huang, “*Non-Chiral S-Matrix of  $N=4$  Super Yang-Mills*”, arxiv:1104.2021.
- [86] T. Lukowski, M. Parisi and L. K. Williams, “*The positive tropical Grassmannian, the hypersimplex, and the  $m=2$  amplituhedron*”, arxiv:2002.06164.
- [87] T. Lukowski and J. Stalknecht, “*The hypersimplex canonical forms and the momentum amplituhedron-like logarithmic forms*”, arxiv:2107.07520.
- [88] T. Lukowski and R. Moerman, “*Boundaries of the amplituhedron with amplituhedronBoundaries*”, Comput. Phys. Commun. 259, 107653 (2021), arxiv:2002.07146.
- [89] L. Ferro, T. Lukowski and R. Moerman, “*From momentum amplituhedron boundaries to amplitude singularities and back*”, JHEP 2007, 201 (2020), arxiv:2003.13704.

- 
- [90] N. Arkani-Hamed, T. Lam and M. Spradlin, “Non-perturbative geometries for planar  $\mathcal{N} = 4$  SYM amplitudes”, JHEP 2103, 065 (2021), [arxiv:1912.08222](https://arxiv.org/abs/1912.08222).
- [91] V. V. Fock and A. B. Goncharov, “Moduli spaces of local systems and higher Teichmüller theory”, arXiv Mathematics e-prints 2103, math/0311149 (2003), [math/0311149](https://arxiv.org/abs/math/0311149).
- [92] R. Britto, F. Cachazo and B. Feng, “New recursion relations for tree amplitudes of gluons”, Nuclear Physics B 715, B. Feng (2005), [http://dx.doi.org/10.1016/j.nuclphysb.2005.02.030](https://doi.org/10.1016/j.nuclphysb.2005.02.030).
- [93] R. Britto, F. Cachazo, B. Feng and E. Witten, “Direct Proof of the Tree-Level Scattering Amplitude Recursion Relation in Yang-Mills Theory”, Physical Review Letters 94, E. Witten (2005), [http://dx.doi.org/10.1103/PhysRevLett.94.181602](https://doi.org/10.1103/PhysRevLett.94.181602).
- [94] A. Postnikov, “Permutohedra, Associahedra, and Beyond”, International Mathematics Research Notices 2009, 1026 (2009).
- [95] J. L. Bourjaily, E. Herrmann, C. Langer and J. Trnka, “Building bases of loop integrands”, JHEP 2011, 116 (2020), [arxiv:2007.13905](https://arxiv.org/abs/2007.13905).
- [96] J. L. Bourjaily, E. Herrmann, C. Langer, A. J. McLeod and J. Trnka, “All-Multiplicity Nonplanar Amplitude Integrands in Maximally Supersymmetric Yang-Mills Theory at Two Loops”, Phys. Rev. Lett. 124, 111603 (2020), [arxiv:1911.09106](https://arxiv.org/abs/1911.09106).
- [97] Z. Bern, J. J. M. Carrasco and H. Johansson, “Perturbative Quantum Gravity as a Double Copy of Gauge Theory”, Phys. Rev. Lett. 105, 061602 (2010), [arxiv:1004.0476](https://arxiv.org/abs/1004.0476).
- [98] J. Trnka, “Towards the Gravituhedron: New Expressions for NMHV Gravity Amplitudes”, JHEP 2104, 253 (2021), [arxiv:2012.15780](https://arxiv.org/abs/2012.15780).
- [99] G. Dian and P. Heslop, “Amplituhedron-like geometries”, [arxiv:2106.09372](https://arxiv.org/abs/2106.09372).
- [100] A. B. Goncharov, M. Spradlin, C. Vergu and A. Volovich, “Classical Polylogarithms for Amplitudes and Wilson Loops”, Physical Review Letters 105, A. Volovich (2010), [http://dx.doi.org/10.1103/PhysRevLett.105.151605](https://doi.org/10.1103/PhysRevLett.105.151605).
- [101] P. Baikov, “Explicit solutions of the multi-loop integral recurrence relations and its application”, Nuclear Instruments and Methods in Physics Research Section A: Accelerators, Spectrometers, Detectors and Associated Equipment 650, 117–120 (2011), [http://dx.doi.org/10.1016/S0168-9002\(97\)00126-5](https://doi.org/10.1016/S0168-9002(97)00126-5).
- [102] J. M. Henn, “Multiloop Integrals in Dimensional Regularization Made Simple”, Physical Review Letters 110, J. M. Henn (2013), [http://dx.doi.org/10.1103/PhysRevLett.110.251601](https://doi.org/10.1103/PhysRevLett.110.251601).